Investigating the role of the circadian clock and timed exercise on mouse skeletal muscle function

Inauguraldissertation

zur

Erlangung der Würde eines Doktors der Philosophie

vorgelegt der

Philosophisch-Naturwissenschaftlichen Fakultät

der Universität Basel

von

Geraldine Maier

Deutschland

Basel, 2020

Genehmigt von der Philosophisch-Naturwissenschaftlichen Fakultät auf Antrag von

Prof. Dr. Christoph Handschin und Prof. Dr. Markus Rüegg

Basel, den 23.06.2020

Prof. Dr. Martin Spiess
Dekan

Table of Contents

Abstract 7
Abbreviations 9
1. Introduction 13
1.1 Circadian Rhythm 13
The molecular clock 13
Central and peripheral clocks 15
Circadian rhythm disruption and consequence 16
1.2 Skeletal Muscle 19
Skeletal muscle function and fiber type 19
Physical exercise 19
Exercise and health 21
1.3 Skeletal Muscle Clock 22
2. Aim of the Thesis 25
Timing of exercise defines the transcriptome, proteome and phosphoproteome responses of mouse skeletal muscle 29
Abstract 30
Introduction 31
Results 33
Time-of-day-dependent variations in mouse treadmill exercise performance. 33
Exercise around the clock induces broad and time-dependent gene responses in skeletal muscle. 35
Daytime vs. nighttime treadmill exercise elicits distinct gene signatures in skeletal muscle. 38
Proteome and secretome changes associated with daytime vs. nighttime treadmill exercise. 41
The phosphorylome of daytime vs. nighttime working muscles. 45
Scheduled daytime wheel-running activity in mice exposed to a skeleton photoperiod. 47
Daytime wheel running is a potent inducer of gene expression in muscle of trained mice. 49
Characterization of the muscle transcriptome, proteome and phosphoproteome responses of daytime wheel active mice. 51
Discussion 55
Understanding the daily variance in maximal exercise capacity 55

Time-dependent activation of skeletal muscle pathways 57
Time, exercise and circadian physiology 58
Limitations of the study 59
Materials and methods 60
Animals 60
Forced high-intensity exercise performance across the day 60
Daytime scheduled wheel-running activity 60
Body temperature and locomotor activity recordings 61
Muscle tissue preparation and blood collection 61
Quantitative Real-Time PCR (Reverse Transcript) 61
Blood parameters analysis 62
RNA sequencing and data analysis 62
Proteomics and data analysis 63
Pathway enrichment analysis 66
Statistics 66
Supplemental Figures 67
References 75
RORα deletion alters mouse spontaneous locomotion and skeletal muscle ROS metabolism 91
Abstract 92
Introduction 93
Results 94
Muscle-specific RORα deletion leads to slight alterations in energy balance and muscle fiber type. 94
RORα deletion leads to a severe dampening of core clock gene oscillations. 95
Decreased spontaneous wheel-running activity in mice with muscle-specific RORα deletion but not forced exercise performance. 97
In-depth proteomic analysis of MKO muscle indicates a role for RORα in ROS detoxification. 99
RORα is essential for the detoxification of ROS produced by exercise 101
Discussion 103
Materials and methods 105
Animals 105
Body composition analysis 105
Body temperature and locomotor activity recordings 105
Comprehensive laboratory animal monitoring system 105

Treadmill 105
ROS detection 106
Muscle tissue preparation and blood collection 106
Quantitative Real-Time PCR (Reverse Transcript) 107
RNA sequencing and data analysis 107
TMT labeling and LC-MS/MS analysis 107
Cell Culture 109
Hypoxia 110
Statistical analysis 110
Supplemental Figures 111
References 116
5 Discussion 123
5.1 On the effects of timed exercise 123
Time, exercise and the skeletal muscle clock 124
Proteomics and circadian proteins 127
Daytime activity, SPP and SCN 127
On the timed effects of regular training 128
Limitations and perspectives 129
5.2 On clock-controlled muscle functions 131
Exercise and the brain 131
The clock and metabolism 132
Limitations and perspectives 132
5.3 Conclusion on Ph.D. work 133
6 References of Thesis 135
7 Appendix 152
Acknowledgments 163

Abstract

An inactive, sedentary lifestyle directly impacts health and increases the risk of premature death. Likewise, circadian rhythm disruption (e.g., shift-work) is linked to various chronic diseases, including diabetes, cardiovascular disease, and cancer. Regular physical exercise is a potent regulator of skeletal muscle and whole-body metabolism and can prevent or even treat chronic medical disorders, including diabetes, cancer, and cardiovascular disease. Moreover, proper sleeping schedules, meal-timing, and chrono-medication all can ameliorate many of the aforementioned diseases. It is unclear, however, whether a chrono-therapeutic approach of exercise can amplify the beneficial health effects of regular training, and whether these effects would be mediated by skeletal muscle.

The first part of my Ph.D. work evaluated the transcriptomic, proteomic, and phosphoproteomic responses of mouse skeletal muscle to two widely used exercise modalities at distinct phases of the light-dark cycle. We found that maximal treadmill exercise capacity varies according to the time of day, and give evidence of subtle changes in systemic and muscle energy levels in response to exercise around the clock. Moreover, we reveal a timely activation of specific biological pathways within working muscles. For instance, mechanisms directing vesicular trafficking, phosphorylation of key regulators of glucose uptake and calcium metabolism, and putative secreted factors affecting hepatic glucose production were induced explicitly by early daytime treadmill exercise and could potentially enhance running exercise capacity. We furthermore established a completely new methodology to examine the effects of spontaneous wheel running. Using this method, we give evidence that exercise is a poor modifier of daily clock gene expression. On the other hand, we show that daytime wheel-running activity is a potent modifier of oxidative metabolism gene expression under constant environmental light conditions; however, food-intake has a more profound effect on the skeletal muscle clock. With our large-scale transcriptomic, proteomic, and phosphoproteomic data, we provide resources for future research projects and validation studies. We also hope that the use of scheduled wheel running at different times of the day could be useful in preclinical mouse models.

Mouse models of whole-body clock gene deletion highlighted the potential role for circadian clock components in muscle cell development and repair, insulin sensitivity, glucose, and lipid metabolism. Yet, global gene deletion leads to multiple effects in other organs, which can be confounding factors for the evaluation of muscle-specific function. The second part of my Ph.D. work was to characterize the specific contribution of the core clock transcription factor RORα in skeletal muscle physiology and exercise behavior. We show that skeletal muscle-specific deletion of RORα significantly decreased spontaneous wheel-running activity in the absence of significant alteration in muscle structure, and systemic metabolism.

Interestingly, in response to exercise, a decrease in the expression of key regulators of oxidative stress was observed. Furthermore, upon exposure to hypoxia, causing abnormal ROS elevation, or directly to H_2O_2, we reveal that RORα overexpression protects from cell death. Our data suggest that skeletal muscle RORα is important for modulating ROS metabolism and possibly the skeletal muscle adaptations to exercise.

Taken together, our data provide new evidence that skeletal muscle molecular and cellular responses are dependent on the time of the day and systemic energy level. Notably, we propose that mechanisms promoting glucose delivery and uptake in muscle tissues, together with those critical for the response to inflammation and the secretion of myokines, are tied to a time period of the day. Our results, moreover, suggest that there is an optimal time to exercise to improve muscle adaptation and probably performance, as well as glucose homeostasis. Finally, the last part of my Ph.D. work gives evidence that the circadian component RORα is required to influence ROS metabolism and the cellular adaptations of skeletal muscle to a prolonged period of exercise training.

Abbreviations

Acaca	acetyl-CoA carboxylase
Acty	ATP-citrate synthase
Akap	A-kinase anchoring protein
Aldo	aldolase
AMPK	adenosine monophosphate (AMP)-activated protein kinase
Arntl	aryl hydrocarbon receptor nuclear translocator like
Atf	AMP-dependent transcription factor
ATP	adenosine triphosphate
bHLH	basic helix-loop-helix
Bmal1	brain and muscle arntl
Cacna1	calcium voltage-gated channel subunit alpha1
CCG	clock-controlled genes
Ciart	circadian associated repressor of transcription
CK1	casein kinase 1
CLAMS	Comprehensive Laboratory Animal Monitoring System
Clock	circadian locomotor output cycles kaput
Cpt1	carnitine palmitoyltransferase 1
CRD	circadian rhythm disruption
Cry	cryptochrome
cTM	circadian treadmill
CTRL	control
Ctsb	cathepsin b
DA	Daytime Activity
Dbp	D-box Binding PAR bZIP Transcription Factor
DD	constant darkness
DEG	differentially expressed genes
DF	Daytime Feeding
Dpb	D-Box Binding Par Bzip Transcription Factor
E-box	enhancer box
EDL	extensor digitalis longus
Eif	eukaryotic translation initiation factor
Elovl	elovl fatty acid elongase
Eno	enolase
ER	endoplasmic reticulum
FAA	free fatty acid
Fasn	fatty acid synthase
Fbn	fibrillin/asprosin
FoxO	forkhead transcription factor O
Gas	gastrocnemius
gKO	global KO
Glut4	glucose transporter type 4
GMC	German Mouse Clinic

GO	Gene Ontology
Grk	Beta-adrenergic receptor kinase
H&E	Hematoxylin & Eosin
Hadh	mitochondrial trifunctional enzyme subunit
Hif-1	hypoxia-inducible factors
HIIT	High Intensity Interval Training
Hk	hexokinase
IARC	International Agency for Research on Cancer
Idh	isocitrate dehydrogenase
Il-6	interleukin-6
Itih	inhibitor heavy chain
Kat	kynurenine aminotransferase
KEGG	Kyoto Encyclopedia of Genes and Genomes
KO	knock out
KYN	kynurenine
KYNA	kynurenic acid
LD	light-dark cycle
Lpin	lipin
MAPK	mitogen-activated protein kinase
MKO	skeletal muscle-specific KO
MS	mass spectrometry
Mt	metallothionein
mTOR	mammalian target of rapamycin
Mup	major urinary proteins
Myh	myosin heavy chain protein
Myod	myogenic differentiation
Ncor	nuclear corepressor
Nfκb	nuclear factor-kappa B
NMD	nonsense mediated decay
Nr1d1	nuclear receptor subfamily 1 group d member 1
Nr1f1	nuclear receptor subfamily 1 group f member 1
Nr3c1/GR	glucocorticoid receptor
Nrf	nuclear respiratory factor
Orai	calcium release-activated calcium channel protein
PCr	phosphocreatine
Pdk	pyruvate dehydrogenase kinase
Per	period
Pfk	phosphofructokinase
Ppargc-1/Pgc-1	peroxisome proliferator-activated receptor gamma coactivator 1
Pld5	phospholipase d family member 5
Plin3	perilipin3
Ppar	peroxisome proliferator-activated receptor
Prdx	peroxiredoxin

Psmd8	Proteasome 26S subunit, non-ATPase 8
Ptpr	protein tyrosine phosphatase
Pyg	glycogen phosphorylase
Rala	GTPase Ras-related protein
RER	respiratory exchange ratio
Rev-Erb	reverse viral erythroblastosis oncogene product
Ror	retinoic acid receptor-related orphan receptor
RORE	REV-ERB/ROR response element
ROS	reactive oxygen species
Rps6	ribosomal protein S6
Scd-1	stearoyl-CoA desaturase
SCN	suprachiasmatic nucleus
Sdh	succinate dehydrogenase
Sed	sedentary
Serca	sarcoplasmic reticulum calcium-ATPase
Sirt	sirtuin
Snap	synaptosomal-associated protein
Sod	superoxide dismutase
Sparcl	SPARC-like protein
SPP	skeleton photoperiod
Stab2	stabilin2
Stx	syntaxin
Tbc1d	TBC1 domain family member 4
TG	triglyceride
TSC	tuberous sclerosis complex
Ttfl	transcriptional-translational (autoregulatory) feedback loop
Vamp	vesicle-associated membrane protein
Vegf	vascular endothelial growth factor
WHO	World Health Organization
Ykt	synaptobrevin homolog YKT
ZT	zeitgeber time

1. Introduction

1.1 Circadian Rhythm

The molecular clock

Due to earth rotation, the environment is changing drastically within 24 hours, including light, temperature, and food availability. A wide range of organisms, including bacteria, plants, fungi, and animals, anticipate those environmental fluctuations and thus increase their chance of survival (Dibner et al., 2010; McClung, 2006; Reppert and Weaver, 2002; Sweeney and Borgese, 1989). Rhythmic changes in physiology and behavior (e.g., sleep/wake cycles, falling/rising of core body temperature, or hormonal levels), even in the absence of external cues, are called circadian rhythms. Circadian originates from the Latin "circa" meaning "about" and "dies" meaning "day" (Halberg, 1977). Those biological rhythms are the result of autonomous, intrinsic clocks found in virtually every cell (Pittendrigh, 1993; Sehgal, 2017). The 2017 Physiology or Medicine Nobel Prize was awarded to Michael Rosbash, Jeffrey C. Hall, and Michael W. Young "for their discoveries of molecular mechanisms controlling the circadian rhythm", proofing the fundamental importance of the circadian clock (Callaway and Ledford, 2017).

The molecular clock, a transcriptional, translational autoregulatory feedback loop (TTFL) is composed of more than a dozen transcription factors, coactivators and -repressors that coordinate a time-delayed activation/repression of transcription, to generate a self-sustained approximately 24-h rhythm (i.e., between 22 to 30 hours) (Mohawk et al., 2012) (**Figure I1**). The primary feedback loop is composed of the basic helix-loop-helix (bHLH) transcription factors circadian locomotor output cycles kaput (CLOCK) and brain and muscle Arnt-like 1 (BMAL1/ARNTL1). CLOCK and BMAL1 form a heterodimer and initiate the transcription of their target genes via an enhancer box (E-box) regulatory sequence Those target genes include the transcriptional corepressors Period (Per1, Per2, and Per3) and Cryptochrome (Cry1 and Cry2) (Kume et al., 1999; Zheng et al., 2001; Zheng et al., 1999), which heterodimerize, translocate to the nucleus and repress the transcriptional activity of the BMAL1:CLOCK heterodimer (Kume et al., 1999; Lee et al., 2001; Tamaru et al., 2015). The secondary feedback loop also begins with the BMAL1:CLOCK heterodimer activating the transcription of the transcriptional enhancer retinoic acid receptor-related orphan receptor (RORα, RORβ, and RORγ) and the transcriptional repressor reverse viral erythroblastosis oncogene product (Rev-erbα and Rev-erbβ) (Akashi and Takumi, 2005; Preitner et al., 2002; Sato et al., 2004; Triqueneaux et al., 2004). REV-ERB and ROR compete to bind the retinoic acid-related orphan receptor response elements (ROREs) in the Bmal1 promoter and thus regulate its expression (Guillaumond et al., 2005). Besides the transcriptional-translational regulation of the clock, post-translational modifications such as phosphorylation and

ubiquitination affecting the stability and nuclear translocation of the core clock proteins play a vital role in sustaining a 24-h rhythm (Akashi et al., 2002; Eide et al., 2005; Eide et al., 2002; Toh et al., 2001). Critical factors that regulate the core circadian protein turnover in mammals are the casein kinase1 (CK1ε and CK1δ) (Akashi et al., 2002; Eide et al., 2002). Mutations altering the kinase activity of CK1ε or CK1δ cause shorter circadian periods in mammals (Xu et al., 2005). Besides the circadian oscillation of the core clock proteins, the transcription of so-called clock-controlled genes (CCGs) is driven by the circadian core clock proteins. The CCGs include the transcription factors D-box binding PAR bZIP transcription factor (DBP), myogenic differentiation (MyoD), and many more. Rhythmic expression of about 3-16% of the transcriptome or about 4000 genes depending on the tissue can be observed (Koike et al., 2012; Mure et al., 2018; Zhang et al., 2014).

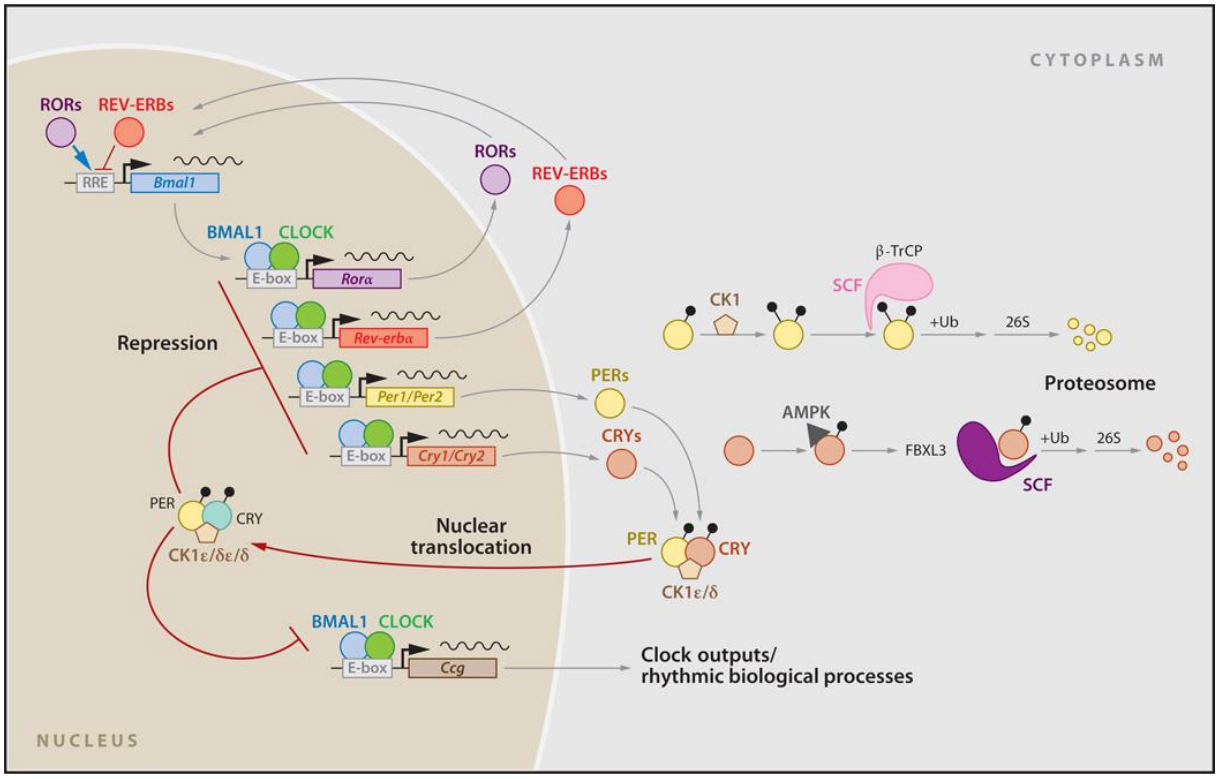

Figure I1. The mammalian circadian clock. In the primary feedback loop, the transcription factors BMAL1 (blue circles) and CLOCK (green circles) bind to E-box promoters, including the genes for PER1/2 (yellow) and CRY1/2 (orange). PERs and CRYs dimerize and translocate to the nucleus and repress their own transcription. In a secondary feedback loop, CLOCK and BMAL1 also regulate the transcription of the nuclear receptors REV-ERBα/β (red circles) and RORα/β/γ (purple circles) which compete for binding to RORE (RRE) elements on the BMAL1 gene promoter, providing both positive (ROR) and negative (REV-ERB) regulation of BMAL1 transcription. In addition, CLOCK/BMAL1, ROR/REV-ERB regulate the transcription of many clock output genes (CCG) (Mohawk et al., 2012).

Central and peripheral clocks

The mammalian circadian system is hierarchically organized, with a central clock in the brain orchestrating the oscillations in the peripheral clocks (Albrecht, 2012; Hastings et al., 2018; Panda et al., 2002). The central clock or suprachiasmatic nucleus (SCN) is located in the hypothalamus, directly above the optic chiasm. The approximately 10'000 neurons, each containing a cell-autonomous circadian oscillator, get direct photic input from the retina via light-sensitive ganglion cells (Hastings et al., 2018; Hatori and Panda, 2010). The light is not driving the molecular clock, but the neuronal input fine-tunes the TTFL via the expression of the Per genes (Sakamoto et al., 2013). Factors entraining the endogenous circadian clocks to the environmental time are known as Zeitgeber ("time-giver" or "synchronizer"). Light, directly adjusting the central clock, is the most prominent Zeitgeber. However, other, so-called non-photic Zeitgebers, such as food-intake for peripheral clocks in metabolic tissues, like the liver, are working SCN-independent (Damiola et al., 2000; Vollmers et al., 2012). As mentioned above, the molecular clock is present in virtually every cell of an organism; therefore, rhythmic expression of clock genes and proteins has been observed in tissues throughout the mammalian body. However, the clock output, i.e., CCGs, in different tissues, are mostly non-overlapping, therefore temporarily control cellular processes relevant to each unique cell type autonomously. The circadian clock controls many biological processes, including the sleep-wake cycle, hormone secretion, and metabolism (Delezie and Challet, 2011). The circadian control of, e.g., metabolism happens on the central as well as local level, involving the clocks of several peripheral tissues, like liver, skeletal muscle, and adipose tissue. Under normal environmental conditions, an internal synchronization of all body clock to the solar time is desirable. For that reason, the central clock orchestras the oscillation of the peripheral clocks through several signals (**Figure I2**). The SCN, as a brain region, projects to several other brain regions, controlling, e.g., sleep, appetite, mood, and alertness. Likewise, the clocks of peripheral tissues, including the liver, intestines, and skeletal muscle, are controlled via neuronal pathways. Besides the direct neuronal projection, the SCN is controlling the release of hormones, changes in body temperature, as well as behaviors like feeding and activity, which are potent synchronizers for the peripheral clocks.

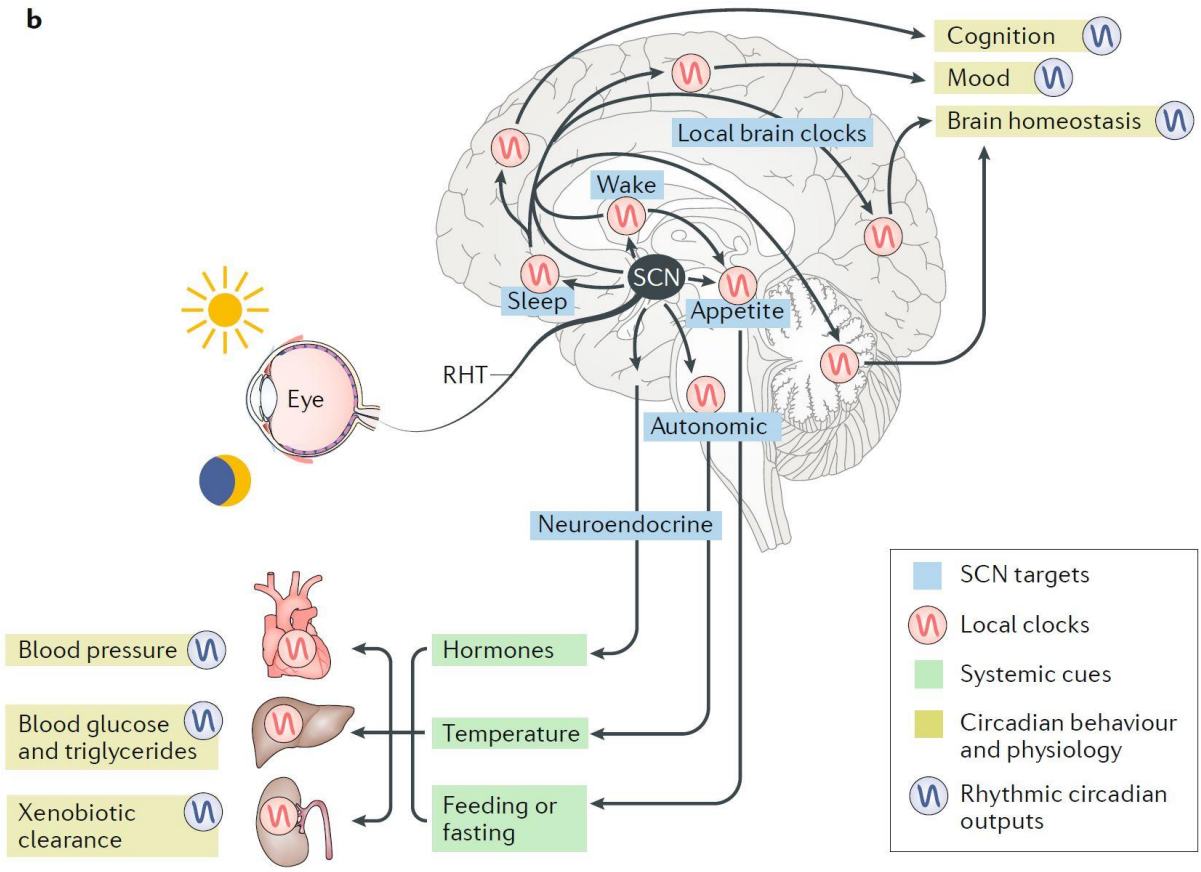

Figure I2. Circadian organization in mammals. The SCN receives direct photic input from the retina and projects to various brain centers, directly influencing behavior. Systemic cues synchronize the molecular clocks of peripheral tissues, leading to tissue-specific circadian gene expression that regulates physiological rhythms critical to health (Hastings et al., 2018).

Circadian rhythm disruption and consequence

Under normal living conditions, daily rhythms emerge from an interaction between the endogenous circadian clock and various rhythmic behaviors or environmental factors. The misalignment of the endogenous clock and the external clues can lead to circadian rhythm disruption (CRD). Between 15 and 20% of people in industrial societies work night shifts, an extreme case of CRD and associated with various chronic diseases, including obesity and diabetes, cardiovascular disease, infections, and cancer (Davis et al., 2001; Kervezee et al., 2020; Knutsson, 2003; Mohren et al., 2002). The International Agency for Research on Cancer (IARC) even classified shift work with CRD as a probable human carcinogen (group 2A carcinogen) (Straif et al., 2007). Over the past century, electric light at night softened the boundaries between day and night, leading to an increase of people with a shift-work-like lifestyle and circadian clock disruption (Dominoni et al., 2016). To further investigate the role of clock genes and the impact of CRD, different circadian clock gene loss-of-function or gain-of-function mouse models have been investigated. Those mice exhibit various diseases, including metabolic (Cho et al., 2012; Marcheva et al., 2010; Turek et al., 2005; Vieira et al.,

2014), inflammatory (Cao et al., 2017; Gibbs et al., 2012; Narasimamurthy et al., 2012) as well as mental disorders (Lamont et al., 2007), cancer (Fu et al., 2002; Lee et al., 2010) and early aging (Dubrovsky et al., 2010; Kondratov et al., 2006) (**Figure I3**). Taken together, the detrimental effects of a disrupted, malfunctioning clock indicates its importance in health and longevity.

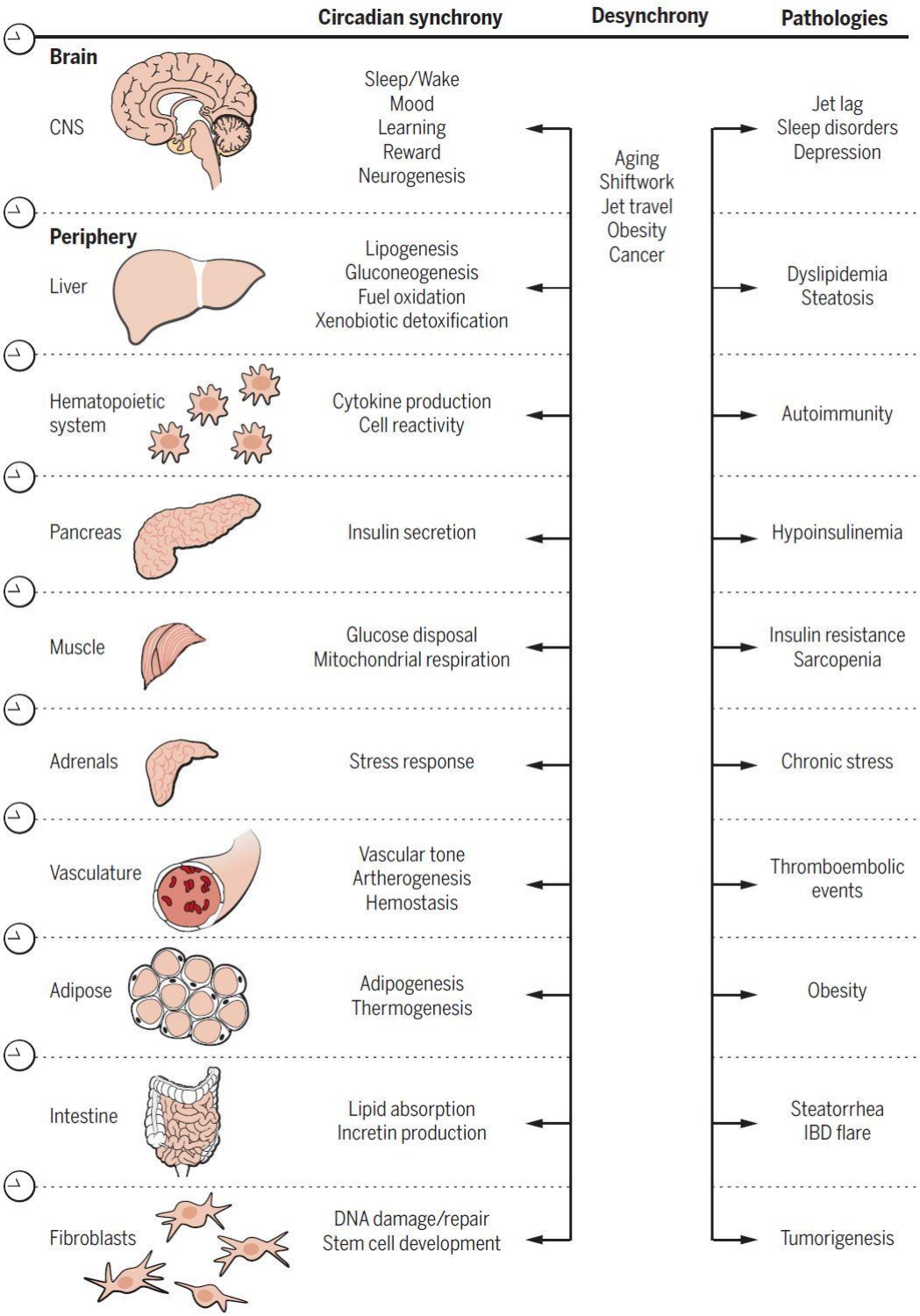

Figure I3. Circadian systems in physiological crosstalk and disease. In the brain, the clock coordinates the timing of sleep/wake cycle relative to light but additionally plays a role in many behaviors, including learning, reward, and neurogenesis. Peripheral tissue clocks are entrained by the SCN, although feeding and temperature can be dominant Zeitgeber in some physiological settings. Peripheral clocks may become uncoupled and desynchronized from the SCN, during aging, shiftwork, jet travel, obesity, or cancer. Circadian disruption contributes to the development of disorders such as metabolic syndrome, obesity, diabetes, autoimmunity, and cancer (Bass and Lazar, 2016).

1.2 Skeletal Muscle

Skeletal muscle function and fiber type

Skeletal muscle, the largest organ in the human body, accounts for approximately 40 % of total body weight and contains 50–75 % of all body proteins. It plays a critical role in locomotion, respiration, and metabolism, and as a consequence, health. Skeletal muscle contributes to basal energy metabolism, serves as storage for essential substrates such as amino acids and carbohydrates, is a significant site for insulin-stimulated glucose uptake (DeFronzo et al., 1981) and consumes the majority of oxygen and fuel during physical exercise (i.e., up to 90% of whole-body energy expenditure) (Egan and Zierath, 2013; Summermatter and Handschin, 2012). Besides its local metabolic activity, skeletal muscle exerts autocrine, paracrine, and long-distance endocrine effects, by secreting so-called myokines (Delezie and Handschin, 2018).

Skeletal muscle fibers, or myofibers, are classified into fiber types, with different metabolic and functional properties, in particular slow-oxidative (Type 1) versus fast-glycolytic (Type 2) fibers. Type 2 fibers are further subdivided into 2A, 2B, and 2X fibers (Schiaffino and Reggiani, 2011). Type I myofibers, rich in myoglobin and mitochondria, with a high oxidative capacity, are ideal for continuous and slow contraction. While, Type 2 (mainly 2B and 2X) myofibers, containing fewer mitochondria and relying on glycolytic metabolism, are ideal for powerful, fast movements, but also fatigue faster. Type 2A shows characteristics between type I and type 2B/2X. As a very dynamic and plastic tissue, skeletal muscle adapts to a variety of activities, from the explosive movement during a sprint to the continuous contraction during a marathon.

Physical exercise

Endurance (aerobic) exercise is characterized by high-repetition, low-resistance muscle contractions during which energy is provided by oxidative metabolism of carbohydrates and fatty acids. Resistance (strength) exercise, on the other hand, stands for a low-repetition, high-resistance load on the muscle where glycolysis provides most of the energy. In general, adenosine triphosphate (ATP) is essential for muscle contraction. However, the amount of ATP stored in muscle is small, and thus ATP needs to be resynthesized using other energy substrates. Within a few seconds of contraction, phosphocreatine (PCr) is broken-down. Glucose (deriving from the plasma or breakdown of muscle glycogen stores) entering anaerobic glycolysis provides ATP for the first minute. However, for longterm exercise, the oxidative phosphorylation of pyruvate (deriving from the glycolysis), fatty acids, or even amino acids is required to sustain the demand for ATP. Skeletal muscle substrate utilization (contributions of carbohydrates and lipids) during exercise is influenced by intensity and duration of exercise, but also by the individual conditions (e.g., sex, age, training status) of the exercising individual.

A single bout of exercise activates multiple signaling pathways (**Figure I4**) including well-known exercise-induced kinases (e.g., AMPK, MAPK, mTOR), regulating downstream transcriptional regulators (e.g., PGC-1α, PPARs, NRFs, SIRTs FOXOs) leading to increase transcription and protein stabilization (Bassel-Duby and Olson, 2006; Egan and Zierath, 2013; Hawley et al., 2014). Cumulative effects of repeated bouts of exercise (training) result in physiological adaptations, e.g., changes in mitochondrial function, substrate metabolism, protein content, and intracellular signaling (Benziane et al., 2008; Green et al., 1992; Pilegaard et al., 2003; Spina et al., 1996; Vargas-Ortiz et al., 2019; Widrick et al., 2002). More specifically, endurance training is associated with muscle capillarization, mitochondrial metabolism, and endurance capacity, while regular strength training is linked to increased fiber size, strength, and basal metabolic rate (Egan and Zierath, 2013). Exercise has a positive impact on many organs throughout the body, in particular by modulating the cardiovascular, respiratory, metabolic, and neuroendocrine systems via the exercise-induced secretion of myokines (Delezie and Handschin, 2018).

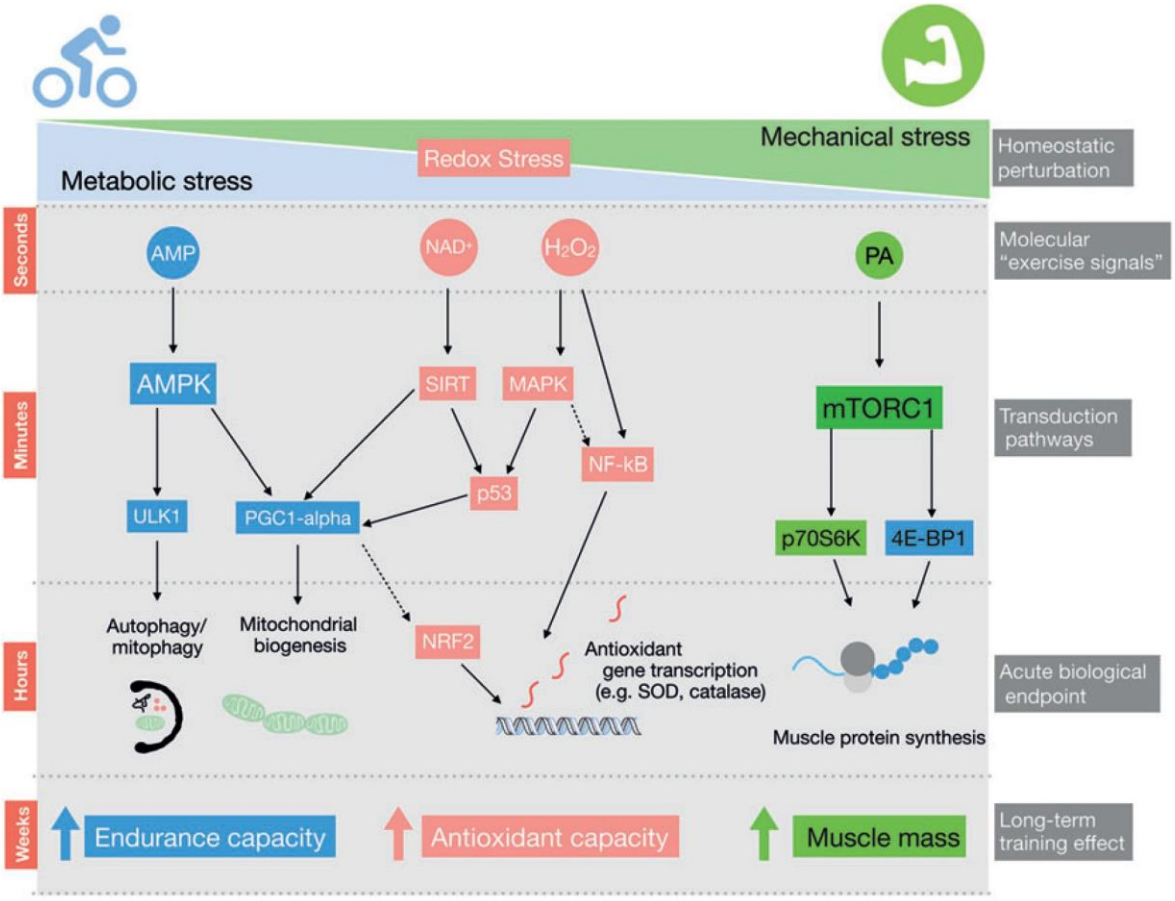

Figure I4. Adaptations to exercise training. Long-term adaptations to regular exercise, like increased endurance capacity with endurance exercise and muscle mass with resistance exercise, are mediated by specific acute signaling events and downstream changes in transcription and translation. The AMPK and mTORC1 pathways are classic examples of endurance and resistance exercise- activated pathways. Redox signaling may act in parallel or interact with these and other signaling pathways to modulate exercise training response (Henriquez-Olguin et al., 2019).

Exercise and health

Even though the quality, quantity, and time of food-intake had been widely studied (Chaix et al., 2019), exercise has been proven to be more effective in treating and preventing chronic diseases (Ding et al., 2016; Lobelo et al., 2014; Pedersen and Saltin, 2015). For example, the link between low cardiometabolic fitness and all-cause mortality is more robust than that of obesity (Lee et al., 1999). Exercise training is sufficient to decrease the prevalence of many chronic metabolic conditions/diseases (Booth et al., 2000; Ruegsegger and Booth, 2018). Regular physical exercise reduces fat (You et al., 2006) while preserving lean mass (Parr et al., 2013). Endurance exercise promotes beneficial changes in whole-body metabolism (Ballor and Keesey, 1991), whereas resistance exercise preserves/increase muscle mass (McGlory et al., 2019). Unfortunately, the compliance of people, even with the minimum recommended quantity and quality of exercise to obtain health benefits, is low (Guthold et al., 2018) (**Figure I5**).

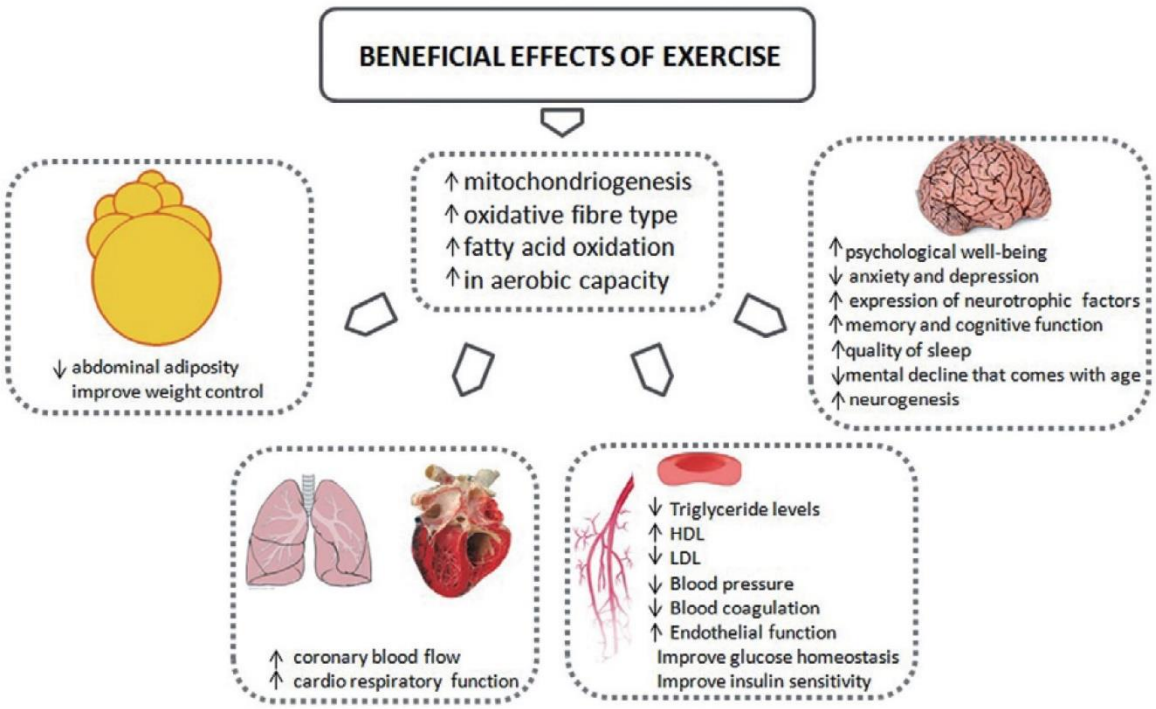

Figure I5. Health benefits of exercise in tissues and organs (Vina et al., 2012).

1.3 Skeletal Muscle Clock

While a bit more than 20 years ago, a few scientists in the field of skeletal muscle and exercise research, were puzzled by the different results of two seemingly identical experiments, it is now clear that timing makes the difference and that the skeletal muscle has a functional clock (Yamazaki et al., 2000; Zambon et al., 2003; Zylka et al., 1998). The molecular mechanism of the circadian clock is conserved between different tissues. However, the CCG expression, partially under the direct control of the BMAL1:CLOCK heterodimer, is tissue-specific. In skeletal muscle, about 10-20% of the transcriptome in humans and mice shows circadian expression, including transcription factors or proteins that control rate-limiting steps in cell physiology (e.g., DBP; MYOD, PGC-1α, PDK4) (Hodge et al., 2015; McCarthy et al., 2007; Miller et al., 2007; Perrin et al., 2018; Pizarro et al., 2013; van Moorsel et al., 2016; Zhang et al., 2014). As a consequence, insulin sensitivity, mitochondrial respiration, glucose, and lipid-related metabolites likewise oscillate (Aviram et al., 2016; Dyar et al., 2018; Loizides-Mangold et al., 2017; Sato et al., 2018). Additionally, to skeletal muscle metabolism and physiological functions, exercise performance and muscle strength in humans changes over a day and is likely influenced by the individual chrono-type (Atkinson and Reilly, 1996; Facer-Childs and Brandstaetter, 2015). However, not as much is known about exercise performance in mice. Recently published data found a difference in exercise performance between the early vs. late active phase (Ezagouri et al., 2019). Besides its potential role in exercise performance, the clock also has a significant impact on the skeletal muscle response to exercise. For instance, while afternoon exercise is more efficient than morning exercise at improving blood glucose levels in type 2 diabetes men (Savikj et al., 2019), early morning aerobic exercise has more significant effects on blood pressure and sleep quality in humans (de Brito et al., 2015; Fairbrother et al., 2014). Furthermore, scheduled exercise is an effective stimulus to regulate circadian timing in skeletal muscle (Ezagouri et al., 2019; Peek et al., 2017; Saner et al., 2018; Sato et al., 2019; Wolff and Esser, 2012a; Zambon et al., 2003) and can partially reverse metabolic defects in clock-deficient animals (Pastore and Hood, 2013).

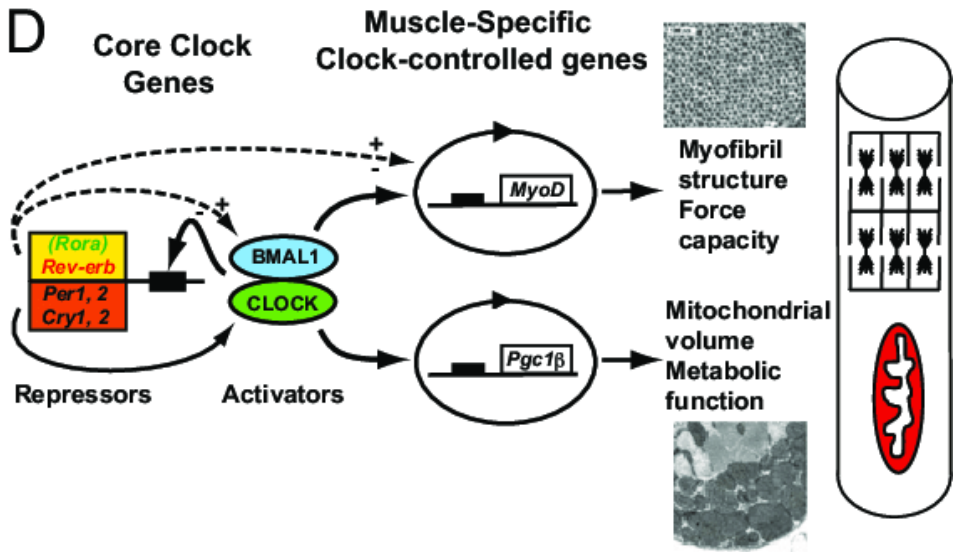

Figure I6. Clock-controlled muscle functions Proposed model of BMAL1:CLOCK regulation of muscle phenotype and function via targeting of MyoD and Pgc-1 expression. Solid lines indicate known molecular links among components of the molecular clock, and dashed lines suggest potential links. (Andrews et al., 2010)

Global circadian clock KO mouse models often show an exercise phenotype, where spontaneous nighttime locomotor activity or forced endurance performance is significantly altered (Delezie et al., 2016; Jordan et al., 2017; Woldt et al., 2013; Zheng et al., 1999). Moreover, clock gene perturbation is associated with disrupted muscle function such as growth and repair, autophagy, lipid homeostasis, insulin sensitivity, mitochondrial metabolism and respiration (Andrews et al., 2010; Dyar et al., 2014; Loizides-Mangold et al., 2017; Woldt et al., 2013). Myoblast determination protein 1 (MYOD), controlling myogenesis, and peroxisome proliferator-activated receptor gamma coactivator 1 (PGC-1), regulating mitochondrial biogenesis, exhibit circadian oscillation in gene expression and might be directly controlled by the BMAL1:CLOCK heterodimer (**Figure I6**). Clock and Bmal1 mutant mice, therefore, show decreased force, changed myofilament structures, and decreased mitochondrial volume (Andrews et al., 2010). Many of the clock components, however, are essential for tissue- and brain development (Dussault et al., 1998; Kobayashi et al., 2015; Noda et al., 2019). Due to tissue-crosstalk and central control of organismal behavior and physiology, the tissue-specific role of the clock genes remains unanswered in the global KO models.

Retinoic acid receptor-related orphan receptor α (RORα; NR1F1) is a transcription factor belonging to the family of steroid/thyroid hormone receptor superfamily, acts as a key regulator of the circadian clock, and competitively binds to the same cis-acting DNA element occupied by REV-ERB (Akashi and Takumi, 2005; Sato et al., 2004). As an orphan nuclear receptor, with a ligand-binding site, it has been suggested as a potential pharmacological target, for which several natural and synthetic activators and inhibitors have been found

(Kojetin and Burris, 2014). RORα deficient mice are protected against the development of diet- and age-induced obesity and show enhanced insulin sensitivity and glucose uptake in skeletal muscle (Lau et al., 2011). However, due to the systemic effects of RORα deletion, including staggering phenotype and a defective cerebellum development (Dussault et al., 1998), conclusions about the skeletal muscle-specific role of RORα cannot be made. Interestingly, RORα has many binding partners. For example, RORα binds peroxisome proliferator-activated receptor gamma coactivator 1 alpha (PGC-1α) through a LXXLL motif to enhance its transcriptional activity on a Bmal1 promoter-reporter (Liu et al., 2007). PGC-1α, on the other hand, competes with the nuclear corepressor (NCoR)1 (Perez-Schindler et al., 2012), which serves as a corepressor for the circadian protein REV-ERBα (Yin and Lazar, 2005). RORα binds and recruits histone deacetylase 3 (HDAC3) to inhibit the transcriptional activity of peroxisome proliferator-activated receptor-gamma (PPARγ) in the liver, and thus prevents high fat diet-induced hepatic steatosis, obesity, and insulin resistance (Kim et al., 2017). RORα plays a vital role in overall health, development, and metabolic homeostasis. Especially the interaction with PGC-1α makes it an attractive candidate to study in skeletal muscle exercise adaptation.

While the exercise-induced responses on a tissue and systemic level are complex, the emerging role of circadian rhythm in organismal physiology is adding another level of complexity. In the last few years, research in the integrative field of exercise physiology and circadian biology has been conducted and revealed the importance of timing on muscle function and metabolism. However, further studies are needed to elucidate how the time of exercise affects exercise outcomes, whether exercise works as a time cue for the skeletal muscle clock, and if the skeletal muscle clock regulates exercise performance, adaptation, and metabolism.

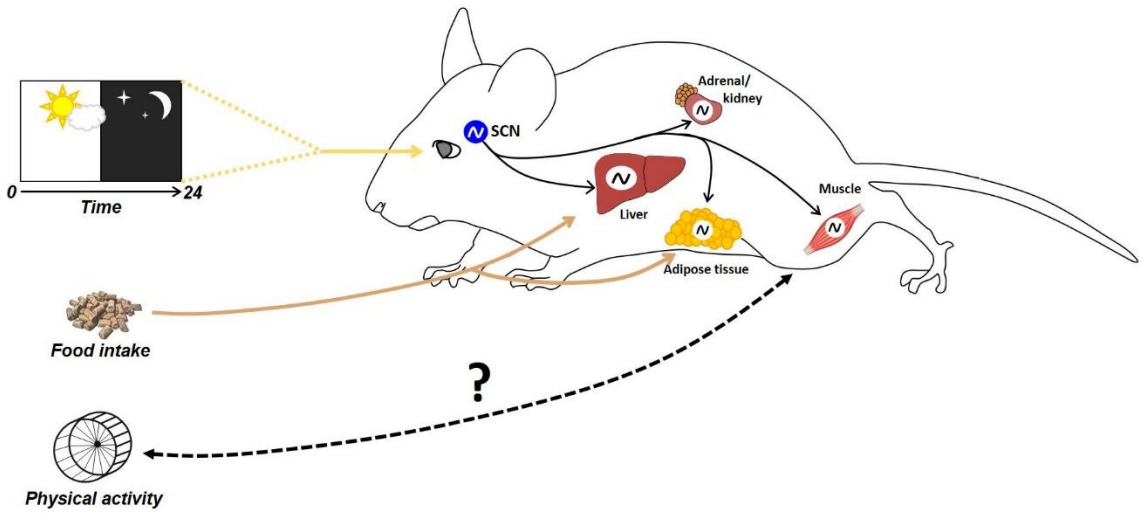

Figure I7. What are the reciprocal interaction of exercise and the skeletal muscle clock?

2. Aim of the Thesis

The circadian clock modulates mammalian physiology and behavior, which is essential for our health. Physical activity is one of the most powerful strategies to prevent and treat chronic diseases. Interestingly, scheduled medications can amplify the beneficial effect of treatments while reducing the harmful side effects. Yet, it is unclear whether chrono-exercise could likewise potentiate the health benefits of physical activity and thus treat various chronic diseases even more effectively. More importantly, despite the substantial variations of muscle metabolism across the 24-h cycle, it is unknown whether muscle cellular processes and the circadian clock respond to exercise in a time-of-day-dependent manner. Finally, despite the strong evidence that, e.g., obesity, cancer, and aging, negatively influence the circadian timing system, with far-reaching consequences on exercise performance, skeletal muscle metabolism, and overall health, the contribution of clock components to skeletal muscle physiology remain poorly explored.

During my Ph.D. work, I have been using different mouse models, and exercise modalities, combined with multi-omics and cell culture approaches, to shed light on the reciprocal interaction between exercise, the circadian clock, and skeletal muscle function. In particular, I focused my work on 4 specific aims:

1. Does skeletal muscle respond to exercise in a time-of-day-dependent manner (study 1)
2. Is scheduled voluntary exercise a strong Zeitgeber for the skeletal muscle clock (study 1)
3. What is the role of the nuclear receptor and circadian gene RORα in skeletal muscle function (study 2)
4. Is RORα required to mediate the adaptations of skeletal muscle to physical exercise (study 2)

Manuscript 1

Timing of exercise defines the transcriptome, proteome and phosphoproteome responses of mouse skeletal muscle

Geraldine Maier[1,*], Julien Delezie[1,*], Pål O. Westermark[2], Gesa Santos[1], Danilo Ritz[1], and Christoph Handschin[1,#]

[1]Biozentrum, University of Basel, CH-4056 Basel, Switzerland

[2]Leibniz-Institut für Nutztierbiologie, Institut für Genetik und Biometrie, D- 18196 Dummerstorf, Germany

[*]Equal first authors

[#]*Correspondence to:* Christoph Handschin, Biozentrum, University of Basel, Klingelbergstrasse 50/70, CH-4056 Basel, Switzerland, phone: +41 61 207 2378, fax: +41 61 207 2208, email: christoph.handschin@unibas.ch

Keywords: exercise; skeletal muscle; transcriptomics; proteomics; metabolism; energy homeostasis; circadian clock; Zeitgeber

In preparation

Abstract

Time-based physical activity interventions may potentiate the health benefits of exercise. However, the underlying signaling events triggered by exercise at different times of the day have not been fully characterized. Here, we analyzed the transcriptomic, proteomic, and phosphoproteomic responses of mouse skeletal muscle to two widely used exercise modalities at distinct phases of the light-dark cycle. We found that time-dependent variations in maximal treadmill exercise capacity were accompanied by subtle changes in energy levels, together with the activation of specific biological pathways. For instance, treadmill exercise in the early daytime elicited mechanisms directing vesicular trafficking. This was supported by the identification of phosphorylation sites on key regulators of glucose uptake. Complementary analysis of the proteome of working muscles implicated putative secreted factors for the timely modulation of hepatic glucose production, potentially enhancing running exercise capacity. Furthermore, using a novel approach, we characterized the exercise-regulated networks robustly activated by voluntary wheel running at the opposite phase of the dark, feeding period. This integrated study provides valuable resources for the discovery of potential exercise regulators and mediators of the skeletal-muscle initiated crosstalk with other tissues, and further highlight the relation between time of day and exercise.

Introduction

Physical activity represents one of the most effective strategies to reduce the prevalence and incidence of chronic illnesses and age-related disorders (Ding et al., 2016; Lobelo et al., 2014; Pedersen and Saltin, 2015). Endurance- and resistance-based training have many positive influences throughout the body, in particular by modulating the musculoskeletal, cardiovascular, respiratory, metabolic, and neuroendocrine systems (Delezie and Handschin, 2018; Hawley et al., 2014). In skeletal muscle, exercise activates multiple signaling pathways, including well-known exercise factors such as AMPK and PGC-1α (Bassel-Duby and Olson, 2006; Egan and Zierath, 2013). Accordingly, a single bout of exercise in mice promotes the transcription of more than 300 genes (Choi et al., 2005; Ezagouri et al., 2019; Perez-Schindler et al., 2017), and is likewise a potent inducer of glucose uptake in skeletal muscle (Richter and Hargreaves, 2013).

Mammalian physiology undergoes changes relative to the time of the day. These changes are driven by the circadian clock—an evolutionary conserved time-keeping mechanism that is present in virtually all cells of the body (Buhr and Takahashi, 2013). Hundreds of skeletal muscle transcripts are oscillating with a 24-h period in humans and mice (McCarthy et al., 2007; Miller et al., 2007; Perrin et al., 2018; van Moorsel et al., 2016; Zhang et al., 2014). Insulin sensitivity, mitochondrial respiration, glucose, and lipid-related metabolites likewise all oscillate in muscle tissues (Dyar et al., 2018; Loizides-Mangold et al., 2017; Sato et al., 2018). Moreover, exercise performance shows clear diurnal variations in humans (Atkinson and Reilly, 1996; Facer-Childs and Brandstaetter, 2015), and fluctuates between the early vs. late part of the dark, active period in the mouse (Ezagouri et al., 2019).

The beneficial effects of physical activity are dependent on several parameters, including the type, duration, frequency, and intensity of a workout (WHO, 2010). The timing of exercise may be another critical determinant for maximizing the positive outcomes of regular training (Gabriel and Zierath, 2019). For instance, afternoon exercise is more efficacious than morning exercise at improving blood glucose levels in type 2 diabetes men (Savikj et al., 2019). Conversely, early morning aerobic exercise has more positive effects on blood pressure and sleep quality in healthy humans (de Brito et al., 2015; Fairbrother et al., 2014; Yamanaka et al., 2015). Moreover, scheduled exercise is a potent stimulus to regulate circadian timing in skeletal muscle (Ezagouri et al., 2019; Peek et al., 2017; Sato et al., 2019; Wolff and Esser, 2012; Zambon et al., 2003), and can partially reverse metabolic defects in clock-deficient animals (Pastore and Hood, 2013). This suggests that time-based physical activity interventions could potentiate the health benefits of exercise and serve as an entrainment cue to restore circadian physiology in human populations experiencing circadian disruptions (e.g., shift-workers and the elderly) (Hood and Amir, 2017; James et al., 2017).

However, the underlying cellular and molecular responses of skeletal muscle to timed exercise remain poorly described.

We evaluated herein maximal treadmill exercise capacity across the 24-h light-dark (LD) cycle and the metabolic outcomes of running around the clock in the untrained wild-type mouse. We furthermore dissected the transcriptome and (phospho-)proteome responses of working muscles at two distinct phases of the light-dark (LD) cycle. Finally, we tested the use of a skeleton photoperiod (SPP) in combination with restricted wheel running access to investigate the consequences of scheduled daytime voluntary training on skeletal muscle gene and protein regulation.

Results

Time-of-day-dependent variations in mouse treadmill exercise performance.

Differences in low- and moderate-intensity treadmill exercise performance were reported within the active phase of wild-type mice (Ezagouri et al., 2019). It is, however, unclear whether mice show broader variations in exercise performance between the light (i.e., resting/inactive) and the dark (i.e., feeding/active) periods. To investigate this, we challenged different groups of untrained C57BL/6J mice to an acute bout of high-intensity exercise every 4 h across the whole 24-h LD cycle and sacrificed them immediately (Ex+0h) or 3 h (Ex+3h) after exhaustion (experimental design and protocol, **Fig. 1A**). We found a significant variation of maximal treadmill running capacity, with a peak and trough of performance at Zeitgeber Time 0 (ZT0; light-onset) and ZT12 (light-offset), respectively (**Fig. 1B, S1A**). Importantly, all mice reached exhaustion (see method for criteria) and displayed a drastic elevation of blood lactate, yet without significant relation to the time of day (**Fig. 1C, S1B**). Conversely, we observed that blood glucose levels significantly dropped at ZT12 and ZT16 upon exercise (**Fig. 1D**; delta glucose basal vs. exercise, **Fig. S1C**). Lastly, higher serum corticosterone levels were observed in all exercised groups regardless of time (**Fig. S1D**).

To further evaluate the metabolic outcomes of strenuous treadmill exercise across the day, we measured circulating energy substrates, muscle, and liver glycogen levels immediately after exercise (Ex+0h). We observed that plasma triglyceride (TG) levels were mainly unchanged at exhaustion (**Fig. 1E**), which is consistent with circulating TG not being the primary source of energy during moderate to high-intensity exercise in untrained animals (Hargreaves and Spriet, 2018). Conversely, plasma free fatty acids (FFA) and glycerol levels—a lipolytic marker—were affected by treadmill exercise in a time-dependent manner (**Fig. 1F-G**). In particular, plasma glycerol levels were significantly upregulated when exercise was performed during the light phase, which might result from higher breakdown of TGs in daytime working muscles. Lastly, muscle glycogen stores were consistently reduced by exercise but not at ZT0—time at which mice show their greatest performance (**Fig. 1H**). In contrast, hepatic glycogen stores—an essential source of glucose during exercise (Richter and Hargreaves, 2013)—were significantly impacted by exercise across the LD cycle but not at ZT4 (**Fig. 1I**).

Altogether, these data demonstrate subtle time-dependent effects of acute exercise on markers of lipid and glucose metabolism and indicate that mice are surprisingly better at performing a maximal running test in the early light, resting phase of the 24-h LD cycle. Furthermore, we show that when basal hepatic glycogen stores are low (i.e., in the early night), mice are unable to sustain a prolonged workout and to maintain homeostatic blood glucose levels.

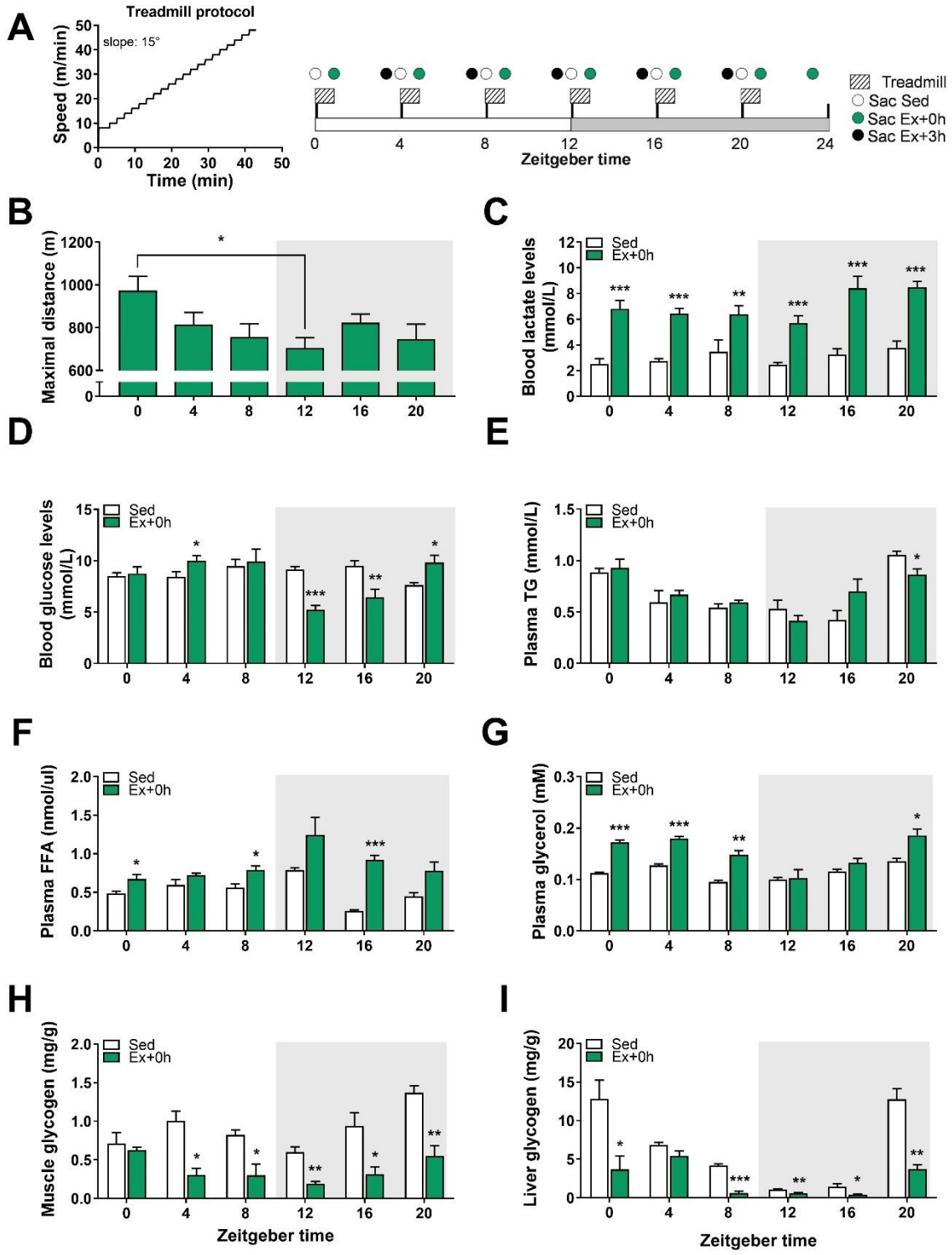

FIGURE 1. Time-of-day-dependent variations in mouse treadmill exercise performance. (A) Treadmill protocol and experimental outline scheme: mice were divided into two groups, sedentary (SED) and treadmill exercised mice. The exercise mice were then further divided into two groups (sacrificed immediately (+0h) or three hours after exercise (+3h)). This setup was repeated every four hours for 24-h (for a more detailed description of the experimental setup, please refer to materials and methods). (B) Maximal distance reached at exhaustion. (C) Blood lactate and (D) glucose levels at rest and within 1 min after exhaustion. Plasma (E) triglyceride (TG), (F) free fatty acid (FAA), and (G) glycerol levels in SED and after exhaustion. (H) Muscle and (I) liver glycogen levels in SED and after exhaustion. Data is shown as the average ± SEM (n=3 per group and time point). * $P < 0.05$; ** $P < 0.01$; *** $P < 0.001$. One-way ANOVA (B) and Unpaired Student's *t*-test (C-I).

Exercise around the clock induces broad and time-dependent gene responses in skeletal muscle.

We then evaluated the expression of genes that are part of the immediate, early response of skeletal muscle to exercise across the day. Importantly, to take into account changes in basal gene expression over time, gene expression data obtained from Ex+0h and Ex+3h mouse groups running, e.g., at ZT0, were compared to sedentary controls sacrificed at ZT0 and ZT4, respectively (see method for details about the statistical analysis and **Fig. S1E**; for each transcript, data normalized at each time point are provided as bar graphs, while data normalized to SED ZT0 are provided as daily curves).

We found that *Nr4a3*—an exercise-responsive gene and member of the nuclear receptor subfamily group A (Mahoney et al., 2005)—was immediately induced after exercise and remained elevated 3 h post-exercise (**Fig. 2A**). Likewise, activating transcription factor 3 (*Atf3*)—involved in the molecular adaptation to endurance exercise (Fernandez-Verdejo et al., 2017)—was significantly upregulated by physical exercise (**Fig. S2A**). Incidentally, the induction of both *Nr4a3* and *Atf3* expression was slightly influenced by the time of day at which treadmill exercise was performed, with higher expression levels at the day-night transition when running capacity was low (**Fig. 2A** and **S2A**). Conversely, the expression of the peroxisome proliferator-activated receptor gamma coactivator-1 alpha 1 (*Pgc-1α1*)—a key isoform involved in oxidative muscle remodeling (Lin et al., 2002)— was mainly induced directly after exercise, while the expression of *Pgc-1a4*—an isoform modulated by resistance exercise (Ruas et al., 2012)—was exclusively upregulated 3 h post-exercise (**Fig. S2A**). Moreover, the vascular endothelial growth factor a (*Vegfa*)—an essential regulator of muscle regeneration, exercise adaptation, and angiogenesis (Delavar et al., 2014)—was only induced when exercise was performed during daytime (**Fig. 2A**). Finally, interleukin-6 (*Il-6*)—a myokine implicated in muscle glycolysis and adipose fat lipolysis (Pedersen and Febbraio, 2008)—was increased immediately post-exercise especially in the late part of the day and at night (i.e., from ZT8-20) (**Fig. 2A**).

We have likewise measured genes involved in the metabolic response of skeletal muscle to exercise. Transcripts such as the peroxisome proliferator-activated receptor δ (*Pparδ)*—an essential regulator of lipid metabolism in contracting muscles (Fan et al., 2017)—was significantly upregulated 3 h after exercise only when the latter was performed during the late day period (ZT8-20; **Fig. 2B**). Similarly, carnitine palmitoyltransferase-1α (*Cpt1α*)—involved in fatty acid oxidation (Bruce et al., 2009)—and pyruvate dehydrogenase kinase 4 (*Pdk4*)—a negative regulator of glucose utilization (Wende et al., 2005)—were mostly induced during the nighttime period (**Fig. 2B**). Conversely, hexokinase 2 (*Hk2*)—encoding for the rate-limiting first step of glycolysis—was broadly induced by acute treadmill exercise (**Fig. 2B**).

Finally, we assessed the expression of core clock genes known to be modulated by O_2 levels, glucocorticoids, calcium signaling and/or previously shown to be induced by acute exercise (Adamovich et al., 2017; Cheon et al., 2013; Dyar et al., 2015; Kinouchi et al., 2018; Zambon et al., 2003). We observed specific, time-dependent changes in, e.g., the expression of brain and muscle arnt-like (*Bmal1),* cryptochrome *(Cry)2,* period *(Per)1,* and *Per2,* circadian associated repressor of transcription *(Ciart)* and D-box binding PAR bZIP transcription factor *(Dbp)* (**Fig. 2C**). In addition, both *Per1* and *Per2,* but not *Per3*, were immediately induced post-exercise at nearly all ZT. Moreover, expression levels of *Cry2*—a known modulator of PPARδ transcriptional activity in muscle (Jordan et al., 2017)—was exclusively upregulated during the late part of the day and 3 h post-exercise alongside *Pparδ* (**Fig. 2B-C**). Lastly, expression of *Dbp* was negatively regulated 3 h post-exercise when performed during the light period (**Fig. 2C**).

Overall, our qPCR data highlight broad (e.g., *Nr4a3, Pgc-1α4, Hk2*) and temporally distinct gene responses (e.g., *Pparδ, Cry2*) in skeletal muscle following treadmill exercise. Moreover, we found that the circadian transcriptional (co-)regulators *Ciart* and *Per1, 2* are part of the immediate, early response to exercise. Importantly, the apparent time-dependent induction of key regulators of lipid oxidation, namely *Cpt1α* and *Pdk4*, could be associated with more significant metabolic stress induced by treadmill exercise at night.

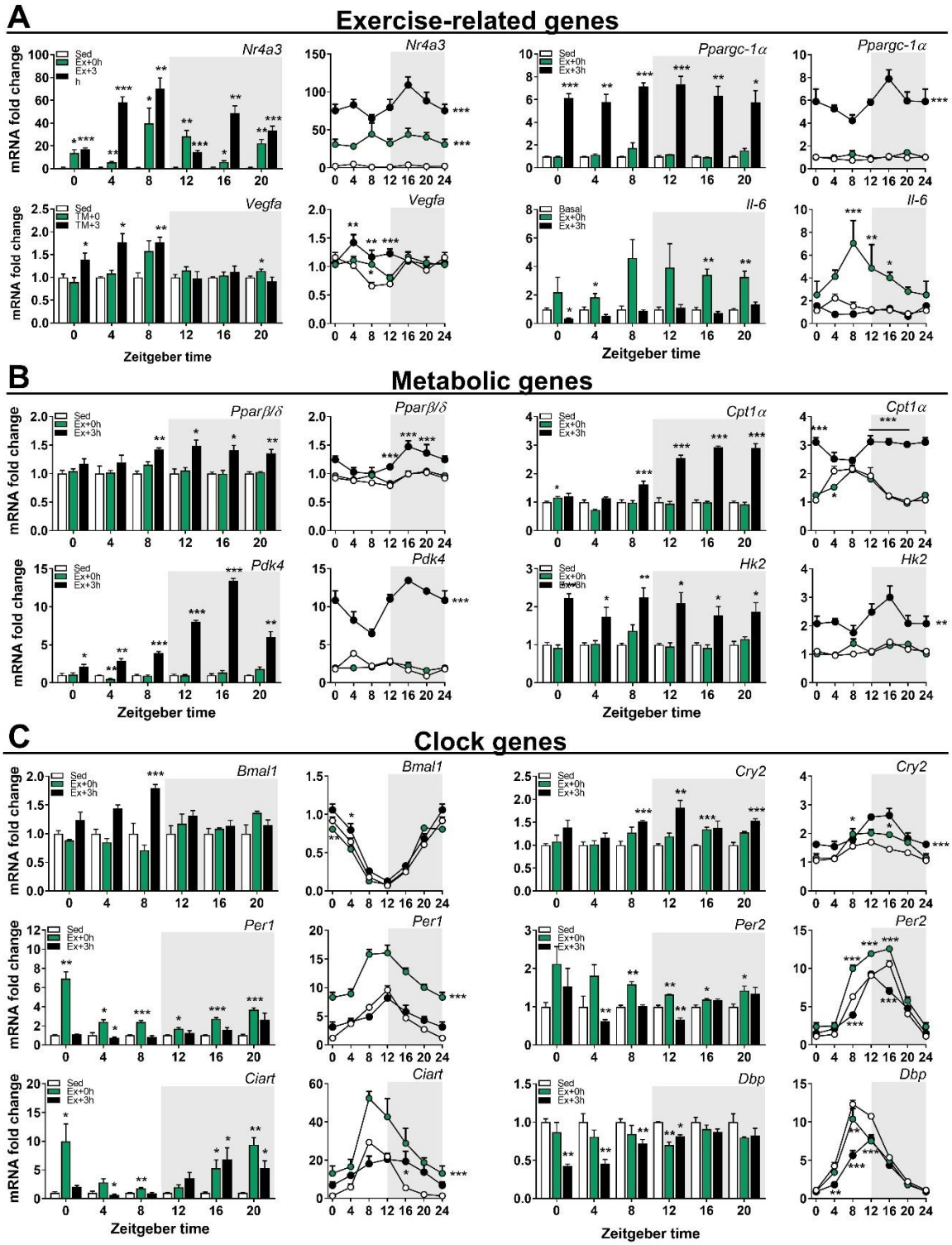

FIGURE 2. Scheduled treadmill induces broad and time-dependent transcriptional responses in skeletal muscle. Gene expression in sedentary (SED), directly (+0h), and 3 h (+3h) after exhaustion. (A) Exercise-related genes, (B) Metabolic genes, (C) Clock genes. Expression values were determined by qPCR and normalized to *Hprt*. Bargraph data is shown as the average fold-change ± SEM (n = 3) relative to the expression in SED set to 1. Curve data is shown as the average fold-change ± SEM (n = 3) relative to the expression in SED ZT0 set to 1 * $P < 0.05$; ** $P < 0.01$; *** $P < 0.001$. Unpaired Student's *t*-test (Bargraphs) and One-way ANOVA (Curves).

Daytime vs. nighttime treadmill exercise elicits distinct gene signatures in skeletal muscle.

In light of our qPCR results, we further explored the transcriptional signatures of working muscles at distinct phases of the LD cycle. We performed RNA-sequencing gene expression profiling of muscles harvested at times when treadmill exercise performance differed the most, namely ZT0 (i.e., light onset) and ZT12 (i.e., light offset). Incidentally, we focused on the effects of exercise at different ZT and did not explore the effects of time on gene expression in sedentary mice, which is characterized elsewhere with a better time resolution (McCarthy et al., 2007; Miller et al., 2007; Sato et al., 2019). As mentioned above, data collected from Ex+0h and Ex+3h mouse groups (whether mice exercised at ZT0 or ZT12) were always normalized to data obtained from sedentary animals sacrificed at a similar phase of the light-dark cycle (see method).

There was a higher number of differentially expressed genes (DEGs) immediately after early daytime exercise (ZT0 Ex+0h = 1440 genes vs. ZT12 Ex+0h = 906 genes) (**Fig. 3A**). In contrast, the transcriptional response of early nighttime exercised muscles was greater 3 h after exercise (ZT12 Ex+3h = 2899 genes vs. ZT0 Ex+3h = 2337 genes) (**Fig. 3B**). Moreover, about 25% of the DEGs were shared between ZT0 and ZT12, regardless of the time of sacrifice (i.e., Ex+0h vs. Ex+3h). In line with qPCR data, *Per1* and *Ciart* transcripts were significantly induced immediately after exercise when performed at ZT0, but not at ZT12 (**Fig. 3C**). Surprisingly, however, only a handful of transcripts were found to be differentially expressed whether exercise was performed at ZT0 vs. ZT12 (**Fig. S3B**). Among these genes, *Arrdc2*—a nutrient-responsive gene (Gordon et al., 2019)—show an induction only when exercise was performed in early daytime (**Fig. S3B**). In contrast, we identified several novel transcripts induced by exercise, regardless of the time of the day. For instance, the MAF transcription factors *Maff* and *Mafk*, implicated in cellular stress response and detoxification (Katsuoka et al., 2005); the metallothionein1/2 (*Mt1/2*), involved in oxidative stress protection and regulation of hypertrophy via the Akt pathway (Di Foggia et al., 2014; Summermatter et al., 2017); and, the A-kinase anchoring protein 12 (*Akap12*), a transcript likely involved in muscle differentiation and maintenance, all show a significant induction at both ZT (**Fig. 3C, 3D**).

To gain more insights into the DEG lists obtained immediately after exercise (Ex+0h), we performed pathway enrichment analysis using g:Profiler (Reimand et al., 2016). Test for overrepresentation of gene ontology (GO) terms returned broad (e.g., Response to apoptosis, Angiogenesis, Muscle development) and distinct terms in response to early morning (e.g., Response to hypoxia, Carbohydrate metabolic process, Circadian regulation) vs. early nighttime exercise (e.g., Proteolysis, Inflammatory response and Cytokine production, Response to glucocorticoid). Extracted KEGG pathways further highlighted time-specific responses triggered by exercise at the transcriptional level. Early daytime treadmill was a strong activator of “Protein processing in the endoplasmic reticulum (ER)” and of the

“Lysosome” and “Phagosome” pathways (**Fig. 3E** yellow). Conversely, there was a robust inflammatory response to nighttime exercise, as evidenced by the activation of “TNF signaling” and “IL-17 signaling” pathways (**Fig. 3E** blue). Moreover, early nighttime exercise promoted the activation of the “MAPK and Hippo signaling pathways”, involved in muscle maintenance and exercise adaptation (**Fig. 3E** blue) (Kramer and Goodyear, 2007; Watt et al., 2018). Lastly, nighttime exercise was a potent activator of the “FoxO signaling” pathway, known to trigger a switch in energy metabolism from glucose oxidation to lipid oxidation by increasing the expression of genes such as *Pdk4* (Gross et al., 2008).

We likewise analyzed the late gene response (Ex+3h) after an acute bout of exercise. While common transcripts were enriched for “Mitophagy”, unique processes were activated 3 h after an exercise challenge. For instance, daytime exercise promoted the expression of several transcripts associated with “Ribosome” and “Protein processing in endoplasmic reticulum” (**Fig. 3F** yellow), suggesting that treadmill exercise in the early light phase is a strong regulator of protein synthesis and conformation. Conversely, nighttime exercise was a potent activator of the “AMPK signaling” pathway (**Fig. 3F** blue)—particularly involved in the switch from anaerobic to aerobic metabolism in contracting muscles (Hardie, 2004). Furthermore, consistent with the activation of FoxO transcription factors immediately post-exercise (Ex+0h) and their role in fine-tuning cellular homeostasis and adaptation to exercise (Sanchez et al., 2014; Zhao et al., 2007), we found a subsequent overrepresentation of the “Autophagic/Lysosomal” and “Proteasomal” pathways in the late response to nighttime treadmill (**Fig. 3F** blue).

Taken together, both early daytime and nighttime exercise activate mitophagy and anti-apoptotic pathways. Daytime exercise furthermore positively regulated transcriptional processes associated with protein synthesis and stability. In contrast, nighttime exercise triggered responses associated with inflammation, energy stress (i.e., FoxO, AMPK), and the transcriptional activation of the ubiquitin-proteasome/autophagy-lysosome systems. This could particularly relate to an increase in muscle amino acid breakdown triggered by exercise at night, in a low energy state, as previously suggested (Sato et al., 2019).

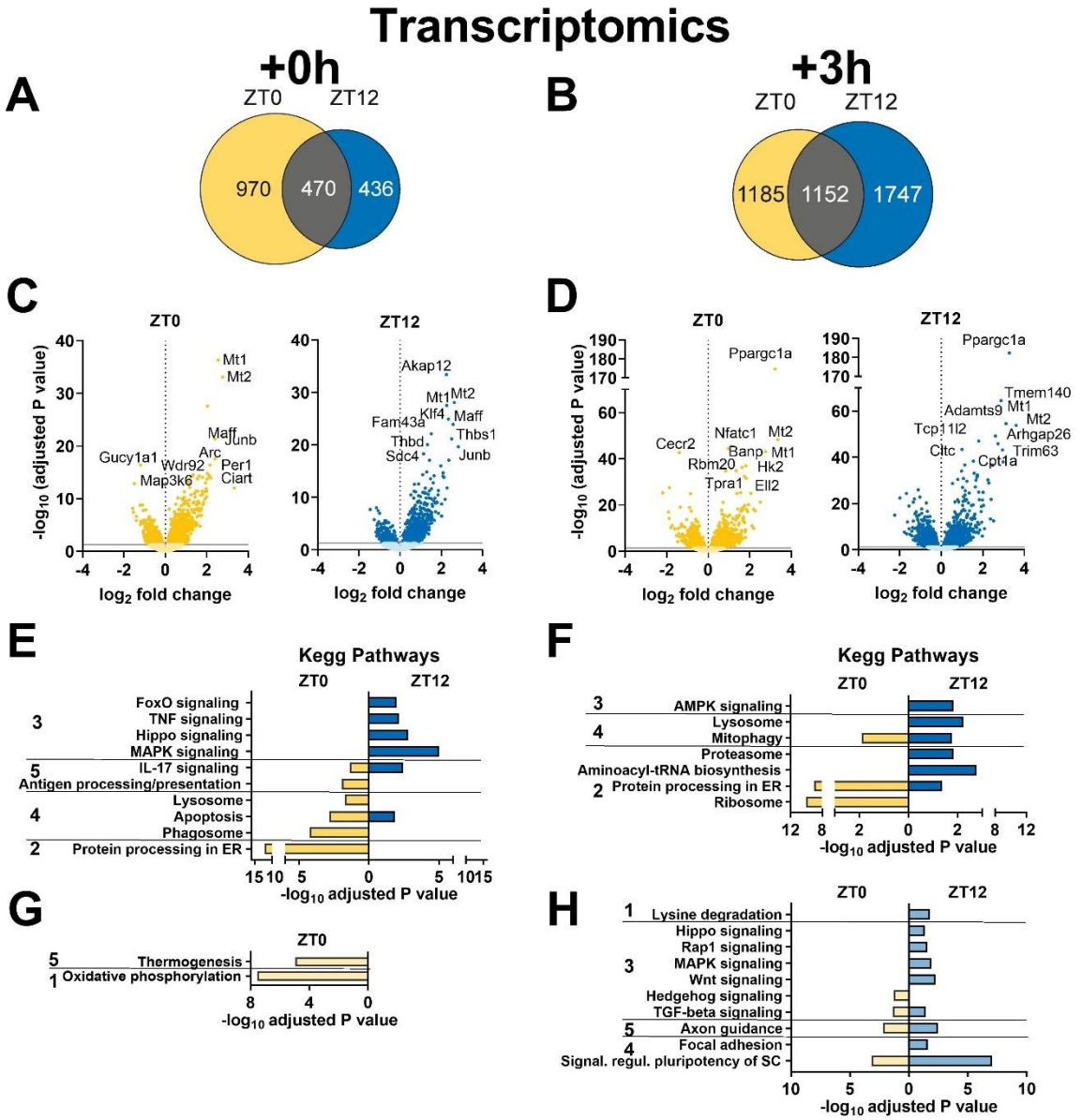

FIGURE 3. Distinct muscle gene expression signatures after early light vs. early dark phase treadmill exercise. Analysis of transcriptomic data directly (Ex+0h) and 3 h (Ex+3h) after exhaustion. (A, B) Venn diagram displaying the number of differentially expressed genes directly (A) and 3 h (B) after early light (ZT0; yellow) and early dark (ZT12; blue) phase exercise as well as the overlapping genes of both conditions (gray). (C, D) Volcano plot displaying the differentially expressed genes directly (C) and 3 h (D) after exercise in the early light (ZT0; yellow) or early dark (ZT12; blue) phase. (E, F) KEGG pathway enrichment analysis for exercise-induced genes directly (E) and 3 h (F) after early light (ZT0; yellow) or early dark (ZT12; blue) phase exercise. (G, H) KEGG pathway enrichment analysis for exercise-decreased genes directly (G) and 3 h (H) after the early light (ZT0; yellow) or early dark (ZT12; blue) phase exercise. KEGG pathway categories: 1. Metabolism; 2. Genetic Information Processing; 3. Environmental Information Processing; 4. Cellular Processes; 5. Organismal Systems.

Proteome and secretome changes associated with daytime vs. nighttime treadmill exercise.

To investigate whether significant modifications at the protein level accompanied the exercise-induced transcriptional changes, we used a state-of-the-art mass spectrometric (MS)-based proteomics workflow (see method). We performed triplicates analyses of muscles from ZT0 and ZT12 exercised mouse groups and analyzed the results together in MaxQuant, specifying a false discovery rate of 5% at the peptide and protein level. We identified a total of about 5300 proteins, in line with previous deep proteome coverage of mouse skeletal muscle tissue (Deshmukh et al., 2015).

Early light and dark phase exercise rapidly altered the expression level of 655 proteins and 811 proteins, respectively (**Fig. 4A**), with a small overlap of 113 proteins returning, however, no KEGG terms (**Fig. 4E, 4G**). The protein distribution 3 h after an exercise bout was also relatively similar between ZT (**Fig. 4B**). Consistent with the transcriptional responses observed at night, we found enrichment for “Ribosome” and “RNA transport” cellular pathways in the immediate response (Ex+0h) (**Fig. 4E** blue), and for “Nitrogen metabolism” in the late response (Ex+3h) to treadmill running (**Fig. 4F** blue)—further illustrating a change in the protein anabolism/catabolism balance triggered by exercise at night. In contrast, early daytime treadmill robustly initiated the “Complement system” (**Fig. 4E** yellow). Complement activation triggers tissue regeneration in response to muscle injury and inflammation (Zhang et al., 2017). Accordingly, the complement C3a, C4b, C8a, C8b, C9, CFD, and CFB proteins, were all upregulated. The “SNARE interactions in vesicular transport” pathway was similarly overrepresented after early daytime exercise (**Fig. 4E** yellow). SNARE elements (Soluble NSF attachment protein receptors) form a class of membrane-associated proteins, which, besides their involvement in neurotransmitter release (Dunant and Israel, 2000; Kasai et al., 2012), particularly regulate GLUT4-containing vesicle trafficking (Cheatham, 2000). In line, we detected a significant elevation in the abundance of the vesicle-associated membrane protein 3 and 8 (VAMP3, 8), syntaxin 6 and 8 (STX6, 8), synaptobrevin homolog YKT6 (YKT6), and of the synaptosomal-associated protein 23 (SNAP23), which are all key mediators of GLUT4 translocation to the cell surface (Bryant and Gould, 2011; Morris et al., 2020; Zong et al., 2011). Moreover, the rho family GTPase RAC1—an essential regulator of glucose transport in contracting muscles (Sylow et al., 2017)—, its upstream regulator protein tyrosine phosphatase α (PTPα; PTPRA) (Sun et al., 2012), together with the GTPase ras-related protein (RALA)—a known mediator of insulin-dependent glucose uptake (Takenaka et al., 2015)—were all consistently elevated. Finally, we observed increased expression of the Rho GTPases RHOA, B, and C, in favor of enhanced GLUT4's intracellular trafficking (Duong and Chun, 2019).

Skeletal muscle tissue is an endocrine organ, releasing small molecules so-called myokines in response to exercise (Delezie and Handschin, 2018). Incidentally, despite some changes at the transcriptional level, we could not detect previously characterized myokines

(e.g., VEGF, IL6) with the exception of the exercise-related cathepsin B (CTSB) protein (Moon et al., 2016), yet without alteration in expression upon exercise. We then used predictive analytics tools to identify other, putatively secreted proteins that could influence muscle performance and metabolism at distinct phases of the LD cycle. Of the top 100 proteins exclusively induced in the immediate response to daytime exercise (Ex+0h), we retrieved 25 candidates predicted as secreted proteins using SignalP 5.0 and 12 additional using SecretomeP 2.0—these tools predict the presence of classical and non-classical signal peptide cleavage sites in amino acid sequences (Bendtsen et al., 2004; Nielsen, 2017) For instance, the major urinary proteins (MUP) 3, 17, and 18 were all upregulated at ZT0 and could potentially be associated with the regulation of systemic blood glucose, liver, and skeletal muscle metabolism (Zhou et al., 2009). We moreover identified fibrillin-1 (FBN1), also called Asprosin—a glucogenic protein hormone that is secreted by adipose cells and recruited at the surface of hepatocytes to increase plasma glucose level (Romere et al., 2016). Expression of the inter-α-trypsin inhibitor heavy chain 5 (ITIH5)—a tumor suppressor and prognostic biomarker in cancer (Sasaki et al., 2017; Veeck et al., 2008)—was similarly induced when exercise was performed at ZT0. Nighttime exercise conversely upregulated 7 proteins, potentially secreted through a standard signal peptide in response to nighttime exercise. This included the SPARC-like protein 1 (SPARCL1)—a member of the SPARC family of proteins that modulate cell interaction with the extracellular milieu (Bradshaw, 2012)—which has a potent tumor-suppressor function (Esposito et al., 2007; Li et al., 2017) and is a marker of cancer disease progression (Turtoi et al., 2012).

Overall, these proteomic results highlight the robust activation of time-dependent cellular responses; enhancing glucose metabolism in the early daytime and, conversely, restoring protein homeostasis when exercise is performed in the early night. Moreover, we identified novel putative myokines that could not only regulate systemic glucose availability but also mediate the health benefits of exercise.

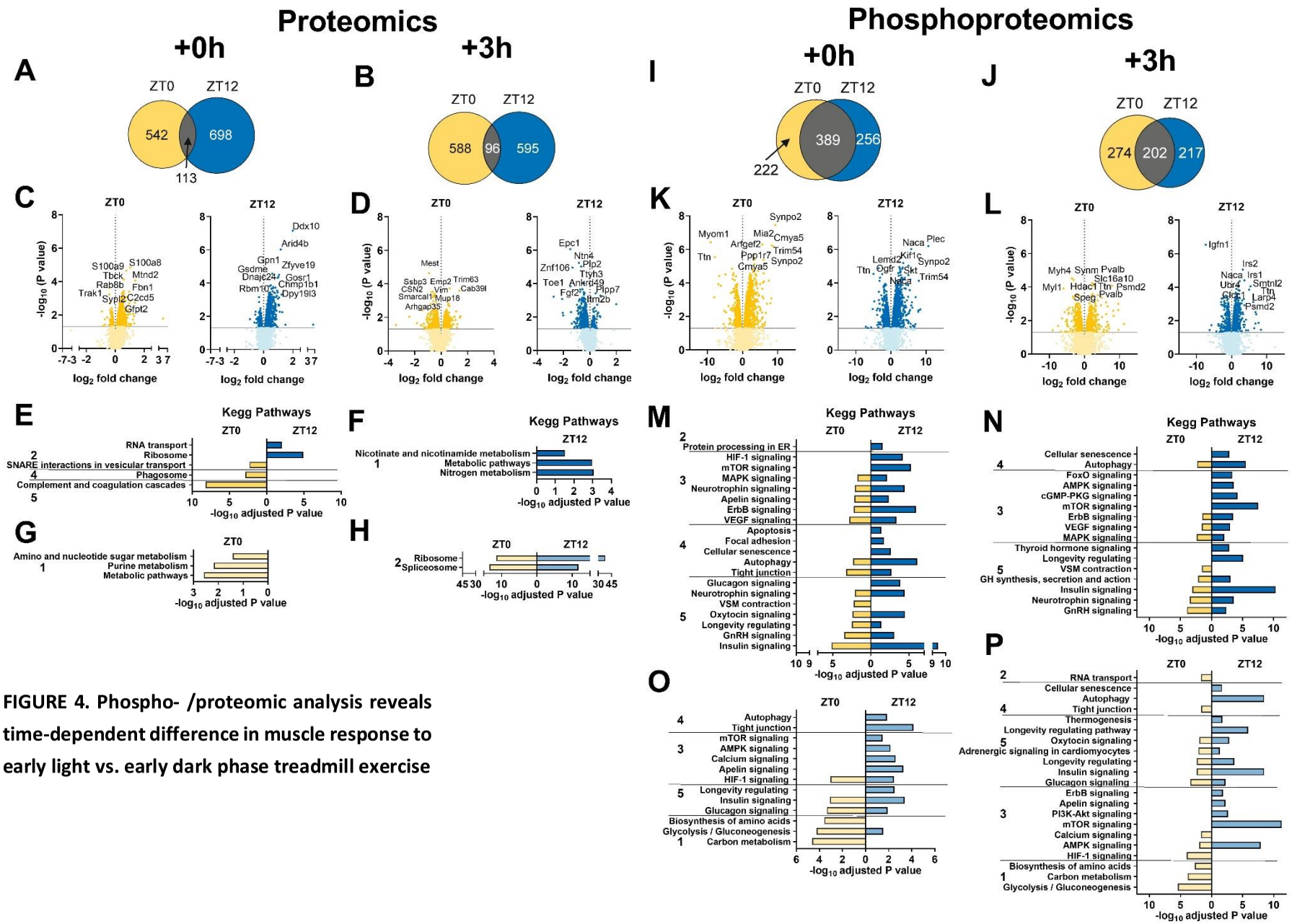

FIGURE 4. Phospho- /proteomic analysis reveals time-dependent difference in muscle response to early light vs. early dark phase treadmill exercise

FIGURE 4. Phospho- /proteomic analysis reveals time-dependent difference in muscle response to early light vs. early dark phase treadmill exercise Analysis of proteomics and phosphoproteomics data directly (Ex+0h) and 3 h (Ex+3h) after exhaustion. (A, B) Venn diagram displaying the number of differentially regulated proteins directly (A) and 3 h (B) after early light (ZT0; yellow) and early dark (ZT12; blue) phase exercise as well as the overlapping proteins of both conditions (gray). (C, D) Volcano plot displaying the differentially regulated proteins directly (C) and 3 h (D) after exercise in the early light (ZT0; yellow) or early dark (ZT12; blue) phase. (E, F) KEGG pathway enrichment analysis for proteins induced directly (E) and 3 h (F) after early light (ZT0; yellow) or early dark (ZT12; blue) phase exercise. (G, H) KEGG pathway enrichment analysis for proteins decreased directly (G) and 3 h (H) after early light (ZT0; yellow) or early dark (ZT12; blue) phase exercise. (I, J) Venn diagram displaying the number of differentially phosphorylated proteins directly (I) and 3 h (J) after early light (ZT0; yellow) and early dark (ZT12; blue) phase exercise as well as the overlapping proteins of both conditions (gray). (K, L) Volcano plot displaying the differentially phosphorylated proteins directly (K) and 3 h (L) after exercise in the early light (ZT0; yellow) or early dark (ZT12; blue) phase. (M, N) KEGG pathway enrichment analysis for protein phosphorylation induced directly (M) and 3 h (N) after early light (ZT0; yellow) or early dark (ZT12; blue) phase exercise. (O, P) KEGG pathway enrichment analysis for protein dephosphorylation directly (O) and 3 h (P) after early light (ZT0; yellow) or early dark (ZT12; blue) phase exercise group. KEGG pathway categories: 1. Metabolism; 2. Genetic Information Processing; 3. Environmental Information Processing; 4. Cellular Processes; 5. Organismal Systems.

The phosphorylome of daytime vs. nighttime working muscles.

Many proteins are regulated by phosphorylation independently of their expression (Huttlin et al., 2010). Protein phosphorylation is a fast and dynamic process in response to exercise, altering the activity of several kinases, including AMPK, MAPK, and mTOR (Deshmukh et al., 2008; Hoffman et al., 2015). Our phosphoproteomic analysis identified up to 7000 sequence ions carrying post-translational modifications in response to exercise mapping to about 1600 unique proteins. As a rapid response to exercise, 611 and 645 proteins were differentially phosphorylated in the early light vs. dark phase, respectively, with an overlap of 389 phosphorylated proteins (Ex+0h; **Fig. 4I**). In contrast, 476 vs. 419 proteins were differentially regulated in the late response to daytime vs. nighttime exercise, with an overlap of 202 proteins (Ex+3h; **Fig. 4J**). Of note, some pathways were found to be both under- and over-represented, which is mainly due to the concurrent phosphorylation/dephosphorylation of the same proteins at multiple sites (**Fig. 4M-P**).

Focusing on protein clusters showing a higher phosphorylation status in the immediate response to exercise (Ex+0h), KEGG analysis returned, e.g., “Insulin”, “Autophagy”, “VEGF”, “MAPK” and “Neurotrophin” signaling pathways, regardless of the time of exercise (**Fig. 4M**). Moreover, a common overrepresented protein subset corresponded to “Oxytocin signaling”, which has been shown to promote muscle regeneration through the activation of the MAPK/ERK signaling pathway (Elabd et al., 2014). We also detected posttranslational modifications of hormone receptors that play a key role in energy metabolism in skeletal muscle (Cohen, 2002). Accordingly, exercise-induced phosphorylation of the β-adrenergic receptor kinase 1 (GRK2) on Ser670 residue was promoted both at ZT0 and at ZT12. In contrast, even though plasma corticosterone levels were similarly elevated by exercise at ZT0 and ZT12 (**Fig. S1D**), only nighttime treadmill promoted the phosphorylation of the glucocorticoid receptor (Nr3c1; GR) on T152 and S275 residues. These sites, however, have not been extensively studied.

Nighttime treadmill running promoted the specific activation of the “HIF-1”, “mTOR”, “AMPK” and “FoxO” pathways (**Fig. 4N** blue)—some of these pathways were similarly overrepresented in our transcriptomic analyses. Incidentally, the α2-subunit of AMPK—the predominant form in the muscle (Garcia and Shaw, 2017)—was consistently dephosphorylated on Ser377 by exercise regardless of ZT; this residue, however, has no reported function (PhosphoSite®). Yet exercise at night induced further changes in the phosphorylation status of both α1/α2 AMPK subunits. Nighttime exercise rapidly phosphorylated α2/α2 at Ser496/491, and we found an increased phosphorylation of the critical regulator of autophagy ULK1 on Ser637, which is dependent on AMPK (Mack et al., 2012). The mTOR protein was similarly phosphorylated on Ser1162/1261 upon exercise at both ZT, yet both TSC1 and TSC2 proteins—important integrators of different signaling

pathways to control mTOR signaling—were predominantly regulated by nighttime exercise. Emblematic of the activation of the "mTOR pathway", there were robust posttranslational changes of, e.g., lipin1 (LPIN1), eukaryotic translation initiation factor 4 (EIF4) B, EIF4E binding protein, and ribosomal protein S6 (RPS6). Similarly, key components of the "HIF-1 signaling" pathway, e.g., enolase 1 (ENO1), phosphofructokinase (PFK) L-M, and aldolase A (ALDOA), displayed unique and/or distinct phosphorylation profiles at night. In line with the decrease in muscle glycogen content upon exercise at ZT12, the muscle-specific isoform of the glycogen phosphorylase (PYGM)—a key enzyme in the first step of glycogenolysis—was specifically phosphorylated on Ser2 and on Ser15—the latter residue is particularly known to enhance phosphorylase activity and the degradation of glycogen (Johnson, 1992). In contrast, these two sites were not phosphorylated in response to early daytime exercise, consistent with muscle glycogen sparing (**Fig. 1H**). Moreover, daytime exercise exclusively enhanced phosphorylation on Ser3/616 residues of TBC1 domain family member 4 (TBC1D4 or AS160)—a strong candidate for controlling GLUT4 trafficking in skeletal muscle (Cartee, 2015b; Sakamoto and Holman, 2008). Finally, besides the increased abundance of Asprosin in daytime contracting muscles, we observed active posttranslational modifications on Ser2566 and Ser2711, which could warrant secretory processing to boost hepatic glucose production.

Broad changes in the phosphorylation of Titin and several myosin heavy chain (i.e., MYH 3, 4, and 9)—proteins associated with modulation of muscle contractile properties (Eckels et al., 2018; Vandenboom, 2016)—were similarly observed, independent of the time of the day (**Fig. 4K, 4L**). Equally, key regulators of muscular excitation and contraction, such as sarcoplasmic reticulum calcium-ATPase 1 and 2 (SERCA1 and 2) show several phosphorylation modifications at multiple sites. However, the "Vascular smooth muscle (VSM) contraction" KEGG pathway was exclusively enriched upon daytime exercise, especially in freshly contracting muscles (Ex+0h) (**Fig. 4M** yellow). Intriguingly, phosphorylation of the calcium voltage-gated channel subunit alpha1 S (CACNA1S) protein—a regulator of contractile force in response to stress, fear, and exercise; the so-called "fight-or-flight" response (Catterall, 2015; Emrick et al., 2010)—was specific to residue Ser5 and Ser1617/1640 and T700. These sites are not yet characterized but could indicate an up-regulation of calcium channel activity, leading to increased force production. In support of this, expression of the calcium release-activated calcium channel protein 1 (ORAI1)—a crucial calcium regulator limiting muscle fatigue (Wei-Lapierre et al., 2013)—was exclusively upregulated in daytime exercised muscles.

Taken together, these data reveal that a vast number of signaling pathways (i.e., insulin, oxytocin, VEGF, and neurotrophin) were similarly regulated by an acute bout of treadmill exercise at the posttranslational level. However, in line with low energy availability and a likely increase in proteolytic activities, the HIF-1, AMPK, FoxO, and mTOR pathways, were all robustly activated by exercise at night. Conversely, in the postprandial energy state,

skeletal muscle responded to daytime treadmill by activating cellular mechanisms to modulate muscle contractile properties.

Scheduled daytime wheel-running activity in mice exposed to a skeleton photoperiod.

Contrary to treadmill exercise (present results and (Ezagouri et al., 2019; Sato et al., 2019)), the effects of wheel running exercise at distinct phases of the LD cycle remain unexplored. Both laboratory and wild mice run spontaneously when they have free access to a running wheel and exhibit much greater running distance than in a treadmill (Ghosh et al., 2010; Meijer and Robbers, 2014). Yet due to the masking (i.e., suppressive) effect of light on nocturnal rodents' behavior, voluntary use of the wheel exclusively spread throughout the dark period—with a peak in the early hours of the night—and is scattered with multiple eating events (Yasumoto et al., 2015). We thus tested the use of a skeleton photoperiod (SPP) in combination with time-restricted wheel and food access to evaluate whether mice would spontaneously run in a wheel during their resting phase (see method and **Fig. 5A**).

Under SPP conditions, DA mice surprisingly used the wheel from the 1st day of daytime-restricted access and maintained a relatively stable onset and level of activity during the following days (**Fig. 5B** and **S4B**). Notably, DA mice exclusively ran within the first 3 h of daytime wheel access (**Fig. 5C**). Even though total wheel-running activity only represented 50% of the control group (**Fig. 5D**), the intensity of running was comparable between the two groups during the first two hours of wheel access (**Fig. 5C**). Of note, daytime-restricted wheel access promoted food intake in the first few hours of the nighttime period but significantly decreased the overall amount of food consumed (**Fig. 5E** and **S4A**)—in line with a lower activity level. As expected, there was an elevation of daytime core body temperature paralleling the increase in wheel-running activity of DA mice (**Fig. 5F, 5G**). Yet the temporal organization of nighttime core body temperature values in DA mice closely resembled those of CTRL mice, as likely caused by feeding activities (**Fig. 5E**). To evaluate whether the experimenter's interventions (i.e., daily delivery/removal of food, manual locking /unlocking of the wheel) caused severe physiological stress, we have measured serum corticosterone levels but did not observe significant changes between DA and CTRL animals (**Fig. 5H**). This also demonstrates that chronic daytime wheel running does not affect the daily rhythm of plasma corticosterone.

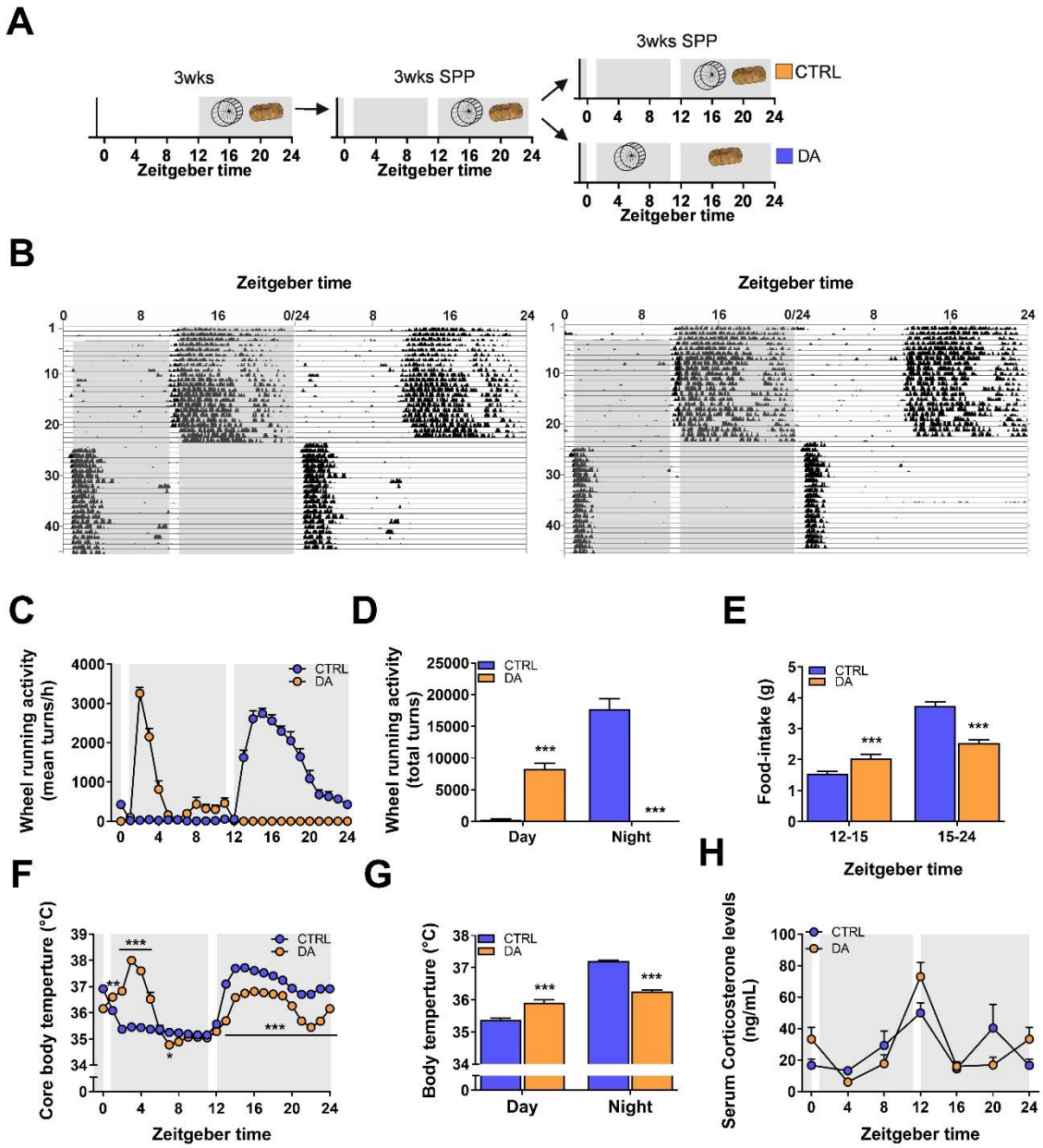

FIGURE 5. Mice run spontaneously during the inactive phase when a wheel is provided (A) Experimental outline scheme: Mice were given running wheel access ad libitum for 3weeks under 12:12 L:D before exposing the all mice to a skeleton photoperiod (SPP). The SPP consists of a 1h light pulse from ZT0 to ZT1 and from ZT11 to ZT12, followed by 10h and 12h without light, respectively. After 3 unrestricted weeks under SPP conditions, one group of mice was restricted to wheel access during day and food access during night. (B) Representative double-plotted actograms of DA mice, the gray background indicates light off (C) Quantified wheel-running activity, averaged over the last 10days in mean turns/h, and (D) per day and night. (D) Food-intake within the first 3 h of the active phase, and second 9 h. (E) Core body temperature averaged over the last 10days, and (F) per day and night. (G) Serum corticosterone levels. Data is shown as the average ± SEM (n = 24). * $P < 0.05$; *** $P < 0.001$. Unpaired Student's *t*-test (D, E, G) and One-way ANOVA (F).

Daytime wheel running is a potent inducer of gene expression in muscle of trained mice.

We then took advantage of the spontaneous motivation of mice to run without food reward at the usual onset of their resting phase, to evaluate muscle gene expression around the clock. Importantly, we only compared daytime and nighttime wheel active animals in our study, trained for a similar length of time; the comparison of sedentary mice with mice given free access to a running wheel is well documented elsewhere (Allen et al., 2001; Holloszy, 1967; McKie et al., 2019). We moreover collected muscle tissues after 3 weeks of daytime wheel access, when running performance already plateaued in particular in DA mice (**Fig. S1B**), without depriving mice of wheel access.

Exercise-related transcripts such as *Nr4a3*, *Atf3* were all induced by daytime wheel running (**Fig. 6A**). Incidentally, *Nr4a3* expression was strictly influenced by wheel running exercise and not by feeding. Total *Pgc-1a* was similarly induced by daytime wheel running (**Fig. 6A**), but only the *Pgc-1α2*, *3,* and *4* responded to daytime activity (**Fig. S5A**). Given the role of *Pgc-1a1* in the adaptation to endurance exercise (Lin et al., 2002), it thus is possible that this transcript isoform is only induced in the early phase of chronic exercise. We likewise evaluated the expression of metabolic genes in light of the strong effect of chronic training on skeletal muscle metabolism (Egan and Zierath, 2013). Unexpectedly, neither the phase nor the level of *Pparδ*, *Hk2,* and *Pdk4* expression was changed by chronic daytime exercise. In contrast, *Pparα*, stearoyl-CoA desaturase (*Scd-1*), ELOVL fatty acid elongase 6 (*Elovl6*) (**Fig. 6B**), and fatty acid synthase (*Fasn*) (**Fig. S5B**) were significantly increased by daytime wheel running, suggesting increased fat storage in muscle tissues of DA mice.

We have shown that treadmill exercise caused the rapid expression of transcriptional (co-)regulators associated with circadian clock function. Moreover, nighttime wheel running exercise modulates the daily amplitude of core clock gene expression (Yasumoto et al., 2015). *Bmal1*, *Clock, Cry1,* and *Rory* expression were all significantly decreased prior to and/or during wheel access in the DA mice (**Fig. 6C**). In contrast, *Per3* transcript was upregulated prior to wheel access, while both *Cry2* and *Per2* were induced during or after wheel access, leading to a phase-advanced peak of expression (**Fig. 6C**). This phase advance could either be caused by an acute, direct effect of wheel exercise or be the result of circadian entrainment. However, the effects of daytime wheel running were rather mild on the expression of circadian-related genes (i.e., *Pdk4, Cpt1α, Tbc1d1*). Finally, 24-h expression levels of *MyoD*—a direct target of the *Clock/Bmal1* complex and an essential regulator of muscle cell differentiation (Andrews et al., 2010)—were unchanged by daytime wheel running.

Taken together, these results show that there is a clear induction of exercise-related genes, including the transcriptional (co-)regulators *Nr4a3* and specific transcript isoforms of *Pgc-1a*, in chronically trained muscles. In contrast, chronic daytime wheel running does not severely alter clock gene oscillations in skeletal muscle.

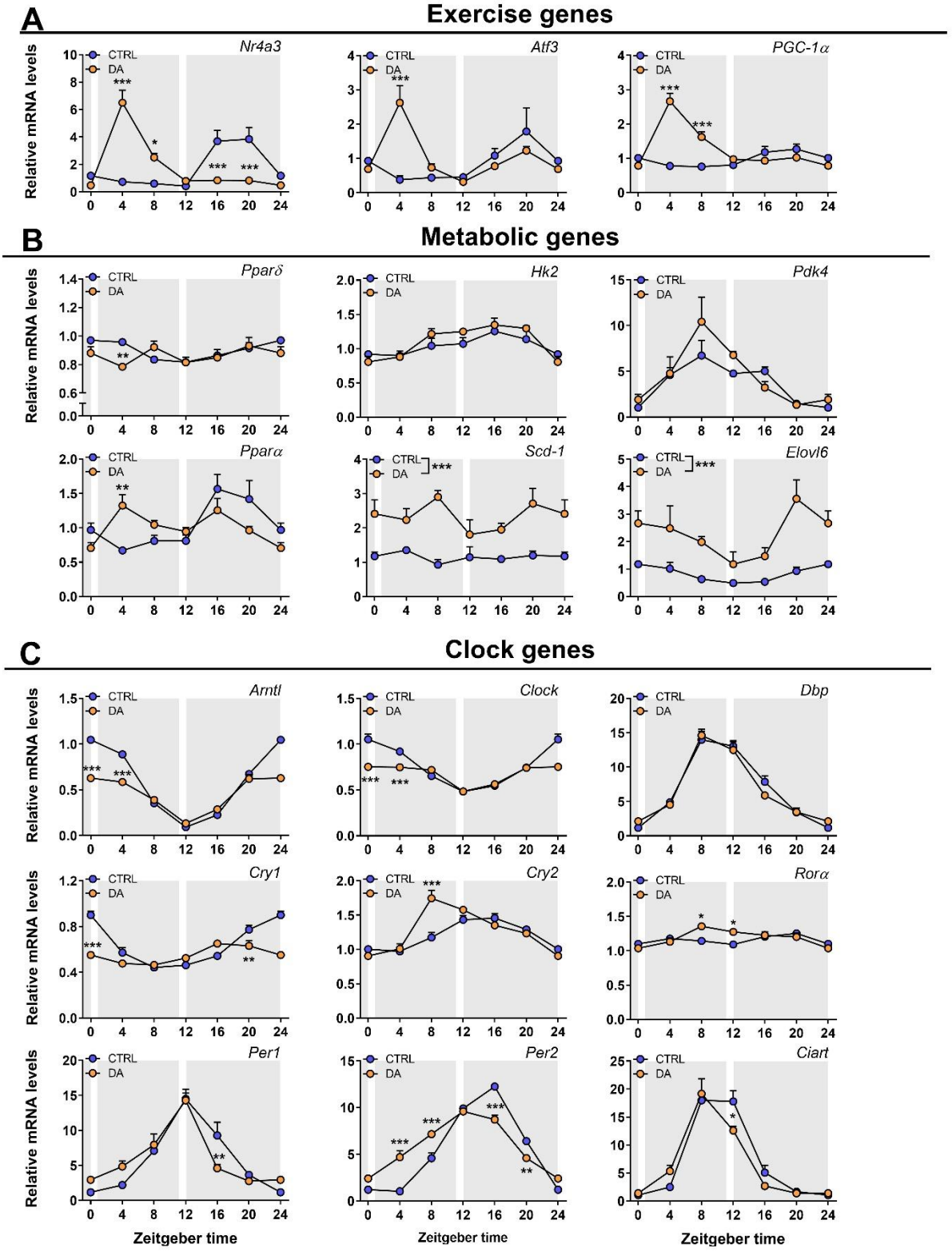

FIGURE 6. Distinct muscle gene expression signatures after daytime vs. nighttime wheel running. Gene expression in control (CTRL) and daytime activity (DA) mice. (A) Exercise-related genes, (B) Metabolic genes, (C) Clock genes. Expression values were determined by qPCR and normalized to Hprt. Data is shown as the average fold-change ± SEM (n = 4) relative to the expression in SED ZT0 set to 1 * $P < 0.05$; ** $P < 0.01$; *** $P < 0.001$. One-way ANOVA.

Characterization of the muscle transcriptome, proteome and phosphoproteome responses of daytime wheel active mice.

Studies on voluntary endurance exercise adaptation at different times of the day have not been reported. The behavioral and gene responses described above prompted us to further dissect the molecular and cellular changes induced by daytime wheel running. Importantly, we focused our multi-omics analysis on ZT4 and ZT16—near the peak of wheel-running activity in DA and CTRL mice, respectively.

Daytime wheel running led to the differential expression of 2094 genes at ZT4, with a similar proportion of down and upregulated transcripts. (**Fig. 7A** and **S6**). Intriguingly, wheel-running activity at nighttime was a poor modifier of gene expression; we only found 368 transcripts for which the expression was different between CTRL muscles and those obtained from daytime trained animals at ZT16. These genes associated with GO terms such as "Angiogenesis", "Regulation of cytoskeleton organization", "Protein folding". We, nonetheless, identified a conserved set of exercise-regulated genes regardless of the timing of wheel running (**Fig. 7A**). This included the KLF gene family (i.e., *Klf4, 5* and *15*), the transcriptional regulators *Maff* and *Mafk, Tbx3, Creb5, Atoh8 Nfe2l2, Noct, Sik1,* and *Nr4a3,* some of which are important for skeletal muscle maintenance and/or mitochondrial function and were similarly activated by an acute bout of treadmill exercise (Onder et al., 2019; Stewart et al., 2013). Incidentally, *Atf3*, *Nr4a3, Per2,* and *Pgc-1α*, were among the top induced genes in daytime working muscles (**Fig.7B**). The nuclear receptor *Pparα*—a regulator of fatty acid oxidation (Muoio et al., 2002)—was likewise specifically induced by daytime wheel running. GO analysis of DA muscles also highlighted gene sets involved in "mRNA metabolic process", "Regulation of catabolic process", "Regulation of cytoskeleton/organelle organization", "Intracellular protein transport" and "Protein stabilization". Moreover, KEGG analysis returned "Protein processing in ER" and "Mitophagy" as overrepresented pathways following daytime wheel running (**Fig.7C**).

Up to 3800 proteins were detected in skeletal muscles of DA and CTRL mice, including 246 for which the expression was exclusively altered by daytime wheel running (**Fig. 7E**). The majority of upregulated proteins were linked to metabolic functions (**Fig. 7G**) including an important cluster regulating fatty acid metabolism, e.g., ATP-citrate synthase (*Acty*), acetyl-CoA carboxylase (*Acaca*), mitochondrial trifunctional enzyme subunit (*Hadh*) α and β), *Fasn* and *Pdk4*; and the citrate cycle, e.g., Isocitrate dehydrogenase (*Idh*)2-3, succinate dehydrogenase (Sdh) a-b) (**Fig. 7F** orange). Incidentally, most of these proteins are direct targets of PPARα (Boergesen et al., 2012; Gan et al., 2018). We similarly observed the differential phosphorylation of 344 and 135 proteins in response to daytime and nighttime wheel running, respectively, with an overlap of 62 protein-specific posttranslational modifications, some of which associated with "Calcium signaling" (**Fig. 7K**). However, most of

the proteins shared between ZT4 and ZT16 were differentially phosphorylated by wheel running exercise. For instance, CACNA1s was phosphorylated on Ser700 in the morning and dephosphorylated on Ser1617 in the evening. Similar results were found for RYR1 and STIM1, with the identification of previously uncharacterized sites. Notably, there was a strong daytime-dependent posttranslational regulation of PYGM on Ser15 (**Fig. 7J**, orange), promoting the degradation of glycogen (Johnson, 1992). Accordingly, "Glycolysis" was enriched in the daytime wheel running group (**Fig. 7K** orange), and ALDOA—a key enzyme in the fourth step of glycolysis—was one of the top phosphorylated enzymes. Finally, major sarcomeric proteins, including Titin and several myosin heavy chain proteins (i.e., MYH1, 4, and 9) all show a significant change in phosphorylation, indicating significant adaptation in contractile properties of daytime working muscles (Eckels et al., 2018; Vandenboom, 2016).

Therefore, even in the late phase of repetitive training, daytime wheel running triggers the activation of vast gene program to particularly promote cytoskeleton and organelle organization, protein folding, and mitochondrial maintenance. We furthermore show that skeletal muscle undergoes a significant metabolic remodeling in response to daytime wheel running at both the proteome and phosphoproteome levels. Unexpectedly, despite the greater running exercise volume of CTRL mice and the strong induction of exercise-related transcriptional regulators in their muscles, nighttime wheel running poorly altered gene and protein expression. This suggests that, e.g., feeding activities have the potential to confound the interpretation of exercise training studies on these parameters.

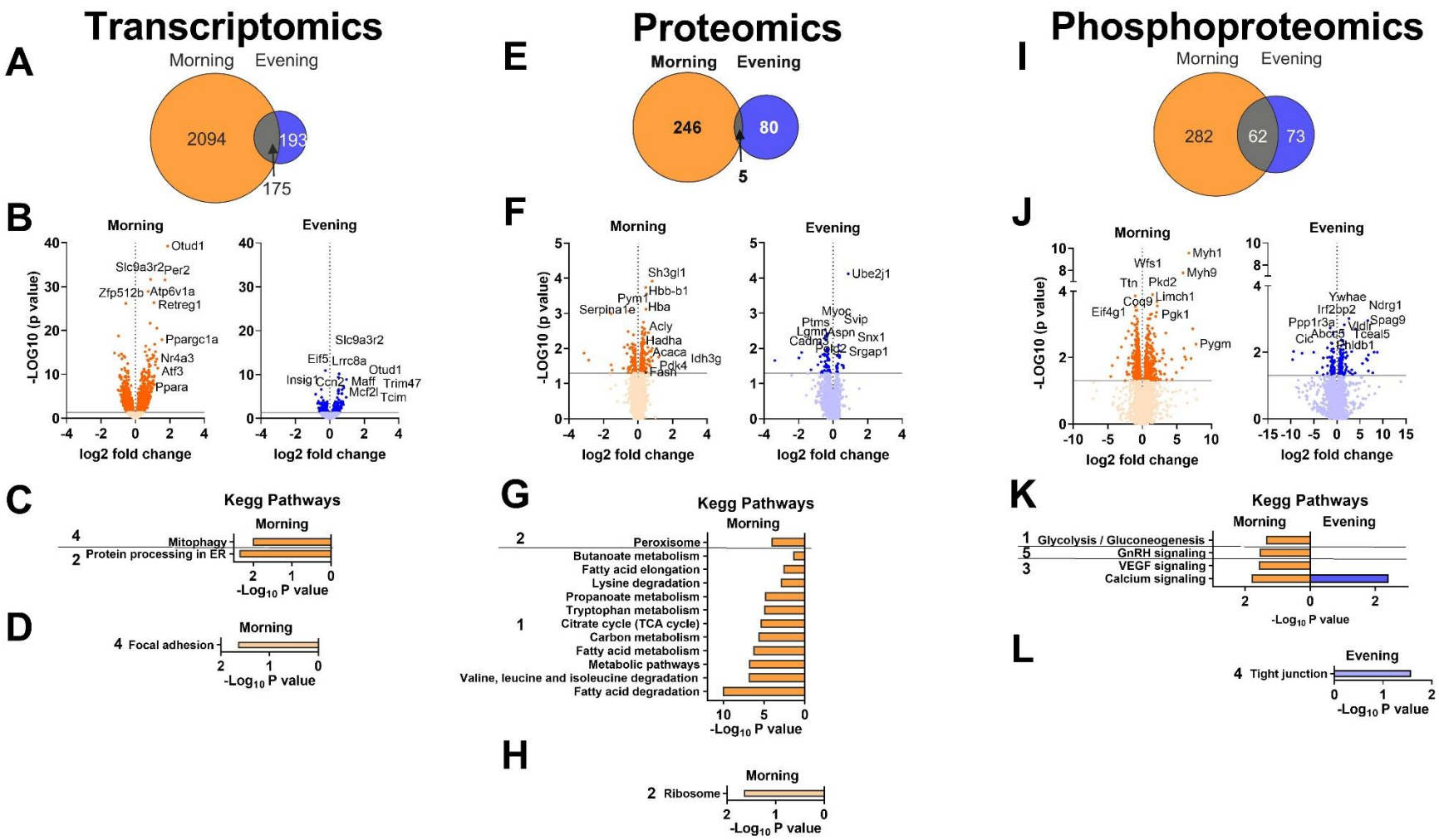

FIGURE 7. The effects of chronic voluntary daytime wheel running on transcriptomics, proteomics, and phosphoproteomics.

FIGURE 7. The effects of chronic voluntary daytime wheel running on transcriptomics, proteomics, and phosphoproteomics. Analysis of transcriptomic, proteomics, and phosphoproteomics data of control (CTRL) and daytime activity (DA) mice. (A) Venn diagram displaying the number of differentially expressed genes by nighttime (blue) and daytime (orange) wheel running as well as the overlapping genes of both conditions (gray). (B) Volcano plot displaying the differentially expressed genes by nighttime (blue) and daytime (orange) wheel running. (C) KEGG pathway enrichment analysis for exercise-induced genes by nighttime (blue) and daytime (orange) wheel running. (D) KEGG pathway enrichment analysis for exercise-decreased genes by nighttime (blue) and daytime (orange) wheel running. (E) Venn diagram displaying the number of differentially regulated proteins nighttime (blue) and daytime (orange) wheel running as well as the overlapping proteins of both conditions (gray). (F) Volcano plot displaying the differentially regulated proteins nighttime (blue) and daytime (orange) wheel running. (G) KEGG pathway enrichment analysis for proteins induced by nighttime (blue) and daytime (orange) wheel running. (H) KEGG pathway enrichment analysis for proteins decreased by nighttime (blue) and daytime (orange) wheel running. (I) Venn diagram displaying the number of differentially phosphorylated proteins by nighttime (blue) and daytime (orange) wheel running as well as the overlapping proteins of both conditions (gray). (J) Volcano plot displaying the differentially phosphorylated proteins by nighttime (blue) and daytime (orange) wheel running. (K) KEGG pathway enrichment analysis for protein phosphorylation induced by nighttime (blue) and daytime (orange) wheel running. (L) KEGG pathway enrichment analysis for protein dephosphorylation by nighttime (blue) and daytime (orange) wheel running. KEGG pathway categories: 1. Metabolism; 2. Genetic Information Processing; 3. Environmental Information Processing; 4. Cellular Processes; 5. Organismal Systems

Discussion

We revealed herein a time-of-day dependent variation in maximal running performance and identified specific, novel cellular pathways that are influenced by exercise in a timely manner. This, with the secretion of putative myokines, may contribute to improving physical exercise performance, skeletal muscle adaptations, and the health benefits associated with regular training. Finally, we propose a new methodology to explore the effects of chronic exercise training at different times of the day in preclinical mouse models. We hope that our large-scale transcriptomic, proteomic, and phosphoproteomic data will serve as a resource for future hypothesis-driven research and validation studies.

Understanding the daily variance in maximal exercise capacity

Fatigue is a complex phenomenon, and several aspects account for the failure to maintain a certain power output during strenuous exercise (Fitts, 1994; Green, 1997). Notably, glycogen depletion is thought to be one of the main determinants—the "glycogen shunt" hypothesis (Shulman and Rothman, 2001). We found that when mice show a peak of performance (i.e., at ZT0), basal liver glycogen levels are high, and this energy source is subsequently mobilized during exercise, at the expanse of muscle glycogen. The importance of muscle vs. liver glycogen in the mouse is still under debate (Pederson et al., 2005; Xirouchaki et al., 2016). Nevertheless, muscle glycogen only represents a minor source of energy in the mouse—about 10-fold lower as compared to humans (Jensen et al., 2011)—and mice with a muscle-specific GLUT4 deletion show decreased glucose uptake and running ability (Richter and Hargreaves, 2013). Moreover, when hepatic glycogen stores are depleted, liver glucose output is reduced, and hypoglycemia ensues (Richter and Hargreaves, 2013), which is consistent with the failure of our nighttime exercised mice to sustain a prolonged treadmill workout and to maintain a physiological blood glucose concentration. This is furthermore in line with the specific activation of energy-sensing pathways, namely HIF-1, AMPK, FoxO, and mTOR, following an exceptional exercise volume at night (Ma and Blenis, 2009; Semenza, 2012). Hence, the better capacity of mice to run on a treadmill appears to mainly depend on the hepatic glycogen reservoir and glucose delivery to contracting muscles (Jensen et al., 2013).

Glucose utilization in working muscles relies on the tight coordination of mechanisms promoting glucose availability, transport, and glycolysis. Our proteomic analyses allowed us to retrieve new potential players in the skeletal muscle crosstalk with other organs. For instance, MUP3, 17, and 18 proteins were all consistently upregulated in daytime exercised muscles and could regulate systemic glucose levels (Zhou et al., 2009). Intriguingly, administration of MUP1 has been shown to increase muscle glucose uptake and locomotor activity in diabetic mice (Hui et al., 2009). Our signal peptide prediction analyses further

identified Asprosin (FBN1). In contrast to the function of Asprosin as an adipokine (Romere et al., 2016), its putative secretion by contracting muscle cells to likewise stimulate hepatic glucose release into the bloodstream remains unexplored. There is, however, evidence that plasma concentration of Asprosin increases in response to exercise in humans (Wiecek et al., 2018) and our observation of active phosphorylation on Ser2566 and Ser2711 residues—further shown in mouse brown fat tissue (Huttlin et al., 2010)—could support a fine-tuning mechanism for active secretion.

In line with a greater reliance on liver-derived glucose, the expression of the Rho family GTPase RAC1—an essential regulator of glucose transport in contracting muscles (Sylow et al., 2017)—along with its upstream regulator PTPα and downstream target GTPase Ras-related protein (RALA), were exclusively elevated when treadmill exercise was performed in the early daytime. Hence, the synergistic expression of RAC1 and its downstream target RALA could facilitate GLUT4 translocation to the muscle cell membrane in response to mechanical stress during exercise, as previously proposed (Sylow et al., 2017). Incidentally, Rac1 imKO mice display a severe reduction in treadmill exercise-stimulated glucose uptake and GLUT4 translocation (Cartee, 2015a; Sylow et al., 2016). Therefore, it would be particularly interesting to evaluate time-dependent variations in maximal exercise performance in this mouse model or in muscle-GLUT4 deficient animals.

TBC1D1 and TBC1D4 (also called AS160) have recently emerged as a strong candidate for controlling GLUT4 trafficking in skeletal muscle (Cartee, 2015b; Sakamoto and Holman, 2008). In the absence of distinct TBC1D1 phosphorylation profiles upon exercise at both ZT, we predict that the time-dependent exercise-mediated phosphorylation of TBC1D4 on Ser3/616 is essential in regulating the translocation of GLUT4 to the membrane. Finally, the strong upregulation of the SNARE proteins—important regulators of vesicular trafficking (Cheatham, 2000; Pessin et al., 1999)—further highlights the time- and energy level-dependent activation of the GLUT4 secretory pathway.

Our data also support a temporal specificity in the expression and phosphorylation of proteins involved in synaptic transmission and the excitation-contraction coupling as potential determinants of running performance. For instance, along SNARE proteins, a collection of Rab GTPases are exclusively upregulated in daytime exercised muscles. Even though these proteins are much less studied at the peripheral synapse, they may play a prominent role in presynaptic vesicle exocytosis and thus acetylcholine release (Kiral et al., 2018; Stenmark, 2009; Tanaka et al., 2001). Moreover, the skeletal muscle calcium channels ORAI1—a major determinant of muscle fatigue (Wei-Lapierre et al., 2013)—was similarly induced in the early daytime. Finally, we identified novel phosphorylation sites on CACNA1S, which could positively regulate its activity and contribute to increased contractility of skeletal muscle (Fuller et al., 2010). We thus believe that the different responses of individual sites under

physiologically relevant conditions will provide valuable resources for further experimental investigation.

Time-dependent activation of skeletal muscle pathways

Several major cellular processes such as apoptosis, autophagy, mitophagy, protein synthesis and conformation, angiogenesis, and insulin signaling, were concurrently modulated by exercise regardless of time of day. Conversely, in the pre-prandial state, an acute bout of strenuous treadmill exercise activated specific pathways, namely HIF-1, AMPK, FoxO, and mTOR, in line with low energy availability at night and a likely increase in amino acid breakdown as previously suggested (Sato et al., 2019). Consequently, exercise in the early night was accompanied by the activation of a robust transcriptional program in response to inflammation. Notably, despite a greater workout, this response was not observed in daytime exercised muscles. On the contrary, daytime treadmill elicited a rapid activation of the complement system at the proteome level. Complement activation is an early priming event with significant influence on subsequent local inflammation and muscle regeneration (Frenette et al., 2000; Zhang et al., 2017). It thus is apparent that the activation of this pathway is tied to a specific time window of the day, and could suggest that exercising mice near ZT0 may facilitate skeletal muscle adaptations to regular training.

The endocrine potential of skeletal muscle represents an essential mechanism to control whole-body homeostasis and to coordinate the physiological adaptations of other organs to exercise (Legård and Pedersen, 2019; Schnyder and Handschin, 2015). Our secretory prediction analyses uncovered several potential myokines. For instance, the glucogenic adipokine Asprosin (FBN1) was exclusively elevated in daytime exercised muscles and is a potential therapeutic agent for the treatment of metabolic diseases, including diabetes (Yuan et al., 2020). Moreover, FBN1 protein is found in tumor cells and could be part of the cancer-induced reprogramming of host glucose metabolism (Schwartsburd, 2019; Zanivan et al., 2008). We also identified ITIH5 in skeletal muscles of daytime exercised mice, which could act as a tumor suppressor (Rose et al., 2017). Supporting its potential secretion, ITIH5 is referenced in the human Plasma Proteome Database (Nanjappa et al., 2014) and the PeptideAtlas plasma proteome repository (Schwenk et al., 2017). We also show a muscle elevation of SPARCL1 in response to nighttime exercise. Importantly, SPARCL1 shares high structural resemblance with SPARC, a protein released by contracting muscles known to inhibit tumor progression (Aoi et al., 2013). Hence, exercising at a specific time of the day could potentiate the health benefits associated with physical activity in normal and pathophysiological contexts. We moreover highlight here the potential of our proteomic data for the discovery of novel secreted factors.

Time, exercise and circadian physiology

Clock components play a major role in the regulation of mammalian physiology. There is moreover a tight relation between exercise-regulated energy sensors (e.g., AMPK, mTOR) and circadian proteins (Panda, 2016). In addition, the timing of exercise is a significant modifier of the subsequent daily oscillation of genes and metabolites in skeletal muscle (Sato et al., 2019). We now give a comprehensive overview of the temporal dynamics of clock gene expression in response to two exercise modalities. We propose that the transcriptional (co-)regulators *Per1, Per2,* and *Ciart* are part of the immediate-early response to acute strenuous exercise. Conversely, we show that the transcriptional changes induced by chronic daytime wheel exercise are very mild in comparison to the effects of scheduled daytime feeding on clock gene oscillations in muscle and liver tissues (Damiola et al., 2000; Reznick et al., 2013). Hence, in the long-term and in the present experimental conditions, we do not provide evidence that daytime wheel running is a strong Zeitgeber for the muscle and liver clocks (**Fig. 6C** and **S7**). Moreover, the robust induction of some of the core clock transcripts observed in previous (Ezagouri et al., 2019; Peek et al., 2017; Sato et al., 2019; Zambon et al., 2003) and in the present exercise study, could be associated with noncircadian function in skeletal muscle.

Our modern-day lifestyle has deleterious effects on the circadian clock, which in turn negatively affects our health (Arendt, 2010; Chellappa et al., 2019; James et al., 2017; Sulli et al., 2018). Designing time-based therapeutic interventions is, therefore, attractive. Accordingly, a recent study reported that afternoon exercise is more efficacious than morning exercise at improving glycemia in type 2 diabetes men (Savikj et al., 2019). Our data now highlight that the timing of exercise differently alters cellular mechanisms of glucose uptake in mouse skeletal muscle, and putatively its endocrine role. Studies of longer training periods would thus be interesting to assess how regular training at different times of day alters systemic function and different organ systems, in particular in preclinical mouse models. Incidentally, exercising mice on a treadmill presents several challenges to the daytime researcher as disruptions of mouse circadian physiology is inevitable (Sasaki et al., 2016). Moreover, selection of specific exercise regimens alongside the animal's compliance to the exercise protocol are important variables eventually changing over time (Ghosh et al., 2010). In this context, we show that under special lighting conditions, mice display a surprising and sustained motivation for voluntary wheel running in the early resting phase. We moreover describe the gene and protein regulatory networks robustly activated in response to chronic daytime training, without the confounding effect of feeding and the negative impact of forced exercise (Sasaki et al., 2016; Svensson et al., 2016). Hence, wheel running represents a better exercise modality to evaluate whether the health benefits of regular training critically depend upon the time of day. Finally, the relentless motivation of mice to be active on an exercise wheel even in their inactive phase could be leveraged to further study the consequence of

internal desynchronization (Salgado-Delgado et al., 2008). For instance, by regularly shifting wheel access under stable light entrainment (SPP), in combination or not with irregular mealtime. This strategy would ultimately better reflect the phase misalignment experienced by humans engaged in shift work (Arendt, 2010; Chellappa et al., 2019; Evans and Davidson, 2013; Wehrens et al., 2017).

Limitations of the study

We have used two different exercise modalities, in acute and chronic modes, and thus did not directly compare our multi-omics datasets. Also of note, despite the use of treadmill exercise at similar phases of the daily cycle, contrary to Sato et al. (Sato et al., 2019) our mice were pushed to run until exhaustion and did not have access to food after the treadmill exercise sessions, making the comparison of our respective gene studies somewhat irrelevant.

Multisite phosphorylation is a widespread phenomenon in eukaryotic cells, and a vast number of phosphorylated sites identified in our study are not yet associated with specific functional characteristics (e.g., enzymatic activity, binding, cellular localization or stability (Salazar and Hofer, 2009; Suwanmajo and Krishnan, 2015). We thus have mainly limited our comparative phosphorylome analyses to proteins showing time- and exercise-dependent phosphorylation on unique residues. We hope that the different responses of individual sites to timed exercise will provide valuable resources for further experimental investigation.

Materials and methods

Animals

8 week old C57BL/6JRj male mice (Janvier Labs) were housed in standard cages under 12:12 light:dark (LD) conditions, with light onset at 6am (Zeitgeber Time 0; ZT0) or entrained to a skeleton photoperiod (SPP) as described below and in Fig. 4, unless otherwise stated. The mice had ad libitum access to a standard chow diet (Maintenance 3432, KLIBA NAFAG) and water, unless otherwise stated. All experiments were performed in agreement with the principles of the Basel Declaration, with Federal and Cantonal Laws regulating the care and use of experimental animals in Switzerland, and the institutional guidelines of the Biozentrum and the University of Basel. The protocol with all methods described here was approved by the "Kantonales Veterinäramt" of the Kanton Basel-Stadt, under consideration of the well-being of the animals and the 3R principle.

Forced high-intensity exercise performance across the day

Sedentary mice were acclimated to the treadmill (Columbus Instruments, Columbus, Ohio, USA) on three consecutive days prior to the experiment. The accommodation period consisted in: Day 1, placing the mice in the treadmill for 10 min without speed followed by 5 min at 5 m/min; Day 2, running at 5 m/min, 7 m/min and 10 m/min for 5 min each; Day 3, running at 8 m/min, 10 m/min and 12 m/min for 5 min each. After one resting day, a maximal exercise capacity test was performed by 3min at 8m/min increasing treadmill speed by 2 m every 2 min, at a 15° slope, until exhaustion. Importantly, we have previously shown that this protocol elicits maximal oxygen uptake (VO_{2max}) in C57BL/6J mice (Delezie et al., 2019). Exhaustion was met if an animal remained on the electrical grid (providing a mild electrical stimulus of 0.5 mA, 200 ms pulse, 1 Hz) for more than 5 s. Tail blood glucose (Accu-Chek, Roche) and lactate (Lactate Plus meter, Nova Biomedical) values were determined immediately prior to treadmill exercise and within 1 min after physical exhaustion. Mice were either sacrificed immediately after exhaustion (≤ 5 min of time delay; Ex+0h) or 3 h after exercise (Ex+3h). For the latter group, mice were returned to their home cages without access to food. This experiment was repeated every 4 h for 24 h starting from ZT0 (6 a.m.; scheme in Fig. 1 (A)). A non-exercised group (Sedentary; Sed) of mice was always sacrificed at a similar ZT (≤ 30 min of time delay) as the exercised mice (Ex+0h and Ex+3h). Note that control Sed mice were placed in new cages, with new bedding but no food access 60 min prior to sacrifice.

Daytime scheduled wheel-running activity

Mice were single-housed in standard cages, within an environment-controlled cabinet (UniProtect Air Flow Cabinet, Bioscape), with the temperature set to 23°C. The mice had access to wheel with rods (∅ 11.5 cm, Starr Life Sciences) under constant 12:12 LD conditions for three weeks prior to exposure to a skeleton photoperiod (SPP). The SPP consisted of two repeated light-pulses (LP): 1 h LP at the beginning of the resting period and 1 h LP at the end

of the resting period, interrupted by 10 h of darkness (Fig. 4A). After three weeks acclimatization to the SPP, three weeks of intervention followed. During the intervention, one group of mice (control, CTRL) had ad libitum access to food, water and free access to running wheels. Another group of mice (Daytime activity, DA) was food-restricted to the longer dark phase (active phase) and had access to a wheel only during the shorter dark period (resting phase) (see Fig. 4). Wheel and food access were controlled manually, without opening the cage to not disturb the animals. Importantly, the use of the wheel (light phase: 309 turns vs. dark phase: 17732 turns) and food intake (light phase: 0.4g vs. dark phase: 4.7g) during the resting/inactive period was virtually absent in the CTRL group.

Body temperature and locomotor activity recordings

General locomotor activity and core body temperature data were acquired with the E-Mitter Telemetry System (Starr Life Sciences) from single-caged animals placed in an environment-controlled cabinet (UniProtect Air Flow Cabinet, Bioscape). Briefly, small transponders (G2 E-Mitter, Starr Life Sciences) were implanted into the abdominal cavity of mice under isoflurane anesthesia (2 % isoflurane + O_2). Mice were treated with Meloxicam (1 mg/kg) pre- and post-operatively and allowed to recover for three weeks. The abovementioned parameters together with the wheel-running activity, were recorded with a PC-based acquisition system connected to ER4000 Receivers (VitalView, Starr Life Sciences).

Muscle tissue preparation and blood collection

Mice from the different experiments were sacrificed by short exposure to CO_2 and immediate exsanguination. Blood was collected in tubes containing lithium heparin (Microvette 500 LH, Sarstedt, 20.1345) centrifuged at 2000 g for 5 min at RT and stored at - 80°C. The glycolytic quadriceps and gastrocnemius muscles, as well as liver samples were quickly snap frozen in liquid nitrogen and stored at - 80°C until further analysis.

Quantitative Real-Time PCR (Reverse Transcript)

Total RNA from muscle tissues was extracted using a hybrid method combining TRI-Reagent (Sigma-Aldrich T9424) and RNeasy Mini Kit (QIAGEN 74104). RNA quantity and purity were measured with a NanoDrop OneC (ThermoFisher Scientific). High-Capacity cDNA Reverse Transcript Kit (Applied Biosystems, 4368814) was used for cDNA synthesis with 1 ug of total RNA. Quantitative real-time PCR was performed with Fast SYBR Green Master Mix (Applied Biosystems, 4385612) in a RT-PCR System (StepOnePlus, Applied Biosystems). PCR reactions were done in duplicate with the addition of negative controls (i.e., no reverse transcription and no template controls). Relative expression levels were determined using the comparative ΔCT method to normalize target gene mRNA to *Hprt*. Primers were designed and tested as previously described (Delezie et al., 2012). Primer sequences are summarized in supplemental Table 1.

Blood parameters analysis

Quantification of plasma triglyceride was done with the Cobas c111 analyzer (Roche). Plasma free fatty acids were analyzed using the Free Fatty Acid Quantification Assay Kit (Abcam, ab65341) following manufacturer's recommendations. Muscle and liver glycogen levels were measured with the Glycogen Assay Kit (Abcam, ab65620).

RNA sequencing and data analysis

RNA quality was determined on the Bioanalyzer instrument (Agilent Technologies, Santa Clara, CA, USA) using the RNA 6000 Nano Chip (Agilent, Cat# 5067-1511) and quantified by Spectrophotometry using the NanoDrop ND-1000 Instrument (NanoDrop Technologies, Wilmington, DE, USA). Library preparation was performed with 1µg total RNA using the TruSeq Stranded mRNA Library Prep Kit High Throughput (Cat# RS-122-2103, Illumina, San Diego, CA, USA). Libraries were quality-checked on the Fragment Analyzer (Advanced Analytical, Ames, IA, USA) using the Standard Sensitivity NGS Fragment Analysis Kit (Cat# DNF-473, Advanced Analytical) revealing excellent quality of libraries (average concentration was 152±9 nmol/L and average library size was 374±4 base pairs). Samples were pooled to equal molarity. Each pool was quantified by PicoGreen Fluorometric measurement in order to be adjusted to 1.8pM and used for clustering on the NextSeq 500 instrument (Illumina). Samples were sequenced Single-reads 76 bases using the NextSeq 500 High Output Kit 75-cycles (Illumina, Cat# FC-404-1005) and primary data analysis was performed with the Illumina RTA version 2.4.11 and Basecalling Version bcl2fastq-2.20.0.422.

To quantify mRNA expression levels, kallisto version 0.46.0 (Bray et al., 2016) was used. To build the index for kallisto, the GRCm38.p6 (mm10) genome assembly and the ncbiRefSeqCurated transcript annotation of the UCSC genome browser were used (Karolchik et al., 2014; Pruitt et al., 2014). microRNAs (miRbase Version 19 (Kozomara and Griffiths-Jones, 2011), translated to RefSeq IDs through BioMart (Durinck et al., 2009)) were excluded. Only one transcript was retained if several had both identical start and end coordinates, slightly flattening the annotation, preference was given to transcripts with IDs starting with “NM_”. Transcripts mapping to more than one chromosome, or to random or chrUn contigs, were discarded. tximport version 1.14.0 (Soneson et al., 2015) was used to transform expression levels to flattened gene level pseudo-counts, using the “lengthScaledTPM” option. For this, RefSeq IDs were mapped to Entrez gene IDs using the org.Mm.eg.db database of R/Bioconductor version 3.10 (Gentleman et al., 2004). DESeq2 version 1.26.0 (Love et al., 2014) was used for statistical analysis of gene level differential expression. Here, $\log_2$ fold changes were estimated by the DESeq2 shrinkage estimator.

Proteomics and data analysis

Phosphopeptide enrichment and LC MS/MS analysis

Tissue was lysed in 8 M Urea, 0.1 M ammonium bicarbonate, phosphatase inhibitors (Sigma P5726&P0044) by sonication (Bioruptor, 10 cycles, 30 seconds on/off, Diagenode, Belgium) and proteins were digested as described previously (Ahrne et al., 2016). Shortly, proteins were reduced with 5 mM TCEP for 60 min at 37 °C and alkylated with 10 mM chloroacetamide for 30 min at 37 °C. After diluting samples with 100 mM ammonium bicarbonate buffer to a final urea concentration of 1.6M, proteins were digested by incubation with sequencing-grade modified trypsin (1/50, w/w; Promega, Madison, Wisconsin) for 12 h at 37°C. After acidification using 5% TFA, peptides were desalted using C18 reverse-phase spin columns (Macrospin, Harvard Apparatus) according to the manufacturer's instructions, dried under vacuum and stored at -20 °C until further use.

Peptide samples were enriched for phosphorylated peptides using Fe(III)-IMAC cartridges on an AssayMAP Bravo platform as recently described (Post et al., 2017). Unmodified peptides ("flowthrough") were subsequently used for TMT analysis.

Phospho-enriched peptides were resuspended in 0.1% aqueous formic acid and subjected to LC–MS/MS analysis using a Q Exactive HF Mass Spectrometer or an Orbitrap Fusion Lumos Mass Spectrometer fitted with an EASY-nLC 1000 or an EASY-nLC 1200, respectively (both Thermo Fisher Scientific) and a custom-made column heater set to 60°C. Peptides were resolved using a RP-HPLC column (75µm × 30cm or 75µm × 36cm, respectively) packed in-house with C18 resin (ReproSil-Pur C18–AQ, 1.9 µm resin; Dr. Maisch GmbH) at a flow rate of 0.2 µl/min. The following gradient was used for peptide separation: Q Exactive HF from 5% B to 8% B over 5 min to 20% B over 45 min to 25% B over 15 min to 30% B over 10 min to 35% B over 7 min to 42% B over 5 min to 50% B over 3min to 95% B over 2 min followed by 18 min at 95% B, Orbitrap Fusion Lumos from 5% B to 8% B over 5 min to 20% B over 45 min to 25% B over 15 min to 30% B over 10 min to 35% B over 7 min to 42% B over 5 min to 50% B over 3min to 95% B over 2 min followed by 18 min at 95% B. Buffer A was 0.1% formic acid in water and buffer B was 80% acetonitrile, 0.1% formic acid in water.

The Q Exactive HF mass spectrometer was operated in DDA mode with a total cycle time of approximately 1 s. Each MS1 scan was followed by high-collision-dissociation (HCD) of the 10 most abundant precursor ions with dynamic exclusion set to 45 seconds. For MS1, 3e6 ions were accumulated in the Orbitrap over a maximum time of 100 ms and scanned at a resolution of 120,000 FWHM (at 200 m/z). MS2 scans were acquired at a target setting of 1e5 ions, maximum accumulation time of 100 ms and a resolution of 30,000 FWHM (at 200 m/z). Singly charged ions and ions with unassigned charge state were excluded from triggering MS2 events. The normalized collision energy was set to 28%, the mass isolation window was set to

1.4 m/z and one microscan was acquired for each spectrum. The Orbitrap Fusion Lumos mass spectrometer was operated in DDA mode with a cycle time of 3 seconds between master scans. Each master scan was acquired in the Orbitrap at a resolution of 120,000 FWHM (at 200 m/z) and a scan range from 375 to 1600 m/z followed by MS2 scans of the most intense precursors in the Orbitrap at a resolution of 30,000 FWHM (at 200 m/z) with isolation width of the quadrupole set to 1.4 m/z. Maximum ion injection time was set to 50ms (MS1) and 54 ms (MS2) with an AGC target set to 1e6 and 5e4, respectively. Only peptides with charge state 2 – 5 were included in the analysis. Monoisotopic precursor selection (MIPS) was set to Peptide, and the Intensity Threshold was set to 2.5e4. Peptides were fragmented by HCD (Higher-energy collisional dissociation) with collision energy set to 30%, and one microscan was acquired for each spectrum. The dynamic exclusion duration was set to 30s.

The acquired raw-files were imported into the Progenesis QI software (v2.0, Nonlinear Dynamics Limited), which was used to extract peptide precursor ion intensities across all samples applying the default parameters. The generated mgf-file was searched using MASCOT against a murine database (consisting of 34026 forward and reverse protein sequences downloaded from Uniprot on 20190129) and 392 commonly observed contaminants using the following search criteria: full tryptic specificity was required (cleavage after lysine or arginine residues, unless followed by proline); 3 missed cleavages were allowed; carbamidomethylation (C) was set as fixed modification; oxidation (M) and phosphorylation (STY) were applied as variable modifications; mass tolerance of 10 ppm (precursor) and 0.02 Da (fragments). The database search results were filtered using the ion score to set the false discovery rate (FDR) to 1% on the peptide and protein level, respectively, based on the number of reverse protein sequence hits in the datasets. Exported peptide intensities were normalized based on the protein regulations observed in the corresponding TMT experiments in order to account for changes in protein abundance. Only peptides corresponding to proteins, which were regulated significantly with a p value ≤ 5% in the TMT analysis were normalized. Quantitative analysis results from label-free quantification were processed using the SafeQuant R package v.2.3.2. (Ahrne et al., 2016), https://github.com/eahrne/SafeQuant/) to obtain peptide relative abundances. This analysis included global data normalization by equalizing the total peak/reporter areas across all LC-MS runs, data imputation using the knn algorithm, summation of peak areas per and LC-MS/MS run, followed by calculation of peptide abundance ratios. Only isoform specific peptide ion signals were considered for quantification. The summarized peptide expression values were used for statistical testing of between condition differentially abundant peptides. Here, empirical Bayes moderated t-Tests were applied, as implemented in the R/Bioconductor limma package (http://bioconductor.org/packages/release/bioc/html/limma.html) were used.TMT labelling and LC MS/MS analysis

Tryptic peptides were labeled with isobaric tandem mass tags (TMT10plex or TMTpro 16plex, Thermo Fisher Scientific). Peptides were resuspended in labeling buffer (2 M urea, 0.2 M HEPES, pH 8.3) by sonication and TMT reagents were added to the individual peptide samples followed by a 1 h incubation at 25°C shaking at 500 rpm. To quench the labelling reaction, aqueous 1.5 M hydroxylamine solution was added and samples were incubated for another 5 min at 25°C shaking at 500 rpm followed by pooling of all samples. The pH of the sample pool was increased to 11.9 by adding 1 M phosphate buffer (pH 12) and incubated for 20 min at 25°C shaking at 500 rpm to remove TMT labels linked to peptide hydroxyl groups. Subsequently, the reaction was stopped by adding 2 M hydrochloric acid until a pH < 2 was reached. Finally, peptide samples were further acidified using 5 % TFA, desalted using Sep-Pak Vac 1cc (50 mg) C18 cartridges (Waters) according to the manufacturer's instructions and dried under vacuum. For TMTpro 16plex analysis, 4 peptide samples were prepared from C2C12 cells, TMT labelled and included in the analysis to boost protein coverage.

TMT-labeled peptides were fractionated by high-pH reversed phase separation using a XBridge Peptide BEH C18 column (3,5 µm, 130 Å, 1 mm x 150 mm, Waters) on an Agilent 1260 Infinity HPLC system. Peptides were loaded on column in buffer A (20 mM ammonium formate in water, pH 10) and eluted using a two-step linear gradient from 2% to 10% in 5 min and then to 50% buffer B (20 mM ammonium formate in 90% acetonitrile, pH 10) over 55 min at a flow rate of 42 µl/min. Elution of peptides was monitored with a UV detector (215 nm, 254 nm) and a total of 36 fractions were collected, pooled into 12 fractions using a post-concatenation strategy as previously described (Wang et al., 2011) and dried under vacuum.

Dried peptides were resuspended in 0.1% aqueous formic acid and subjected to LC–MS/MS analysis using a Q Exactive HF Mass Spectrometer or an Orbitrap Fusion Lumos Mass Spectrometer fitted with an EASY-nLC 1000 or an EASY-nLC 1200, respectively (both Thermo Fisher Scientific) and a custom-made column heater set to 60°C. Peptides were resolved using a RP-HPLC column (75µm × 30cm or 75µm × 36cm, respectively) packed in-house with C18 resin (ReproSil-Pur C18–AQ, 1.9 µm resin; Dr. Maisch GmbH) at a flow rate of 0.2 µLmin-1. The following gradient was used for peptide separation: Q Exactive HF from 5% B to 15% B over 10 min to 30% B over 60 min to 45 % B over 20 min to 95% B over 2 min followed by 18 min at 95% B, Orbitrap Fusion Lumos from 5% B to 15% B over 9 min to 30% B over 90 min to 45 % B over 21 min to 95% B over 2 min followed by 18 min at 95% B. Buffer A was 0.1% formic acid in water and buffer B was 80% acetonitrile, 0.1% formic acid in water.

The Q Exactive HF mass spectrometer was operated in DDA mode with a total cycle time of approximately 1 s. Each MS1 scan was followed by high-collision-dissociation (HCD) of the 10 most abundant precursor ions with dynamic exclusion set to 30 seconds. For MS1, 3e6 ions were accumulated in the Orbitrap over a maximum time of 100 ms and scanned at a resolution of 120,000 FWHM (at 200 m/z). MS2 scans were acquired at a target setting of 1e5

ions, maximum accumulation time of 100 ms and a resolution of 30,000 FWHM (at 200 m/z). Singly charged ions and ions with unassigned charge state were excluded from triggering MS2 events. The normalized collision energy was set to 30%, the mass isolation window was set to 1.1 m/z and one microscan was acquired for each spectrum. The Orbitrap Fusion Lumos mass spectrometer was operated in DDA mode with a cycle time of 3 seconds between master scans. Each master scan was acquired in the Orbitrap at a resolution of 120,000 FWHM (at 200 m/z) and a scan range from 375 to 1600 m/z followed by MS2 scans of the most intense precursors in the Orbitrap at a resolution of 30,000 FWHM (at 200 m/z) with isolation width of the quadrupole set to 1.1 m/z. Maximum ion injection time was set to 50ms (MS1) and 54 ms (MS2) with an AGC target set to 1e6 and 1e5, respectively. Monoisotopic precursor selection (MIPS) was set to Peptide, and the Intensity Threshold was set to 5e4. Peptides were fragmented by HCD (Higher-energy collisional dissociation) with collision energy set to 38%, and one microscan was acquired for each spectrum. The dynamic exclusion duration was set to 45s.

The acquired raw-files were analysed using the SpectroMine software (Biognosis AG, Schlieren, Switzerland). Spectra were searched against a murine database consisting of 17013 protein sequences (downloaded from Uniprot on 20190307) and 392 commonly observed contaminants. Standard Pulsar search settings for TMT10plex ("TMT10plex Quantification") and TMTpro 16plex ("TMTpro Quantification") were used and resulting identifications and corresponding quantitative values were exported on the PSM level using the "Export Report" function. Acquired reporter ion intensities in the experiments were employed for automated quantification and statistical analysis using our in-house developed SafeQuant R script v2.3.2, (Ahrne et al., 2016). This analysis included adjustment of reporter ion intensities, global data normalization by equalizing the total reporter ion intensity across all channels, summation of reporter ion intensities per protein and channel, calculation of protein abundance ratios and testing for differential abundance using empirical Bayes moderated t-statistics.

Pathway enrichment analysis

For the pathway enrichment analysis with g:Profiler (Reimand et al., 2016), all genes and (phospho-)proteins of a time point were used, including the overlap.

Statistics

The n number used per genotype for each experiment is indicated in the figure legend. Data are represented as mean±SEM and statistically analyzed with GraphPad Prism 8. Student t-test was performed to evaluate statistical difference between two groups. For multiple comparisons, data were analyzed using 2-Way ANOVA followed by Sidak's multiple comparisons test. Corresponding symbols to highlight statistical significance are the following: *: $p \leq 0.05$; **: $p \leq 0.01$; ***: $p \leq 0.001$.

Supplemental Figures

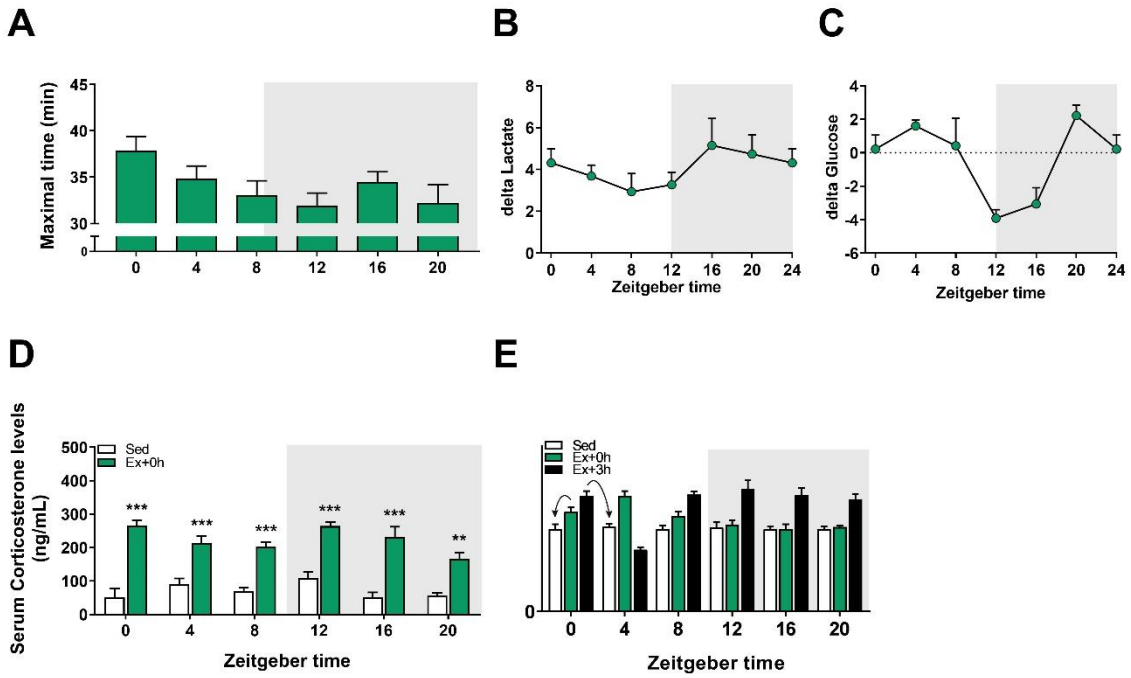

SUPP. FIGURE 1. Time-of-day-dependent variations in mouse treadmill exercise performance (A) Maximal time reached at exhaustion. (B) Delta blood lactate and (C) delta glucose levels (rest subtracted from after exhaustion value). (D) Serum corticosterone levels in SED and after exhaustion. Data is shown as the average ± SEM (n=3 per group and time point). ** P < 0.01; *** P < 0.001. One-way ANOVA (D). (E) Example for the analysis of the bar graph plots, arrows indicate normalization. Note, values are plotted according to their exercise time, while the normalization was performed corresponding to their sacrification time. (i.e., the gene expression of a mouse trained at ZT0 and sacrificed directly after exhaustion was normalized to the expression of Sed ZT0 plotted at ZT0, while the gene expression of a mouse trained at ZT0 and sacrificed 3 h after exhaustion was normalized to the expression of Sed ZT4, but plotted at ZT0, at its training time.)

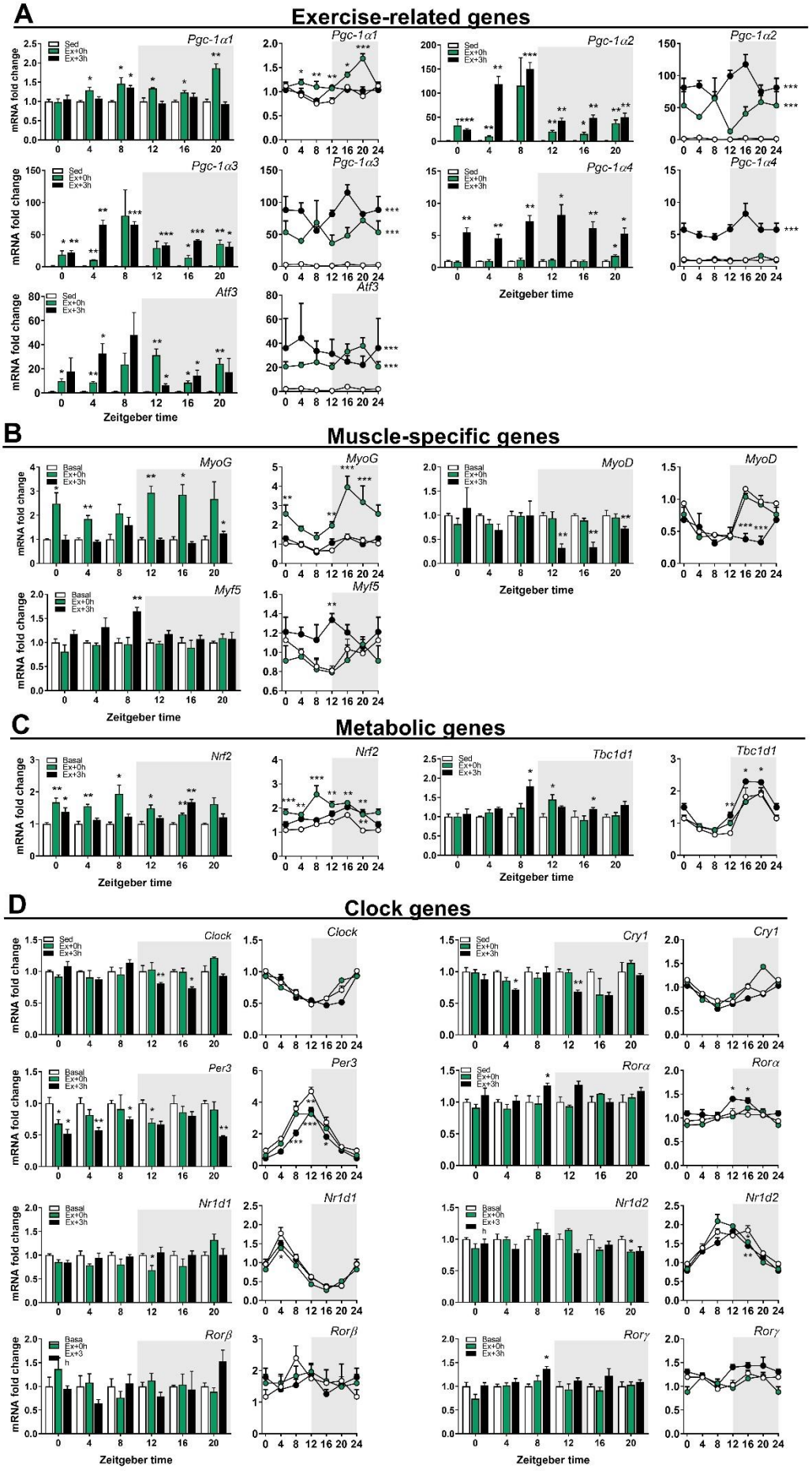
A
Exercise-related genes
Pgc-1α1
Pgc-1α2
Pgc-1α3
Pgc-1α4
Atf3
Sed
Ex+0h
Ex+3h
mRNA fold change
Zeitgeber time
B
Muscle-specific genes
MyoG
MyoD
Myf5
Basal
C
Metabolic genes
Nrf2
Tbc1d1
D
Clock genes
Clock
Cry1
Per3
Rorα
Nr1d1
Nr1d2
Rorβ
Rorγ

SUPP. FIGURE 2. Scheduled treadmill induces broad and time-dependent transcriptional responses in skeletal muscle. Gene expression in sedentary (SED), directly (+0h) and 3 h (+3h) after exhaustion. (A) Exercise-related genes, (B) Muscle-specific genes, (C) Metabolic genes, (D) Clock genes. Expression values were determined by qPCR and normalized to *Hprt*. Bargraph data is shown as the average fold-change ± SEM (n = 3) relative to the expression in SED set to 1. Curve data is shown as the average fold-change ± SEM (n = 3) relative to the expression in SED ZT0 set to 1 * $P < 0.05$; ** $P < 0.01$; *** $P < 0.001$. Unpaired Student's *t*-test (Bargraphs) and One-way ANOVA (Curves).

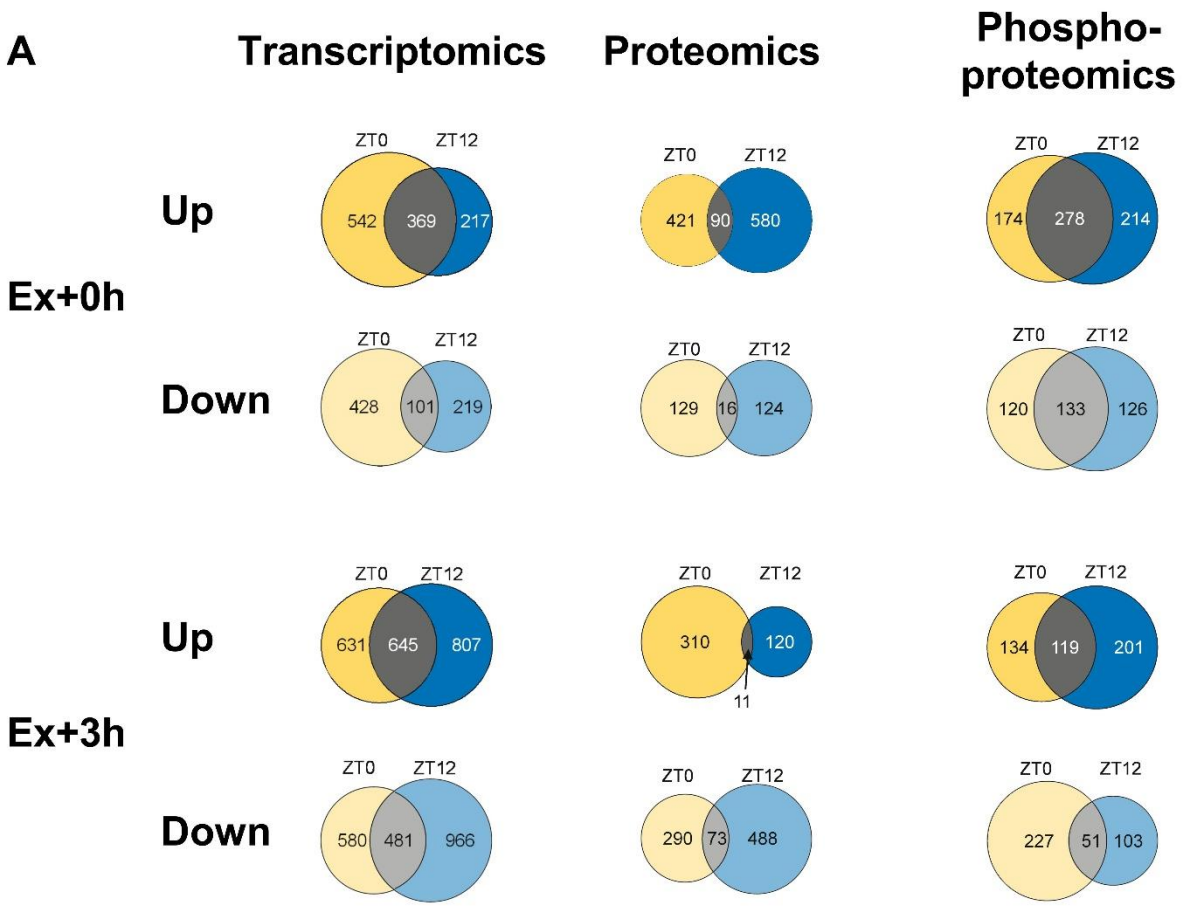

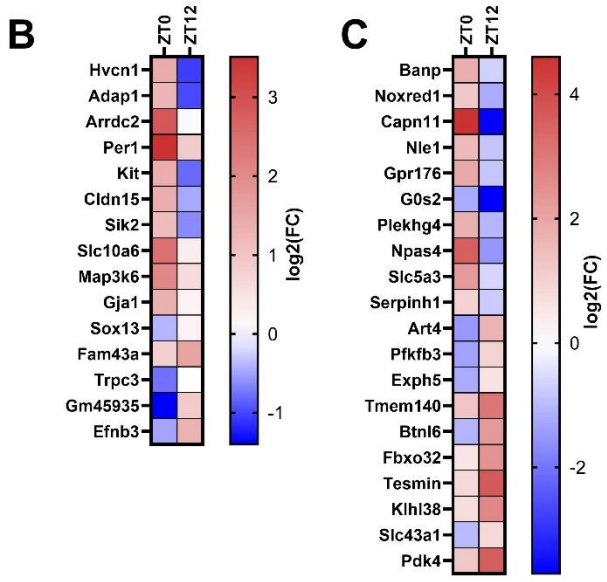

SUPP. FIGURE 3. Distinct muscle gene expression signatures after early light vs. early dark phase treadmill exercise. (A) Venn diagram displaying the number of differentially regulated genes, proteins and phosphosites directly and 3 h after early light (ZT0; yellow) and early dark (ZT12; blue) phase exercise as well as the overlapping genes of both conditions (gray). (B) Heatmap of differentially expressed genes directly after and (C) 3 h after exercise.

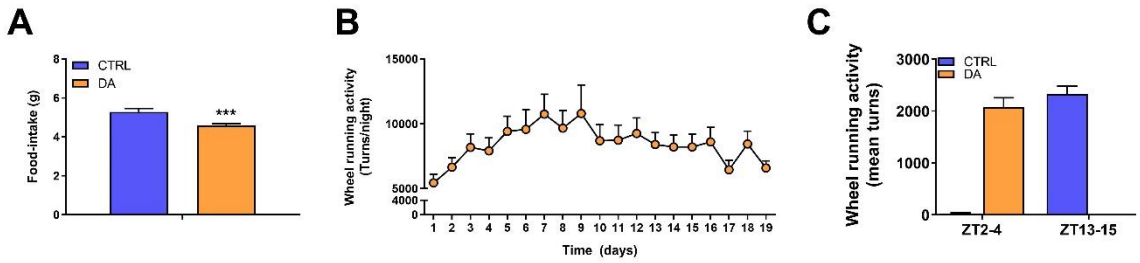

SUPP. FIGURE 4. Slightly decreased food intake in DA mice (A) Food-intake average over the full food access period. (B) Daily wheel-running activity from the first day of restriction of the DA mice. Data is shown as the average fold-change ± SEM (n = 24). (C) Quantified wheel-running activity during the first 3 h of wheel excess. *** P < 0.001. Unpaired Student's t-test (A).

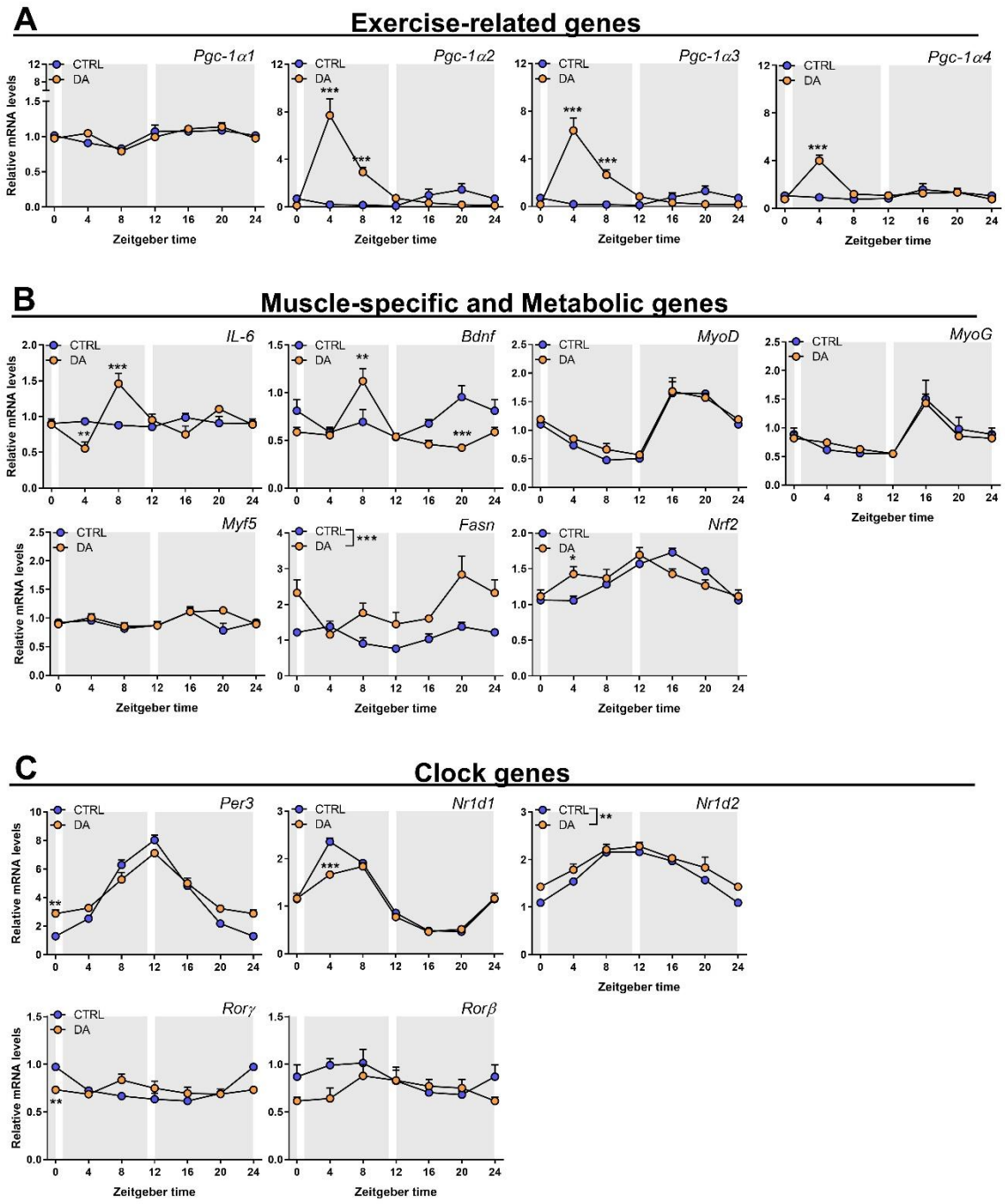

SUPP. FIGURE 5. Distinct muscle gene expression signatures after daytime vs. nighttime wheel running. Gene expression in control (CTRL) and daytime activity (DA) mice. (A) Exercise-related genes, (B) Muscle-specific and Metabolic genes, (C) Clock genes. Expression values were determined by qPCR and normalized to Hprt. Data is shown as the average fold-change ± SEM (n = 4) relative to the expression in SED ZT0 set to 1 * P < 0.05; ** P < 0.01; *** P < 0.001. One-way ANOVA.

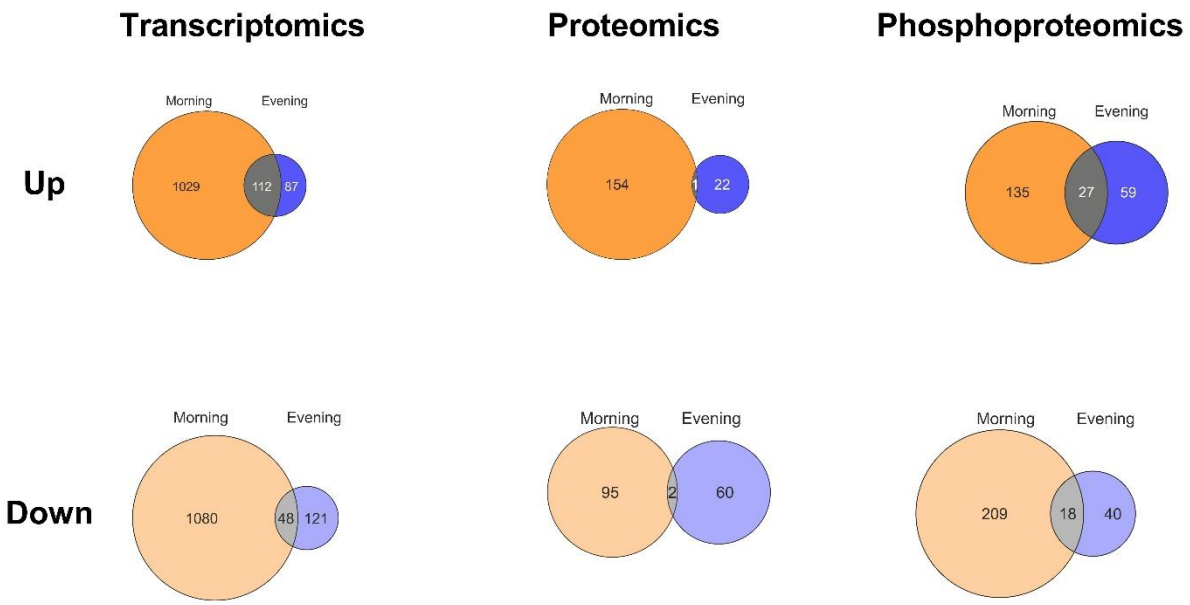

SUPP. FIGURE 6. The effects of chronic voluntary daytime wheel running on transcriptomics, proteomics, and phosphoproteomics Venn diagram displaying the number of differentially regulated genes, proteins and phosphosites by nighttime (blue) and daytime (orange) wheel running as well as the overlapping genes of both conditions (gray).

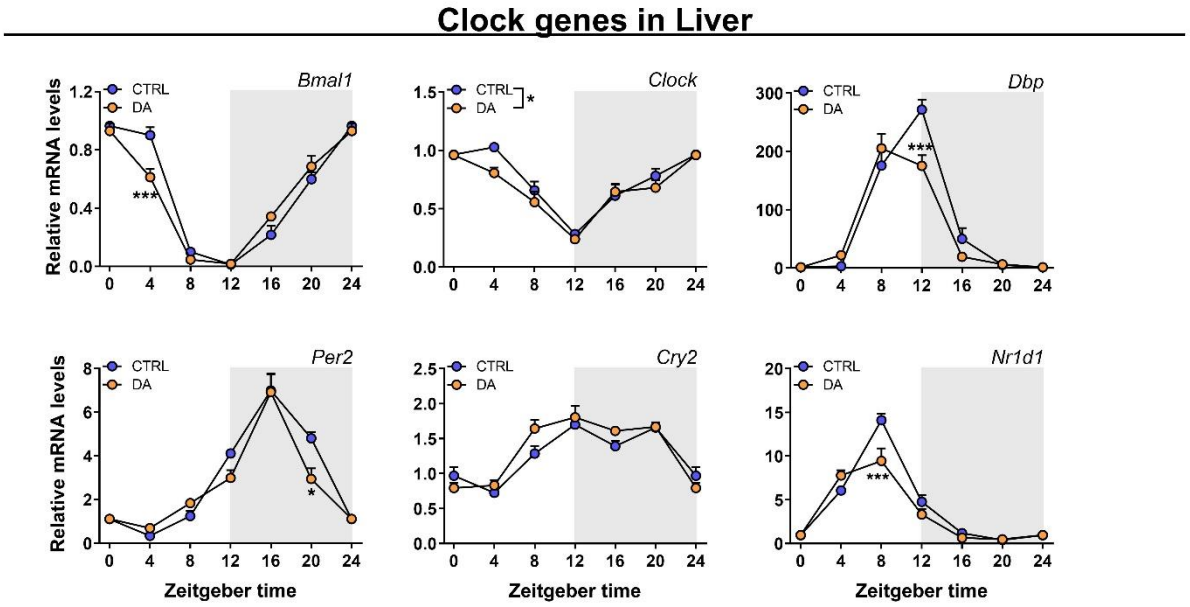

SUPP. FIGURE 7. Distinct liver gene expression signatures after daytime vs. nighttime wheel running. Gene expression in control (CTRL) and daytime activity (DA) mice. Clock genes. Expression values were determined by qPCR and normalized to Hprt. Data is shown as the average fold-change ± SEM (n = 4) relative to the expression in SED ZT0 set to 1 * $P < 0.05$; *** $P < 0.001$. One-way ANOVA.

Table 1. Primers

Gene	Fwd	Rvs
Arntl	CTCATTGATGCCAAGACTGG	GGTGGCCAGCTTTTCAAATA
Atf3	ACCGTCAACAACAGACCCC	TTTCTGCAGGCACTCTGTCTT
Bdnf	GGGTCACAGCGGCAGATAAA	GCCTTTGGATACCGGGACTT
Ciart	ACTCAAGATGGGTCGCTTTG	GGGCAGCTATGTGAGGAAAC
Clock	CACAGGGCACCACCAATAAT	CATATCCACTGCTGGCCTTT
Cpt1a	TACTACGCCATGGAGATGCT	TGACGTGTTGGATGGTGTCT
Cry1	CTGGCGTGGAAGTCATCGT	CTGTCCGCCATTGAGTTCTATG
Cry2	ACCGATGGAGGTTCCTACTG	AGCCTTGGGAACACATCAG
Dbp	ACCGTGGAGGTGCTAATGAC	TGGCTGCTTCATTGTTCTTG
Hk2	CCCTGCCACCAGACGAAA	GACTTGAACCCCTTAGTCCATGA
Il-6	CTGCAAGAGACTTCCATCCAGTT	GAAGTAGGGAAGGCCGTGG
Myf5	TGAGGGAACAGGTGGAGAAC	AGCTGGACACGGAGCTTTTA
MyoD	GCCGCCTGAGCAAAGTGAATG	CAGCGGTCCAGGTGCGTAGAAG
MyoG	GCAATGCACTGGAGTTCG	ACGATGGACGTAAGGGAGTG
Nr1d1	AGACTTCCCGCTTCACCAAG	AGCTTCTCGGAATGCATGTT
Nr1d2	TCTTTCGGAGGAGCATTCAG	GAATTCGGCCAAATCGAAC
Nr4a3	GATCACAGAGCGACATGGGTTA	GAGCCTGTCCCTTCCTCTGG
Nrf2	AGGACATGGAGCAAGTTTGG	TTCTTTTTCCAGCGAGGAGA
Pdk4	CCGCTGTCCATGAAGCA	GCAGAAAAGCAAAGGACGTT
Pdp1	TGTTGACCTCCATGTGGCTA	TCCTGCTTTACCACGCTCTT
Per1	ACCAGCGTGTCATGATGACATAC	CTCTCCCGGTCTTGCTTCAG
Per2	ATGCTCGCCATCCACAAGA	GCGGAATCGAATGGGAGAAT
Per3	GTGATTGTTCACGCGTCTGT	CACTGCCATCTCGAGTTCAA
Pgc-1a	TGATGTGAATGACTTGGATACAGACA	GCTCATTGTTGTACTGGTTGGATATG
Pgc-1a1	GGACATGTGCAGCCAAGACTCT	CACTTCAATCCACCCAGAAAGCT
Pgc-1a2	CCACCAGAATGAGTGACATGGA	GTTCAGCAAGATCTGGGCAAA
Pgc-1a3	AAGTGAGTAACCGGAGGCATTC	TTCAGGAAGATCTGGGCAAAGA
Pgc-1a4	TCACACCAAACCCACAGAAA	CTGGAAGATATGGCACAT
Ppara	CCACGAAGCCTACCTGAAGA	ACTGGCAGCAGTGGAAGAAT
Ppard	GCCTCGGGCTTCCACTAC	AGATCCGATCGCACTTCTCA
Pparg	TGTGGGGATAAAGCATCAGGC	CCGGCAGTTAAGATCACACCTAT
Rora	CCCCTACTGTTCCTTCACCA	ACAGCTGCCACATCACCTCT
Rorb	TGGACATGACTGGGATCAAA	GCCAGCTGATGGAGTTCTTC
Rorg	AGTCCTTCCGAGAGACATGC	TCCCACATTGACTTCCTCTG
Tbc1d1	CATAAAGAACACACTCCCCAACCT	TGCTTGGCGATGTCCATCT
Vegfa	CTGTAACGATGAAGCCCTGGAG	TGGTGAGGTTTGATCCGCAT

References

Adamovich, Y., Ladeuix, B., Golik, M., Koeners, M.P., and Asher, G. (2017). Rhythmic Oxygen Levels Reset Circadian Clocks through HIF1alpha. Cell Metab 25, 93-101.

Ahrne, E., Glatter, T., Vigano, C., Schubert, C., Nigg, E.A., and Schmidt, A. (2016). Evaluation and Improvement of Quantification Accuracy in Isobaric Mass Tag-Based Protein Quantification Experiments. J Proteome Res 15, 2537-2547.

Allen, D.L., Harrison, B.C., Maass, A., Bell, M.L., Byrnes, W.C., and Leinwand, L.A. (2001). Cardiac and skeletal muscle adaptations to voluntary wheel running in the mouse. J Appl Physiol (1985) 90, 1900-1908.

Andrews, J.L., Zhang, X., McCarthy, J.J., McDearmon, E.L., Hornberger, T.A., Russell, B., Campbell, K.S., Arbogast, S., Reid, M.B., Walker, J.R., et al. (2010). CLOCK and BMAL1 regulate MyoD and are necessary for maintenance of skeletal muscle phenotype and function. Proceedings of the National Academy of Sciences of the United States of America 107, 19090-19095.

Aoi, W., Naito, Y., Takagi, T., Tanimura, Y., Takanami, Y., Kawai, Y., Sakuma, K., Hang, L.P., Mizushima, K., Hirai, Y., et al. (2013). A novel myokine, secreted protein acidic and rich in cysteine (SPARC), suppresses colon tumorigenesis via regular exercise. Gut 62, 882-889.

Arendt, J. (2010). Shift work: coping with the biological clock. Occup Med (Lond) 60, 10-20.

Atkinson, G., and Reilly, T. (1996). Circadian variation in sports performance. Sports Med 21, 292-312.

Bassel-Duby, R., and Olson, E.N. (2006). Signaling pathways in skeletal muscle remodeling. Annu Rev Biochem 75, 19-37.

Bendtsen, J.D., Jensen, L.J., Blom, N., Von Heijne, G., and Brunak, S. (2004). Feature-based prediction of non-classical and leaderless protein secretion. Protein Eng Des Sel 17, 349-356.

Boergesen, M., Pedersen, T.A., Gross, B., van Heeringen, S.J., Hagenbeek, D., Bindesboll, C., Caron, S., Lalloyer, F., Steffensen, K.R., Nebb, H.I., et al. (2012). Genome-wide profiling of liver X receptor, retinoid X receptor, and peroxisome proliferator-activated receptor alpha in mouse liver reveals extensive sharing of binding sites. Mol Cell Biol 32, 852-867.

Bradshaw, A.D. (2012). Diverse biological functions of the SPARC family of proteins. Int J Biochem Cell Biol 44, 480-488.

Bray, N.L., Pimentel, H., Melsted, P., and Pachter, L. (2016). Near-optimal probabilistic RNA-seq quantification. Nat Biotechnol 34, 525-527.

Bruce, C.R., Hoy, A.J., Turner, N., Watt, M.J., Allen, T.L., Carpenter, K., Cooney, G.J., Febbraio, M.A., and Kraegen, E.W. (2009). Overexpression of carnitine palmitoyltransferase-1 in skeletal muscle is sufficient to enhance fatty acid oxidation and improve high-fat diet-induced insulin resistance. Diabetes 58, 550-558.

Bryant, N.J., and Gould, G.W. (2011). SNARE proteins underpin insulin-regulated GLUT4 traffic. Traffic 12, 657-664.

Buhr, E.D., and Takahashi, J.S. (2013). Molecular components of the Mammalian circadian clock. Handb Exp Pharmacol, 3-27.

Cartee, G.D. (2015a). Mechanisms for greater insulin-stimulated glucose uptake in normal and insulin-resistant skeletal muscle after acute exercise. Am J Physiol Endocrinol Metab 309, E949-959.

Cartee, G.D. (2015b). Roles of TBC1D1 and TBC1D4 in insulin- and exercise-stimulated glucose transport of skeletal muscle. Diabetologia 58, 19-30.

Catterall, W.A. (2015). Regulation of Cardiac Calcium Channels in the Fight-or-Flight Response. Curr Mol Pharmacol 8, 12-21.

Cheatham, B. (2000). GLUT4 and company: SNAREing roles in insulin-regulated glucose uptake. Trends Endocrinol Metab 11, 356-361.

Chellappa, S.L., Vujovic, N., Williams, J.S., and Scheer, F. (2019). Impact of Circadian Disruption on Cardiovascular Function and Disease. Trends Endocrinol Metab 30, 767-779.

Cheon, S., Park, N., Cho, S., and Kim, K. (2013). Glucocorticoid-mediated Period2 induction delays the phase of circadian rhythm. Nucleic Acids Res 41, 6161-6174.

Choi, S., Liu, X., Li, P., Akimoto, T., Lee, S.Y., Zhang, M., and Yan, Z. (2005). Transcriptional profiling in mouse skeletal muscle following a single bout of voluntary running: evidence of increased cell proliferation. J Appl Physiol (1985) 99, 2406-2415.

Cohen, P. (2002). The origins of protein phosphorylation. Nat Cell Biol 4, E127-130.

Damiola, F., Le Minh, N., Preitner, N., Kornmann, B., Fleury-Olela, F., and Schibler, U. (2000). Restricted feeding uncouples circadian oscillators in peripheral tissues from the central pacemaker in the suprachiasmatic nucleus. Genes & development 14, 2950-2961.

de Brito, L.C., Rezende, R.A., da Silva Junior, N.D., Tinucci, T., Casarini, D.E., Cipolla-Neto, J., and Forjaz, C.L. (2015). Post-Exercise Hypotension and Its Mechanisms Differ after Morning and Evening Exercise: A Randomized Crossover Study. PLoS One 10, e0132458.

Delavar, H., Nogueira, L., Wagner, P.D., Hogan, M.C., Metzger, D., and Breen, E.C. (2014). Skeletal myofiber VEGF is essential for the exercise training response in adult mice. Am J Physiol Regul Integr Comp Physiol 306, R586-595.

Delezie, J., Dumont, S., Dardente, H., Oudart, H., Grechez-Cassiau, A., Klosen, P., Teboul, M., Delaunay, F., Pevet, P., and Challet, E. (2012). The nuclear receptor REV-ERBalpha is required for the daily balance of carbohydrate and lipid metabolism. FASEB journal : official publication of the Federation of American Societies for Experimental Biology 26, 3321-3335.

Delezie, J., and Handschin, C. (2018). Endocrine Crosstalk Between Skeletal Muscle and the Brain. Front Neurol 9, 698.

Delezie, J., Weihrauch, M., Maier, G., Tejero, R., Ham, D.J., Gill, J.F., Karrer-Cardel, B., Ruegg, M.A., Tabares, L., and Handschin, C. (2019). BDNF is a mediator of glycolytic fiber-type specification in mouse skeletal muscle. Proc Natl Acad Sci U S A 116, 16111-16120.

Deshmukh, A.S., Hawley, J.A., and Zierath, J.R. (2008). Exercise-induced phospho-proteins in skeletal muscle. Int J Obes (Lond) 32 Suppl 4, S18-23.

Deshmukh, A.S., Murgia, M., Nagaraj, N., Treebak, J.T., Cox, J., and Mann, M. (2015). Deep proteomics of mouse skeletal muscle enables quantitation of protein isoforms, metabolic pathways, and transcription factors. Mol Cell Proteomics 14, 841-853.

Di Foggia, V., Zhang, X., Licastro, D., Gerli, M.F., Phadke, R., Muntoni, F., Mourikis, P., Tajbakhsh, S., Ellis, M., Greaves, L.C., et al. (2014). Bmi1 enhances skeletal muscle regeneration through MT1-mediated oxidative stress protection in a mouse model of dystrophinopathy. J Exp Med 211, 2617-2633.

Ding, D., Lawson, K.D., Kolbe-Alexander, T.L., Finkelstein, E.A., Katzmarzyk, P.T., van Mechelen, W., Pratt, M., and Lancet Physical Activity Series 2 Executive, C. (2016). The economic burden of physical inactivity: a global analysis of major non-communicable diseases. Lancet 388, 1311-1324.

Dunant, Y., and Israel, M. (2000). Neurotransmitter release at rapid synapses. Biochimie 82, 289-302.

Duong, K.H.M., and Chun, K.H. (2019). Regulation of glucose transport by RhoA in 3T3-L1 adipocytes and L6 myoblasts. Biochem Biophys Res Commun 519, 880-886.

Durinck, S., Spellman, P.T., Birney, E., and Huber, W. (2009). Mapping identifiers for the integration of genomic datasets with the R/Bioconductor package biomaRt. Nat Protoc 4, 1184-1191.

Dyar, K.A., Ciciliot, S., Tagliazucchi, G.M., Pallafacchina, G., Tothova, J., Argentini, C., Agatea, L., Abraham, R., Ahdesmaki, M., Forcato, M., et al. (2015). The calcineurin-NFAT pathway controls activity-dependent circadian gene expression in slow skeletal muscle. Mol Metab 4, 823-833.

Dyar, K.A., Lutter, D., Artati, A., Ceglia, N.J., Liu, Y., Armenta, D., Jastroch, M., Schneider, S., de Mateo, S., Cervantes, M., et al. (2018). Atlas of Circadian Metabolism Reveals System-wide Coordination and Communication between Clocks. Cell 174, 1571-1585 e1511.

Eckels, E.C., Tapia-Rojo, R., Rivas-Pardo, J.A., and Fernandez, J.M. (2018). The Work of Titin Protein Folding as a Major Driver in Muscle Contraction. Annu Rev Physiol 80, 327-351.

Egan, B., and Zierath, J.R. (2013). Exercise metabolism and the molecular regulation of skeletal muscle adaptation. Cell Metab 17, 162-184.

Elabd, C., Cousin, W., Upadhyayula, P., Chen, R.Y., Chooljian, M.S., Li, J., Kung, S., Jiang, K.P., and Conboy, I.M. (2014). Oxytocin is an age-specific circulating hormone that is necessary for muscle maintenance and regeneration. Nat Commun 5, 4082.

Emrick, M.A., Sadilek, M., Konoki, K., and Catterall, W.A. (2010). Beta-adrenergic-regulated phosphorylation of the skeletal muscle Ca(V)1.1 channel in the fight-or-flight response. Proc Natl Acad Sci U S A 107, 18712-18717.

Esposito, I., Kayed, H., Keleg, S., Giese, T., Sage, E.H., Schirmacher, P., Friess, H., and Kleeff, J. (2007). Tumor-suppressor function of SPARC-like protein 1/Hevin in pancreatic cancer. Neoplasia 9, 8-17.

Evans, J.A., and Davidson, A.J. (2013). Health consequences of circadian disruption in humans and animal models. Prog Mol Biol Transl Sci 119, 283-323.

Ezagouri, S., Zwighaft, Z., Sobel, J., Baillieul, S., Doutreleau, S., Ladeuix, B., Golik, M., Verges, S., and Asher, G. (2019). Physiological and Molecular Dissection of Daily Variance in Exercise Capacity. Cell Metabolism.

Facer-Childs, E., and Brandstaetter, R. (2015). The impact of circadian phenotype and time since awakening on diurnal performance in athletes. Curr Biol 25, 518-522.

Fairbrother, K., Cartner, B., Alley, J.R., Curry, C.D., Dickinson, D.L., Morris, D.M., and Collier, S.R. (2014). Effects of exercise timing on sleep architecture and nocturnal blood pressure in prehypertensives. Vasc Health Risk Manag 10, 691-698.

Fan, W., Waizenegger, W., Lin, C.S., Sorrentino, V., He, M.X., Wall, C.E., Li, H., Liddle, C., Yu, R.T., Atkins, A.R., et al. (2017). PPARdelta Promotes Running Endurance by Preserving Glucose. Cell Metab 25, 1186-1193 e1184.

Fernandez-Verdejo, R., Vanwynsberghe, A.M., Essaghir, A., Demoulin, J.B., Hai, T., Deldicque, L., and Francaux, M. (2017). Activating transcription factor 3 attenuates chemokine and cytokine expression in mouse skeletal muscle after exercise and facilitates molecular adaptation to endurance training. FASEB J 31, 840-851.

Fitts, R.H. (1994). Cellular mechanisms of muscle fatigue. Physiol Rev 74, 49-94.

Frenette, J., Cai, B., and Tidball, J.G. (2000). Complement activation promotes muscle inflammation during modified muscle use. Am J Pathol 156, 2103-2110.

Fuller, M.D., Emrick, M.A., Sadilek, M., Scheuer, T., and Catterall, W.A. (2010). Molecular mechanism of calcium channel regulation in the fight-or-flight response. Sci Signal 3, ra70.

Gabriel, B.M., and Zierath, J.R. (2019). Circadian rhythms and exercise - re-setting the clock in metabolic disease. Nat Rev Endocrinol 15, 197-206.

Gan, Z., Fu, T., Kelly, D.P., and Vega, R.B. (2018). Skeletal muscle mitochondrial remodeling in exercise and diseases. Cell Res 28, 969-980.

Garcia, D., and Shaw, R.J. (2017). AMPK: Mechanisms of Cellular Energy Sensing and Restoration of Metabolic Balance. Mol Cell 66, 789-800.

Gentleman, R.C., Carey, V.J., Bates, D.M., Bolstad, B., Dettling, M., Dudoit, S., Ellis, B., Gautier, L., Ge, Y., Gentry, J., et al. (2004). Bioconductor: open software development for computational biology and bioinformatics. Genome Biol 5, R80.

Ghosh, S., Golbidi, S., Werner, I., Verchere, B.C., and Laher, I. (2010). Selecting exercise regimens and strains to modify obesity and diabetes in rodents: an overview. Clin Sci (Lond) 119, 57-74.

Gordon, B.S., Rossetti, M.L., and Eroshkin, A.M. (2019). Arrdc2 and Arrdc3 elicit divergent changes in gene expression in skeletal muscle following anabolic and catabolic stimuli. Physiol Genomics 51, 208-217.

Green, H.J. (1997). Mechanisms of muscle fatigue in intense exercise. J Sports Sci 15, 247-256.

Gross, D.N., van den Heuvel, A.P., and Birnbaum, M.J. (2008). The role of FoxO in the regulation of metabolism. Oncogene 27, 2320-2336.

Hardie, D.G. (2004). The AMP-activated protein kinase pathway--new players upstream and downstream. J Cell Sci 117, 5479-5487.

Hargreaves, M., and Spriet, L.L. (2018). Exercise Metabolism: Fuels for the Fire. Cold Spring Harb Perspect Med 8.

Hawley, J.A., Hargreaves, M., Joyner, M.J., and Zierath, J.R. (2014). Integrative biology of exercise. Cell 159, 738-749.

Hoffman, N.J., Parker, B.L., Chaudhuri, R., Fisher-Wellman, K.H., Kleinert, M., Humphrey, S.J., Yang, P., Holliday, M., Trefely, S., Fazakerley, D.J., et al. (2015). Global Phosphoproteomic Analysis of Human Skeletal Muscle Reveals a Network of Exercise-Regulated Kinases and AMPK Substrates. Cell Metab 22, 922-935.

Holloszy, J.O. (1967). Biochemical adaptations in muscle. Effects of exercise on mitochondrial oxygen uptake and respiratory enzyme activity in skeletal muscle. J Biol Chem 242, 2278-2282.

Hood, S., and Amir, S. (2017). The aging clock: circadian rhythms and later life. J Clin Invest 127, 437-446.

Hui, X., Zhu, W., Wang, Y., Lam, K.S., Zhang, J., Wu, D., Kraegen, E.W., Li, Y., and Xu, A. (2009). Major urinary protein-1 increases energy expenditure and improves glucose intolerance through enhancing mitochondrial function in skeletal muscle of diabetic mice. J Biol Chem 284, 14050-14057.

Huttlin, E.L., Jedrychowski, M.P., Elias, J.E., Goswami, T., Rad, R., Beausoleil, S.A., Villen, J., Haas, W., Sowa, M.E., and Gygi, S.P. (2010). A tissue-specific atlas of mouse protein phosphorylation and expression. Cell 143, 1174-1189.

James, S.M., Honn, K.A., Gaddameedhi, S., and Van Dongen, H.P.A. (2017). Shift Work: Disrupted Circadian Rhythms and Sleep-Implications for Health and Well-Being. Curr Sleep Med Rep 3, 104-112.

Jensen, J., Rustad, P.I., Kolnes, A.J., and Lai, Y.C. (2011). The role of skeletal muscle glycogen breakdown for regulation of insulin sensitivity by exercise. Front Physiol 2, 112.

Jensen, T.L., Kiersgaard, M.K., Sorensen, D.B., and Mikkelsen, L.F. (2013). Fasting of mice: a review. Lab Anim 47, 225-240.

Johnson, L.N. (1992). Glycogen phosphorylase: control by phosphorylation and allosteric effectors. FASEB J 6, 2274-2282.

Jordan, S.D., Kriebs, A., Vaughan, M., Duglan, D., Fan, W., Henriksson, E., Huber, A.L., Papp, S.J., Nguyen, M., Afetian, M., et al. (2017). CRY1/2 Selectively Repress PPARdelta and Limit Exercise Capacity. Cell Metab 26, 243-255 e246.

Karolchik, D., Barber, G.P., Casper, J., Clawson, H., Cline, M.S., Diekhans, M., Dreszer, T.R., Fujita, P.A., Guruvadoo, L., Haeussler, M., et al. (2014). The UCSC Genome Browser database: 2014 update. Nucleic Acids Res 42, D764-770.

Kasai, H., Takahashi, N., and Tokumaru, H. (2012). Distinct initial SNARE configurations underlying the diversity of exocytosis. Physiol Rev 92, 1915-1964.

Katsuoka, F., Motohashi, H., Ishii, T., Aburatani, H., Engel, J.D., and Yamamoto, M. (2005). Genetic evidence that small maf proteins are essential for the activation of antioxidant response element-dependent genes. Mol Cell Biol 25, 8044-8051.

Kinouchi, K., Magnan, C., Ceglia, N., Liu, Y., Cervantes, M., Pastore, N., Huynh, T., Ballabio, A., Baldi, P., Masri, S., et al. (2018). Fasting Imparts a Switch to Alternative Daily Pathways in Liver and Muscle. Cell Rep 25, 3299-3314 e3296.

Kiral, F.R., Kohrs, F.E., Jin, E.J., and Hiesinger, P.R. (2018). Rab GTPases and Membrane Trafficking in Neurodegeneration. Curr Biol 28, R471-R486.

Kozomara, A., and Griffiths-Jones, S. (2011). miRBase: integrating microRNA annotation and deep-sequencing data. Nucleic Acids Res 39, D152-157.

Kramer, H.F., and Goodyear, L.J. (2007). Exercise, MAPK, and NF-kappaB signaling in skeletal muscle. J Appl Physiol (1985) 103, 388-395.

Legård, G.E., and Pedersen, B.K. (2019). Chapter 13 - Muscle as an Endocrine Organ. In Muscle and Exercise Physiology. J.A. Zoladz, ed. (Academic Press), pp. 285-307.

Li, T., Liu, X., Yang, A., Fu, W., Yin, F., and Zeng, X. (2017). Associations of tumor suppressor SPARCL1 with cancer progression and prognosis. Oncol Lett 14, 2603-2610.

Lin, J., Wu, H., Tarr, P.T., Zhang, C.Y., Wu, Z., Boss, O., Michael, L.F., Puigserver, P., Isotani, E., Olson, E.N., et al. (2002). Transcriptional co-activator PGC-1 alpha drives the formation of slow-twitch muscle fibres. Nature 418, 797-801.

Lobelo, F., Stoutenberg, M., and Hutber, A. (2014). The Exercise is Medicine Global Health Initiative: a 2014 update. Br J Sports Med 48, 1627-1633.

Loizides-Mangold, U., Perrin, L., Vandereycken, B., Betts, J.A., Walhin, J.P., Templeman, I., Chanon, S., Weger, B.D., Durand, C., Robert, M., et al. (2017). Lipidomics reveals diurnal lipid oscillations in human skeletal muscle persisting in cellular myotubes cultured in vitro. Proc Natl Acad Sci U S A 114, E8565-E8574.

Love, M.I., Huber, W., and Anders, S. (2014). Moderated estimation of fold change and dispersion for RNA-seq data with DESeq2. Genome Biol 15, 550.

Ma, X.M., and Blenis, J. (2009). Molecular mechanisms of mTOR-mediated translational control. Nat Rev Mol Cell Biol 10, 307-318.

Mack, H.I., Zheng, B., Asara, J.M., and Thomas, S.M. (2012). AMPK-dependent phosphorylation of ULK1 regulates ATG9 localization. Autophagy 8, 1197-1214.

Mahoney, D.J., Parise, G., Melov, S., Safdar, A., and Tarnopolsky, M.A. (2005). Analysis of global mRNA expression in human skeletal muscle during recovery from endurance exercise. FASEB J 19, 1498-1500.

McCarthy, J.J., Andrews, J.L., McDearmon, E.L., Campbell, K.S., Barber, B.K., Miller, B.H., Walker, J.R., Hogenesch, J.B., Takahashi, J.S., and Esser, K.A. (2007). Identification of the circadian transcriptome in adult mouse skeletal muscle.

McKie, G.L., Medak, K.D., Knuth, C.M., Shamshoum, H., Townsend, L.K., Peppler, W.T., and Wright, D.C. (2019). Housing temperature affects the acute and chronic metabolic adaptations to exercise in mice. J Physiol 597, 4581-4600.

Meijer, J.H., and Robbers, Y. (2014). Wheel running in the wild. Proc Biol Sci 281.

Miller, B.H., McDearmon, E.L., Panda, S., Hayes, K.R., Zhang, J., Andrews, J.L., Antoch, M.P., Walker, J.R., Esser, K.A., Hogenesch, J.B., et al. (2007). Circadian and CLOCK-controlled regulation of the mouse transcriptome and cell proliferation. Proc Natl Acad Sci U S A 104, 3342-3347.

Moon, H.Y., Becke, A., Berron, D., Becker, B., Sah, N., Benoni, G., Janke, E., Lubejko, S.T., Greig, N.H., Mattison, J.A., et al. (2016). Running-Induced Systemic Cathepsin B Secretion Is Associated with Memory Function. Cell Metab 24, 332-340.

Morris, S., Geoghegan, N.D., Sadler, J.B.A., Koester, A.M., Black, H.L., Laub, M., Miller, L., Heffernan, L., Simpson, J.C., Mastick, C.C., et al. (2020). Characterisation of GLUT4 trafficking in HeLa cells: comparable kinetics and orthologous trafficking mechanisms to 3T3-L1 adipocytes. PeerJ 8, e8751.

Muoio, D.M., MacLean, P.S., Lang, D.B., Li, S., Houmard, J.A., Way, J.M., Winegar, D.A., Corton, J.C., Dohm, G.L., and Kraus, W.E. (2002). Fatty acid homeostasis and induction of lipid regulatory genes in skeletal muscles of peroxisome proliferator-activated receptor (PPAR) alpha knock-out mice. Evidence for compensatory regulation by PPAR delta. J Biol Chem 277, 26089-26097.

Nanjappa, V., Thomas, J.K., Marimuthu, A., Muthusamy, B., Radhakrishnan, A., Sharma, R., Ahmad Khan, A., Balakrishnan, L., Sahasrabuddhe, N.A., Kumar, S., et al. (2014). Plasma Proteome Database as a resource for proteomics research: 2014 update. Nucleic Acids Res 42, D959-965.

Nielsen, H. (2017). Predicting Secretory Proteins with SignalP. Methods Mol Biol 1611, 59-73.

Onder, Y., Laothamatas, I., Berto, S., Sewart, K., Kilaru, G., Bordieanu, B., Stubblefield, J.J., Konopka, G., Mishra, P., and Green, C.B. (2019). The Circadian Protein Nocturnin Regulates Metabolic Adaptation in Brown Adipose Tissue. iScience 19, 83-92.

Panda, S. (2016). Circadian physiology of metabolism. Science 354, 1008-1015.

Pastore, S., and Hood, D.A. (2013). Endurance training ameliorates the metabolic and performance characteristics of circadian Clock mutant mice. J Appl Physiol (1985) 114, 1076-1084.

Pedersen, B.K., and Febbraio, M.A. (2008). Muscle as an endocrine organ: Focus on muscle-derived interleukin-6. Physiological Reviews 88, 1379-1406.

Pedersen, B.K., and Saltin, B. (2015). Exercise as medicine - evidence for prescribing exercise as therapy in 26 different chronic diseases. Scand J Med Sci Sports 25 Suppl 3, 1-72.

Pederson, B.A., Cope, C.R., Schroeder, J.M., Smith, M.W., Irimia, J.M., Thurberg, B.L., DePaoli-Roach, A.A., and Roach, P.J. (2005). Exercise capacity of mice genetically lacking muscle glycogen synthase: in mice, muscle glycogen is not essential for exercise. J Biol Chem 280, 17260-17265.

Peek, C.B., Levine, D.C., Cedernaes, J., Taguchi, A., Kobayashi, Y., Tsai, S.J., Bonar, N.A., McNulty, M.R., Ramsey, K.M., and Bass, J. (2017). Circadian Clock Interaction with HIF1alpha Mediates Oxygenic Metabolism and Anaerobic Glycolysis in Skeletal Muscle. Cell Metab 25, 86-92.

Perez-Schindler, J., Kanhere, A., Edwards, L., Allwood, J.W., Dunn, W.B., Schenk, S., and Philp, A. (2017). Exercise and high-fat feeding remodel transcript-metabolite interactive networks in mouse skeletal muscle. Sci Rep 7, 13485.

Perrin, L., Loizides-Mangold, U., Chanon, S., Gobet, C., Hulo, N., Isenegger, L., Weger, B.D., Migliavacca, E., Charpagne, A., Betts, J.A., et al. (2018). Transcriptomic analyses reveal rhythmic and CLOCK-driven pathways in human skeletal muscle. Elife 7.

Pessin, J.E., Thurmond, D.C., Elmendorf, J.S., Coker, K.J., and Okada, S. (1999). Molecular basis of insulin-stimulated GLUT4 vesicle trafficking. Location! Location! Location! J Biol Chem 274, 2593-2596.

Post, H., Penning, R., Fitzpatrick, M.A., Garrigues, L.B., Wu, W., MacGillavry, H.D., Hoogenraad, C.C., Heck, A.J., and Altelaar, A.F. (2017). Robust, Sensitive, and Automated Phosphopeptide Enrichment Optimized for Low Sample Amounts Applied to Primary Hippocampal Neurons. J Proteome Res 16, 728-737.

Pruitt, K.D., Brown, G.R., Hiatt, S.M., Thibaud-Nissen, F., Astashyn, A., Ermolaeva, O., Farrell, C.M., Hart, J., Landrum, M.J., McGarvey, K.M., et al. (2014). RefSeq: an update on mammalian reference sequences. Nucleic Acids Res 42, D756-763.

Reimand, J., Arak, T., Adler, P., Kolberg, L., Reisberg, S., Peterson, H., and Vilo, J. (2016). g:Profiler-a web server for functional interpretation of gene lists (2016 update). Nucleic Acids Res 44, W83-89.

Reznick, J., Preston, E., Wilks, D.L., Beale, S.M., Turner, N., and Cooney, G.J. (2013). Altered feeding differentially regulates circadian rhythms and energy metabolism in liver and muscle of rats. Biochimica et biophysica acta 1832, 228-238.

Richter, E.A., and Hargreaves, M. (2013). Exercise, GLUT4, and skeletal muscle glucose uptake. Physiol Rev 93, 993-1017.

Romere, C., Duerrschmid, C., Bournat, J., Constable, P., Jain, M., Xia, F., Saha, P.K., Del Solar, M., Zhu, B., York, B., et al. (2016). Asprosin, a Fasting-Induced Glucogenic Protein Hormone. Cell 165, 566-579.

Rose, M., Kloten, V., Noetzel, E., Gola, L., Ehling, J., Heide, T., Meurer, S.K., Gaiko-Shcherbak, A., Sechi, A.S., Huth, S., et al. (2017). ITIH5 mediates epigenetic reprogramming of breast cancer cells. Mol Cancer 16, 44.

Ruas, J.L., White, J.P., Rao, R.R., Kleiner, S., Brannan, K.T., Harrison, B.C., Greene, N.P., Wu, J., Estall, J.L., Irving, B.A., et al. (2012). A PGC-1alpha isoform induced by resistance training regulates skeletal muscle hypertrophy. Cell 151, 1319-1331.

Sakamoto, K., and Holman, G.D. (2008). Emerging role for AS160/TBC1D4 and TBC1D1 in the regulation of GLUT4 traffic. Am J Physiol Endocrinol Metab 295, E29-37.

Salazar, C., and Hofer, T. (2009). Multisite protein phosphorylation--from molecular mechanisms to kinetic models. FEBS J 276, 3177-3198.

Salgado-Delgado, R., Angeles-Castellanos, M., Buijs, M.R., and Escobar, C. (2008). Internal desynchronization in a model of night-work by forced activity in rats. Neuroscience 154, 922-931.

Sanchez, A.M., Candau, R.B., and Bernardi, H. (2014). FoxO transcription factors: their roles in the maintenance of skeletal muscle homeostasis. Cell Mol Life Sci 71, 1657-1671.

Sasaki, H., Hattori, Y., Ikeda, Y., Kamagata, M., Iwami, S., Yasuda, S., Tahara, Y., and Shibata, S. (2016). Forced rather than voluntary exercise entrains peripheral clocks via a corticosterone/noradrenaline increase in PER2::LUC mice. Sci Rep 6, 27607.

Sasaki, K., Kurahara, H., Young, E.D., Natsugoe, S., Ijichi, A., Iwakuma, T., and Welch, D.R. (2017). Genome-wide in vivo RNAi screen identifies ITIH5 as a metastasis suppressor in pancreatic cancer. Clin Exp Metastasis 34, 229-239.

Sato, S., Basse, A.L., Schönke, M., Chen, S., Samad, M., Altıntaş, A., Laker, R.C., Dalbram, E., Barrès, R., Baldi, P., et al. (2019). Time of Exercise Specifies the Impact on Muscle Metabolic Pathways and Systemic Energy Homeostasis. Cell Metabolism.

Sato, S., Parr, E.B., Devlin, B.L., Hawley, J.A., and Sassone-Corsi, P. (2018). Human metabolomics reveal daily variations under nutritional challenges specific to serum and skeletal muscle. Mol Metab 16, 1-11.

Savikj, M., Gabriel, B.M., Alm, P.S., Smith, J., Caidahl, K., Bjornholm, M., Fritz, T., Krook, A., Zierath, J.R., and Wallberg-Henriksson, H. (2019). Afternoon exercise is more efficacious than morning exercise at improving blood glucose levels in individuals with type 2 diabetes: a randomised crossover trial. Diabetologia 62, 233-237.

Schnyder, S., and Handschin, C. (2015). Skeletal muscle as an endocrine organ: PGC-1alpha, myokines and exercise. Bone 80, 115-125.

Schwartsburd, P. (2019). Cancer-Induced Reprogramming of Host Glucose Metabolism: "Vicious Cycle" Supporting Cancer Progression. Front Oncol 9, 218.

Schwenk, J.M., Omenn, G.S., Sun, Z., Campbell, D.S., Baker, M.S., Overall, C.M., Aebersold, R., Moritz, R.L., and Deutsch, E.W. (2017). The Human Plasma Proteome Draft of 2017: Building on the Human Plasma PeptideAtlas from Mass Spectrometry and Complementary Assays. J Proteome Res 16, 4299-4310.

Semenza, G.L. (2012). Hypoxia-inducible factors in physiology and medicine. Cell 148, 399-408.

Shulman, R.G., and Rothman, D.L. (2001). The "glycogen shunt" in exercising muscle: A role for glycogen in muscle energetics and fatigue. Proc Natl Acad Sci U S A 98, 457-461.

Soneson, C., Love, M.I., and Robinson, M.D. (2015). Differential analyses for RNA-seq: transcript-level estimates improve gene-level inferences. F1000Res 4, 1521.

Stenmark, H. (2009). Rab GTPases as coordinators of vesicle traffic. Nat Rev Mol Cell Biol 10, 513-525.

Stewart, R., Akhmedov, D., Robb, C., Leiter, C., and Berdeaux, R. (2013). Regulation of SIK1 abundance and stability is critical for myogenesis. Proc Natl Acad Sci U S A 110, 117-122.

Sulli, G., Manoogian, E.N.C., Taub, P.R., and Panda, S. (2018). Training the Circadian Clock, Clocking the Drugs, and Drugging the Clock to Prevent, Manage, and Treat Chronic Diseases. Trends Pharmacol Sci 39, 812-827.

Summermatter, S., Bouzan, A., Pierrel, E., Melly, S., Stauffer, D., Gutzwiller, S., Nolin, E., Dornelas, C., Fryer, C., Leighton-Davies, J., et al. (2017). Blockade of Metallothioneins 1 and 2 Increases Skeletal Muscle Mass and Strength. Mol Cell Biol 37.

Sun, G., Cheng, S.Y., Chen, M., Lim, C.J., and Pallen, C.J. (2012). Protein tyrosine phosphatase alpha phosphotyrosyl-789 binds BCAR3 to position Cas for activation at integrin-mediated focal adhesions. Mol Cell Biol 32, 3776-3789.

Suwanmajo, T., and Krishnan, J. (2015). Mixed mechanisms of multi-site phosphorylation. J R Soc Interface 12.

Svensson, M., Rosvall, P., Boza-Serrano, A., Andersson, E., Lexell, J., and Deierborg, T. (2016). Forced treadmill exercise can induce stress and increase neuronal damage in a mouse model of global cerebral ischemia. Neurobiol Stress 5, 8-18.

Sylow, L., Kleinert, M., Richter, E.A., and Jensen, T.E. (2017). Exercise-stimulated glucose uptake - regulation and implications for glycaemic control. Nat Rev Endocrinol 13, 133-148.

Sylow, L., Nielsen, I.L., Kleinert, M., Moller, L.L., Ploug, T., Schjerling, P., Bilan, P.J., Klip, A., Jensen, T.E., and Richter, E.A. (2016). Rac1 governs exercise-stimulated glucose uptake in skeletal muscle through regulation of GLUT4 translocation in mice. J Physiol 594, 4997-5008.

Takenaka, N., Sumi, Y., Matsuda, K., Fujita, J., Hosooka, T., Noguchi, T., Aiba, A., and Satoh, T. (2015). Role for RalA downstream of Rac1 in skeletal muscle insulin signalling. Biochem J 469, 445-454.

Tanaka, M., Miyoshi, J., Ishizaki, H., Togawa, A., Ohnishi, K., Endo, K., Matsubara, K., Mizoguchi, A., Nagano, T., Sato, M., et al. (2001). Role of Rab3 GDP/GTP exchange protein in synaptic vesicle trafficking at the mouse neuromuscular junction. Mol Biol Cell 12, 1421-1430.

Turtoi, A., Musmeci, D., Naccarato, A.G., Scatena, C., Ortenzi, V., Kiss, R., Murtas, D., Patsos, G., Mazzucchelli, G., De Pauw, E., et al. (2012). Sparc-like protein 1 is a new marker of human glioma progression. J Proteome Res 11, 5011-5021.

van Moorsel, D., Hansen, J., Havekes, B., Scheer, F.A.J.L., Jörgensen, J.A., Hoeks, J., Schrauwen-Hinderling, V.B., Duez, H., Lefebvre, P., Schaper, N.C., et al. (2016). Demonstration of a day-night rhythm in human skeletal muscle oxidative capacity. Molecular Metabolism 5, 635-645.

Vandenboom, R. (2016). Modulation of Skeletal Muscle Contraction by Myosin Phosphorylation. Compr Physiol 7, 171-212.

Veeck, J., Chorovicer, M., Naami, A., Breuer, E., Zafrakas, M., Bektas, N., Durst, M., Kristiansen, G., Wild, P.J., Hartmann, A., et al. (2008). The extracellular matrix protein ITIH5 is a novel prognostic marker in invasive node-negative breast cancer and its aberrant expression is caused by promoter hypermethylation. Oncogene 27, 865-876.

Wang, Y., Yang, F., Gritsenko, M.A., Wang, Y., Clauss, T., Liu, T., Shen, Y., Monroe, M.E., Lopez-Ferrer, D., Reno, T., et al. (2011). Reversed-phase chromatography with multiple fraction concatenation strategy for proteome profiling of human MCF10A cells. Proteomics 11, 2019-2026.

Watt, K.I., Goodman, C.A., Hornberger, T.A., and Gregorevic, P. (2018). The Hippo Signaling Pathway in the Regulation of Skeletal Muscle Mass and Function. Exerc Sport Sci Rev 46, 92-96.

Wehrens, S.M.T., Christou, S., Isherwood, C., Middleton, B., Gibbs, M.A., Archer, S.N., Skene, D.J., and Johnston, J.D. (2017). Meal Timing Regulates the Human Circadian System. Curr Biol 27, 1768-1775 e1763.

Wei-Lapierre, L., Carrell, E.M., Boncompagni, S., Protasi, F., and Dirksen, R.T. (2013). Orai1-dependent calcium entry promotes skeletal muscle growth and limits fatigue. Nat Commun 4, 2805.

Wende, A.R., Huss, J.M., Schaeffer, P.J., Giguere, V., and Kelly, D.P. (2005). PGC-1alpha coactivates PDK4 gene expression via the orphan nuclear receptor ERRalpha: a mechanism for transcriptional control of muscle glucose metabolism. Mol Cell Biol 25, 10684-10694.

WHO (2010). Global Recommendations on Physical Activity for Health. In Global Recommendations on Physical Activity for Health (Geneva).

Wiecek, M., Szymura, J., Maciejczyk, M., Kantorowicz, M., and Szygula, Z. (2018). Acute Anaerobic Exercise Affects the Secretion of Asprosin, Irisin, and Other Cytokines - A Comparison Between Sexes. Front Physiol 9, 1782.

Wolff, G., and Esser, K.A. (2012). Scheduled exercise phase shifts the circadian clock in skeletal muscle. Medicine and science in sports and exercise 44, 1663-1670.

Xirouchaki, C.E., Mangiafico, S.P., Bate, K., Ruan, Z., Huang, A.M., Tedjosiswoyo, B.W., Lamont, B., Pong, W., Favaloro, J., Blair, A.R., et al. (2016). Impaired glucose metabolism and exercise capacity with muscle-specific glycogen synthase 1 (gys1) deletion in adult mice. Mol Metab 5, 221-232.

Yamanaka, Y., Hashimoto, S., Takasu, N.N., Tanahashi, Y., Nishide, S.Y., Honma, S., and Honma, K. (2015). Morning and evening physical exercise differentially regulate the autonomic nervous system during nocturnal sleep in humans. Am J Physiol Regul Integr Comp Physiol 309, R1112-1121.

Yasumoto, Y., Nakao, R., and Oishi, K. (2015). Free access to a running-wheel advances the phase of behavioral and physiological circadian rhythms and peripheral molecular clocks in mice. PLoS One 10, e0116476.

Yuan, M., Li, W., Zhu, Y., Yu, B., and Wu, J. (2020). Asprosin: A Novel Player in Metabolic Diseases. Front Endocrinol (Lausanne) 11, 64.

Zambon, A.C., McDearmon, E.L., Salomonis, N., Vranizan, K.M., Johansen, K.L., Adey, D., Takahashi, J.S., Schambelan, M., and Conklin, B.R. (2003). Time- and exercise-dependent gene regulation in human skeletal muscle. Genome Biol 4, R61.

Zanivan, S., Gnad, F., Wickstrom, S.A., Geiger, T., Macek, B., Cox, J., Fassler, R., and Mann, M. (2008). Solid tumor proteome and phosphoproteome analysis by high resolution mass spectrometry. J Proteome Res 7, 5314-5326.

Zhang, C., Wang, C., Li, Y., Miwa, T., Liu, C., Cui, W., Song, W.C., and Du, J. (2017). Complement C3a signaling facilitates skeletal muscle regeneration by regulating monocyte function and trafficking. Nat Commun 8, 2078.

Zhang, R., Lahens, N.F., Ballance, H.I., Hughes, M.E., and Hogenesch, J.B. (2014). A circadian gene expression atlas in mammals: implications for biology and medicine. Proceedings of the National Academy of Sciences of the United States of America 111, 16219-16224.

Zhao, J., Brault, J.J., Schild, A., Cao, P., Sandri, M., Schiaffino, S., Lecker, S.H., and Goldberg, A.L. (2007). FoxO3 coordinately activates protein degradation by the autophagic/lysosomal and proteasomal pathways in atrophying muscle cells. Cell Metab 6, 472-483.

Zhou, Y., Jiang, L., and Rui, L. (2009). Identification of MUP1 as a regulator for glucose and lipid metabolism in mice. J Biol Chem 284, 11152-11159.

Zong, H., Wang, C.C., Vaitheesvaran, B., Kurland, I.J., Hong, W., and Pessin, J.E. (2011). Enhanced energy expenditure, glucose utilization, and insulin sensitivity in VAMP8 null mice. Diabetes 60, 30-38.

Manuscript 2

RORα deletion alters mouse spontaneous locomotion and skeletal muscle ROS metabolism

Geraldine Maier[1], Julien Delezie[1], Pål Westermark[2], Gesa Santos[1], Joaquín Pérez-Schindler[1], Danilo Ritz[1] and Christoph Handschin[1,#]

[1]Biozentrum, University of Basel, CH-4056 Basel, Switzerland

[2]Leibniz-Institut für Nutztierbiologie, Institut für Genetik und Biometrie, D- 18196 Dummerstorf, Germany

[#]*Correspondence to:* Christoph Handschin, Biozentrum, University of Basel, Klingelbergstrasse 50/70, CH-4056 Basel, Switzerland, phone: +41 61 207 2378, fax: +41 61 207 2208, email: christoph.handschin@unibas.ch

In preparation

Abstract

Objective: Skeletal muscle is a highly metabolic organ that plays a significant role in whole-body homeostasis. About 10-20% of the skeletal muscle transcriptome exhibits circadian oscillation, leading to fluctuations in muscle tissue function, including insulin sensitivity, mitochondrial respiration, lipid, and glucose metabolism. However, the role of circadian clock components in skeletal muscle remains poorly defined. Here, we evaluated the specific contribution of RORα in skeletal muscle for the regulation of metabolism and exercise behavior.

Methods: We generated mice lacking the *Rorα* gene, specifically in skeletal muscle (MKO). Assessment of mouse behavior and metabolism, together with the evaluation of skeletal muscle gene and protein expression, was performed under basal fed conditions and in response to different running exercise challenges.

Results: We found that skeletal muscle-specific deletion of RORα significantly decreased spontaneous wheel-running activity in the absence of significant alteration in muscle structure and systemic metabolism. Our transcriptome and proteome investigations of exercised muscles revealed a decrease in the expression of key regulators of oxidative stress. Furthermore, upon exposure to hypoxia, causing abnormal ROS elevation or H_2O_2, we reveal that RORα overexpression protects from cell death.

Conclusion: Our data suggest that skeletal muscle RORα is important for ROS detoxification and thus the adaptations of skeletal muscle physiology to chronic physical activity.

Introduction

Circadian clocks are evolutionary conserved time-keeping mechanisms adjusting behavioral and physiological processes to daily changes in the environment (Takahashi, 2017). Importantly, perturbations of the circadian machinery (e.g., shift-work, disease, and aging) are associated with various pathologies, including obesity, diabetes, cancer, and cardiovascular complications (Mayeuf-Louchart et al., 2017; Sulli et al., 2018).

Skeletal muscle is the largest organ of the human body and an essential regulator of whole-body energy homeostasis (Delezie and Handschin, 2018). About 10-20% of the transcriptome is oscillating with a 24-h period in human (Perrin et al., 2018; van Moorsel et al., 2016) and in mouse muscles (McCarthy et al., 2007; Miller et al., 2007; Zhang et al., 2014). Most of these transcripts associate with a broad range of cellular functions, e.g., transcriptional regulation, cell signaling, protein, and energy metabolism (McCarthy et al., 2007). Accordingly, glucose and lipid-related metabolites oscillate in a cell-autonomous manner in both human and mouse muscle tissues (Aviram et al., 2016; Dyar et al., 2018; Loizides-Mangold et al., 2017; Sato et al., 2018), and clock gene perturbation in the mouse is associated with disrupted muscle function such as growth and repair and insulin sensitivity (Andrews et al., 2010; Dyar et al., 2014; Loizides-Mangold et al., 2017; Woldt et al., 2013). Moreover, global clock KO mouse models often show an exercise phenotype, in that spontaneous nighttime locomotor activity or forced endurance performance is significantly altered (Delezie et al., 2016; Jordan et al., 2017; Woldt et al., 2013; Zheng et al., 1999).

The Retinoic acid receptor-related orphan receptor α (RORα; NR1F1) is a transcription factor belonging to the steroid/thyroid hormone receptor superfamily. It is a key regulator of the circadian clock (Akashi and Takumi, 2005; Sato et al., 2004) and various biological functions such as cerebellum development, cancer, and hepatic lipid homeostasis (Kim et al., 2017). Interestingly, whole-body deficiency of RORα alters insulin sensitivity and glucose uptake in mouse skeletal muscle (Lau et al., 2011). However, this mouse model develops an ataxic phenotype, which severely impacts spontaneous locomotion and, thus, muscle function (Dussault et al., 1998; Steinmayr et al., 1998).

We thus generated a muscle-specific RORα knockout mouse model (MKO) and used different exercise protocols, -omics and cell culture approach, to study the specific role of RORα in skeletal muscle physiology.

Results

Muscle-specific RORα deletion leads to slight alterations in energy balance and muscle fiber type.

Deletion of RORα in skeletal muscle was achieved by crossing mice with a floxed *RORα* allele together with mice that express Cre recombinase under the control of the skeletal muscle-specific HAS-promoter (see method "animals"); hereafter called RORα MKO mice. The deletion of RORα was detected in the skeletal muscle and slightly in the heart, as determined by qPCR analysis of the RORα mRNA **(Figure 1A)**. Moreover, the protein deletion in the gastrocnemius (GAS) was assessed using western blot (**Figure 1B**). General locomotor activity did not differ between the control littermates and the RORα MKO mice (**Figure 1C**), while core body temperature was increased during the inactive phase (**Supp. Figure 1A**). Under *ad libitum* feeding conditions, daily food intake (**Supp. Figure 1D**) and body mass were comparable between littermate controls and RORα MKO mice (**Figure 1D**). Similarly, lean and fat mass were unchanged in RORα MKO (**Figure 1D**).

We then used a comprehensive animal metabolic monitoring system (CLAMS) to evaluate energy homeostasis in RORα-MKO mice in a broad manner. In basal fed conditions, O_2 consumption, and energy expenditure were higher in RORα MKO mice (**Supp. Figure 1C-D**), while energy substrate utilization (respiratory exchange ratio; RER) was unaltered (**Supp. Figure 1E**). The skeletal muscle structure and structural integrity were unchanged, as determined by H&E staining (**Figure 1E**). However, the fiber type composition of the oxidative part of the tibialis anterior was shifted towards more type 2X fibers in the RORα MKO mice (**Figure 1F** and **Supp. Figure 1G**).

These results indicate that the deletion of RORα specifically affects core body temperature together with energy expenditure. Moreover, loss of RORα slightly alters muscle fiber composition.

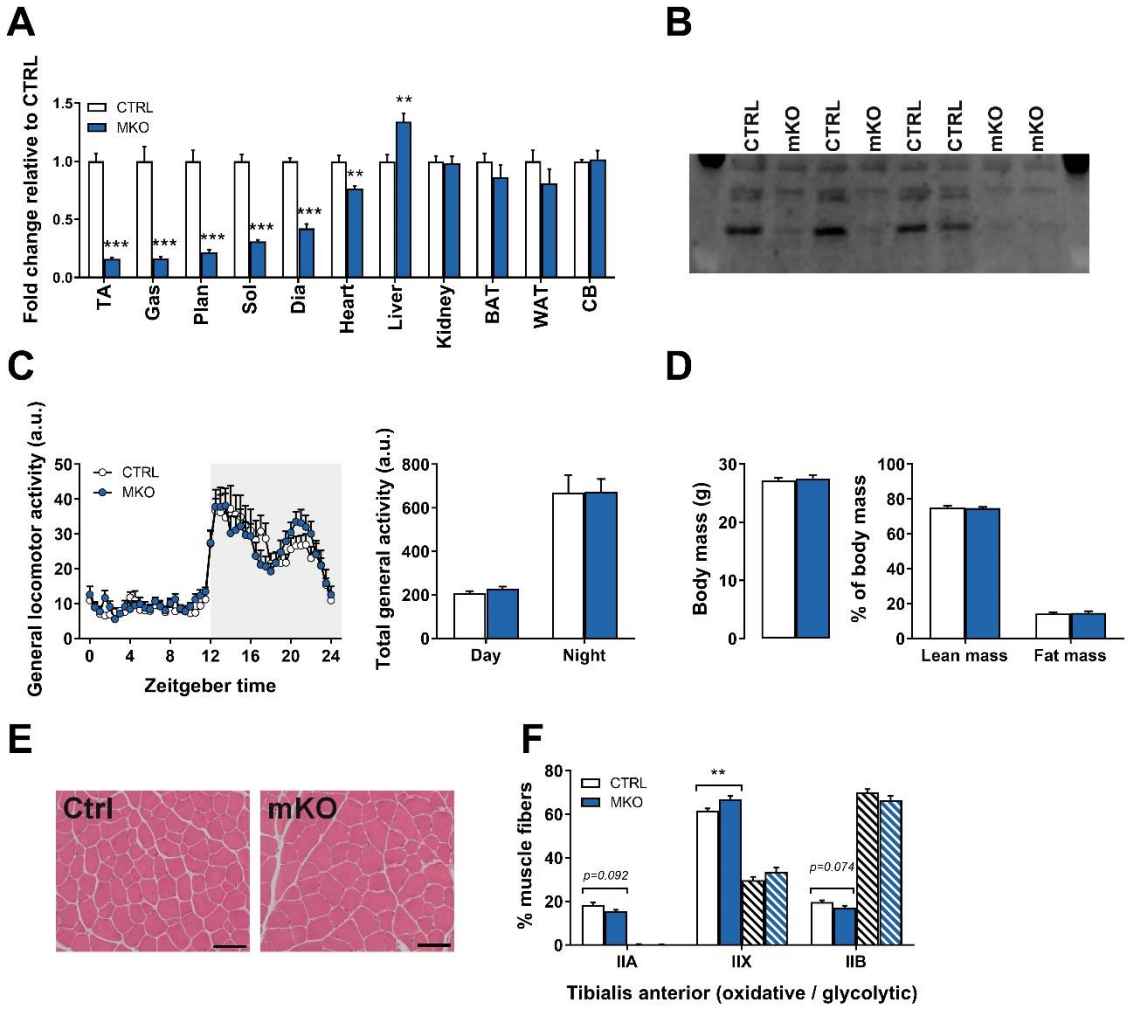

Figure 1. RORα deletion is skeletal muscle does not affect muscle structure. (A) RORα mRNA is decreased by 80% in skeletal muscle and slightly in the heart. (B)Western blot assessment of RORα KO in gastrocnemius muscle. (C) General locomotor activity is unchanged between groups. (D) Body mass and composition are unchanged in MKO mice compared to CTRL. (E) H&E staining of tibialis anterior (TA) muscle shows no difference in muscle integrity. (D) Fiber type shift towards type 2X fibers in the oxidative part of the TA in the MKO mice. Tibialis anterior (TA); Gastrocnemius (Gas); Plantaris (Plan); Soleus (Sol); Diaphragm (Dia); Brown- and white-adipose tissue (BAT and WAT); Cerebellum (CB). n= 4 per genotype for A and B, n = 7-8 per genotype for C and D, n = 5-6 per genotype for F. Results are expressed as mean ± SEM. * $P < 0.05$; ** $P < 0.01$; *** $P < 0.001$. Two-way ANOVA (a, c, and f).

RORα deletion leads to a severe dampening of core clock gene oscillations.

RORα is a transcription factor belonging to the family of steroid/thyroid hormone receptor superfamily and a key regulator of the circadian clock (Akashi and Takumi, 2005; Sato et al., 2004). Therefore, we investigated the effect of the RORα deletion on daily gene expression. We observed a decreased expression level of almost all clock genes except for *Clock*, *Per1,* and *RORγ*; the latter was increased (**Supp Figure 2A**). The transcriptome analysis revealed the differential expression of 1956 and 1461genes at Zeitgeber time (ZT) 4 or ZT16, respectively (**Figure 2A**), (Upregulated: 995 vs. 673 genes; Downregulated: 1002 vs. 789 genes;

Supp Figure 2B). Despite the role of RORα in the circadian clock, the effects of its deletion seem to be vastly independent of time, as more than half of the genes differentially regulated were overlapping between ZT4 and ZT16 (**Figure 2A**). Especially highly significant genes, including Stabilin2 (*Stab2*), Perilipin3 (*Plin3*), Phospholipase D Family Member 5 (*Pld5*) and Proteasome 26S Subunit, Non-ATPase 8 (*Psmd8*) were found in both analysis (**Figure 2B).** Therefore, the overlap of several Reactome terms between ZT4 and ZT16 was not surprising (**Figure 2C)**. A majority of the terms were indeed associated with increased "mitochondrial biogenesis" and "oxidative phosphorylation" (**Figure 2B**).

Our results could point to a possible role of RORα in skeletal muscle glucose transport and glycolysis as its deletion leads to a compensatory increase of oxidative metabolism genes.

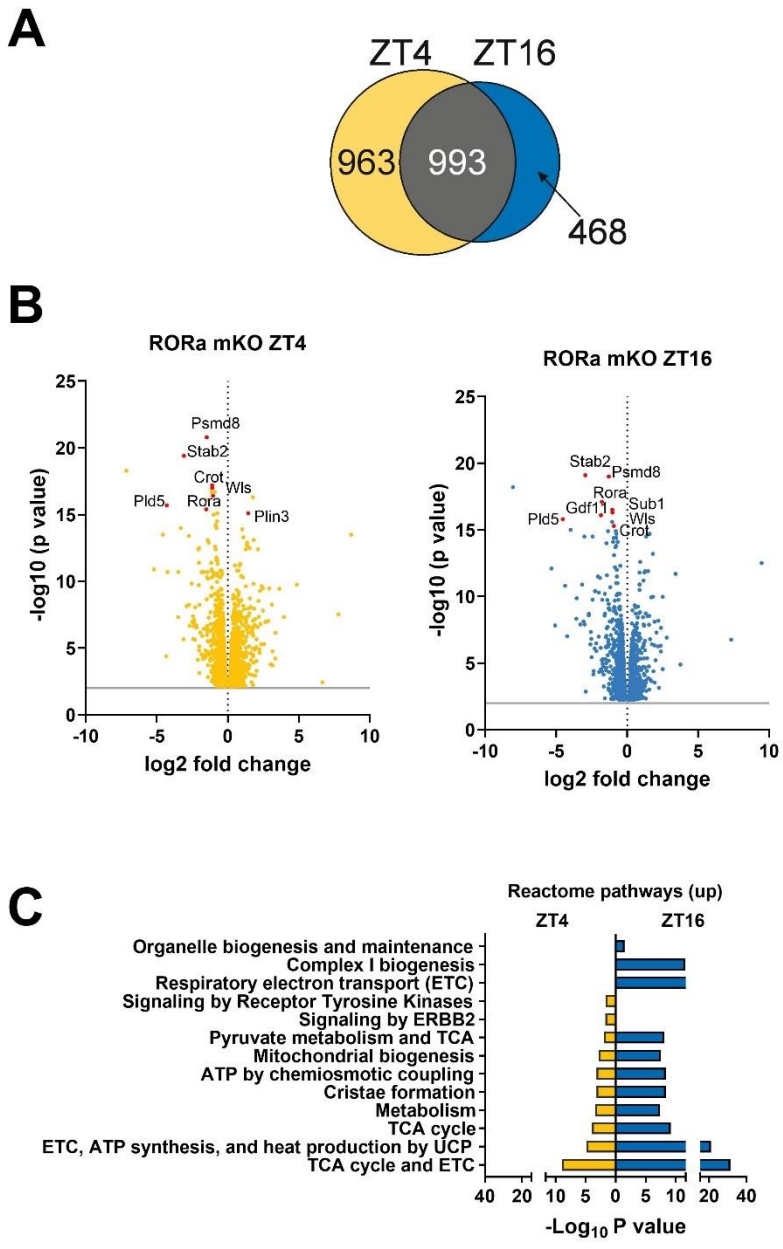

Figure 2. RORα expression in skeletal muscle is essential for transcriptome oscillation. (A) Venn diagram displaying the number of differentially expressed genes at ZT4 (yellow) and ZT16 (blue). (B) Volcano plot displaying the differentially expressed genes at ZT4 (yellow) or ZT16 (blue). (C) Reactome pathway enrichment analysis for genes increased at ZT4 (yellow) or ZT16 (blue). n= 4 per genotype for A, B and C.

Decreased spontaneous wheel-running activity in mice with muscle-specific RORα deletion but not forced exercise performance.

To better explore a potential role for RORα in muscle energy metabolism, we challenged our mice with different exercise modalities. For instance, treadmill running is used to evaluate maximal exercise capacity in untrained animals, while wheel running is often used as a chronic exercise model in laboratory mice, because it better reflects the natural locomotion of the mice (Allen et al., 2001; Kim et al., 2020; Manzanares et al., 2018) and as mice run spontaneously when given access to a running wheel (Ghosh et al., 2010; Meijer and Robbers, 2014).

RORα MKO mice show a significantly decreased wheel-running activity and run about half of the CTRL mice, while no difference in the time of running was observed (**Figure 3A**). As the wheel running was significantly decreased between ZT12 and ZT18, we performed a maximal exercise capacity test in the early night. The respiratory exchange ratio (RER), is used as an indirect measure of energy substrate utilization, indicating the relative contribution of carbohydrates (high RER) and lipids (low RER) to overall energy expenditure (Pendergast et al., 2000; Simonson and DeFronzo, 1990). RER was increased in the MKO mice at rest, but not different at exhaustion (**Figure 3B-D**). O_2 consumption was not different between the two groups at any point during the exercise (**Figure 3E**). Blood glucose levels decreased in both groups (**Figure 3F**), while blood lactate levels increased (**Figure 3G**); however, no difference was observed between the CTRL and MKO group. Interestingly, although wheel-running activity was significantly decreased (**Figure 3A**), the total running distance on the treadmill was significantly higher in the MKO mice compared to the CTRL mice (**Figure 3H**). After the maximal exercise capacity, we also investigated the endurance capacity of the mice, observing similar results for the RER, which was increased at rest (**Figure 3I-J**), but not different at exhaustion (**Figure 3K**). O_2 consumption was not significantly altered between the two groups during the exercise (**Figure 3L**). Blood glucose level decreased in both groups (**Figure 3M**), while blood lactate levels were unchanged (**Figure 3N**); again, no difference was observed between the CTRL and MKO group. Remarkably, we also observed an increased endurance capacity in the MKO mice compared to the CTRL mice (**Figure 3O**).

Overall, these results indicate that despite decreased voluntary wheel running, RORα MKO mice show increased exercise capacity when forced. This also shows that the alteration in the expression of oxidative metabolic genes does not affect muscle metabolism in particular during an exercise challenge.

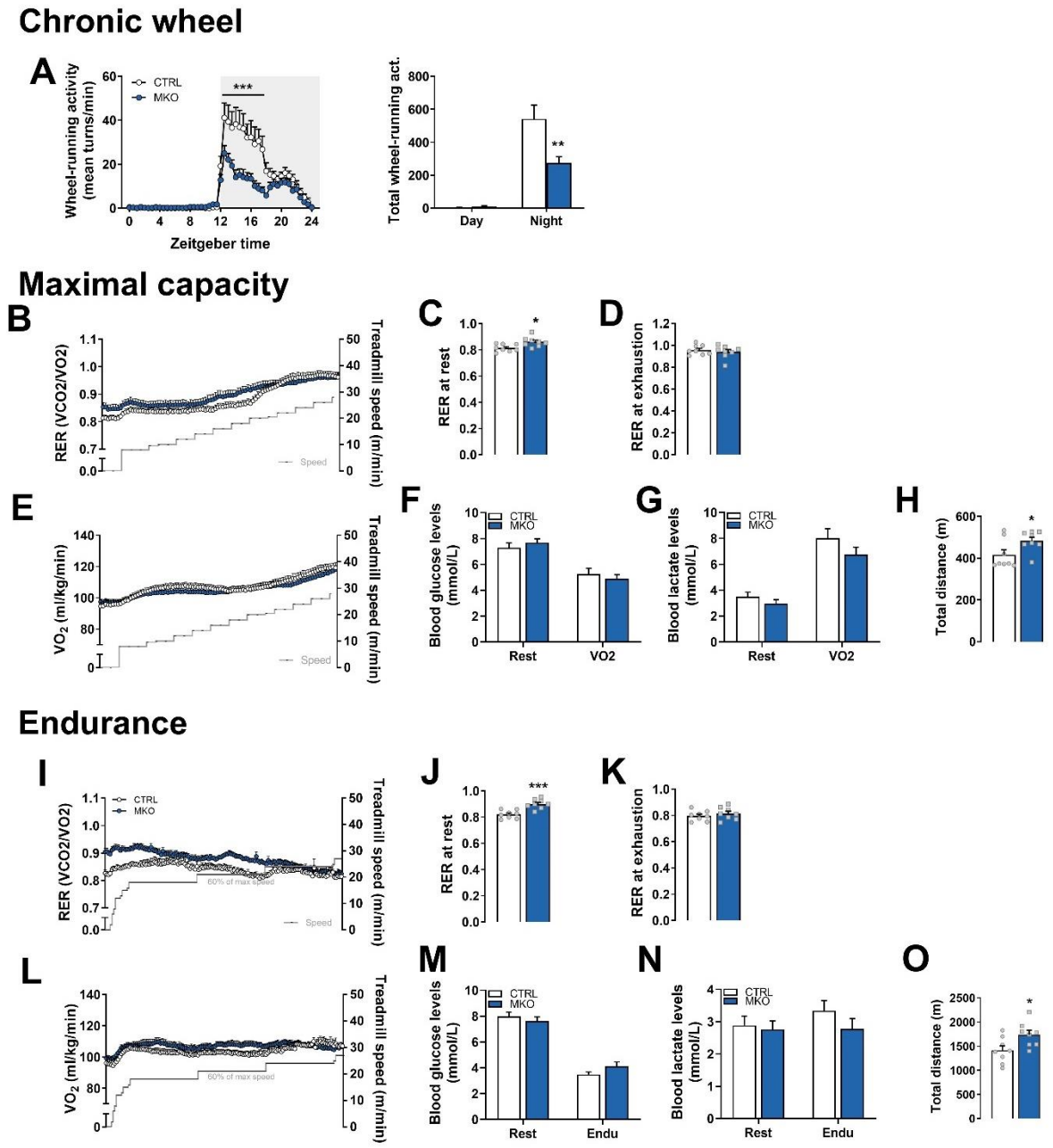

Figure 3. Despite decreased voluntary wheel running, RORα MKO mice show increased exercise capacity. (A) Wheel-running activity over a 7-d period (Light and dark periods are depicted by white and gray rectangles, respectively). Results are expressed as the total number of wheel revolutions per minute ± SEM (n = 8 per genotype) and the sum of the activity for the day and the night. (B) Respiratory exchange ratio (RER) as a function of speed in CTRL and MKO animals during maximal exercise capacity test. (C) RER at rest and (D) RER at exhaustion. (E) O2 consumption as a function of speed in CTRL and MKO animals during maximal exercise capacity test. Note that data in panel B and E are only depicted until speed 27 as beyond mice started to reach exhaustion (F) glucose levels and (G) Blood lactate at rest and within 1 min after exhaustion. (H) total distance reached at exhaustion. Results are expressed as mean ± SEM (n = 8-9 per genotype). (I) Respiratory exchange ratio (RER) as a function of speed in CTRL and MKO animals during endurance exercise test. (J) RER at rest and (K) RER at exhaustion. (L) O2 consumption as a function of speed in CTRL and MKO animals during endurance exercise test. Note that data in panels I and L are only depicted until speed 27 m/min. (M) glucose levels and (N) Blood lactate at rest and within 1 min after exhaustion. (O) total distance reached at exhaustion. Results are expressed as mean ± SEM (n = 8-9 per genotype). Note that B to O were performed around ZT16. * $P < 0.05$; ** $P < 0.01$; *** $P < 0.001$. Two-way ANOVA (a) and Unpaired Student's t-test (c, h, j, and o).

In-depth proteomic analysis of MKO muscle indicates a role for RORα in ROS detoxification.

The results above show that there is no strong correlation between the changes observed at the transcriptional level and the metabolism of skeletal muscle lacking RORα in basal conditions and response to an exercise challenge. We thus analyzed the protein content of the muscle of sedentary mice harvested at ZT4 (resting period) and ZT16 (active/feeding period) by mass spectrometry (MS)-based proteomic analysis. Muscle-specific deletion of RORα altered the expression level of 300 proteins and 413 proteins at ZT4 or ZT16, respectively, under basal conditions (**Figure 4A**) (Upregulated: 98 vs. 104 proteins; Downregulated: 202 vs. 313 proteins; **Supp Figure 4A-B**). RORα is a transcriptional activator (Akashi and Takumi, 2005), explaining the more significant decrease in protein expression compared to its increase. The Reactome pathway enrichment analysis indicated that the decreased proteins were involved in different pathways depending on the time of the day. At ZT4, proteins involved in "muscle contraction" and "amino acid metabolism" were decreased (**Figure 4C**). While at ZT16, when mice are active, the decreased proteins were involved in "metabolism" and "reactive oxygen species (ROS) detoxification" (**Figure 4C**). The proteomic analysis in basal conditions already gave us an insight on the function of RORα in skeletal muscle, indicating a role in muscle contraction during the inactive phase, ROS detoxification and metabolism during the active phase.

Chronically increased ROS concentration could result in muscle damage (Zuo and Pannell, 2015), possibly explaining the decreased running wheel activity. We, therefore, wanted to investigate whether the decreased wheel-running activity is due to impaired exercise adaptation or ROS induced muscle damage. We trained the mice for 34 consecutive nights (ZT 13) for 1 h, using a high-intensity interval treadmill (HIIT) protocol (**Figure 4D**; see method "treadmill"), starting at 60% (19 m/min) of maximal running speed determined beforehand, and increased every 5 days until we reach a 100% of the maximal running speed (31 m/min). We observed an increase in maximal exercise capacity of both groups (**Figure 4E**), indicating that the exercise adaptation to this exercise protocol is not impaired in the RORα MKO mice.

To further examine the molecular basis of our observations, we collected the muscle 24 h after the last training bout and performed mass-spectrometry based proteomic analysis on the samples. Skeletal muscle-specific deletion of RORα leads to the differential induction of 373 proteins (161 up and 257 down) by exercise compared to CTRL littermates (**Figure 4G**). The decreased proteins are involved in "metabolism" and "reactive oxygen species detoxification" (**Figure 4H**), as observed in the sedentary group (**Figure 4C**). The heatmap illustrates the decrease of important ROS detoxification enzymes, including superoxide dismutase 1 (SOD1), and Peroxiredoxin (PRDX) 1, 4, and 6 (**Figure 4I**).

These results indicate that RORα might play an important role in ROS metabolism.

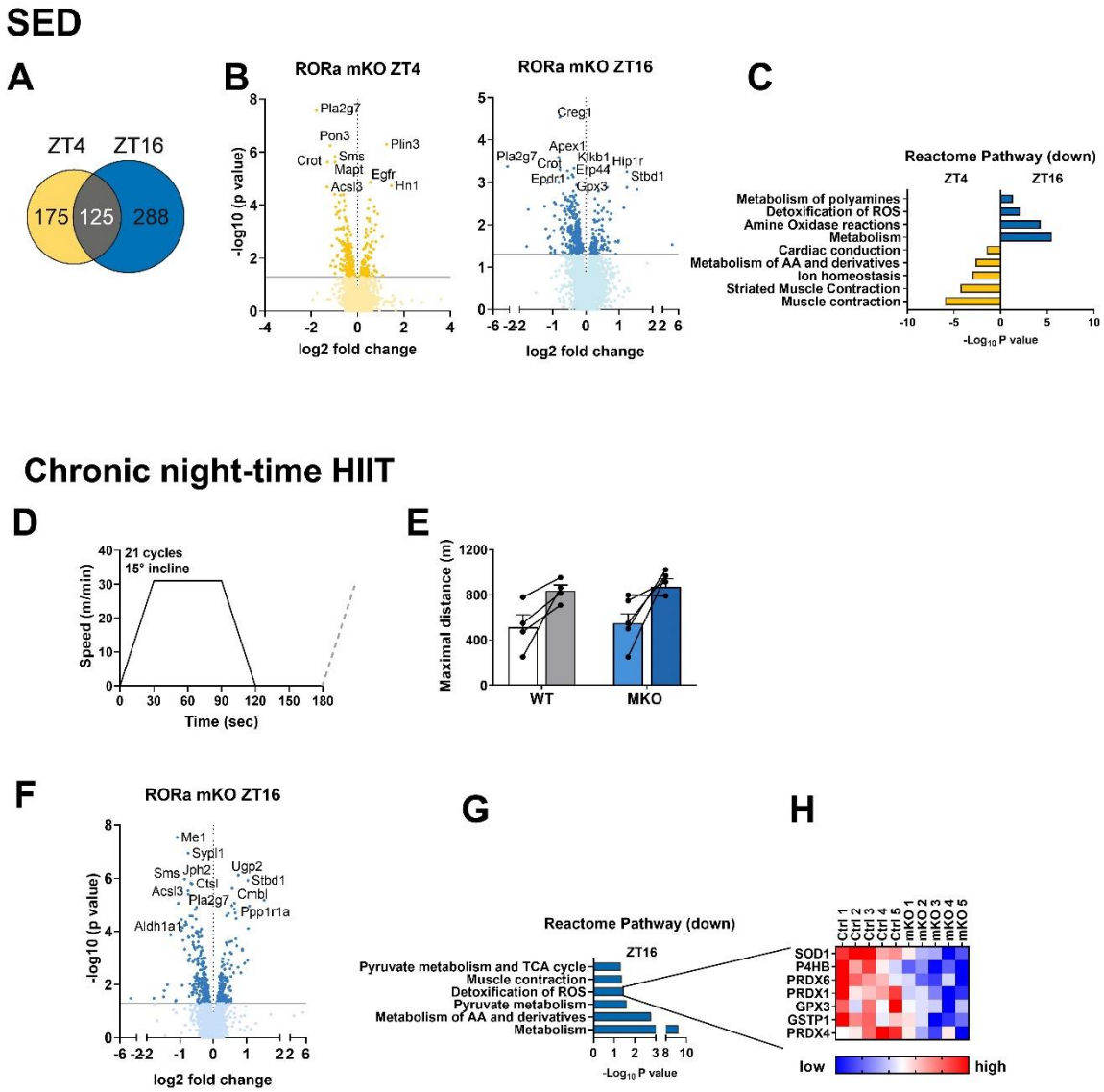

Figure 4. In-depth proteomic analysis of MKO muscle indicates a role of RORα in ROS detoxification. (A) Venn diagram displaying the number of differentially regulated proteins at ZT4 (yellow) and ZT16 (blue). (B) Volcano plot displaying the differentially regulated proteins at ZT4 (yellow) or ZT16 (blue). (C) Reactome pathway enrichment analysis for decreased proteins at ZT4 (yellow) or ZT16 (blue). n= 5 per genotype for A, B, and C. (D) High-intensity –interval treadmill (HIIT)protocol. (E) maximal exercise capacity of CTRL and MKO, before and after the training (white and gray or light blue and dark blue, respectively). Results are expressed as mean ± SEM (n = 4-5 per genotype). (F) Volcano plot displaying the differentially regulated proteins at ZT16 (blue). (G) Reactome pathway enrichment analysis for decreased proteins at ZT16 (blue). (H) heatmap of changed ROS detoxification enzymes.

RORα is essential for the detoxification of ROS produced by exercise.

ROS produced during exercise is thought to be important in exercise adaptation (Margaritelis et al., 2018; Silveira et al., 2006). However, as some ROS detoxification enzymes are decreased in the MKO mice, they might have a problem with the clearance of ROS, this might lead to muscle damage (Anderson et al., 2009; Powers et al., 2011; Zuo and Pannell, 2015).

To investigate the putative modulation of ROS levels by RORα, we used primary cell isolated from mouse extensor digitalis longus (EDL), and we differentiated into myotubes and infected with an adenovirus to drive *Rorα* overexpression. The decrease of oxygen to a hypoxic level is inducing ROS production in the muscle (Clanton, 2007). Therefore, we exposed control cells to hypoxic conditions for different amounts of time and observed an increase in Vascular endothelial growth factor a (*Vegfa*) and Hexokinase 2 (*Hk2*) expression (**Figure5A**). *Vegfa* and *Hk2* are Hypoxia-inducible factors 1(HIF1)-target genes (Favier et al., 2015), and their induction indicates that the hypoxic conditions were sufficient to induce HIF-1α signaling. Surprisingly, besides the HIF-1α target genes, *Rorα* expression was induced by hypoxia after 2h, and further increased after 6h and 48h (**Figure 5A**), indicating a possible role in cell survival under hypoxic conditions.

Abnormal ROS production can lead to cell death (Ghosh et al., 2018). The reduction of MTT, the mitochondrial succinate dehydrogenase, is often used to assess cell viability (Kumar et al., 2018). Therefore, we exposed cells to hypoxia, increasing ROS in skeletal muscle (Clanton, 2007), and observed a decreased cytotoxicity in the cells overexpressing RORα (**Figure 5B**). Additionally, we treated cells with different concentrations of hydrogen peroxide (H_2O_2), and likewise observed a decrease in cytotoxicity (**Figure 5C**). In order to translate our in vitro finding to an in vivo physiological context, ROS accumulation in RORα MKO muscle in sedentary, 9-day wheel running, and an acute bout of exercise was evaluated. Although we did not observe an increase in H_2O_2 in the muscle of those mice (**Figure 5D**), we were able to show an increased peroxidase activity in the mice lacking RORα (**Figure 5E**).

Our findings indicate a strong induction of *Rorα* expression in response to hypoxia and a positive effect of RORα overexpression on cell survival under hypoxic conditions.

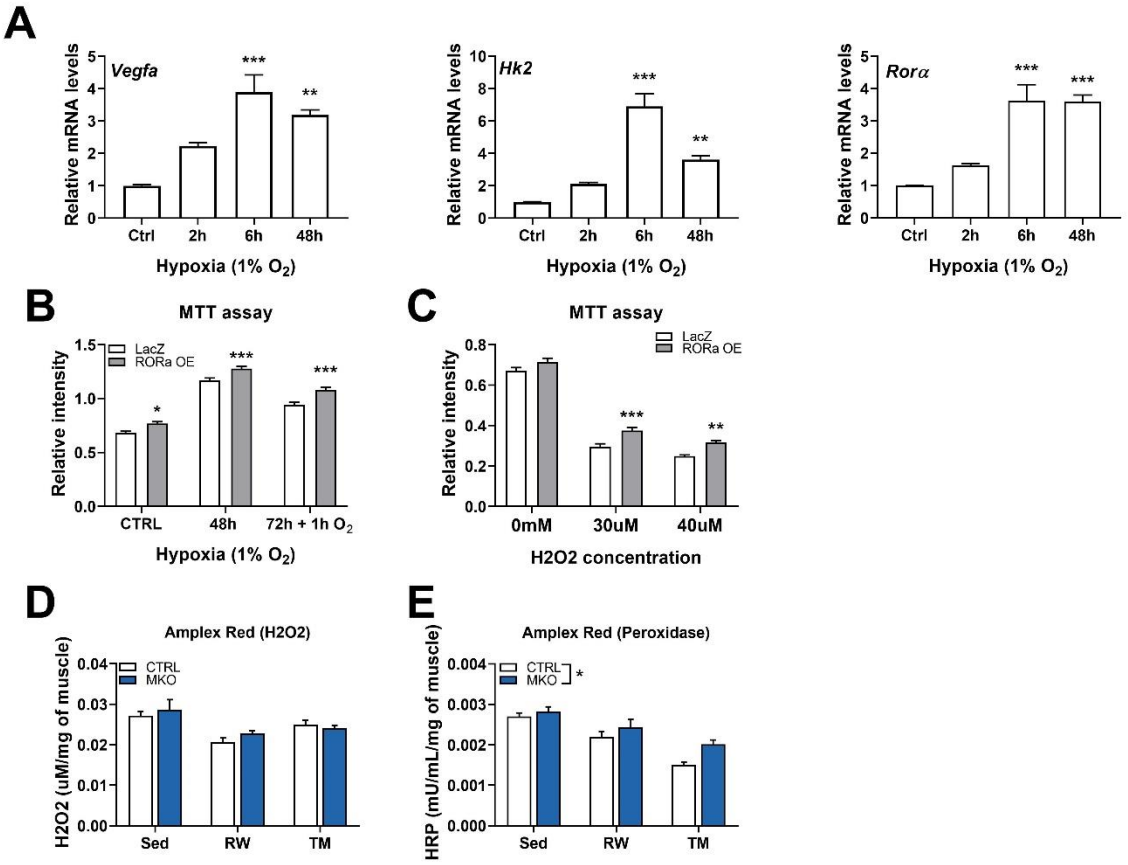

Figure 5. RORα is important in the detoxification of ROS produced by exercise. (A) *Rorα* gene expression in primary myotubes after exposure to hypoxia (1%O2). Results are expressed as mean ± SEM (n = 3 per condition). Cell viability assay in control (LacZ) or *Rorα* overexpressing (RORα OE) cells after (B) H_2O_2 treatment, (C) exposure to hypoxic conditions. Results are expressed as mean ± SEM (n = 7-8 per condition). (D) H_2O_2 amount and (E) peroxidase activity measurement in mouse muscle after 7 days of wheel access (RW) or a maximal exercise capacity test (TM). * $P < 0.05$; ** $P < 0.01$; *** $P < 0.001$. One-way ANOVA (a) and Two-way ANOVA (b, c).

Discussion

Physical exercise is an indispensable element of a healthy lifestyle and a potent intervention to reduce the prevalence and incidence of metabolic, cancer, and age-related disorders (Ding et al., 2016; Lobelo et al., 2014; Pedersen and Saltin, 2015). Skeletal muscle adaptation to acute and chronic exercise is critical for improved performance and health benefits. An acute increase in ROS concentration during contraction is essential for exercise-induced glucose uptake (Henriquez-Olguin et al., 2019) and skeletal muscle exercise adaptation (Margaritelis et al., 2018; Silveira et al., 2006). However, chronically elevated levels of ROS in skeletal muscle are detrimental (Zuo and Pannell, 2015) and associated with metabolic perturbations, particularly with insulin resistance (Anderson et al., 2009; Hoehn et al., 2009; Houstis et al., 2006). Besides exercise, an increase in mitochondrial oxidative phosphorylation has been associated with an increase in ROS production (Fleury et al., 2002; Murphy, 2009). We here proposed a role for muscle RORα in the modulation of ROS metabolism during physical activity.

We show that skeletal muscle-specific *Rorα* KO mice displayed decreased voluntary wheel-running activity, but improved acute treadmill exercise capacity when forced. This paradoxical phenotype can be related to the chronic aspect of voluntary wheel running. We therefore equally trained animals on a treadmill for about 5 weeks in the early nighttime and measured muscle gene and protein expression. We specifically found a decrease in proteins essential for ROS detoxification, including SOD1 and several peroxiredoxins. Interestingly, SOD1 global KO and muscle-specific KO mice show signs of impaired redox signaling and muscle damage indicated by centralized nuclei (Nagahisa et al., 2016; Sakellariou et al., 2018). However, exercise performance and spontaneous locomotor activity were not measured in these mouse models. We also observed the parallel decrease of several other antioxidant enzymes in skeletal muscle lacking RORα, which could have detrimental effects as observed in the liver lacking both Peroxiredoxin 4 (Prdx4) and SOD1 (Homma et al., 2018). It would, however, be important to evaluate muscle damage (e.g., centralized nuclei) in response to exercise in our mouse model.

Running wheel behavior—besides its voluntary and motivational aspects (Meijer and Robbers, 2014)—better reflects rodent's natural running pattern. Moreover, mice exhibit much greater running distance in wheels over a single night as compared to a unique treadmill exercise session (Ghosh et al., 2010). While both intensity and duration are relevant for ROS accumulation (He et al., 2016), 1 h of high-intensity interval treadmill exercise (~1000m/h), might lead to much less ROS accumulation and thus detrimental effects, compared to nighttime wheel running (>5000m). Furthermore, ROS gene and protein alterations were not only observed when animals are active at night but also when they feed. Indeed, nutritional oxidative stress could be another, additional aspect leading to increase oxidative damage in

muscle lacking RORα, thereby negatively impacting on muscle function (Sies et al., 2005; Simioni et al., 2018; van Dijk et al., 2016). Hence, dietary supplementation with antioxidants could be tested in RORα KO mice to potentially reduce postprandial oxidative stress and evaluate whether this impacts on their spontaneous locomotion and skeletal muscle adaptation to chronic wheel running.

The intriguing overrepresentation of oxidative metabolism and mitochondria-associated genes in our transcriptome analysis can indicate altered mitochondrial homeostasis in the absence of RORα. For instance, we observed a decreased expression of several members of the peroxiredoxin (PRDX) family, which remove peroxides, including hydrogen peroxide (H_2O_2). Interestingly, peroxiredoxin 3 (Prx3) deletion results in altered mitochondrial network and membrane potential of myotubes, in which ROS levels were increased (Lee et al., 2014). In the mouse, both deletion of Prx3 and 6 alters muscle force and exercise performance (Lee et al., 2014; Lee, 2020; Zhang et al., 2016). Importantly, we demonstrate that primary myotubes overexpressing RORα are resistant to cell death in response to hypoxia, known to elevate cellular ROS levels (Munoz-Sanchez and Chanez-Cardenas, 2019), or H_2O_2 directly. Although we neither observe increased H_2O_2 levels in muscles of RORα MKO mice after wheel running nor treadmill exercise, further investigations to reveal the role of RORα in skeletal muscle function, ROS detoxification, and exercise adaptation will be needed.

Materials and methods

Animals

Rorα$^{flox/flox}$ mice (Mouse Clinical Institute, Strasbourg, France) were crossed with HSA-Cre transgenic mice (purchased from the Jackson Laboratory; stock no. 006149). All mice were maintained on a C57BL/6J genetic background in the animal facility of the Biozentrum (University of Basel) under a 12:12 h light/dark cycle (lights on at 6:00 A.M.). Unless specifically mentioned, all experiments were performed in young adult male mice (3- to 6-mo-old) housed in standard cages with bedding substrates and free access to regular chow diet (# 3432, KLIBA NAFAG) and water. The temperature was constantly between 21 °C to 22 °C. All experiments were performed in accordance with the principles of the Basel Declaration and with Federal and Cantonal Laws regulating the care and use of experimental animals in Switzerland, as well as institutional guidelines of the Biozentrum and the University of Basel. The protocol with all methods described here was approved by the "Kantonales Veterinäramt" of the Kanton Basel-Stadt, under consideration of the well-being of the animals and the 3R principle.

Body composition analysis

Body composition was assessed with an EchoMRI-100 analyzer (EchoMRI Medical Systems). Fat and lean mass were normalized to total body mass.

Body temperature and locomotor activity recordings

General locomotor activity and core body temperature data were acquired with the E-Mitter Telemetry System (Starr Life Sciences) from single-caged animals placed in an environment-controlled cabinet (UniProtect Air Flow Cabinet, Bioscape). Briefly, small transponders (G2 E-Mitter, Starr Life Sciences) were implanted into the abdominal cavity of mice under isoflurane anesthesia (2 % isoflurane + O2). Mice were treated with Meloxicam (1 mg/kg) pre- and post-operatively and allowed to recover for three weeks. The abovementioned parameters, together with the wheel-running activity, were recorded with a PC-based acquisition system connected to ER4000 Receivers (VitalView, Starr Life Sciences).

Comprehensive laboratory animal monitoring system

A comprehensive animal metabolic monitoring system (CLAMS; Columbus Instruments) was used to evaluate food consumption, oxygen consumption (VO2) and CO2 production (VCO2) from singly housed mice within an environment-controlled cabinet with a temperature set at 23°C. Feeding was measured by recording the difference in the scale measurement of the center feeder from one time point to another. We studied 8 mice per genotype in both basal fed and 24-h fasted/refed conditions, after acclimatization of 2 days.

Treadmill

Sedentary mice were acclimated to the treadmill (Columbus Instruments, Columbus, Ohio, USA) on three consecutive days prior to the experiment. The accommodation period

consisted in: Day 1, placing the mice in the treadmill for 10 min without speed followed by 5 min at 5 m/min; Day 2, running at 5 m/min, 7 m/min and 10 m/min for 5 min each; Day 3, running at 8 m/min, 10 m/min and 12 m/min for 5 min each.

After one resting day, a maximal exercise capacity test was performed by 3min at 8 m/min, increasing treadmill speed by 2 m every 2 min, at a 15° slope, until exhaustion. Exhaustion was met if an animal remained on the electrical grid (providing a mild electrical stimulus of 0.5 mA, 200 ms pulse, 1 Hz) for more than 5 s. Tail blood glucose (Accu-Chek, Roche) and lactate (Lactate Plus meter, Nova Biomedical) values were determined immediately prior to treadmill exercise and within 1 min after physical exhaustion.

One week later, the same group of mice performed an endurance type protocol in early morning during which, after a brief warm-up, speed was successively adjusted to 60, 70, 80, 90 and 100% of maximal mean running speed, every 20 min (5° slope), until exhaustion. Stainless steel grids at the end of each lane provided a mild electrical stimulus (0.5 mA, 200 ms pulse, 1 Hz) to keep the mice running. Exhaustion was met when VO2 and respiratory exchange ratio values plateaued and/or if the animal remained on the electrical grid for more than 5 s without any attempt to go back on the treadmill. Tail blood glucose (Accu-Chek, Roche) and lactate (Lactate Plus meter, Nova Biomedical) values were determined immediately prior to treadmill exercise and within 1 min after physical exhaustion.

Chronically trained mice were also acclimatized to the treadmill as stated above prior to evaluation of their maximal exercise capacity. Then, mice were trained every day at ZT13 with a newly established high-intensity interval treadmill (HIIT) protocol particularly suitable to long-term studies. A daily session started with a ramping speed acceleration for 30 sec, a steady speed was then maintained for 1 min, followed by a progressive speed decrement to 0 m/min within 30 sec, and 1 min of rest. This was repeated 20 times for a total of 1 h of exercise. The first 5 days, steady speed corresponded to 60% of total max speed as determined in the maximal test (here 19 m/min), then an increase of 10% was implemented every 5 days over about 25 days prior to the repetition of a maximal exercise capacity test. The mice were finally trained for 5 additional more days before sacrifice.

ROS detection

(Experiment pending)

Muscle tissue preparation and blood collection

Mice from the different experiments were sacrificed by short exposure to CO2 and immediate exsanguination. Blood was collected in tubes containing lithium heparin (Microvette 500 LH, Sarstedt, 20.1345) centrifuged at 2000 g for 5 min at RT and stored at - 80°C. The glycolytic quadriceps and gastrocnemius muscles, as well as liver samples, were quickly snap frozen in liquid nitrogen and stored at - 80°C until further analysis.

Quantitative Real-Time PCR (Reverse Transcript)

Total RNA from muscle tissues was extracted using a hybrid method combining TRI-Reagent (Sigma-Aldrich T9424) and RNeasy Mini Kit (QIAGEN 74104). RNA quantity and purity were measured with a NanoDrop OneC (ThermoFisher Scientific). High-Capacity cDNA Reverse Transcript Kit (Applied Biosystems, 4368814) was used for cDNA synthesis with 1 ug of total RNA. Quantitative real-time PCR was performed with Fast SYBR Green Master Mix (Applied Biosystems, 4385612) in a RT-PCR System (StepOnePlus, Applied Biosystems). PCR reactions were done in duplicate with the addition of negative controls (i.e., no reverse transcription and no template controls). Relative expression levels were determined using the comparative ΔCT method to normalize target gene mRNA to Hprt. Primers were designed and tested as previously described (Delezie et al., 2012). Primer sequences are summarized in supplemental Table 1.

RNA sequencing and data analysis

RNA quality was determined on the Bioanalyzer instrument (Agilent Technologies, Santa Clara, CA, USA) using the RNA 6000 Nano Chip (Agilent, Cat# 5067-1511) and quantified by Spectrophotometry using the NanoDrop ND-1000 Instrument (NanoDrop Technologies, Wilmington, DE, USA). Library preparation was performed with 1µg total RNA using the TruSeq Stranded mRNA Library Prep Kit High Throughput (Cat# RS-122-2103, Illumina, San Diego, CA, USA). Libraries were quality-checked on the Fragment Analyzer (Advanced Analytical, Ames, IA, USA) using the Standard Sensitivity NGS Fragment Analysis Kit (Cat# DNF-473, Advanced Analytical) revealing excellent quality of libraries (average concentration was 152±9 nmol/L and average library size was 374±4 base pairs). Samples were pooled to equal molarity. Each pool was quantified by PicoGreen Fluorometric measurement in order to be adjusted to 1.8pM and used for clustering on the NextSeq 500 instrument (Illumina). Samples were sequenced Single-reads 76 bases using the NextSeq 500 High Output Kit 75-cycles (Illumina, Cat# FC-404-1005), and primary data analysis was performed with the Illumina RTA version 2.4.11 and Basecalling Version bcl2fastq-2.20.0.422.

TMT labeling and LC-MS/MS analysis

Sample aliquots comprising 25 µg of peptides were labeled with isobaric tandem mass tags (TMT 10-plex, Thermo Fisher Scientific) as described previously (Ahrne et al., 2016). Shortly, peptides were resuspended in 20 µl labeling buffer (2 M urea, 0.2 M HEPES, pH 8.3) and 5 µL of each TMT reagent were added to the individual peptide samples followed by a 1 h incubation at 25 °C. To control for ratio distortion during quantification, a peptide calibration mixture consisting of six digested standard proteins mixed in different amounts was added to each sample before TMT labeling (for details see (Ahrne et al., 2016)). To quench the labeling reaction, 1.5 µL aqueous 1.5 M hydroxylamine solution was added, and samples were incubated for another 10 min at 25°C followed by pooling of all samples. The pH of the sample

pool was increased to 11.9 by adding 1 M phosphate buffer (pH 12) and incubated for 20 min at 25 °C to remove TMT labels linked to peptide hydroxyl groups. Subsequently, the reaction was stopped by adding 2 M hydrochloric acid until a pH < 2 was reached. Finally, peptide samples were further acidified using 5% TFA, desalted using Sep-Pak Vac 1cc (50 mg) C18 cartridges (Waters) according to the manufacturer's instructions, dried under vacuum and stored at -20 °C. TMT-labeled peptides were fractionated by high-pH reversed-phase separation using a XBridge Peptide BEH C18 column (3,5 µm, 130 Å, 1 mm x 150 mm, Waters) on an Agilent 1260 Infinity HPLC system. Peptides were loaded on a column in buffer A (20 mM ammonium formate in water, pH 10) and eluted using a two-step linear gradient from 2% to 10% in 5 min and then to 50% buffer B (20 mM ammonium formate in 90% acetonitrile, pH 10) over 55 min at a flow rate of 42 µl/min. Elution of peptides was monitored with a UV detector (215 nm, 254 nm), and a total of 36 fractions were collected, pooled into 12 fractions using a post-concatenation strategy as previously described (Wang et al., 2011) and dried under vacuum. Dried peptides were resuspended in 0.1% aqueous formic acid and subjected to LC-MS/MS analysis using a Q Exactive HF Mass Spectrometer fitted with an EASY-nLC 1000 (both Thermo Fisher Scientific) and a custom-made column heater set to 60 °C. Peptides were resolved using a RP-HPLC column (75µm × 30cm) packed in-house with C18 resin (ReproSil-Pur C18–AQ, 1.9 µm resin; Dr. Maisch GmbH) at a flow rate of 0.2 µLmin-1. The following gradient was used for peptide separation: from 5% B to 15% B over 10 min to 30% B over 60 min to 45 % B over 20 min to 95% B over 2 min followed by 18 min at 95% B. Buffer A was 0.1% formic acid in water, and buffer B was 80% acetonitrile, 0.1% formic acid in water. The mass spectrometer was operated in DDA mode with a total cycle time of approximately 1 s. Each MS1 scan was followed by high-collision-dissociation (HCD) of the 10 most abundant precursor ions with dynamic exclusion set to 30 seconds. For MS1, 3e6 ions were accumulated in the Orbitrap over a maximum time of 100 ms and scanned at a resolution of 120,000 FWHM (at 200 m/z). MS2 scans were acquired at a target setting of 1e5 ions, maximum accumulation time of 100 ms and a resolution of 30,000 FWHM (at 200 m/z). Singly charged ions and ions with unassigned charge state were excluded from triggering MS2 events. The normalized collision energy was set to 35%, the mass isolation window was set to 1.1 m/z, and one microscan was acquired for each spectrum. The acquired raw-files were converted to the mascot generic file (mgf) format using the msconvert tool (part of ProteoWizard, version 3.0.4624 (2013-6-3)) and searched using MASCOT against a murine database (consisting of 49434 forward and reverse protein sequences downloaded from Uniprot on 20141124), the six calibration mix proteins (Ahrne et al., 2016) and 390 commonly observed contaminants. The precursor ion tolerance was set to 10 ppm, and fragment ion tolerance was set to 0.02 Da. The search criteria were set as follows: full tryptic specificity was required (cleavage after lysine or arginine residues unless followed by proline), 3 missed cleavages were allowed, carbamidomethylation (C) and TMT6plex (K and peptide N-terminus) were set as fixed

modification and oxidation (M) as a variable modification. Next, the database search results were imported into the Scaffold Q+ software (version 4.3.2, Proteome Software Inc., Portland, OR), and the protein false identification rate was set to 1% based on the number of decoy hits. Proteins that contained similar peptides and could not be differentiated based on MS/MS analysis alone were grouped to satisfy the principles of parsimony. Proteins sharing significant peptide evidence were grouped into clusters. Acquired reporter ion intensities in the experiments were employed for automated quantification and statistical analysis using a modified version of our in-house developed SafeQuant R script (v2.3, (Ahrne et al., 2016)). This analysis included adjustment of reporter ion intensities, global data normalization by equalizing the total reporter ion intensity across all channels, summation of reporter ion intensities per protein and channel, calculation of protein abundance ratios and testing for differential abundance using empirical Bayes moderated t-statistics. Finally, the calculated p-values were corrected for multiple testing using the Benjamini−Hochberg method.

Cell Culture

Primary myoblasts were isolated from three-week-old male Per2 flx or PGC-1a gKO mice, as previously described (Pasut et al., 2013; Rion et al., 2019). In short, after CO2 euthanasia, the EDL was isolated, digested with 2mg/ml Collagenase A (Roche 10103586001) in DMEM Glutamax (Gibco 31966-021) with 1% penicillin-streptomycin for 1.5h at 37°C. After the EDL was triturated into singly myofibers using a large bore glass pipette, the single fibers were cultured in multiple dishes previously coated with 10% Corning Matrigel Basement Membrane Matrix (Corning, 354234), contained DMEM Glutamax, 10% horse serum, 1% Pen/Strep, 0.5% Chicken Embryo Extract (CEE) (US Biological Life Science, C3999) and 5ng/ml β-FGF (Invitrogen, PHG0023), at 37°C with 5% CO2. After 48h, the medium was exchanged by DMEM Glutamax, 20% Fetal Bovine Serum, 10% horse serum, 1% CEE, and 5ng/ml β-FGF for an additional 48h. Cells were either proliferated further up to passage 5 or frozen in medium containing 10% DMSO for long-term storage. To passage, the cells were washed once with prewarmed PBS and incubated for 5min in 500ul Trypsin. Cells were collected in DMEM Glutamax, 20% Fetal Bovine Serum, 10% horse serum, 1% CEE and 5ng/ml β-FGF and distributed into 10cm dishes with a density of 50000 cells per plate. For experiments, plates were coated with Matrigel Basement Membrane Matrix (Corning, 354234), incubated for 1min at RT, excess Matrigel was removed, and plates were dried for 1h at RT. Cells were harvested as described above, with Trypsin, and plated in DMEM Glutamax, 20% Fetal Bovine Serum, 10% horse serum, 1% CEE and 5ng/ml β-FGF. When the cells reached 90% confluency, the medium was removed, cells were washed with prewarmed PBS, and DMEM Glutamax, 4% HS, 1% CEE was added. During 4 days of differentiation, 80% of the media was exchanged every day without exposing the cells to air. On the 2nd day of differentiation, the cells were infected with either LacZ or RORα virus.

Hypoxia

The oxygen (O2) concentration in the Hypoxia Workstation (Scitive, Baker Ruskinn) was decreased to 1%, while CO2 was kept at 5% CO2. The cells were placed in the hood for the described amount of time. Cells were also treated with hydrogen peroxide (H_2O_2) with different concentrations for 6 h.

Statistical analysis

The n number used per genotype for each experiment is indicated in the figure legend. Data are represented as mean±SEM and statistically analyzed with GraphPad Prism 8. A student t-test was performed to evaluate statistical differences between the two groups. For multiple comparisons, data were analyzed using 2-Way ANOVA followed by Sidak's multiple comparisons test. Corresponding symbols to highlight statistical significance are the following: *: $p \leq 0.05$; **: $p \leq 0.01$; ***: $p \leq 0.001$.

Supplemental Figures

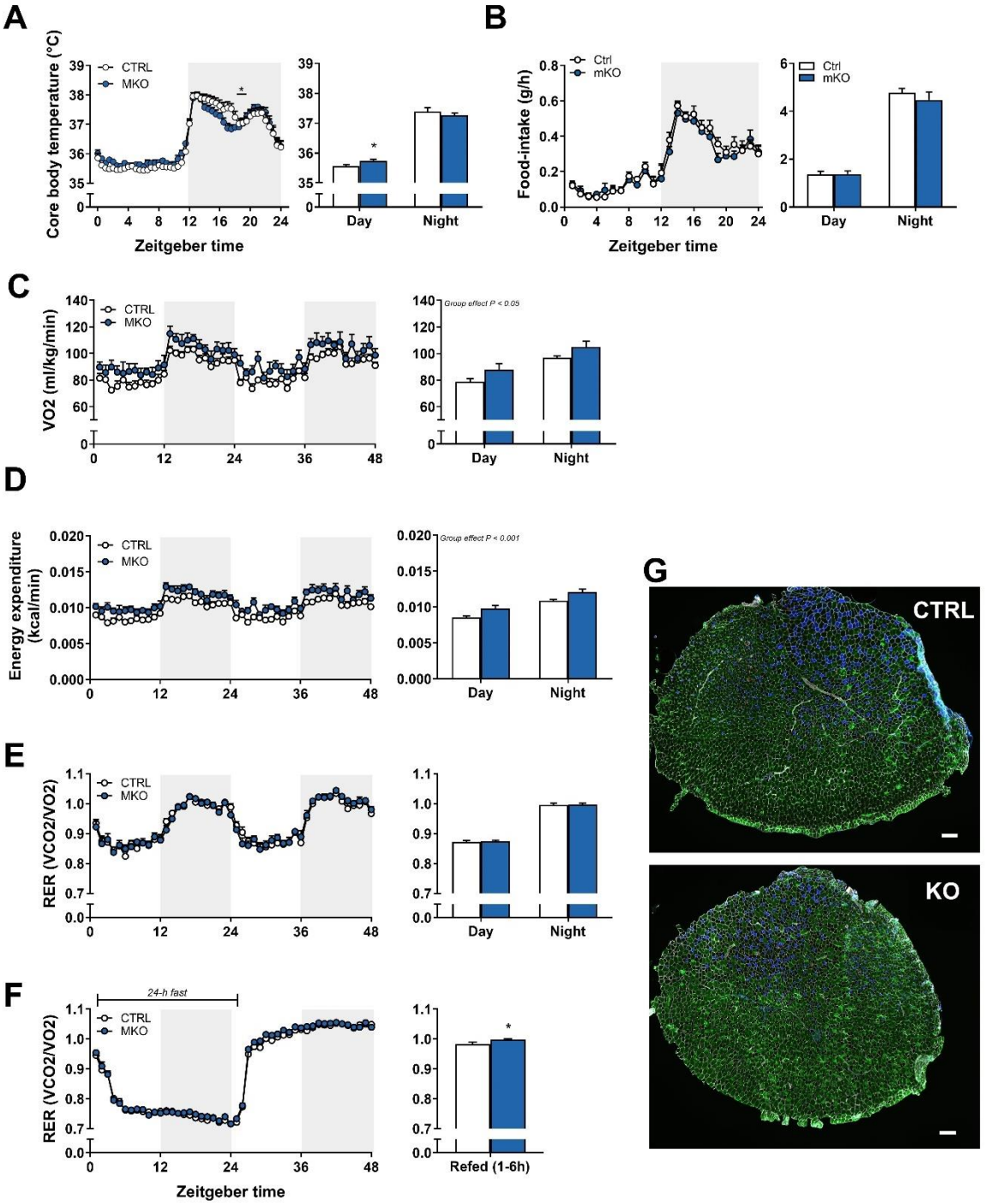

Supp. Figure 1. Energy balance in RORα MKO (A) Core body temperature is increased during the inactive phase in MKO mice. (B)Food intake is unaltered in MKO mice. (C) O2 consumption and thus (D) energy expenditure are slightly increased in MKO mice. (E) Energy substrate utilization is unaltered in MKO mice under basal conditions, but (F) slightly increased in MKO mice after refeeding. (G) Representative fluorescence microscopy images illustrating the fiber type composition in the TA muscle of CTRL and MKO animals. Corresponding color legend for fiber types: type I = red, type IIA = blue, type IIX = unstained (black), type IIB = green, and laminin = white. (Scale bar: 200 µm.) representative fiber type staining of tibialis anterior sections n = 7-8 per genotype for A, B, C, and D, n = 5-6 per genotype for F. Results are expressed as mean ± SEM. ** $P < 0.01$; *** $P < 0.001$. Two-way ANOVA (a, c, d, and f).

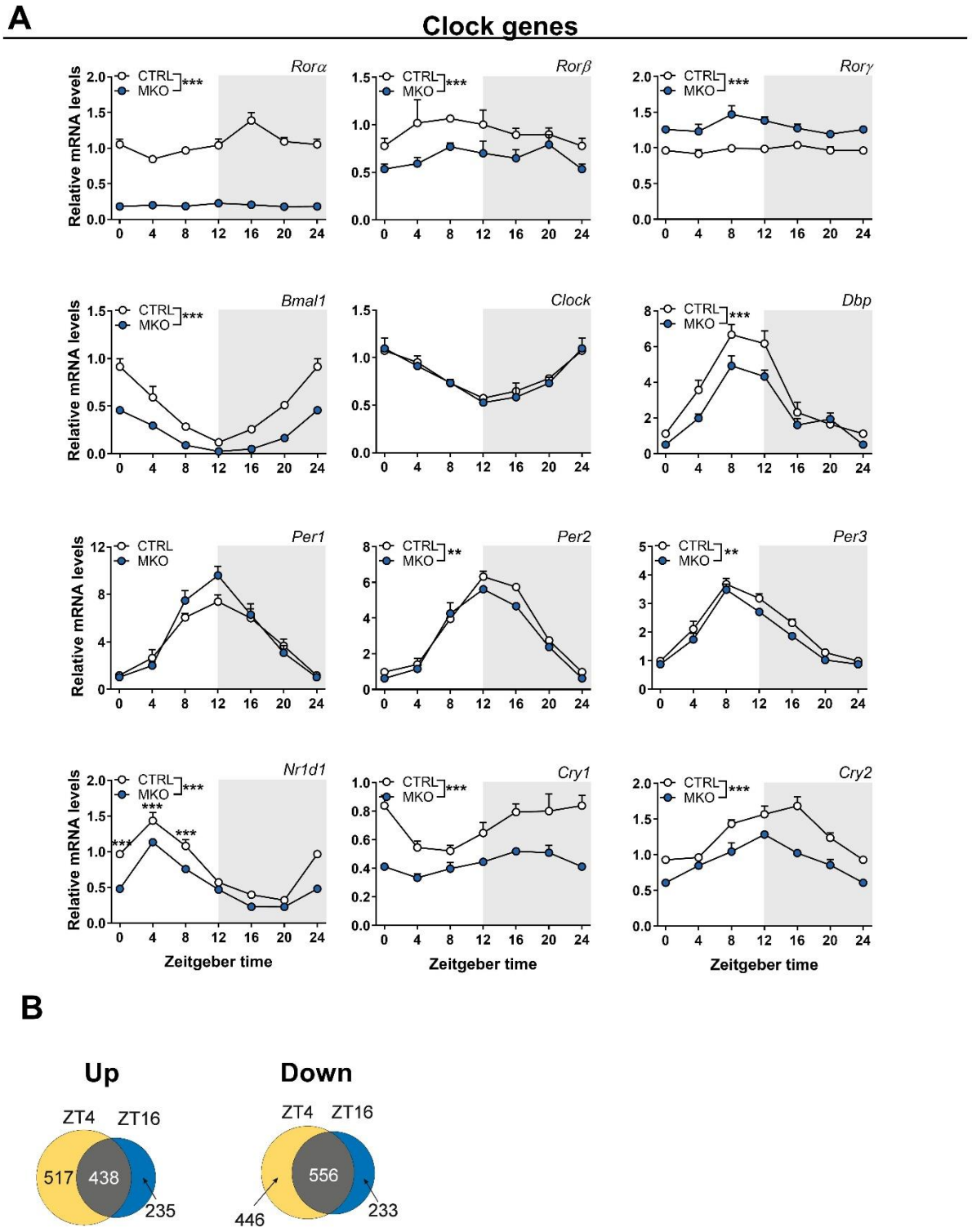

Supp. Figure 2. Clock genes expression altered by RORα deletion Clock gene expression in control (CTRL), and RORα MKO mice (Light and dark periods are depicted by white and gray rectangles, respectively). Expression values were determined by qPCR and normalized to *Hprt*. Data is shown as the average fold-change ± SEM (n = 4) relative to the expression in CTRL ZT0 set to 1 * $P < 0.05$; ** $P < 0.01$; *** $P < 0.001$. One-way ANOVA.

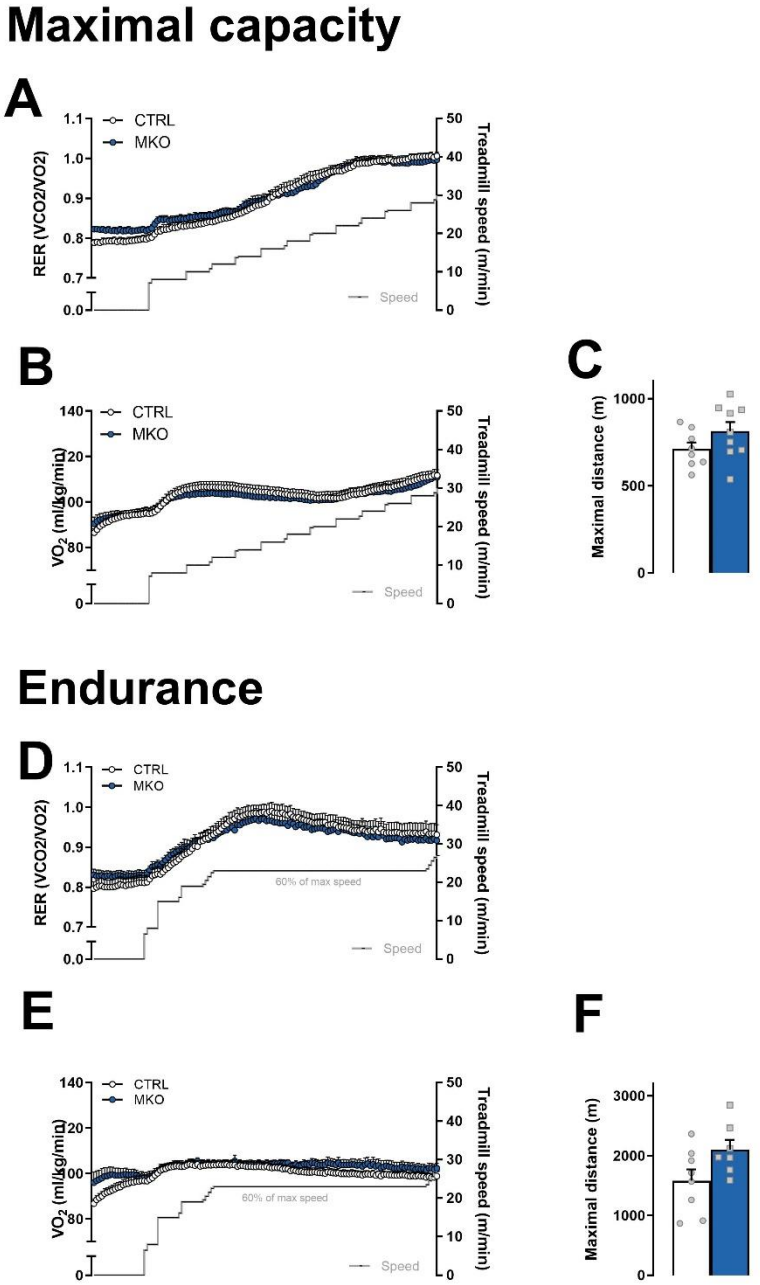

Supp. Figure 3. Treadmill during inactive phase does not reveal differences in exercise performance (A) Respiratory exchange ratio (RER) as a function of speed in CTRL and MKO animals during maximal exercise capacity test. (B) O2 consumption as a function of speed in CTRL and MKO animals during maximal exercise capacity test. Note that data in panel A and E are only depicted until speed 27 as beyond mice started to reach exhaustion (C) total distance reached at exhaustion. Results are expressed as mean ± SEM (n = 8-9 per genotype). (D) Respiratory exchange ratio (RER) as a function of speed in CTRL and MKO animals during endurance exercise test. (E) O2 consumption as a function of speed in CTRL and MKO animals during endurance exercise test. Note that data in panel D and E are only depicted until speed 27 m/min. (F) total distance reached at exhaustion. Results are expressed as mean ± SEM (n = 8-9 per genotype). Note that A to F were performed around ZT4.

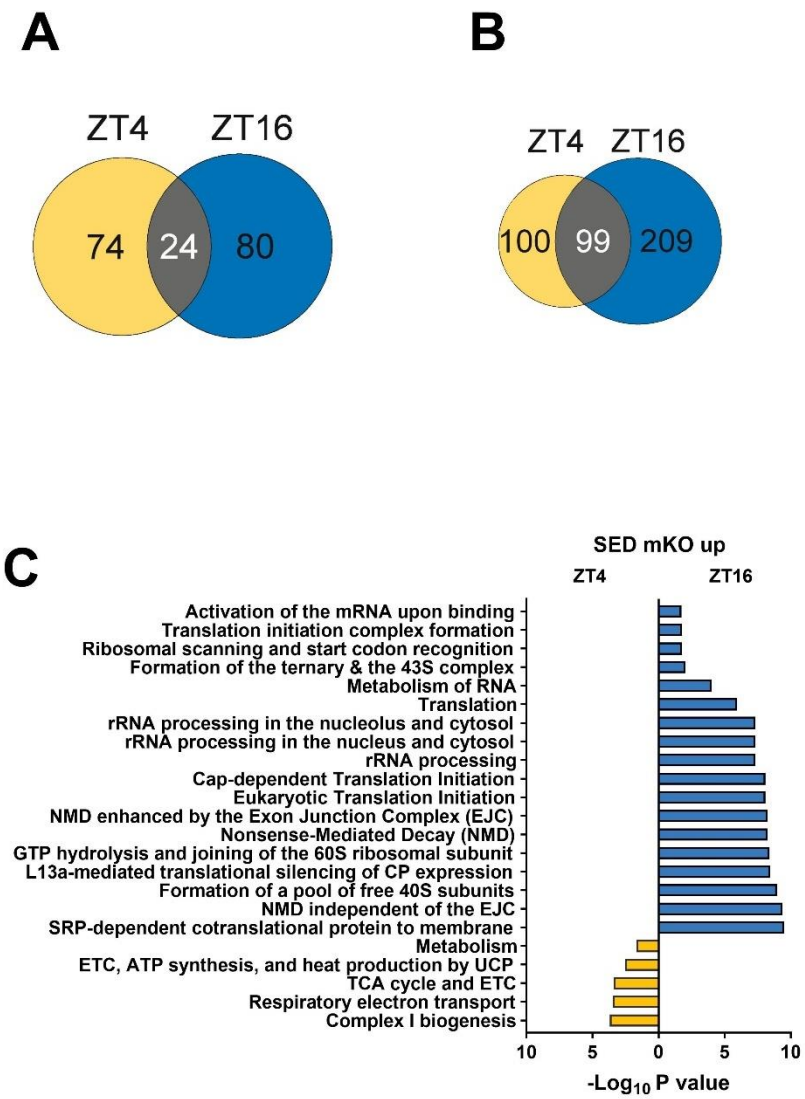

Supp. Figure 4. In-depth proteomic analysis of MKO muscle. Venn diagram displaying the number of differentially regulated proteins at ZT4 (yellow) and ZT16 (blue) (A) up and (B) downregulated). (C) Reactome pathway enrichment analysis for increased proteins at ZT4 (yellow) or ZT16 (blue). (D) Reactome pathway enrichment analysis for increased proteins at ZT16 (blue). n= 5 per genotype for A, B, C, and D.

Table 1. Primers

Name	Fwd	Rvs
Bmal1	CTCATTGATGCCAAGACTGG	GGTGGCCAGCTTTTCAAATA
Clock	CACAGGGCACCACCAATAAT	CATATCCACTGCTGGCCTTT
Cry1	CTGGCGTGGAAGTCATCGT	CTGTCCGCCATTGAGTTCTATG
Cry2	ACCGATGGAGGTTCCTACTG	AGCCTTGGGAACACATCAG
Dbp	ACCGTGGAGGTGCTAATGAC	TGGCTGCTTCATTGTTCTTG
Nr1d1	AGACTTCCCGCTTCACCAAG	AGCTTCTCGGAATGCATGTT
Per1	ACCAGCGTGTCATGATGACATAC	CTCTCCCGGTCTTGCTTCAG
Per2	ATGCTCGCCATCCACAAGA	GCGGAATCGAATGGGAGAAT
Per3	GTGATTGTTCACGCGTCTGT	CACTGCCATCTCGAGTTCAA
Rora	CCCCTACTGTTCCTTCACCA	ACAGCTGCCACATCACCTCT
Rorb	TGGACATGACTGGGATCAAA	GCCAGCTGATGGAGTTCTTC
Rorg	AGTCCTTCCGAGAGACATGC	TCCCACATTGACTTCCTCTG

References

Ahrne, E., Glatter, T., Vigano, C., Schubert, C., Nigg, E.A., and Schmidt, A. (2016). Evaluation and Improvement of Quantification Accuracy in Isobaric Mass Tag-Based Protein Quantification Experiments. J Proteome Res 15, 2537-2547.

Akashi, M., and Takumi, T. (2005). The orphan nuclear receptor RORalpha regulates circadian transcription of the mammalian core-clock Bmal1. Nat Struct Mol Biol 12, 441-448.

Allen, D.L., Harrison, B.C., Maass, A., Bell, M.L., Byrnes, W.C., and Leinwand, L.A. (2001). Cardiac and skeletal muscle adaptations to voluntary wheel running in the mouse. J Appl Physiol (1985) 90, 1900-1908.

Anderson, E.J., Lustig, M.E., Boyle, K.E., Woodlief, T.L., Kane, D.A., Lin, C.T., Price, J.W., 3rd, Kang, L., Rabinovitch, P.S., Szeto, H.H., et al. (2009). Mitochondrial H2O2 emission and cellular redox state link excess fat intake to insulin resistance in both rodents and humans. J Clin Invest 119, 573-581.

Aviram, R., Manella, G., Kopelman, N., Neufeld-Cohen, A., Zwighaft, Z., Elimelech, M., Adamovich, Y., Golik, M., Wang, C., Han, X., et al. (2016). Lipidomics Analyses Reveal Temporal and Spatial Lipid Organization and Uncover Daily Oscillations in Intracellular Organelles. Mol Cell 62, 636-648.

Clanton, T.L. (2007). Hypoxia-induced reactive oxygen species formation in skeletal muscle. J Appl Physiol (1985) 102, 2379-2388.

Delezie, J., Dumont, S., Dardente, H., Oudart, H., Grechez-Cassiau, A., Klosen, P., Teboul, M., Delaunay, F., Pevet, P., and Challet, E. (2012). The nuclear receptor REV-ERBalpha is required for the daily balance of carbohydrate and lipid metabolism. FASEB journal : official publication of the Federation of American Societies for Experimental Biology 26, 3321-3335.

Delezie, J., Dumont, S., Sandu, C., Reibel, S., Pevet, P., and Challet, E. (2016). Rev-erbalpha in the brain is essential for circadian food entrainment. Sci Rep 6, 29386.

Delezie, J., and Handschin, C. (2018). Endocrine Crosstalk Between Skeletal Muscle and the Brain. Front Neurol 9, 698.

Ding, D., Lawson, K.D., Kolbe-Alexander, T.L., Finkelstein, E.A., Katzmarzyk, P.T., van Mechelen, W., Pratt, M., and Lancet Physical Activity Series 2 Executive, C. (2016). The economic burden of physical inactivity: a global analysis of major non-communicable diseases. Lancet 388, 1311-1324.

Dussault, I., Fawcett, D., Matthyssen, A., Bader, J.A., and Giguere, V. (1998). Orphan nuclear receptor ROR alpha-deficient mice display the cerebellar defects of staggerer. Mech Dev 70, 147-153.

Dyar, K.A., Lutter, D., Artati, A., Ceglia, N.J., Liu, Y., Armenta, D., Jastroch, M., Schneider, S., de Mateo, S., Cervantes, M., et al. (2018). Atlas of Circadian Metabolism Reveals System-wide Coordination and Communication between Clocks. Cell 174, 1571-1585 e1511.

Favier, F.B., Britto, F.A., Freyssenet, D.G., Bigard, X.A., and Benoit, H. (2015). HIF-1-driven skeletal muscle adaptations to chronic hypoxia: molecular insights into muscle physiology. Cellular and Molecular Life Sciences 72, 4681-4696.

Fleury, C., Mignotte, B., and Vayssiere, J.L. (2002). Mitochondrial reactive oxygen species in cell death signaling. Biochimie 84, 131-141.

Ghosh, N., Das, A., Chaffee, S., Roy, S., and Sen, C.K. (2018). Chapter 4 - Reactive Oxygen Species, Oxidative Damage and Cell Death. In Immunity and Inflammation in Health and Disease. S. Chatterjee, W. Jungraithmayr, and D. Bagchi, eds. (Academic Press), pp. 45-55.

Ghosh, S., Golbidi, S., Werner, I., Verchere, B.C., and Laher, I. (2010). Selecting exercise regimens and strains to modify obesity and diabetes in rodents: an overview. Clin Sci (Lond) 119, 57-74.

He, F., Li, J., Liu, Z., Chuang, C.C., Yang, W., and Zuo, L. (2016). Redox Mechanism of Reactive Oxygen Species in Exercise. Front Physiol 7, 486.

Henriquez-Olguin, C., Knudsen, J.R., Raun, S.H., Li, Z., Dalbram, E., Treebak, J.T., Sylow, L., Holmdahl, R., Richter, E.A., Jaimovich, E., et al. (2019). Cytosolic ROS production by NADPH oxidase 2 regulates muscle glucose uptake during exercise. Nat Commun 10, 4623.

Hoehn, K.L., Salmon, A.B., Hohnen-Behrens, C., Turner, N., Hoy, A.J., Maghzal, G.J., Stocker, R., Van Remmen, H., Kraegen, E.W., Cooney, G.J., et al. (2009). Insulin resistance is a cellular antioxidant defense mechanism. Proc Natl Acad Sci U S A 106, 17787-17792.

Homma, T., Kurahashi, T., Lee, J., Nabeshima, A., Yamada, S., and Fujii, J. (2018). Double Knockout of Peroxiredoxin 4 (Prdx4) and Superoxide Dismutase 1 (Sod1) in Mice Results in Severe Liver Failure. Oxid Med Cell Longev 2018, 2812904.

Houstis, N., Rosen, E.D., and Lander, E.S. (2006). Reactive oxygen species have a causal role in multiple forms of insulin resistance. Nature 440, 944-948.

Jordan, S.D., Kriebs, A., Vaughan, M., Duglan, D., Fan, W., Henriksson, E., Huber, A.L., Papp, S.J., Nguyen, M., Afetian, M., et al. (2017). CRY1/2 Selectively Repress PPARdelta and Limit Exercise Capacity. Cell Metab 26, 243-255 e246.

Kim, K., Boo, K., Yu, Y.S., Oh, S.K., Kim, H., Jeon, Y., Bhin, J., Hwang, D., Kim, K.I., Lee, J.S., et al. (2017). RORalpha controls hepatic lipid homeostasis via negative regulation of PPARgamma transcriptional network. Nat Commun 8, 162.

Kim, Y.J., Kim, H.J., Lee, W.J., and Seong, J.K. (2020). A comparison of the metabolic effects of treadmill and wheel running exercise in mouse model. Lab Anim Res 36, 3.

Kumar, P., Nagarajan, A., and Uchil, P.D. (2018). Analysis of Cell Viability by the MTT Assay. Cold Spring Harb Protoc 2018.

Lau, P., Fitzsimmons, R.L., Pearen, M.A., Watt, M.J., and Muscat, G.E. (2011). Homozygous staggerer (sg/sg) mice display improved insulin sensitivity and enhanced glucose uptake in skeletal muscle. Diabetologia 54, 1169-1180.

Lee, K.P., Shin, Y.J., Cho, S.C., Lee, S.M., Bahn, Y.J., Kim, J.Y., Kwon, E.S., Jeong, D.Y., Park, S.C., Rhee, S.G., et al. (2014). Peroxiredoxin 3 has a crucial role in the contractile function of skeletal muscle by regulating mitochondrial homeostasis. Free Radic Biol Med 77, 298-306.

Lee, Y.J. (2020). Knockout Mouse Models for Peroxiredoxins. Antioxidants (Basel) 9.

Lobelo, F., Stoutenberg, M., and Hutber, A. (2014). The Exercise is Medicine Global Health Initiative: a 2014 update. Br J Sports Med 48, 1627-1633.

Loizides-Mangold, U., Perrin, L., Vandereycken, B., Betts, J.A., Walhin, J.P., Templeman, I., Chanon, S., Weger, B.D., Durand, C., Robert, M., et al. (2017). Lipidomics reveals diurnal lipid oscillations in human skeletal muscle persisting in cellular myotubes cultured in vitro. Proc Natl Acad Sci U S A 114, E8565-E8574.

Manzanares, G., Brito-da-Silva, G., and Gandra, P.G. (2018). Voluntary wheel running: patterns and physiological effects in mice. Braz J Med Biol Res 52, e7830.

Margaritelis, N.V., Theodorou, A.A., Paschalis, V., Veskoukis, A.S., Dipla, K., Zafeiridis, A., Panayiotou, G., Vrabas, I.S., Kyparos, A., and Nikolaidis, M.G. (2018). Adaptations to endurance training depend on exercise-induced oxidative stress: exploiting redox interindividual variability. Acta Physiol (Oxf) 222.

Mayeuf-Louchart, A., Zecchin, M., Staels, B., and Duez, H. (2017). Circadian control of metabolism and pathological consequences of clock perturbations. Biochimie.

McCarthy, J.J., Andrews, J.L., McDearmon, E.L., Campbell, K.S., Barber, B.K., Miller, B.H., Walker, J.R., Hogenesch, J.B., Takahashi, J.S., and Esser, K.A. (2007). Identification of the circadian transcriptome in adult mouse skeletal muscle.

Meijer, J.H., and Robbers, Y. (2014). Wheel running in the wild. Proc Biol Sci 281.

Miller, B.H., McDearmon, E.L., Panda, S., Hayes, K.R., Zhang, J., Andrews, J.L., Antoch, M.P., Walker, J.R., Esser, K.A., Hogenesch, J.B., et al. (2007). Circadian and CLOCK-controlled regulation of the mouse transcriptome and cell proliferation. Proc Natl Acad Sci U S A 104, 3342-3347.

Munoz-Sanchez, J., and Chanez-Cardenas, M.E. (2019). The use of cobalt chloride as a chemical hypoxia model. J Appl Toxicol 39, 556-570.

Murphy, M.P. (2009). How mitochondria produce reactive oxygen species. Biochem J 417, 1-13.

Nagahisa, H., Okabe, K., Iuchi, Y., Fujii, J., and Miyata, H. (2016). Characteristics of Skeletal Muscle Fibers of SOD1 Knockout Mice. Oxid Med Cell Longev 2016, 9345970.

Pasut, A., Jones, A.E., and Rudnicki, M.A. (2013). Isolation and culture of individual myofibers and their satellite cells from adult skeletal muscle. J Vis Exp, e50074.

Pedersen, B.K., and Saltin, B. (2015). Exercise as medicine - evidence for prescribing exercise as therapy in 26 different chronic diseases. Scand J Med Sci Sports 25 Suppl 3, 1-72.

Pendergast, D.R., Leddy, J.J., and Venkatraman, J.T. (2000). A perspective on fat intake in athletes. J Am Coll Nutr 19, 345-350.

Perrin, L., Loizides-Mangold, U., Chanon, S., Gobet, C., Hulo, N., Isenegger, L., Weger, B.D., Migliavacca, E., Charpagne, A., Betts, J.A., et al. (2018). Transcriptomic analyses reveal rhythmic and CLOCK-driven pathways in human skeletal muscle. Elife 7.

Powers, S.K., Ji, L.L., Kavazis, A.N., and Jackson, M.J. (2011). Reactive oxygen species: impact on skeletal muscle. Compr Physiol 1, 941-969.

Rion, N., Castets, P., Lin, S., Enderle, L., Reinhard, J.R., and Ruegg, M.A. (2019). mTORC2 affects the maintenance of the muscle stem cell pool. Skelet Muscle 9, 30.

Sakellariou, G.K., McDonagh, B., Porter, H., Giakoumaki, II, Earl, K.E., Nye, G.A., Vasilaki, A., Brooks, S.V., Richardson, A., Van Remmen, H., et al. (2018). Comparison of Whole Body SOD1 Knockout with Muscle-Specific SOD1 Knockout Mice Reveals a Role for Nerve Redox Signaling in Regulation of Degenerative Pathways in Skeletal Muscle. Antioxid Redox Signal 28, 275-295.

Sato, S., Parr, E.B., Devlin, B.L., Hawley, J.A., and Sassone-Corsi, P. (2018). Human metabolomics reveal daily variations under nutritional challenges specific to serum and skeletal muscle. Mol Metab 16, 1-11.

Sato, T.K., Panda, S., Miraglia, L.J., Reyes, T.M., Rudic, R.D., McNamara, P., Naik, K.A., FitzGerald, G.A., Kay, S.A., and Hogenesch, J.B. (2004). A functional genomics strategy reveals Rora as a component of the mammalian circadian clock. Neuron 43, 527-537.

Sies, H., Stahl, W., and Sevanian, A. (2005). Nutritional, dietary and postprandial oxidative stress. J Nutr 135, 969-972.

Silveira, L.R., Pilegaard, H., Kusuhara, K., Curi, R., and Hellsten, Y. (2006). The contraction induced increase in gene expression of peroxisome proliferator-activated receptor (PPAR)-gamma coactivator 1alpha (PGC-1alpha), mitochondrial uncoupling protein 3 (UCP3) and hexokinase II (HKII) in primary rat skeletal muscle cells is dependent on reactive oxygen species. Biochim Biophys Acta 1763, 969-976.

Simioni, C., Zauli, G., Martelli, A.M., Vitale, M., Sacchetti, G., Gonelli, A., and Neri, L.M. (2018). Oxidative stress: role of physical exercise and antioxidant nutraceuticals in adulthood and aging. Oncotarget 9, 17181-17198.

Simonson, D.C., and DeFronzo, R.A. (1990). Indirect calorimetry: methodological and interpretative problems. Am J Physiol 258, E399-412.

Steinmayr, M., Andre, E., Conquet, F., Rondi-Reig, L., Delhaye-Bouchaud, N., Auclair, N., Daniel, H., Crepel, F., Mariani, J., Sotelo, C., et al. (1998). staggerer phenotype in retinoid-related orphan receptor alpha-deficient mice. Proc Natl Acad Sci U S A 95, 3960-3965.

Sulli, G., Manoogian, E.N.C., Taub, P.R., and Panda, S. (2018). Training the Circadian Clock, Clocking the Drugs, and Drugging the Clock to Prevent, Manage, and Treat Chronic Diseases. Trends Pharmacol Sci 39, 812-827.

Takahashi, J.S. (2017). Transcriptional architecture of the mammalian circadian clock. Nat Rev Genet 18, 164-179.

van Dijk, M., Dijk, F.J., Bunschoten, A., van Dartel, D.A., van Norren, K., Walrand, S., Jourdan, M., Verlaan, S., and Luiking, Y. (2016). Improved muscle function and quality after diet intervention with leucine-enriched whey and antioxidants in antioxidant deficient aged mice. Oncotarget 7, 17338-17355.

van Moorsel, D., Hansen, J., Havekes, B., Scheer, F.A.J.L., Jörgensen, J.A., Hoeks, J., Schrauwen-Hinderling, V.B., Duez, H., Lefebvre, P., Schaper, N.C., et al. (2016). Demonstration of a day-night rhythm in human skeletal muscle oxidative capacity. Molecular Metabolism 5, 635-645.

Wang, Y., Yang, F., Gritsenko, M.A., Wang, Y., Clauss, T., Liu, T., Shen, Y., Monroe, M.E., Lopez-Ferrer, D., Reno, T., et al. (2011). Reversed-phase chromatography with multiple fraction concatenation strategy for proteome profiling of human MCF10A cells. Proteomics 11, 2019-2026.

Woldt, E., Sebti, Y., Solt, L.A., Duhem, C., Lancel, S., Eeckhoute, J., Hesselink, M.K.C., Paquet, C., Delhaye, S., Shin, Y., et al. (2013). Rev-erb-[alpha] modulates skeletal muscle oxidative capacity by regulating mitochondrial biogenesis and autophagy. Nat Med 19, 1039-1046.

Zhang, R., Lahens, N.F., Ballance, H.I., Hughes, M.E., and Hogenesch, J.B. (2014). A circadian gene expression atlas in mammals: implications for biology and medicine. Proceedings of the National Academy of Sciences of the United States of America 111, 16219-16224.

Zhang, Y.G., Wang, L., Kaifu, T., Li, J., Li, X., and Li, L. (2016). Featured Article: Accelerated decline of physical strength in peroxiredoxin-3 knockout mice. Exp Biol Med (Maywood) 241, 1395-1400.

Zheng, B., Larkin, D.W., Albrecht, U., Sun, Z.S., Sage, M., Eichele, G., Lee, C.C., and Bradley, A. (1999). The mPer2 gene encodes a functional component of the mammalian circadian clock. Nature 400, 169-173.

Zuo, L., and Pannell, B.K. (2015). Redox Characterization of Functioning Skeletal Muscle. Front Physiol 6, 338.

5 Discussion

Circadian rhythm disruption (CRD) is associated with various chronic diseases, including obesity and diabetes, cardiovascular disease, inflammation, and cancer (Davis et al., 2001; Kervezee et al., 2020; Knutsson, 2003; Loef et al., 2019). Remarkably, clock disruption was likewise connected to perturbations in muscle functions like repair, autophagy, lipid homeostasis, insulin sensitivity, mitochondrial metabolism and respiration (Andrews et al., 2010; Dyar et al., 2014; Loizides-Mangold et al., 2017; Woldt et al., 2013), which has detrimental effects on whole-body metabolism and overall health. Likewise, physical inactivity and a sedentary lifestyle have been linked to chronic disorders like type-2-diabetes, obesity, cardiovascular diseases, cancer, and an increased risk of premature death (Ding et al., 2016; Gonzalez et al., 2017; Patterson et al., 2018). Regular physical activity could prevent or treat most of the syndromes mentioned above (Lavie et al., 2019; McTiernan et al., 2019; Pedersen and Saltin, 2015). The myriad effects of exercise are not merely achieved by skeletal muscle adaptation, but owed to exercise-induced changes in other organs, like the liver, fat, and brain. Myokines are cytokines produced and released by the muscle, especially after exercise (Delezie and Handschin, 2018; Schnyder and Handschin, 2015). They play a crucial role in organ crosstalk to promote exercise adaptation in other tissues and control whole-body homeostasis (Whitham and Febbraio, 2016). In human skeletal muscle cells, myokine release is clock-controlled (Perrin et al., 2015). Therefore, additionally to skeletal muscle exercise adaptation, whole-body beneficial effects are likely guided by the skeletal muscle clock.

We investigated the skeletal muscle response to exercise in a time-of-day-dependent manner, effects of exercise on the skeletal muscle clock, and the significance of the circadian clock on muscle function and exercise performance.

5.1 On the effects of timed exercise

Our first study revealed a variation in maximal exercise performance over the 24-h LD cycle and identified specific, novel cellular pathways that are influenced by exercise in a time-of-day-dependent manner. The timely secretion of putative myokines might improve exercise performance, skeletal muscle adaptations, and the health benefits related to regular training. Especially coordinating the muscle-stimulated glucose release by the liver with glucose uptake and metabolism by the muscle could significantly improve exercise performance. We propose a new methodology to explore the effects of chronic exercise training at different times of the day in preclinical mouse models, and provide large-scale transcriptomic, proteomic, and phosphoproteomic data, serving as a resource for future hypothesis-driven research and validation studies.

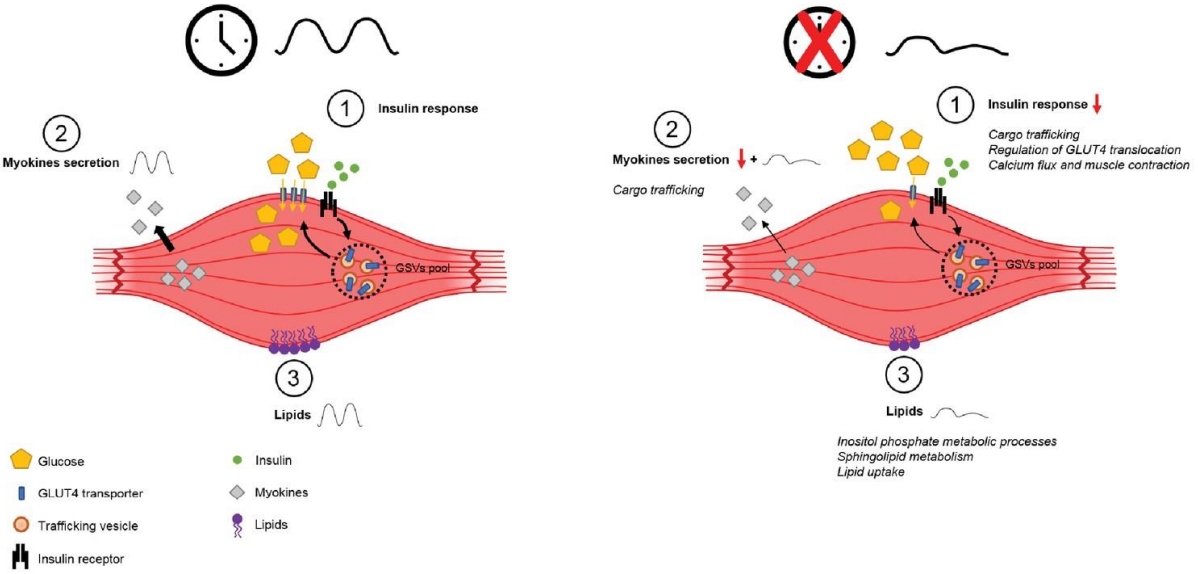

Figure D1. Schema summarizing the impact of clock disruption on muscle metabolic function. Disruption of the clock leads to impaired insulin sensitivity and decreased glucose uptake (1), causes dysregulation of genes involved in vesicle trafficking (2) and impacts lipid metabolism and lipid metabolite oscillations (3) as reported in Loizides-Mangold et al. (2017). (Perrin et al., 2018)

Time, exercise and the skeletal muscle clock

Contrary to Sato et al., (Sato et al., 2019), our study was not designed to assess the impact of scheduled acute treadmill exercise on the subsequent 24-h oscillations of metabolic and muscle-specific genes in skeletal muscle. We did evaluate, however, 24-h core clock and clock-controlled gene expression patterns in muscles of daytime vs. nighttime wheel active mice by conventional qPCR. We show that the phase of expression of some core clock genes is altered by daytime wheel access. For instance, *Per2* and *Cry2* genes displayed a phase-advance of expression in response to daytime wheel running. Interestingly, daytime exercise also produced a significant phase shift of PER2::LUC bioluminescence rhythms as measured from mouse skeletal muscle explants (Wolff and Esser, 2012b). Hence, the advanced expression of, e.g., *Per2* and *Cry2* transcripts observed in the muscles of DA mice, is likely the results of entrainment and not a mere response to an acute bout of wheel running. Moreover, we observed decreased expression levels of *Bmal1, Clock*, *Cry1,* and *Per3* prior to wheel access in DA animals, further suggesting a sustained effect of chronic daytime activity. Even though exercise has been proposed as a potent Zeitgeber for the skeletal muscle clock (Kemler et al., 2020; Wolff and Esser, 2012b), the transcriptional changes induced by daytime wheel exercise are rather mild, especially in comparison to the effects of daytime feeding on core clock gene oscillations in both liver and muscle tissues (Damiola et al., 2000; Reznick et al., 2013) (**Figure D2B**). Moreover, we did not observe changes in the daily expression of downstream targets of the clock e.g., *Cpt1a, Pdk4, Tbc1d1* and *MyoD*. Finally, we were unable to detect altered protein abundance or posttranslational modification of circadian proteins in response to

chronic daytime activity—at least for those proteins covered by our MS analysis. Hence, in the long-term and in the present experimental conditions, we do not provide evidence that daytime wheel running is a strong Zeitgeber for the skeletal muscle clock.

Many experiments, studying exercise as Zeitgeber in wild-type mice, included daily handling, and thus possibly stress-induced hormone signaling. For instance, glucocorticoid hormones (e.g., corticosterone), are secreted upon stress and have significant circadian signaling properties (Spencer et al., 2018), making stress a Zeitgeber for peripheral clocks (Sasaki et al., 2016; Tahara et al., 2015). The absence of differences in corticosterone levels, together with mild effects of voluntary wheel exercise on the muscle clock in our experiment, indicate that stress might be one of the major feedbacks to the muscle clock during exercise.

Additionally, to exercise, we investigated the role of food in the synchronization of the skeletal muscle clock. Contrary to previously published data (Reznick et al., 2013), we provided wheel access during the active phase (to CTRL and daytime feeding (DF) mice). We observed increased wheel-running activity in the DF mice compared to the CTRL group (**Figure D2A**). Moreover, we observed changes in the daily expression of metabolic genes, e.g., *Pdk4* and *Fasn* expression was inverted in DF mouse muscle (**Figure D2C**). Nutritional availability, insulin signaling, and changes in body temperature due to food intake are systemic synchronization cues (Crosby et al., 2019; Morf and Schibler, 2013) and thus affect both liver and muscle core clock gene expression more substantially.

Using PER1/2 null mice, Ezagouri et al. (Ezagouri et al., 2019) found that exercise variation within the active phase of the mouse relies on the circadian clock and produces a distinct daytime-dependent response in the muscle. However, constitutive, whole-body clock-compromised mouse models often show a complex behavioral and metabolic phenotype (Andrews et al., 2010; Delezie et al., 2012; Delezie et al., 2016; Jordan et al., 2017; Woldt et al., 2013; Zheng et al., 1999). Future studies, using conditional knockout mouse models, to control the temporal suppression of clock components specifically in skeletal muscle, could shed light on the specific involvement of the circadian clock in the regulation of muscle contractile and metabolic properties, and likewise on the skeletal muscle-initiated crosstalk with other organs, at specific phases of the LD cycle. Finally, it would be interesting to investigate the “trainability” of mice at different times of the day in muscle-specific clock KO and wild-type mouse models, in combination or not with nutritional strategies.

As previously discussed, muscle and liver glycogen depletion is thought to be one of the main determinants of exercise capacity (Shulman and Rothman, 2001). Further studies, restricting food access to the inactive phase one day prior to a maximal exercise capacity test, to prevent glycogen depletion during the inactive phase, could shed light on the importance of glycogen stores and feeding status in mouse maximal exercise performance.

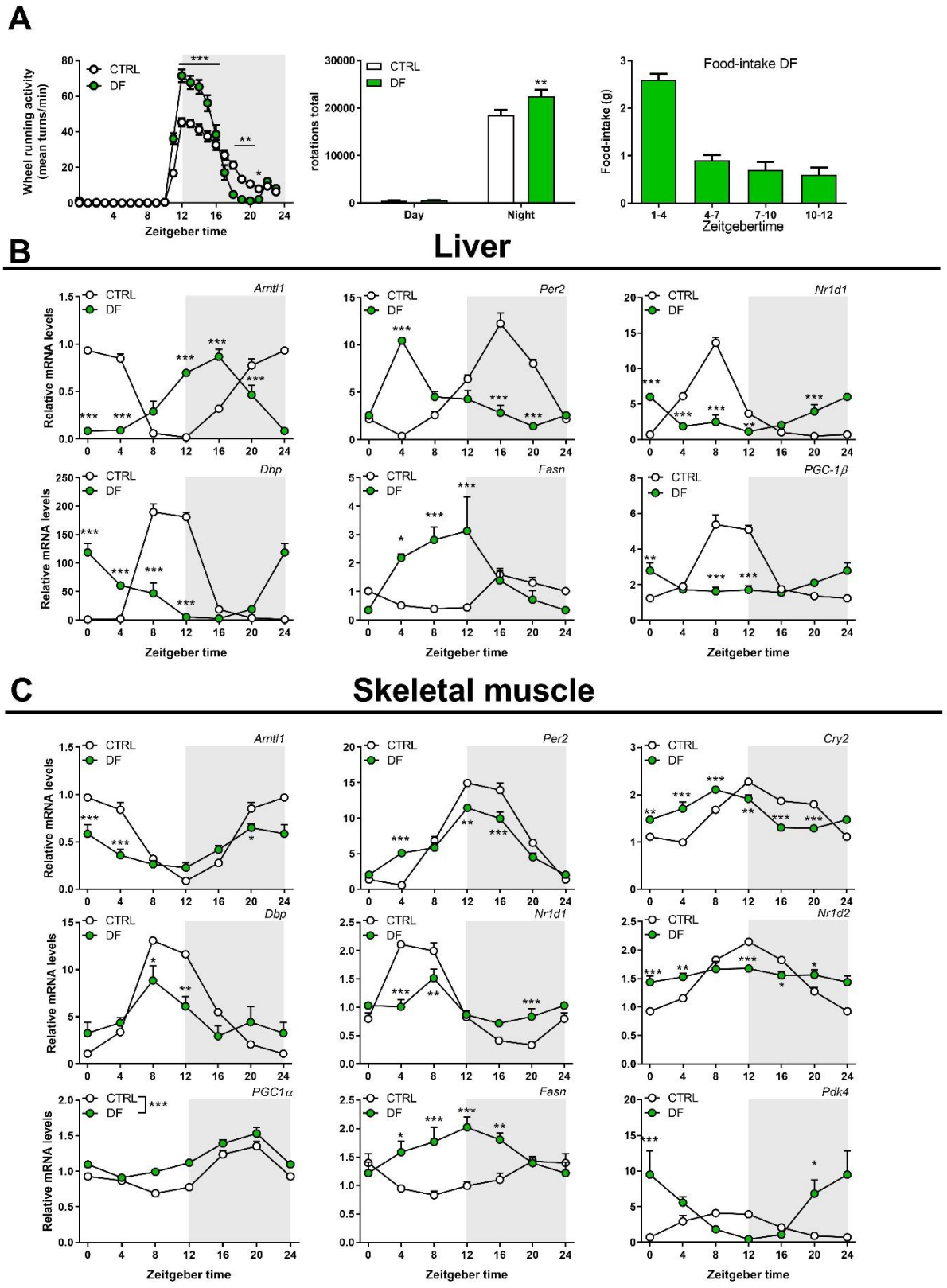

FIGURE D2. Daytime vs. nighttime feeding. (A) wheel running and food-intake in daytime fed mice. Clock gene expression in control (CTRL) and daytime feeding (DF) mice. (B) in liver, (C) in muscle. Expression values were determined by qPCR and normalized to Hprt. Data is shown as the average fold-change ± SEM (n = 4) relative to the expression in SED ZT0 set to 1 * P < 0.05; ** P < 0.01; *** P < 0.001. One-way ANOVA.

However, although critical enzymes for glycogen synthesis and breakdown are controlled by the circadian clock (Doi et al., 2010; Roesler and Khandelwal, 1985), fatigue is much more complex. For instance, although the energy stores (i.e., glycogen) in muscle and liver were replenished at ZT20, exercise performance at that time was poor. While in-depth transcriptomic, proteomic, or phosphoproteomic analysis could reveal underlying molecular processes of muscle-derived fatigue in these mice, the low performance could have been controlled by the SCN directly. The phenomenon of a "nocturnal break" or "siesta" can be observed in a drop of wheel running and general activity, core body temperature, and food intake in C57BL/6 mice around ZT20 (**Figure D3**), and is SCN-controlled (Dudley et al., 2003; Ehlen et al., 2015).

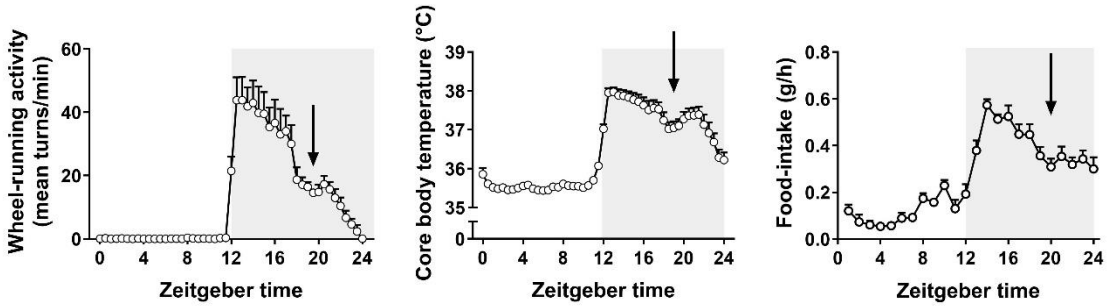

FIGURE D3. "siesta" in CTRL mice wheel running, core body temperature, and food-intake.

Proteomics and circadian proteins

Our MS coverage allowed us to detect some of the circadian proteins in mouse skeletal muscle (i.e., CSNk1a1, CSNk1d, CSNk1e, CLOCK, DBP). However, their abundance and posttranslational status were only mildly affected by acute treadmill exercise. Only CLOCK protein level was increased 3 h after treadmill exercise when performed at ZT0, while CSNk1 proteins were down-regulated 3 h after treadmill exercise was performed at ZT12. The decreased abundance of CSNK1 protein isoforms could thus parallel an increase of PER protein stability at night (Kojima et al., 2011). However, even though PER1/2 affect many biochemical processes such as metabolism (Grimaldi et al., 2010; Liu et al., 2014), the role of the PER proteins in skeletal muscle function and response to exercise remains unknown.

Daytime activity, SPP and SCN

In mammals, light directly entrains the endogenous suprachiasmatic nucleus (SCN) clock but likewise affects spontaneous behavior by suppressing locomotor activity in nocturnal species. This phenomenon, called masking (Aschoff, 1960; Pendergast and Yamazaki, 2011), is particularly observed in daytime food-restricted animals exposed to a standard LD cycle (Delezie et al., 2016). To investigate the effects of chronic daytime voluntary wheel running, we have exposed our mice to a skeleton photoperiod (SPP), which consist of pulses of light

given at dusk and dawn (Rosenwasser et al., 1983). Notably, daily expression of *Per1* and *Per2* transcripts is robustly maintained in the SCN of mice exposed to SPP vs. to a standard 12:12 LD cycle (Oishi et al., 2002). However, we did not investigate whether daytime wheel running under a SPP alter gene oscillations in the SCN. At least, we show that rhythmic parameters known to be influenced by the SCN clock, such as plasma corticosterone and liver gene expression (Kalsbeek et al., 2011; Saini et al., 2013), remain unchanged in DA mice. Furthermore, previous studies did not detect change in the expression pattern of *Per1* and *Per2* in the SCN of rodents forced to exercise during the light phase of a standard LD cycle (Salgado-Delgado et al., 2008; Sasaki et al., 2016; Wolff and Esser, 2012b). Hence, it is unlikely that the combination of SPP and daytime-restricted wheel activity affects the phase of the SCN clock.

On the timed effects of regular training

A single bout of voluntary wheel running exercise rapidly alters the expression of up to 200 genes in skeletal muscle of untrained mice (Choi et al., 2005). However, it remains unclear whether an acute bout of wheel activity is likewise a potent inducer of gene expression in a trained state. We observed a robust transcriptional response in skeletal muscle of daytime active animals with the induction of up to a 1000 genes, without the confounding effect of feeding. This clearly shows that transcriptional reprogramming in skeletal muscle still plays an important role even in long-term exercised mice. A specific response to daytime wheel exercise was observed at both the proteome and phosphoproteome levels, further highlighting the metabolic remodeling occurring in daytime contracting muscles. A similar methodology using SPP exposure and time-controlled wheel access could thus be used to further investigate the effects of spontaneous activity at unusual times of the day on other physiological aspects, including the crosstalk between skeletal muscle and other organs (Delezie and Handschin, 2018). Incidentally, we did not observe great changes in the muscle transcriptome, proteome and phosphoproteome of CTRL animals at ZT16 (i.e., those with wheel access only at night)) as compared to DA animals (i.e., those with wheel access only during the day)—despite the similar level of activity achieved by both groups between ZT2 and 4 and ZT13 and 15 (**Figure S7C** MS-1). It is thus likely that other aspects such as feeding activities have the potential to confound the results of studies investigating the effect of nighttime wheel running on skeletal muscle.

In humans, shift-workers are compelled to work at night during their sleep phase or to rotate shifts, which lead to a misalignment between external signals (e.g., light and food) and rhythmic physiological parameters (e.g., sleep, metabolism, and hormonal secretions) (Arendt, 2010; Chellappa et al., 2019). Importantly, more than working/being active at the wrong time of the day, irregular timing of eating may be the major contributor to internal desynchronization in humans (reviewed in (Chaix et al., 2019; Lowden et al., 2010)). This is

especially supported by studies of peripheral desynchronization in rodent models (Barclay et al., 2012; Delezie et al., 2016; Reznick et al., 2013; Salgado-Delgado et al., 2008; Salgado-Delgado et al., 2013). For instance, feeding during the usual resting period, together or without forced locomotion, alters the rhythmic pattern of gene expression in the liver, skeletal muscle, and of corticosterone release—a major internal Zeitgeber for multiple peripheral organs (Oster et al., 2017; Sasaki et al., 2016). Importantly, the effects of daytime feeding on the aforementioned parameters are now clearly dissociated from the effects of scheduled wheel activity. Indeed, we show that regular daytime wheel running exercise—at the opposite phase of the normal daily cycle—does not promote peripheral desynchronization in liver and muscle tissues. Even though physical activity is a rather weak Zeitgeber for skeletal muscle clock—at least in the present experimental conditions—, it is a potent modulator of the cardiovascular, respiratory, metabolic, and neuroendocrine systems, and thus justifies further studies. We think that time-restricted wheel access in the absence of the interfering masking effects of light could further be used to investigate whether the chrono-therapeutic approach of exercising can offset many of the detrimental effects of irregular feeding. Besides, the use of wheel running exercise as an approach to reduce desynchrony is a more natural exercise modality and presents several advantages for long-term studies as compared to treadmill exercise (discussed in (Ghosh et al., 2010)).

Limitations and perspectives

Data suggest that C57BL6 mice are not the best model for treadmill exercise performance and training adaptation/improvement while being one of the top runners in voluntary wheel running (Ghosh et al., 2010). Indicating that the appropriate mouse strains are important and may strongly influence the outcome of laboratory research. Moreover, besides the protocol, the timing of peak exercise might differ between mouse strains, and housing conditions might similarly affect exercise performance and training (Raun et al., 2020), as it does metabolism (Corrigan et al., 2020).

A specific evaluation of all exercise-responsive genes and gene sets at all ZT is beyond the scope of this study; we focused our multi-omics investigations at times points where treadmill exercise performance varies the most, and at opposite phases of mouse' spontaneous motivation for wheel running. Finally, we did not compare the multi-omics datasets obtained from treadmill-exercised mice with those obtained from chronically wheel-trained animals. These are different exercise modalities: treadmill running is forced (thus, generator of stress), sustained and similar to endurance exercise; wheel running is motivation-based, intermittent and resembles High-Intensity Interval Training (HIIT)-like activity (De Bono et al., 2006; Ghosh et al., 2010).

We suggest a time coordinated response of the muscle to exercise and especially the coordination of cross-tissue communication with muscle activation of metabolic pathways to

take up and metabolize glucose. In order to elucidate and verify the mechanism behind our observations, additional experiments would need to be conducted. For instance, the Glucose Transporter Type 4 (GLUT4) translocation to the membrane after an exercise bout by muscle cross-section staining (Bradley et al., 2014) could be investigated. Moreover, the activity of the Glucose 6-Phosphate Dehydrogenase (G6PD) in the liver could be measured after exercise in the early light vs. the early dark phase (Lee, 1982).

We show here that mice under SPP and daytime-restricted wheel access self-imposed a time-limited and relatively constant running distance during their resting period over three weeks. In our study, however, wheel access was manually unlocked from ZT1 (i.e., immediately after the 1 h light-pulse). It would thus be interesting to unlock the wheel at different ZT of the resting period and evaluate whether mice would still spontaneously run and to which extent. The consequences of an acute phase-shift of wheel running access on the skeletal muscle and whole-body responses, in particular at the circadian level, could similarly be investigated in animals pre-trained in wheels. Notably, this could be done in synchronized animals exposed to a SPP as in the present study or in free-running animals exposed to constant darkness.

In summary, we show for the first time, that maximal exercise performance varies over the 24-h LD cycle. We identified specific, novel cellular pathways that are influenced by exercise in a time-of-day-dependent manner. The timely secretion of putative myokines might improve exercise performance, skeletal muscle adaptations, and the health benefits related to regular training. Moreover, we provide evidence that under environmental light conditions, food-intake is a stronger Zeitgeber for the skeletal muscle clock than wheel running. We propose a new methodology to explore the effects of chronic exercise training at different times of the day in preclinical mouse models without the confining effect of food-intake. Our large-scale transcriptomic, proteomic, and phosphoproteomic data, hopefully, will serve as a resource for future hypothesis-driven research and validation studies.

5.2 On clock-controlled muscle functions

Our second study investigated the role of retinoic acid receptor-related orphan receptor α (RORα) in skeletal muscle. RORα, a transcription factor and key regulator of the circadian clock (Akashi and Takumi, 2005; Sato et al., 2004), binds to PGC-1a (Liu et al., 2007) and inhibits PPARγ activity in the liver (Kim et al., 2017). The binding partners in the liver indicate a possibly important role in skeletal muscle metabolism and exercise performance. We observed decreased voluntary wheel running in the Rorα MKO mice, while the distance on the treadmill in the maximal capacity, as well as the endurance capacity test was significantly increased. As previously discussed, reactive oxygen species (ROS) detoxification enzymes are decreased in RORα MKO muscle, which could lead to a ROS accumulation and thus muscle damage upon chronic long-term exercise.

Exercise and the brain

Chronic stress, a depression model in mice (Willner, 2017), leads to decreased wheel activity (DeVallance et al., 2017). Hence, besides a possible contribution in ROS detoxification, Rorα could be necessary for myokine production or release upon exercise (Schnyder and Handschin, 2015). Especially the crosstalk between the muscle and the brain is essential for the mood and memory-enhancing effects of exercise (Delezie and Handschin, 2018). Recently the critical role of skeletal muscle BMAL1 in sleep homeostasis was observed in BMAL1 gKO mice, in which the skeletal muscle-specific rescue was sufficient to restore normal sleeping patterns, while the brain-specific rescue was not (Ehlen et al., 2017). While no difference in sleep was observed in the RORα mice (data unpublished), other factors like mood or neuronal innervation could be altered in skeletal muscle-specific RORα MKO mice. Indeed, Kynurenine aminotransferase 3 (KAT3), catalyzing the conversion of the neurotoxic kynurenine (KYN) to kynurenic acid (KYNA), which is unable to cross the brain-blood-barrier, was decreased in our proteomic analysis after chronic nighttime treadmill training. KATs are essential enzymes in the exercise-related amelioration of depression (Agudelo et al., 2014; Schlittler et al., 2016). Besides, cathepsin D (CTSD) is decreased after exercise in MKO. Although less is known about its function in exercise mediated effects than for CTSB (Moon et al., 2016), its decrease in plasma has been associated with aging (Zhong et al., 2016).

To further investigate the possible role of RORα in muscle brain crosstalk and thus behavioral changes and anxiety/depression, we sent a group of mice to the German Mouse Clinic (GMC) in Munich, where different behavioral tests are performed. So far, no difference in locomotion or anxiety-related behavior; however, a slight decrease in acoustic startle reactivity has been found. Acoustic startle reactivity is a reflex (Davis, 1980), and changes indicate a possible impaired neuromuscular recruitment.

The clock and metabolism

Whole-body RORα deficiency leads to abnormal circadian behavior (Akashi and Takumi, 2005) and metabolic changes (Lau et al., 2008). Likewise, in skeletal muscle, RORα has been linked to the coordination of energy metabolism (Lau et al., 2011; Lau et al., 2004). Both models, however, have significant drawbacks. The first model was the whole-body Rorα deficient "staggerer" mice (Sidman et al., 1962), possessing a mutation in the Rorα gene (Hamilton et al., 1996). As indicated by Sidman and others, Rorα is essential for cerebellum development (Dussault et al., 1998; Guissart et al., 2018; Sidman et al., 1962). Defects in brain structure and development are often associated with behavioral changes and thus might alter whole-body metabolism. The second model was the overexpression of a dominant-negative form of Rorα in skeletal muscle cells. While the dominant-negative RORα protein prevents the binding of the endogenous protein, it likewise possibly prevents the competitively binding of Rev-erb to its target promoter. With the previously indicated role of RORα in mind, we performed oral glucose tolerance and insulin tolerance tests (under chow and high-fat diet conditions) and did not observe significant differences between the CTRL and MKO group. The Transcriptomic analysis revealed a possible increase in mitochondrial biogenesis and oxidative phosphorylation. However, no significant increase in mitochondrial DNA, nor changes in oxygen consumption using a mitochondrial stress assay kit (Seahorse) were observed.

Limitations and perspectives

Difficulties in confirming a metabolic involvement of RORα in skeletal muscle could arise from early deletion and possible compensatory mechanisms (Bunton-Stasyshyn et al., 2019; El-Brolosy and Stainier, 2017). Indeed, we detected an increased expression of *Rorγ* in the muscle of the *Rorα* MKO mice. RORα and RORγ show some redundancy in the regulation of glucose and lipid metabolic genes (Duez and Staels, 2008; Jetten et al., 2013). However, the functionality of such compensation needs to be further investigated. An elegant solution to bypass early compensation and exclude developmental defects is to use an inducible mouse model.

Although our studies revealed interest aspects of a transcriptional activator in skeletal muscle function, the datasets we generated still have a lot to explore. On the one hand, the failure to fully explore the potential of the data sets, due to missing expertise could be seen as a limitation of the study. On the other hand, with the help of collaborations (e.g., with Dr. Pål Westermark), the data could lead to many fruitful and exciting projects integrating muscle physiology and circadian biology.

The synchrony of biological clocks is tightly linked to health across the lifespan. With increasing age, a dampening–decrease of amplitude–of clock gene oscillations in the SCN and peripheral tissues has been observed in rodents (Agudelo et al., 2014). Although we did not observe premature death in the Rorα MKO mice, they might serve as a premature aging model

for skeletal muscle, as the majority of the clock gene expression is dampened. If RORα is coordinating the crosstalk between skeletal muscle and other tissues, including the brain, this animal model might help to reveal possible mechanisms of muscle aging and new insights in therapeutical approaches, including exercise, to sustain a healthy body communication.

The RORα function in muscle could be complex and versatile, ranging from ROS detoxification, over energy metabolism, to myokine secretion, yet, follow-up experiments have to be performed to reveal its importance.

5.3 Conclusion on Ph.D. work

The mechanisms by which exercise exerts health benefits have been relatively well studied on the tissue level; however, the systemic influence is not entirely understood. Clock-coordinated responses might partially mediate the local and systemic benefits of exercise. Taken together, we provide evidence that exercise performance, response, and adaptation are strongly influenced by timed muscle functions—for instance, myokine secretion, energy substrate metabolism, and ROS detoxification. During early light phase exercise, for instance, the request, uptake, and metabolism of energy substrate seem to be optimized, possibly improving exercise performance. This time-of-day dependent cross-organ communication with the liver and brain is possibly mediating the systemic exercise response. Therefore, dependent on the desired outcome, the time of exercise might be crucial for the successful treatment of diseases, boost of health benefits, and improved performance in elite athletes.

FIGURE D4. Graphical abstract of proposed clock function in skeletal muscle.

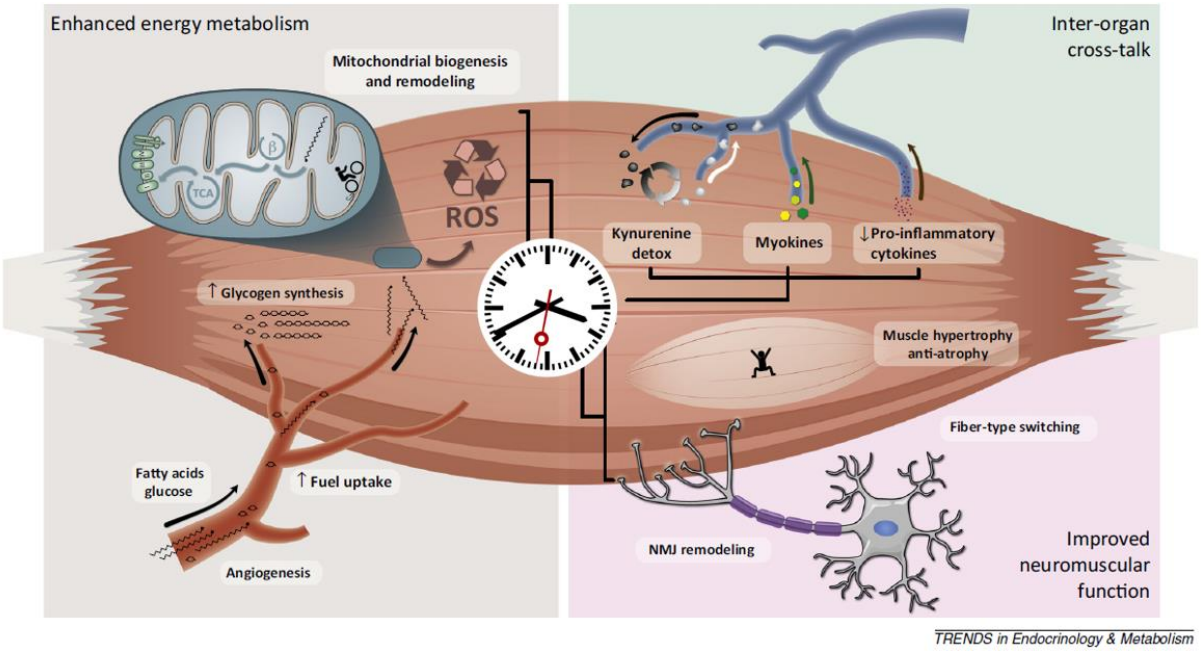

(modified from (Correia et al., 2015))

6 References of Thesis

Agudelo, L.Z., Femenia, T., Orhan, F., Porsmyr-Palmertz, M., Goiny, M., Martinez-Redondo, V., Correia, J.C., Izadi, M., Bhat, M., Schuppe-Koistinen, I., et al. (2014). Skeletal muscle PGC-1alpha1 modulates kynurenine metabolism and mediates resilience to stress-induced depression. Cell 159, 33-45.

Akashi, M., and Takumi, T. (2005). The orphan nuclear receptor RORalpha regulates circadian transcription of the mammalian core-clock Bmal1. Nat Struct Mol Biol 12, 441-448.

Akashi, M., Tsuchiya, Y., Yoshino, T., and Nishida, E. (2002). Control of intracellular dynamics of mammalian period proteins by casein kinase I epsilon (CKIepsilon) and CKIdelta in cultured cells. Mol Cell Biol 22, 1693-1703.

Albrecht, U. (2012). Timing to Perfection: The Biology of Central and Peripheral Circadian Clocks. Neuron 74, 246-260.

Andrews, J.L., Zhang, X., McCarthy, J.J., McDearmon, E.L., Hornberger, T.A., Russell, B., Campbell, K.S., Arbogast, S., Reid, M.B., Walker, J.R., et al. (2010). CLOCK and BMAL1 regulate MyoD and are necessary for maintenance of skeletal muscle phenotype and function. Proceedings of the National Academy of Sciences of the United States of America 107, 19090-19095.

Arendt, J. (2010). Shift work: coping with the biological clock. Occup Med (Lond) 60, 10-20.

Aschoff, J. (1960). Exogenous and endogenous components in circadian rhythms. Cold Spring Harb Symp Quant Biol 25, 11-28.

Atkinson, G., and Reilly, T. (1996). Circadian variation in sports performance. Sports Med 21, 292-312.

Aviram, R., Manella, G., Kopelman, N., Neufeld-Cohen, A., Zwighaft, Z., Elimelech, M., Adamovich, Y., Golik, M., Wang, C., Han, X., et al. (2016). Lipidomics Analyses Reveal Temporal and Spatial Lipid Organization and Uncover Daily Oscillations in Intracellular Organelles. Mol Cell 62, 636-648.

Ballor, D.L., and Keesey, R.E. (1991). A meta-analysis of the factors affecting exercise-induced changes in body mass, fat mass and fat-free mass in males and females. Int J Obes 15, 717-726.

Barclay, J.L., Husse, J., Bode, B., Naujokat, N., Meyer-Kovac, J., Schmid, S.M., Lehnert, H., and Oster, H. (2012). Circadian desynchrony promotes metabolic disruption in a mouse model of shiftwork. PLoS One 7, e37150.

Bass, J., and Lazar, M.A. (2016). Circadian time signatures of fitness and disease. Science 354, 994-999.

Bassel-Duby, R., and Olson, E.N. (2006). Signaling pathways in skeletal muscle remodeling. Annu Rev Biochem 75, 19-37.

Benziane, B., Burton, T.J., Scanlan, B., Galuska, D., Canny, B.J., Chibalin, A.V., Zierath, J.R., and Stepto, N.K. (2008). Divergent cell signaling after short-term intensified endurance training in human skeletal muscle. Am J Physiol Endocrinol Metab 295, E1427-1438.

Booth, F.W., Gordon, S.E., Carlson, C.J., and Hamilton, M.T. (2000). Waging war on modern chronic diseases: primary prevention through exercise biology. J Appl Physiol (1985) 88, 774-787.

Bradley, H., Shaw, C.S., Worthington, P.L., Shepherd, S.O., Cocks, M., and Wagenmakers, A.J. (2014). Quantitative immunofluorescence microscopy of subcellular GLUT4 distribution in human skeletal muscle: effects of endurance and sprint interval training. Physiol Rep 2.

Bunton-Stasyshyn, R.K.A., Wells, S., and Teboul, L. (2019). When all is not lost: considering genetic compensation in laboratory animals. Lab Anim (NY) 48, 282-284.

Callaway, E., and Ledford, H. (2017). Medicine Nobel awarded for work on circadian clocks. Nature 550, 18.

Cao, Q., Zhao, X., Bai, J., Gery, S., Sun, H., Lin, D.C., Chen, Q., Chen, Z., Mack, L., Yang, H., et al. (2017). Circadian clock cryptochrome proteins regulate autoimmunity. Proc Natl Acad Sci U S A 114, 12548-12553.

Chaix, A., Manoogian, E.N.C., Melkani, G.C., and Panda, S. (2019). Time-Restricted Eating to Prevent and Manage Chronic Metabolic Diseases. Annu Rev Nutr 39, 291-315.

Chellappa, S.L., Vujovic, N., Williams, J.S., and Scheer, F. (2019). Impact of Circadian Disruption on Cardiovascular Function and Disease. Trends Endocrinol Metab 30, 767-779.

Cho, H., Zhao, X., Hatori, M., Yu, R.T., Barish, G.D., Lam, M.T., Chong, L.W., DiTacchio, L., Atkins, A.R., Glass, C.K., et al. (2012). Regulation of circadian behaviour and metabolism by REV-ERB-alpha and REV-ERB-beta. Nature 485, 123-127.

Choi, S., Liu, X., Li, P., Akimoto, T., Lee, S.Y., Zhang, M., and Yan, Z. (2005). Transcriptional profiling in mouse skeletal muscle following a single bout of voluntary running: evidence of increased cell proliferation. J Appl Physiol (1985) 99, 2406-2415.

Correia, J.C., Ferreira, D.M., and Ruas, J.L. (2015). Intercellular: local and systemic actions of skeletal muscle PGC-1s. Trends Endocrinol Metab 26, 305-314.

Corrigan, J.K., Ramachandran, D., He, Y., Palmer, C.J., Jurczak, M.J., Chen, R., Li, B., Friedline, R.H., Kim, J.K., Ramsey, J.J., et al. (2020). A big-data approach to understanding metabolic rate and response to obesity in laboratory mice. Elife 9.

Crosby, P., Hamnett, R., Putker, M., Hoyle, N.P., Reed, M., Karam, C.J., Maywood, E.S., Stangherlin, A., Chesham, J.E., Hayter, E.A., et al. (2019). Insulin/IGF-1 Drives PERIOD Synthesis to Entrain Circadian Rhythms with Feeding Time. Cell 177, 896-909 e820.

Damiola, F., Le Minh, N., Preitner, N., Kornmann, B., Fleury-Olela, F., and Schibler, U. (2000). Restricted feeding uncouples circadian oscillators in peripheral tissues from the central pacemaker in the suprachiasmatic nucleus. Genes & development 14, 2950-2961.

Davis, M. (1980). Neurochemical modulation of sensory-motor reactivity: acoustic and tactile startle reflexes. Neurosci Biobehav Rev 4, 241-263.

Davis, S., Mirick, D.K., and Stevens, R.G. (2001). Night shift work, light at night, and risk of breast cancer. J Natl Cancer Inst 93, 1557-1562.

De Bono, J.P., Adlam, D., Paterson, D.J., and Channon, K.M. (2006). Novel quantitative phenotypes of exercise training in mouse models. Am J Physiol Regul Integr Comp Physiol 290, R926-934.

de Brito, L.C., Rezende, R.A., da Silva Junior, N.D., Tinucci, T., Casarini, D.E., Cipolla-Neto, J., and Forjaz, C.L. (2015). Post-Exercise Hypotension and Its Mechanisms Differ after Morning and Evening Exercise: A Randomized Crossover Study. PLoS One 10, e0132458.

DeFronzo, R.A., Jacot, E., Jequier, E., Maeder, E., Wahren, J., and Felber, J.P. (1981). The effect of insulin on the disposal of intravenous glucose. Results from indirect calorimetry and hepatic and femoral venous catheterization. Diabetes 30, 1000-1007.

Delezie, J., and Challet, E. (2011). Interactions between metabolism and circadian clocks: reciprocal disturbances. Ann N Y Acad Sci 1243, 30-46.

Delezie, J., Dumont, S., Dardente, H., Oudart, H., Grechez-Cassiau, A., Klosen, P., Teboul, M., Delaunay, F., Pevet, P., and Challet, E. (2012). The nuclear receptor REV-ERBalpha is required for the daily balance of carbohydrate and lipid metabolism. FASEB journal : official publication of the Federation of American Societies for Experimental Biology 26, 3321-3335.

Delezie, J., Dumont, S., Sandu, C., Reibel, S., Pevet, P., and Challet, E. (2016). Rev-erbalpha in the brain is essential for circadian food entrainment. Sci Rep 6, 29386.

Delezie, J., and Handschin, C. (2018). Endocrine Crosstalk Between Skeletal Muscle and the Brain. Front Neurol 9, 698.

DeVallance, E., Riggs, D., Jackson, B., Parkulo, T., Zaslau, S., Chantler, P.D., Olfert, I.M., and Bryner, R.W. (2017). Effect of chronic stress on running wheel activity in mice. PLoS One 12, e0184829.

Dibner, C., Schibler, U., and Albrecht, U. (2010). The mammalian circadian timing system: organization and coordination of central and peripheral clocks. Annu Rev Physiol 72, 517-549.

Ding, D., Lawson, K.D., Kolbe-Alexander, T.L., Finkelstein, E.A., Katzmarzyk, P.T., van Mechelen, W., Pratt, M., and Lancet Physical Activity Series 2 Executive, C. (2016). The economic burden of physical inactivity: a global analysis of major non-communicable diseases. Lancet 388, 1311-1324.

Doi, R., Oishi, K., and Ishida, N. (2010). CLOCK regulates circadian rhythms of hepatic glycogen synthesis through transcriptional activation of Gys2. J Biol Chem 285, 22114-22121.

Dominoni, D.M., Borniger, J.C., and Nelson, R.J. (2016). Light at night, clocks and health: from humans to wild organisms. Biol Lett 12, 20160015.

Dubrovsky, Y.V., Samsa, W.E., and Kondratov, R.V. (2010). Deficiency of circadian protein CLOCK reduces lifespan and increases age-related cataract development in mice. Aging (Albany NY) 2, 936-944.

Dudley, C.A., Erbel-Sieler, C., Estill, S.J., Reick, M., Franken, P., Pitts, S., and McKnight, S.L. (2003). Altered patterns of sleep and behavioral adaptability in NPAS2-deficient mice. Science 301, 379-383.

Duez, H., and Staels, B. (2008). The nuclear receptors Rev-erbs and RORs integrate circadian rhythms and metabolism. Diab Vasc Dis Res 5, 82-88.

Dussault, I., Fawcett, D., Matthyssen, A., Bader, J.A., and Giguere, V. (1998). Orphan nuclear receptor ROR alpha-deficient mice display the cerebellar defects of staggerer. Mech Dev 70, 147-153.

Dyar, K.A., Lutter, D., Artati, A., Ceglia, N.J., Liu, Y., Armenta, D., Jastroch, M., Schneider, S., de Mateo, S., Cervantes, M., et al. (2018). Atlas of Circadian Metabolism Reveals System-wide Coordination and Communication between Clocks. Cell 174, 1571-1585 e1511.

Egan, B., and Zierath, J.R. (2013). Exercise metabolism and the molecular regulation of skeletal muscle adaptation. Cell Metab 17, 162-184.

Ehlen, J.C., Brager, A.J., Baggs, J., Pinckney, L., Gray, C.L., DeBruyne, J.P., Esser, K.A., Takahashi, J.S., and Paul, K.N. (2017). Bmal1 function in skeletal muscle regulates sleep. Elife 6.

Ehlen, J.C., Jones, K.A., Pinckney, L., Gray, C.L., Burette, S., Weinberg, R.J., Evans, J.A., Brager, A.J., Zylka, M.J., Paul, K.N., et al. (2015). Maternal Ube3a Loss Disrupts Sleep

Homeostasis But Leaves Circadian Rhythmicity Largely Intact. J Neurosci 35, 13587-13598.

Eide, E.J., Kang, H., Crapo, S., Gallego, M., and Virshup, D.M. (2005). Casein kinase I in the mammalian circadian clock. Methods Enzymol 393, 408-418.

Eide, E.J., Vielhaber, E.L., Hinz, W.A., and Virshup, D.M. (2002). The circadian regulatory proteins BMAL1 and cryptochromes are substrates of casein kinase Iepsilon. J Biol Chem 277, 17248-17254.

El-Brolosy, M.A., and Stainier, D.Y.R. (2017). Genetic compensation: A phenomenon in search of mechanisms. PLoS Genet 13, e1006780.

Ezagouri, S., Zwighaft, Z., Sobel, J., Baillieul, S., Doutreleau, S., Ladeuix, B., Golik, M., Verges, S., and Asher, G. (2019). Physiological and Molecular Dissection of Daily Variance in Exercise Capacity. Cell Metabolism.

Facer-Childs, E., and Brandstaetter, R. (2015). The impact of circadian phenotype and time since awakening on diurnal performance in athletes. Curr Biol 25, 518-522.

Fairbrother, K., Cartner, B., Alley, J.R., Curry, C.D., Dickinson, D.L., Morris, D.M., and Collier, S.R. (2014). Effects of exercise timing on sleep architecture and nocturnal blood pressure in prehypertensives. Vasc Health Risk Manag 10, 691-698.

Fu, L., Pelicano, H., Liu, J., Huang, P., and Lee, C. (2002). The circadian gene Period2 plays an important role in tumor suppression and DNA damage response in vivo. Cell 111, 41-50.

Ghosh, S., Golbidi, S., Werner, I., Verchere, B.C., and Laher, I. (2010). Selecting exercise regimens and strains to modify obesity and diabetes in rodents: an overview. Clin Sci (Lond) 119, 57-74.

Gibbs, J.E., Blaikley, J., Beesley, S., Matthews, L., Simpson, K.D., Boyce, S.H., Farrow, S.N., Else, K.J., Singh, D., Ray, D.W., et al. (2012). The nuclear receptor REV-ERBalpha mediates circadian regulation of innate immunity through selective regulation of inflammatory cytokines. Proc Natl Acad Sci U S A 109, 582-587.

Gonzalez, K., Fuentes, J., and Marquez, J.L. (2017). Physical Inactivity, Sedentary Behavior and Chronic Diseases. Korean J Fam Med 38, 111-115.

Green, H.J., Helyar, R., Ball-Burnett, M., Kowalchuk, N., Symon, S., and Farrance, B. (1992). Metabolic adaptations to training precede changes in muscle mitochondrial capacity. J Appl Physiol (1985) 72, 484-491.

Grimaldi, B., Bellet, M.M., Katada, S., Astarita, G., Hirayama, J., Amin, R.H., Granneman, J.G., Piomelli, D., Leff, T., and Sassone-Corsi, P. (2010). PER2 controls lipid metabolism by direct regulation of PPARgamma. Cell Metab 12, 509-520.

Guillaumond, F., Dardente, H., Giguere, V., and Cermakian, N. (2005). Differential control of Bmal1 circadian transcription by REV-ERB and ROR nuclear receptors. J Biol Rhythms 20, 391-403.

Guissart, C., Latypova, X., Rollier, P., Khan, T.N., Stamberger, H., McWalter, K., Cho, M.T., Kjaergaard, S., Weckhuysen, S., Lesca, G., et al. (2018). Dual Molecular Effects of Dominant RORA Mutations Cause Two Variants of Syndromic Intellectual Disability with Either Autism or Cerebellar Ataxia. Am J Hum Genet 102, 744-759.

Guthold, R., Stevens, G.A., Riley, L.M., and Bull, F.C. (2018). Worldwide trends in insufficient physical activity from 2001 to 2016: a pooled analysis of 358 population-based surveys with 1.9 million participants. Lancet Glob Health 6, e1077-e1086.

Halberg, F. (1977). Implications of biologic rhythms for clinical practice. Hosp Pract 12, 139-149.

Hamilton, B.A., Frankel, W.N., Kerrebrock, A.W., Hawkins, T.L., FitzHugh, W., Kusumi, K., Russell, L.B., Mueller, K.L., van Berkel, V., Birren, B.W., et al. (1996). Disruption of the nuclear hormone receptor RORalpha in staggerer mice. Nature 379, 736-739.

Hastings, M.H., Maywood, E.S., and Brancaccio, M. (2018). Generation of circadian rhythms in the suprachiasmatic nucleus. Nat Rev Neurosci 19, 453-469.

Hatori, M., and Panda, S. (2010). The emerging roles of melanopsin in behavioral adaptation to light. Trends Mol Med 16, 435-446.

Hawley, J.A., Hargreaves, M., Joyner, M.J., and Zierath, J.R. (2014). Integrative biology of exercise. Cell 159, 738-749.

Henriquez-Olguin, C., Boronat, S., Cabello-Verrugio, C., Jaimovich, E., Hidalgo, E., and Jensen, T.E. (2019). The Emerging Roles of Nicotinamide Adenine Dinucleotide Phosphate Oxidase 2 in Skeletal Muscle Redox Signaling and Metabolism. Antioxid Redox Signal 31, 1371-1410.

Hodge, B.A., Wen, Y., Riley, L.A., Zhang, X., England, J.H., Harfmann, B.D., Schroder, E.A., and Esser, K.A. (2015). The endogenous molecular clock orchestrates the temporal separation of substrate metabolism in skeletal muscle. Skeletal muscle 5, 17.

Jetten, A., Kang, H.S., and Takeda, Y. (2013). Retinoic acid-related orphan receptors α and γ: key regulators of lipid/glucose metabolism, inflammation, and insulin sensitivity. Frontiers in Endocrinology 4.

Jordan, S.D., Kriebs, A., Vaughan, M., Duglan, D., Fan, W., Henriksson, E., Huber, A.L., Papp, S.J., Nguyen, M., Afetian, M., et al. (2017). CRY1/2 Selectively Repress PPARdelta and Limit Exercise Capacity. Cell Metab 26, 243-255 e246.

Kalsbeek, A., Scheer, F.A., Perreau-Lenz, S., La Fleur, S.E., Yi, C.X., Fliers, E., and Buijs, R.M. (2011). Circadian disruption and SCN control of energy metabolism. FEBS Lett 585, 1412-1426.

Kemler, D., Wolff, C.A., and Esser, K.A. (2020). Time of Day Dependent Effects of Contractile Activity on the Phase of the Skeletal Muscle Clock. bioRxiv, 2020.2003.2005.978759.

Kervezee, L., Kosmadopoulos, A., and Boivin, D.B. (2020). Metabolic and cardiovascular consequences of shift work: The role of circadian disruption and sleep disturbances. Eur J Neurosci 51, 396-412.

Kim, K., Boo, K., Yu, Y.S., Oh, S.K., Kim, H., Jeon, Y., Bhin, J., Hwang, D., Kim, K.I., Lee, J.S., et al. (2017). RORalpha controls hepatic lipid homeostasis via negative regulation of PPARgamma transcriptional network. Nat Commun 8, 162.

Knutsson, A. (2003). Health disorders of shift workers. Occup Med (Lond) 53, 103-108.

Kobayashi, Y., Ye, Z., and Hensch, T.K. (2015). Clock genes control cortical critical period timing. Neuron 86, 264-275.

Koike, N., Yoo, S.H., Huang, H.C., Kumar, V., Lee, C., Kim, T.K., and Takahashi, J.S. (2012). Transcriptional architecture and chromatin landscape of the core circadian clock in mammals. Science 338, 349-354.

Kojetin, D.J., and Burris, T.P. (2014). REV-ERB and ROR nuclear receptors as drug targets. Nature reviews. Drug discovery 13, 197-216.

Kojima, S., Shingle, D.L., and Green, C.B. (2011). Post-transcriptional control of circadian rhythms. J Cell Sci 124, 311-320.

Kondratov, R.V., Kondratova, A.A., Gorbacheva, V.Y., Vykhovanets, O.V., and Antoch, M.P. (2006). Early aging and age-related pathologies in mice deficient in BMAL1, the core componentof the circadian clock. Genes Dev 20, 1868-1873.

Kume, K., Zylka, M.J., Sriram, S., Shearman, L.P., Weaver, D.R., Jin, X., Maywood, E.S., Hastings, M.H., and Reppert, S.M. (1999). mCRY1 and mCRY2 are essential components of the negative limb of the circadian clock feedback loop. Cell 98, 193-205.

Lamont, E.W., Legault-Coutu, D., Cermakian, N., and Boivin, D.B. (2007). The role of circadian clock genes in mental disorders. Dialogues Clin Neurosci 9, 333-342.

Lau, P., Fitzsimmons, R.L., Pearen, M.A., Watt, M.J., and Muscat, G.E. (2011). Homozygous staggerer (sg/sg) mice display improved insulin sensitivity and enhanced glucose uptake in skeletal muscle. Diabetologia 54, 1169-1180.

Lau, P., Fitzsimmons, R.L., Raichur, S., Wang, S.C., Lechtken, A., and Muscat, G.E. (2008). The orphan nuclear receptor, RORalpha, regulates gene expression that controls lipid metabolism: staggerer (SG/SG) mice are resistant to diet-induced obesity. The Journal of biological chemistry 283, 18411-18421.

Lau, P., Nixon, S.J., Parton, R.G., and Muscat, G.E. (2004). RORalpha regulates the expression of genes involved in lipid homeostasis in skeletal muscle cells: caveolin-3 and CPT-1 are direct targets of ROR. The Journal of biological chemistry 279, 36828-36840.

Lavie, C.J., Ozemek, C., Carbone, S., Katzmarzyk, P.T., and Blair, S.N. (2019). Sedentary Behavior, Exercise, and Cardiovascular Health. Circ Res 124, 799-815.

Lee, C., Etchegaray, J.P., Cagampang, F.R., Loudon, A.S., and Reppert, S.M. (2001). Posttranslational mechanisms regulate the mammalian circadian clock. Cell 107, 855-867.

Lee, C.D., Blair, S.N., and Jackson, A.S. (1999). Cardiorespiratory fitness, body composition, and all-cause and cardiovascular disease mortality in men. Am J Clin Nutr 69, 373-380.

Lee, C.Y. (1982). Glucose-6-phosphate dehydrogenase from mouse. Methods Enzymol 89 Pt D, 252-257.

Lee, S., Donehower, L.A., Herron, A.J., Moore, D.D., and Fu, L. (2010). Disrupting circadian homeostasis of sympathetic signaling promotes tumor development in mice. PLoS One 5, e10995.

Liu, C., Li, S., Liu, T., Borjigin, J., and Lin, J.D. (2007). Transcriptional coactivator PGC-1alpha integrates the mammalian clock and energy metabolism. Nature 447, 477-481.

Liu, Z., Huang, M., Wu, X., Shi, G., Xing, L., Dong, Z., Qu, Z., Yan, J., Yang, L., Panda, S., et al. (2014). PER1 phosphorylation specifies feeding rhythm in mice. Cell Rep 7, 1509-1520.

Lobelo, F., Stoutenberg, M., and Hutber, A. (2014). The Exercise is Medicine Global Health Initiative: a 2014 update. Br J Sports Med 48, 1627-1633.

Loef, B., Nanlohy, N.M., Jacobi, R.H.J., van de Ven, C., Mariman, R., van der Beek, A.J., Proper, K.I., and van Baarle, D. (2019). Immunological effects of shift work in healthcare workers. Sci Rep 9, 18220.

Loizides-Mangold, U., Perrin, L., Vandereycken, B., Betts, J.A., Walhin, J.P., Templeman, I., Chanon, S., Weger, B.D., Durand, C., Robert, M., et al. (2017). Lipidomics reveals diurnal

lipid oscillations in human skeletal muscle persisting in cellular myotubes cultured in vitro. Proc Natl Acad Sci U S A 114, E8565-E8574.

Lowden, A., Moreno, C., Holmback, U., Lennernas, M., and Tucker, P. (2010). Eating and shift work - effects on habits, metabolism and performance. Scand J Work Environ Health 36, 150-162.

Marcheva, B., Ramsey, K.M., Buhr, E.D., Kobayashi, Y., Su, H., Ko, C.H., Ivanova, G., Omura, C., Mo, S., Vitaterna, M.H., et al. (2010). Disruption of the clock components CLOCK and BMAL1 leads to hypoinsulinaemia and diabetes. Nature 466, 627-631.

McCarthy, J.J., Andrews, J.L., McDearmon, E.L., Campbell, K.S., Barber, B.K., Miller, B.H., Walker, J.R., Hogenesch, J.B., Takahashi, J.S., and Esser, K.A. (2007). Identification of the circadian transcriptome in adult mouse skeletal muscle.

McClung, C.R. (2006). Plant circadian rhythms. Plant Cell 18, 792-803.

McGlory, C., van Vliet, S., Stokes, T., Mittendorfer, B., and Phillips, S.M. (2019). The impact of exercise and nutrition on the regulation of skeletal muscle mass. J Physiol 597, 1251-1258.

McTiernan, A., Friedenreich, C.M., Katzmarzyk, P.T., Powell, K.E., Macko, R., Buchner, D., Pescatello, L.S., Bloodgood, B., Tennant, B., Vaux-Bjerke, A., et al. (2019). Physical Activity in Cancer Prevention and Survival: A Systematic Review. Med Sci Sports Exerc 51, 1252-1261.

Miller, B.H., McDearmon, E.L., Panda, S., Hayes, K.R., Zhang, J., Andrews, J.L., Antoch, M.P., Walker, J.R., Esser, K.A., Hogenesch, J.B., et al. (2007). Circadian and CLOCK-controlled regulation of the mouse transcriptome and cell proliferation. Proc Natl Acad Sci U S A 104, 3342-3347.

Mohawk, J.A., Green, C.B., and Takahashi, J.S. (2012). Central and peripheral circadian clocks in mammals. Annu Rev Neurosci 35, 445-462.

Mohren, D.C., Jansen, N.W., Kant, I.J., Galama, J., van den Brandt, P.A., and Swaen, G.M. (2002). Prevalence of common infections among employees in different work schedules. J Occup Environ Med 44, 1003-1011.

Moon, H.Y., Becke, A., Berron, D., Becker, B., Sah, N., Benoni, G., Janke, E., Lubejko, S.T., Greig, N.H., Mattison, J.A., et al. (2016). Running-Induced Systemic Cathepsin B Secretion Is Associated with Memory Function. Cell Metab 24, 332-340.

Morf, J., and Schibler, U. (2013). Body temperature cycles: gatekeepers of circadian clocks. Cell Cycle 12, 539-540.

Mure, L.S., Le, H.D., Benegiamo, G., Chang, M.W., Rios, L., Jillani, N., Ngotho, M., Kariuki, T., Dkhissi-Benyahya, O., Cooper, H.M., et al. (2018). Diurnal transcriptome atlas of a primate across major neural and peripheral tissues. Science 359.

Narasimamurthy, R., Hatori, M., Nayak, S.K., Liu, F., Panda, S., and Verma, I.M. (2012). Circadian clock protein cryptochrome regulates the expression of proinflammatory cytokines. Proc Natl Acad Sci U S A 109, 12662-12667.

Noda, M., Iwamoto, I., Tabata, H., Yamagata, T., Ito, H., and Nagata, K.I. (2019). Role of Per3, a circadian clock gene, in embryonic development of mouse cerebral cortex. Sci Rep 9, 5874.

Oishi, K., Fukui, H., Sakamoto, K., Miyazaki, K., Kobayashi, H., and Ishida, N. (2002). Differential expressions of mPer1 and mPer2 mRNAs under a skeleton photoperiod and a complete light-dark cycle. Brain Res Mol Brain Res 109, 11-17.

Oster, H., Challet, E., Ott, V., Arvat, E., de Kloet, E.R., Dijk, D.J., Lightman, S., Vgontzas, A., and Van Cauter, E. (2017). The Functional and Clinical Significance of the 24-Hour Rhythm of Circulating Glucocorticoids. Endocr Rev 38, 3-45.

Panda, S., Antoch, M.P., Miller, B.H., Su, A.I., Schook, A.B., Straume, M., Schultz, P.G., Kay, S.A., Takahashi, J.S., and Hogenesch, J.B. (2002). Coordinated transcription of key pathways in the mouse by the circadian clock. Cell 109, 307-320.

Parr, E.B., Coffey, V.G., and Hawley, J.A. (2013). 'Sarcobesity': a metabolic conundrum. Maturitas 74, 109-113.

Pastore, S., and Hood, D.A. (2013). Endurance training ameliorates the metabolic and performance characteristics of circadian Clock mutant mice. J Appl Physiol (1985) 114, 1076-1084.

Patterson, R., McNamara, E., Tainio, M., de Sa, T.H., Smith, A.D., Sharp, S.J., Edwards, P., Woodcock, J., Brage, S., and Wijndaele, K. (2018). Sedentary behaviour and risk of all-cause, cardiovascular and cancer mortality, and incident type 2 diabetes: a systematic review and dose response meta-analysis. Eur J Epidemiol 33, 811-829.

Pedersen, B.K., and Saltin, B. (2015). Exercise as medicine - evidence for prescribing exercise as therapy in 26 different chronic diseases. Scand J Med Sci Sports 25 Suppl 3, 1-72.

Peek, C.B., Levine, D.C., Cedernaes, J., Taguchi, A., Kobayashi, Y., Tsai, S.J., Bonar, N.A., McNulty, M.R., Ramsey, K.M., and Bass, J. (2017). Circadian Clock Interaction with HIF1alpha Mediates Oxygenic Metabolism and Anaerobic Glycolysis in Skeletal Muscle. Cell Metab 25, 86-92.

Pendergast, J.S., and Yamazaki, S. (2011). Masking responses to light in period mutant mice. Chronobiol Int 28, 657-663.

Perez-Schindler, J., Summermatter, S., Salatino, S., Zorzato, F., Beer, M., Balwierz, P.J., van Nimwegen, E., Feige, J.N., Auwerx, J., and Handschin, C. (2012). The corepressor NCoR1 antagonizes PGC-1alpha and estrogen-related receptor alpha in the regulation of skeletal muscle function and oxidative metabolism. Mol Cell Biol 32, 4913-4924.

Perrin, L., Loizides-Mangold, U., Chanon, S., Gobet, C., Hulo, N., Isenegger, L., Weger, B.D., Migliavacca, E., Charpagne, A., Betts, J.A., et al. (2018). Transcriptomic analyses reveal rhythmic and CLOCK-driven pathways in human skeletal muscle. Elife 7.

Perrin, L., Loizides-Mangold, U., Skarupelova, S., Pulimeno, P., Chanon, S., Robert, M., Bouzakri, K., Modoux, C., Roux-Lombard, P., Vidal, H., et al. (2015). Human skeletal myotubes display a cell-autonomous circadian clock implicated in basal myokine secretion. Mol Metab 4, 834-845.

Pilegaard, H., Saltin, B., and Neufer, P.D. (2003). Exercise induces transient transcriptional activation of the PGC-1alpha gene in human skeletal muscle. The Journal of physiology 546, 851-858.

Pittendrigh, C.S. (1993). Temporal organization: reflections of a Darwinian clock-watcher. Annu Rev Physiol 55, 16-54.

Pizarro, A., Hayer, K., Lahens, N.F., and Hogenesch, J.B. (2013). CircaDB: a database of mammalian circadian gene expression profiles. Nucleic Acids Res 41, D1009-1013.

Preitner, N., Damiola, F., Lopez-Molina, L., Zakany, J., Duboule, D., Albrecht, U., and Schibler, U. (2002). The orphan nuclear receptor REV-ERBalpha controls circadian transcription within the positive limb of the mammalian circadian oscillator. Cell 110, 251-260.

Raun, S.H., Henriquez-Olguin, C., Karavaeva, I., Ali, M., Moller, L.L.V., Kot, W., Castro-Mejia, J.L., Nielsen, D.S., Gerhart-Hines, Z., Richter, E.A., et al. (2020). Housing temperature influences exercise training adaptations in mice. Nat Commun 11, 1560.

Reppert, S.M., and Weaver, D.R. (2002). Coordination of circadian timing in mammals. Nature 418, 935-941.

Reznick, J., Preston, E., Wilks, D.L., Beale, S.M., Turner, N., and Cooney, G.J. (2013). Altered feeding differentially regulates circadian rhythms and energy metabolism in liver and muscle of rats. Biochimica et biophysica acta 1832, 228-238.

Roesler, W.J., and Khandelwal, R.L. (1985). Diurnal variations in the activities of the glycogen metabolizing enzymes in mouse liver. Int J Biochem 17, 81-85.

Rosenwasser, A.M., Boulos, Z., and Terman, M. (1983). Circadian feeding and drinking rhythms in the rat under complete and skeleton photoperiods. Physiol Behav 30, 353-359.

Ruegsegger, G.N., and Booth, F.W. (2018). Health Benefits of Exercise. Cold Spring Harb Perspect Med 8.

Saini, C., Liani, A., Curie, T., Gos, P., Kreppel, F., Emmenegger, Y., Bonacina, L., Wolf, J.P., Poget, Y.A., Franken, P., et al. (2013). Real-time recording of circadian liver gene expression in freely moving mice reveals the phase-setting behavior of hepatocyte clocks. Genes & development 27, 1526-1536.

Sakamoto, K., Norona, F.E., Alzate-Correa, D., Scarberry, D., Hoyt, K.R., and Obrietan, K. (2013). Clock and light regulation of the CREB coactivator CRTC1 in the suprachiasmatic circadian clock. J Neurosci 33, 9021-9027.

Salgado-Delgado, R., Angeles-Castellanos, M., Buijs, M.R., and Escobar, C. (2008). Internal desynchronization in a model of night-work by forced activity in rats. Neuroscience 154, 922-931.

Salgado-Delgado, R.C., Saderi, N., Basualdo Mdel, C., Guerrero-Vargas, N.N., Escobar, C., and Buijs, R.M. (2013). Shift work or food intake during the rest phase promotes metabolic disruption and desynchrony of liver genes in male rats. PLoS One 8, e60052.

Saner, N.J., Bishop, D.J., and Bartlett, J.D. (2018). Is exercise a viable therapeutic intervention to mitigate mitochondrial dysfunction and insulin resistance induced by sleep loss? Sleep Med Rev 37, 60-68.

Sasaki, H., Hattori, Y., Ikeda, Y., Kamagata, M., Iwami, S., Yasuda, S., Tahara, Y., and Shibata, S. (2016). Forced rather than voluntary exercise entrains peripheral clocks via a corticosterone/noradrenaline increase in PER2::LUC mice. Sci Rep 6, 27607.

Sato, S., Basse, A.L., Schönke, M., Chen, S., Samad, M., Altıntaş, A., Laker, R.C., Dalbram, E., Barrès, R., Baldi, P., et al. (2019). Time of Exercise Specifies the Impact on Muscle Metabolic Pathways and Systemic Energy Homeostasis. Cell Metabolism.

Sato, S., Parr, E.B., Devlin, B.L., Hawley, J.A., and Sassone-Corsi, P. (2018). Human metabolomics reveal daily variations under nutritional challenges specific to serum and skeletal muscle. Mol Metab 16, 1-11.

Sato, T.K., Panda, S., Miraglia, L.J., Reyes, T.M., Rudic, R.D., McNamara, P., Naik, K.A., FitzGerald, G.A., Kay, S.A., and Hogenesch, J.B. (2004). A functional genomics strategy reveals Rora as a component of the mammalian circadian clock. Neuron 43, 527-537.

Savikj, M., Gabriel, B.M., Alm, P.S., Smith, J., Caidahl, K., Bjornholm, M., Fritz, T., Krook, A., Zierath, J.R., and Wallberg-Henriksson, H. (2019). Afternoon exercise is more

efficacious than morning exercise at improving blood glucose levels in individuals with type 2 diabetes: a randomised crossover trial. Diabetologia 62, 233-237.

Schiaffino, S., and Reggiani, C. (2011). Fiber types in mammalian skeletal muscles. Physiol Rev 91, 1447-1531.

Schlittler, M., Goiny, M., Agudelo, L.Z., Venckunas, T., Brazaitis, M., Skurvydas, A., Kamandulis, S., Ruas, J.L., Erhardt, S., Westerblad, H., et al. (2016). Endurance exercise increases skeletal muscle kynurenine aminotransferases and plasma kynurenic acid in humans. Am J Physiol Cell Physiol 310, C836-840.

Schnyder, S., and Handschin, C. (2015). Skeletal muscle as an endocrine organ: PGC-1alpha, myokines and exercise. Bone 80, 115-125.

Sehgal, A. (2017). Physiology Flies with Time. Cell 171, 1232-1235.

Shulman, R.G., and Rothman, D.L. (2001). The "glycogen shunt" in exercising muscle: A role for glycogen in muscle energetics and fatigue. Proc Natl Acad Sci U S A 98, 457-461.

Sidman, R.L., Lane, P.W., and Dickie, M.M. (1962). Staggerer, a new mutation in the mouse affecting the cerebellum. Science 137, 610-612.

Spencer, R.L., Chun, L.E., Hartsock, M.J., and Woodruff, E.R. (2018). Glucocorticoid hormones are both a major circadian signal and major stress signal: How this shared signal contributes to a dynamic relationship between the circadian and stress systems. Front Neuroendocrinol 49, 52-71.

Spina, R.J., Chi, M.M., Hopkins, M.G., Nemeth, P.M., Lowry, O.H., and Holloszy, J.O. (1996). Mitochondrial enzymes increase in muscle in response to 7-10 days of cycle exercise. J Appl Physiol (1985) 80, 2250-2254.

Straif, K., Baan, R., Grosse, Y., Secretan, B., El Ghissassi, F., Bouvard, V., Altieri, A., Benbrahim-Tallaa, L., Cogliano, V., and Group, W.H.O.I.A.F.R.o.C.M.W. (2007). Carcinogenicity of shift-work, painting, and fire-fighting. Lancet Oncol 8, 1065-1066.

Summermatter, S., and Handschin, C. (2012). PGC-1alpha and exercise in the control of body weight. Int J Obes (Lond) 36, 1428-1435.

Sweeney, B.M., and Borgese, M.B. (1989). A Circadian-Rhythm in Cell-Division in a Prokaryote, the Cyanobacterium Synechococcus Wh7803. J Phycol 25, 183-186.

Tahara, Y., Shiraishi, T., Kikuchi, Y., Haraguchi, A., Kuriki, D., Sasaki, H., Motohashi, H., Sakai, T., and Shibata, S. (2015). Entrainment of the mouse circadian clock by sub-acute physical and psychological stress. Sci Rep 5, 11417.

Tamaru, T., Hattori, M., Honda, K., Nakahata, Y., Sassone-Corsi, P., van der Horst, G.T., Ozawa, T., and Takamatsu, K. (2015). CRY Drives Cyclic CK2-Mediated BMAL1 Phosphorylation to Control the Mammalian Circadian Clock. PLoS Biol 13, e1002293.

Toh, K.L., Jones, C.R., He, Y., Eide, E.J., Hinz, W.A., Virshup, D.M., Ptacek, L.J., and Fu, Y.H. (2001). An hPer2 phosphorylation site mutation in familial advanced sleep phase syndrome. Science 291, 1040-1043.

Triqueneaux, G., Thenot, S., Kakizawa, T., Antoch, M.P., Safi, R., Takahashi, J.S., Delaunay, F., and Laudet, V. (2004). The orphan receptor Rev-erbalpha gene is a target of the circadian clock pacemaker. J Mol Endocrinol 33, 585-608.

Turek, F.W., Joshu, C., Kohsaka, A., Lin, E., Ivanova, G., McDearmon, E., Laposky, A., Losee-Olson, S., Easton, A., Jensen, D.R., et al. (2005). Obesity and metabolic syndrome in circadian Clock mutant mice. Science 308, 1043-1045.

van Moorsel, D., Hansen, J., Havekes, B., Scheer, F.A.J.L., Jörgensen, J.A., Hoeks, J., Schrauwen-Hinderling, V.B., Duez, H., Lefebvre, P., Schaper, N.C., et al. (2016). Demonstration of a day-night rhythm in human skeletal muscle oxidative capacity. Molecular Metabolism 5, 635-645.

Vargas-Ortiz, K., Perez-Vazquez, V., and Macias-Cervantes, M.H. (2019). Exercise and Sirtuins: A Way to Mitochondrial Health in Skeletal Muscle. Int J Mol Sci 20.

Vieira, E., Burris, T.P., and Quesada, I. (2014). Clock genes, pancreatic function, and diabetes. Trends Mol Med 20, 685-693.

Vina, J., Sanchis-Gomar, F., Martinez-Bello, V., and Gomez-Cabrera, M.C. (2012). Exercise acts as a drug; the pharmacological benefits of exercise. Br J Pharmacol 167, 1-12.

Vollmers, C., Schmitz, R.J., Nathanson, J., Yeo, G., Ecker, J.R., and Panda, S. (2012). Circadian oscillations of protein-coding and regulatory RNAs in a highly dynamic mammalian liver epigenome. Cell Metab 16, 833-845.

Whitham, M., and Febbraio, M.A. (2016). The ever-expanding myokinome: discovery challenges and therapeutic implications. Nature reviews. Drug discovery 15, 719-729.

Widrick, J.J., Stelzer, J.E., Shoepe, T.C., and Garner, D.P. (2002). Functional properties of human muscle fibers after short-term resistance exercise training. Am J Physiol Regul Integr Comp Physiol 283, R408-416.

Willner, P. (2017). The chronic mild stress (CMS) model of depression: History, evaluation and usage. Neurobiol Stress 6, 78-93.

Woldt, E., Sebti, Y., Solt, L.A., Duhem, C., Lancel, S., Eeckhoute, J., Hesselink, M.K.C., Paquet, C., Delhaye, S., Shin, Y., et al. (2013). Rev-erb-[alpha] modulates skeletal muscle

oxidative capacity by regulating mitochondrial biogenesis and autophagy. Nat Med 19, 1039-1046.

Wolff, G., and Esser, K.A. (2012a). Scheduled exercise phase shifts the circadian clock in skeletal muscle. Medicine and science in sports and exercise 44, 1663-1670.

Wolff, G., and Esser, K.A. (2012b). Scheduled exercise phase shifts the circadian clock in skeletal muscle. Med Sci Sports Exerc 44, 1663-1670.

Xu, Y., Padiath, Q.S., Shapiro, R.E., Jones, C.R., Wu, S.C., Saigoh, N., Saigoh, K., Ptacek, L.J., and Fu, Y.H. (2005). Functional consequences of a CKIdelta mutation causing familial advanced sleep phase syndrome. Nature 434, 640-644.

Yamazaki, S., Numano, R., Abe, M., Hida, A., Takahashi, R., Ueda, M., Block, G.D., Sakaki, Y., Menaker, M., and Tei, H. (2000). Resetting central and peripheral circadian oscillators in transgenic rats. Science 288, 682-685.

Yin, L., and Lazar, M.A. (2005). The orphan nuclear receptor Rev-erbalpha recruits the N-CoR/histone deacetylase 3 corepressor to regulate the circadian Bmal1 gene. Mol Endocrinol 19, 1452-1459.

You, T., Murphy, K.M., Lyles, M.F., Demons, J.L., Lenchik, L., and Nicklas, B.J. (2006). Addition of aerobic exercise to dietary weight loss preferentially reduces abdominal adipocyte size. Int J Obes (Lond) 30, 1211-1216.

Zambon, A.C., McDearmon, E.L., Salomonis, N., Vranizan, K.M., Johansen, K.L., Adey, D., Takahashi, J.S., Schambelan, M., and Conklin, B.R. (2003). Time- and exercise-dependent gene regulation in human skeletal muscle. Genome Biol 4, R61.

Zhang, R., Lahens, N.F., Ballance, H.I., Hughes, M.E., and Hogenesch, J.B. (2014). A circadian gene expression atlas in mammals: implications for biology and medicine. Proceedings of the National Academy of Sciences of the United States of America 111, 16219-16224.

Zheng, B., Albrecht, U., Kaasik, K., Sage, M., Lu, W., Vaishnav, S., Li, Q., Sun, Z.S., Eichele, G., Bradley, A., et al. (2001). Nonredundant roles of the mPer1 and mPer2 genes in the mammalian circadian clock. Cell 105, 683-694.

Zheng, B., Larkin, D.W., Albrecht, U., Sun, Z.S., Sage, M., Eichele, G., Lee, C.C., and Bradley, A. (1999). The mPer2 gene encodes a functional component of the mammalian circadian clock. Nature 400, 169-173.

Zhong, Y., Chen, A.F., Zhao, J., Gu, Y.J., and Fu, G.X. (2016). Serum levels of cathepsin D, sirtuin1, and endothelial nitric oxide synthase are correlatively reduced in elderly healthy people. Aging Clin Exp Res 28, 641-645.

Zylka, M.J., Shearman, L.P., Weaver, D.R., and Reppert, S.M. (1998). Three period homologs in mammals: differential light responses in the suprachiasmatic circadian clock and oscillating transcripts outside of brain. Neuron 20, 1103-1110.

Appendix

7 Appendix

BDNF is a mediator of glycolytic fiber-type specification in mouse skeletal muscle

Julien Delezie[a], Martin Weihrauch[a], Geraldine Maier[a], Rocío Tejero[b], Daniel J. Ham[a], Jonathan F. Gill[a], Bettina Karrer-Cardel[a], Markus A. Rüegg[a], Lucía Tabares[b], and Christoph Handschin[a,1]

[a]Biozentrum, University of Basel, CH-4056 Basel, Switzerland; and [b]Department of Medical Physiology and Biophysics, School of Medicine, University of Seville, 41009 Seville, Spain

Edited by Louis M. Kunkel, Boston Children's Hospital, Harvard Medical School, Boston, MA, and approved June 24, 2019 (received for review January 11, 2019)

Brain-derived neurotrophic factor (BDNF) influences the differentiation, plasticity, and survival of central neurons and likewise, affects the development of the neuromuscular system. Besides its neuronal origin, BDNF is also a member of the myokine family. However, the role of skeletal muscle-derived BDNF in regulating neuromuscular physiology in vivo remains unclear. Using gain- and loss-of-function animal models, we show that muscle-specific ablation of BDNF shifts the proportion of muscle fibers from type IIB to IIX, concomitant with elevated slow muscle-type gene expression. Furthermore, BDNF deletion reduces motor end plate volume without affecting neuromuscular junction (NMJ) integrity. These morphological changes are associated with slow muscle function and a greater resistance to contraction-induced fatigue. Conversely, BDNF overexpression promotes a fast muscle-type gene program and elevates glycolytic fiber number. These findings indicate that BDNF is required for fiber-type specification and provide insights into its potential modulation as a therapeutic target in muscle diseases.

neurotrophic factor | myokine | oxidative fiber | neuromuscular junction | endurance exercise

Neurotrophins (NTs) are members of a subfamily of structurally related trophic factors that regulate the differentiation, survival, and function of neuronal cells by modulating the $p75^{NTR}$ receptor and members of the Trk family of receptor tyrosine kinases (1, 2). Besides the central nervous system, skeletal muscle is an abundant source of trophic factors during development (3, 4). In particular, NTs can be released from muscle fibers, acting on the nerve terminals of motor neurons (5, 6), in addition to using retrograde routes to be transported to the cell body (7, 8).

Inactivation or overexpression of NTs in mouse models demonstrates their broad involvement in neuromuscular physiology. For instance, chronic deprivation of the nerve growth factor leads to muscular dystrophy (9). Deficiency in NT-3 or its receptor TrkC decreases proprioceptive afferents and muscle spindles, resulting in severe movement defects (10, 11). Lack of NT-4/5 induces the disassembly of postsynaptic acetylcholine receptor (AChR) clusters in association with neurotransmission failure and decreased fatigue resistance (12).

Similar to these NT family members, the brain-derived neurotrophic factor (BDNF) also exerts diverse roles in the neuromuscular system. For example, BDNF regulates agrin-induced AChR clustering in cultured myotubes (13). Moreover, precursor and mature forms of BDNF influence the survival and innervation pattern of developing motor neurons by modulating both $p75^{NTR}$ and TrkB receptors (8, 14). Accordingly, mice heterozygous for TrkB display altered neuromuscular junction (NMJ) structure and function as well as muscle weakness and sarcopenia (6, 15). In contrast to BDNF of neuronal origin, the role of BDNF in muscle function is much less studied, in part due to controversial BDNF detection in this tissue (16). There is, however, evidence that BDNF is a contraction-induced myokine likely involved in autocrine and/or paracrine regulation of muscle fat metabolism (17). Moreover, specific loss of BDNF within the satellite cell niche affects early stages of the regenerative process after muscle cardiotoxin injury (18). However, no study to date has comprehensively investigated the potential contribution of skeletal muscle-derived BDNF to both muscle and NMJ physiology in the postnatal mouse in vivo.

Using functional, cellular, and molecular approaches, we show that mice lacking BDNF specifically in striated muscle fibers do not exhibit any developmental neuromuscular or metabolic deficits. Intriguingly, we discovered that loss of BDNF within muscle fibers induces structural and functional remodeling of the NMJ toward a slower phenotype. In line, our data indicate that muscle BDNF loss or gain of function is sufficient to decrease or increase, respectively, the proportion of types IIB and IIX muscle fibers along with a broad range of oxidative and glycolytic marker genes.

Results

BDNF Muscle Knockout Mice Show Altered Spontaneous Gait Behavior and Locomotion. To restrict the Cre-induced recombination of the *Bdnf* floxed allele to skeletal muscle cells, we used the human α-skeletal actin (HSA) promoter (19, 20). $Bdnf^{flox/flox}$;HSA-Cre mice (hereafter referred as muscle knockout [MKO]) were born at Mendelian ratios and exhibited an average lifespan comparable with their $Bdnf^{flox/flox}$ control (CTRL) littermates (CTRL: 833.1 ± 38.2 d vs. MKO: 880 ± 31.3 d; $n = 10$ per genotype; not significant).

Significance

The brain-derived neurotrophic factor (BDNF) is essential to promote neuronal differentiation, plasticity, and survival. Altered BDNF expression is associated with several pathologies, including neuropsychiatric and neurodegenerative disorders, cardiovascular diseases, diabetes, and motor neuron diseases. Although BDNF has been identified as a contraction-induced myokine, its involvement in muscle physiology is unclear. Using functional, cellular, and molecular approaches, we report here that the myokine BDNF regulates glycolytic muscle fiber-type identity. Our findings warrant additional studies to determine whether modulating the activity of BDNF represents an effective therapeutic strategy to delay or even prevent muscle wasting disorders in which the function of glycolytic muscle fibers is compromised (e.g., in Duchenne muscular dystrophy, muscle insulin resistance).

Author contributions: J.D. and C.H. designed research; J.D., M.W., G.M., R.T., D.J.H., J.F.G., and B.K.-C. performed research; M.A.R. and L.T. contributed new reagents/analytic tools; J.D., R.T., and D.J.H. analyzed data; and J.D. and C.H. wrote the paper.

The authors declare no conflict of interest.

This article is a PNAS Direct Submission.

[1]To whom correspondence may be addressed. Email: christoph.handschin@unibas.ch.

This article contains supporting information online at www.pnas.org/lookup/suppl/doi:10.1073/pnas.1900544116/-/DCSupplemental.

Published online July 18, 2019.

Analysis of *Bdnf* transcript expression in 3-mo-old MKO mice revealed a ≤70% reduction in both oxidative and glycolytic skeletal muscle (Fig. 1*A* and *SI Appendix*, Fig. S1*A*). Interestingly, while *TrkB* levels were not affected by BDNF depletion, other NTs, such as *NT-3* and *NT-4/5*, show increased and decreased transcript expression, respectively, in the glycolytic gastrocnemius (GAS) muscle (*SI Appendix*, Fig. S1*A*). We, however, could not reveal changes in circulating BDNF; the latter was undetectable in mouse serum (*SI Appendix*, Fig. S1*B*) in agreement with previous studies (21, 22). Because BDNF is associated with fatty acid oxidation (17, 23, 24), we evaluated systemic and muscle metabolism of mice lacking muscle BDNF in a broad manner. MKO mice did not show an overt metabolic phenotype in terms of daily food intake (CTRL: 3.43 ± 0.11 g vs. MKO: 3.17 ± 0.26 g; $n = 5$ to 6; not significant), body, lean and fat mass, glucose tolerance, daily body temperature, VO_2 consumption, or energy substrate utilization (respiratory exchange ratio [RER]), which were all not significantly different from CTRL mice (*SI Appendix*, Fig. S1 *C–I*).

In line with unchanged whole-body lean mass, individual weights of different oxidative and glycolytic muscles were indistinguishable in BDNF MKO mice (*SI Appendix*, Fig. S1*E*). Basic histological evaluation of glycolytic tibialis anterior (TA) muscle revealed normal muscle structure (Fig. 1*B*). Using a telemetry system to record spontaneous, in-cage locomotion over a 10-d period, we observed that nighttime general locomotor activity was significantly reduced in MKO mice (Fig. 1*C*). A more detailed characterization of locomotor and gait behavior using the CatWalk XT system indicated that MKO gait velocity was slightly reduced as supported by parameters associated with walking speed (Fig. 1*D*). Overall, these data show that, even though spontaneous locomotion and walking speed are reduced in MKO mice, BDNF deletion is not linked to pathological changes in whole-body metabolism, body composition, and muscle mass and morphology.

Muscle-Specific BDNF Deletion Reduces Motor End Plate Volume in the Extensor Digitorum Longus Muscle. The BDNF-TrkB signaling pathway plays an essential role in the maturation and maintenance of the developing mammalian motor unit (6, 8, 13, 25). We thus investigated whether the locomotor phenotype of MKO mice was associated with NMJ abnormalities. We first evaluated the expression of transcripts playing a key role in the function and maintenance of the neuromuscular synapse and observed a significant reduction of the *Muscle-specific Kinase* (*MuSK*) and its downstream regulator *Docking Protein 7* (*Dok7*) in glycolytic muscles of MKO mice (Fig. 2*A* and *SI Appendix*, Fig. S2*A*). Of note, loss of MuSK abolishes synapse formation in mice (26). However, a closer examination of *MuSK* expression in subsynaptic regions—where it is preferentially expressed at the adult NMJ—did not reveal any significant reduction on BDNF deletion (*SI Appendix*, Fig. S2*A*). Moreover, MuSK protein showed a normal presence at synaptic sites, colocalizing with AChR clusters as in CTRL muscle (*SI Appendix*, Fig. S2*B*). Lastly, transcripts encoding for the α-and ε-AChR subunits were similarly enriched in the synaptic area of both genotypes (*SI Appendix*, Fig. S2*C*), further suggesting that molecules involved in NMJ maintenance are likely present at similar levels in adult MKO vs. CTRL muscles. Incidentally, transcript levels

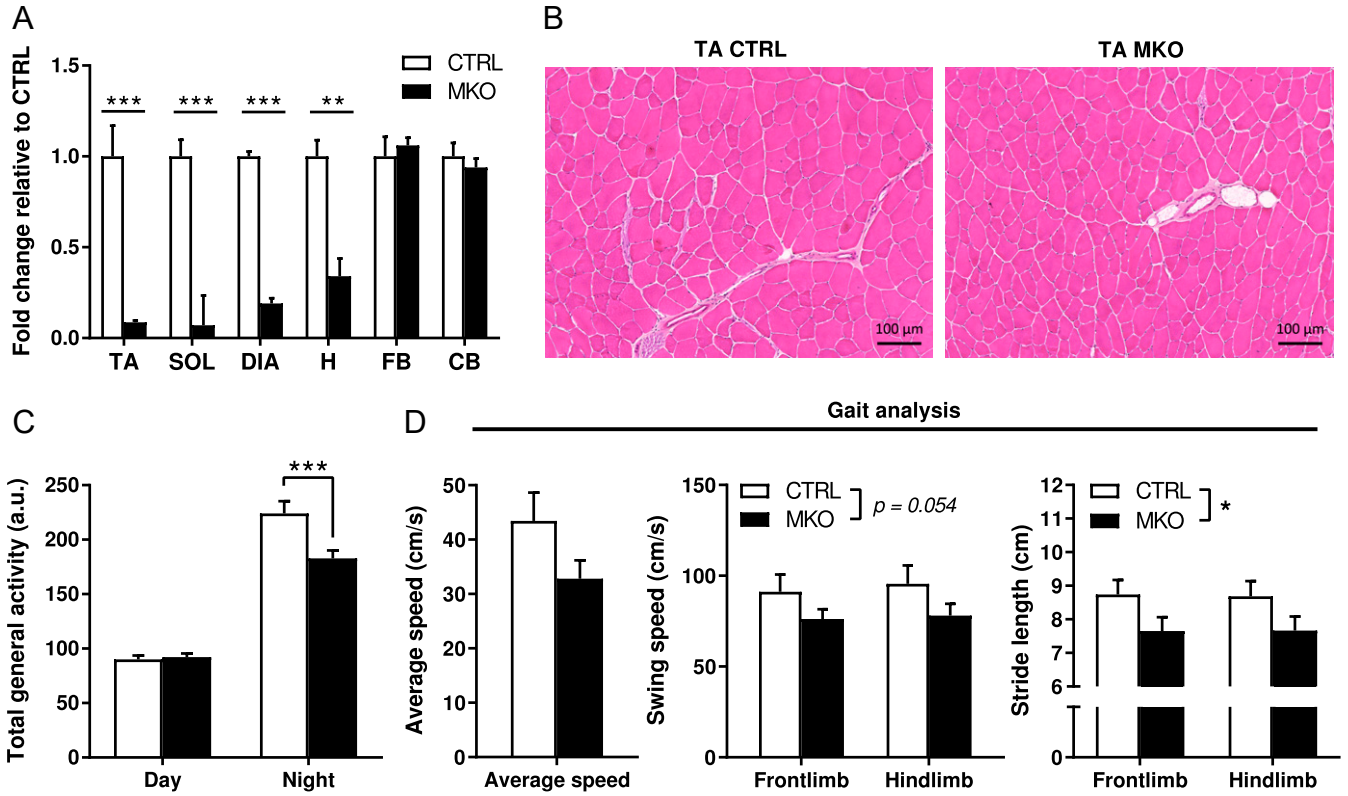

Fig. 1. BDNF MKO mice show altered spontaneous gait behavior and locomotion. (*A*) *Bdnf* gene expression in CTRL and BDNF MKO tissues. Expression values were determined by qPCR and normalized to *Hprt*. Data are shown as the average fold change ± SEM ($n = 3$ to 9 per genotype per tissue) relative to the expression in CTRL set to 1. CB, cerebellum; DIA, diaphragm; FB, forebrain; H, heart. (*B*) Histology of CTRL and MKO TA muscles as determined by hematoxylin and eosin staining. (Scale bar: 100 µm.) (*C*) Total gross locomotor activity ($n = 15$ per genotype, average of a 10-d period) and (*D*) gait locomotor parameters ($n = 8$ per genotype) of CTRL and MKO animals. Results are expressed as mean ± SEM. Unpaired Student's *t* test (*A* and *D*) and 2-way ANOVA followed by Sidak's multiple comparisons (*C* and *D*). $^*P < 0.05$; $^{**}P < 0.01$; $^{***}P < 0.001$.

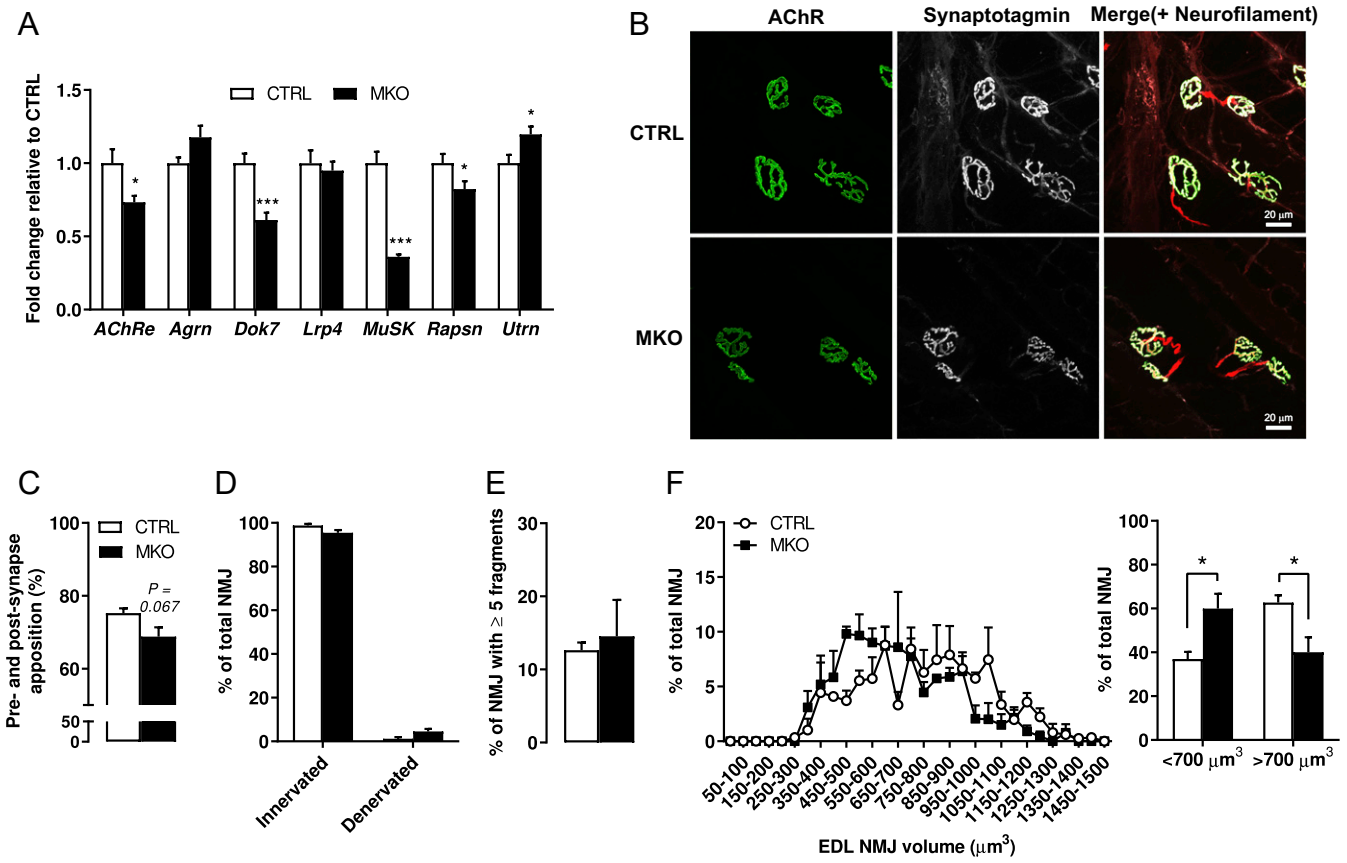

Fig. 2. Muscle-specific BDNF deletion reduces motor end plate size in the EDL muscle. (*A*) Gene expression in CTRL and BDNF MKO GAS muscles. Expression values were determined by qPCR and normalized to *Hprt*. Data are shown as the average fold change ± SEM ($n = 12$ per genotype) relative to the expression in CTRL set to 1. (*B*) Confocal microscopy images illustrating the apposition of both pre- and postsynaptic markers and the motor neuron innervation of EDL NMJs from CTRL and MKO mice. (Scale bar: 20 µm.) Quantification of (*C*) pre- and postsynapse apposition, (*D*) NMJ innervation, and (*E*) NMJ fragmentation. (*F*) NMJ volume distribution from CTRL and MKO EDL muscles (*Materials and Methods* has the number of NMJ analyzed per muscle per genotype). Results are expressed as percentage (mean ± SEM; $n = 4$ per genotype). Unpaired Student's *t* test (*A*, *C*, and *E*) and 2-way ANOVA followed by Sidak's multiple comparisons (*D* and *F*). $^*P < 0.05$; $^{***}P < 0.001$.

of *Bdnf* and *TrkB* were not enriched in microdissected synaptic regions of adult CTRL muscles (*SI Appendix*, Fig. S2*D*), hinting at synaptic and extrasynaptic functions of this signaling pathway.

We then examined the morphology of NMJs from the extensor digitorum longus (EDL)—a fast-twitch muscle used in rapid movements of hind limb digits—of CTRL and MKO animals by confocal microscopy. We used synaptotagmin, a synaptic vesicle-associated Ca^{2+} protein, as a presynaptic marker; α-bungarotoxin, a selective and potent ligand for AChR, to visualize the postsynaptic membrane; and an antineurofilament antibody to label motor nerve axons. Knockdown of muscle BDNF did not impair synapse structure in regard to presynaptic–postsynaptic apposition (Fig. 2 *B* and *C*). Similarly, no evidence of increased NMJ fragmentation and denervation was observed in MKO mice, indicating that muscle BDNF is not essential to maintain NMJ integrity (Fig. 2 *D* and *E*). Strikingly, however, lack of muscle BDNF led to a significant reduction of the motor end plate volume (Fig. 2*F*). Importantly, the reduction in NMJ volume was not associated with significant changes in the expression of $p75^{NTR}$ and both full-length and truncated forms of TrkB and TrkC in motor neurons and interneurons that lie in the lumbar portion of the spinal cord (*SI Appendix*, Fig. S2 *E–G*). Moreover, these receptors were not or only poorly detected in the GAS muscle (*SI Appendix*, Fig. S2 *E–G*), in keeping with their low expression levels postdifferentiation (16, 17, 27). In summary, muscle-specific ablation of BDNF does not affect NMJ apposition and integrity but evokes a shift in motor end plate size that is reminiscent of slow-type muscles (28).

Loss of BDNF Promotes Slow Contraction Velocity and Fatigue Resistance. We next assessed whether the morphological and molecular changes in the NMJs of MKO animals had any functional consequences on muscle contractile and fatigue properties and neuromuscular transmission. We first performed in situ measurements of TA muscle function in response to sciatic nerve stimulation. MKO muscles produced similar twitch and tetanic force as their CTRL counterparts (Fig. 3*A*, force frequency curve, and Fig. 3*E*, cross-sectional area [CSA]-normalized maximal twitch and tetanic forces), in line with in vivo measures of grip strength (*SI Appendix*, Fig. S2*J*). In contrast, time-to-peak tension and half-relaxation time were significantly longer in MKO mice (Fig. 3 *B–D*), indicating slower contraction velocities. Next, we studied force production during a fatigue protocol consisting of intermittent 100-Hz tetanic stimulations. After 1 min of repeated stimulation, contraction force started to drop faster in CTRL than in MKO TA muscles and remained lower until the end of the fatigue protocol (Fig. 3*F*). Consistent with fatigue resistance, BDNF knockout muscles recovered significantly faster than CTRL muscles, returning to ∼95% of baseline peak force, while CTRL muscles reached ∼84% of peak force 3 min after the fatigue protocol (Fig. 3*F*).

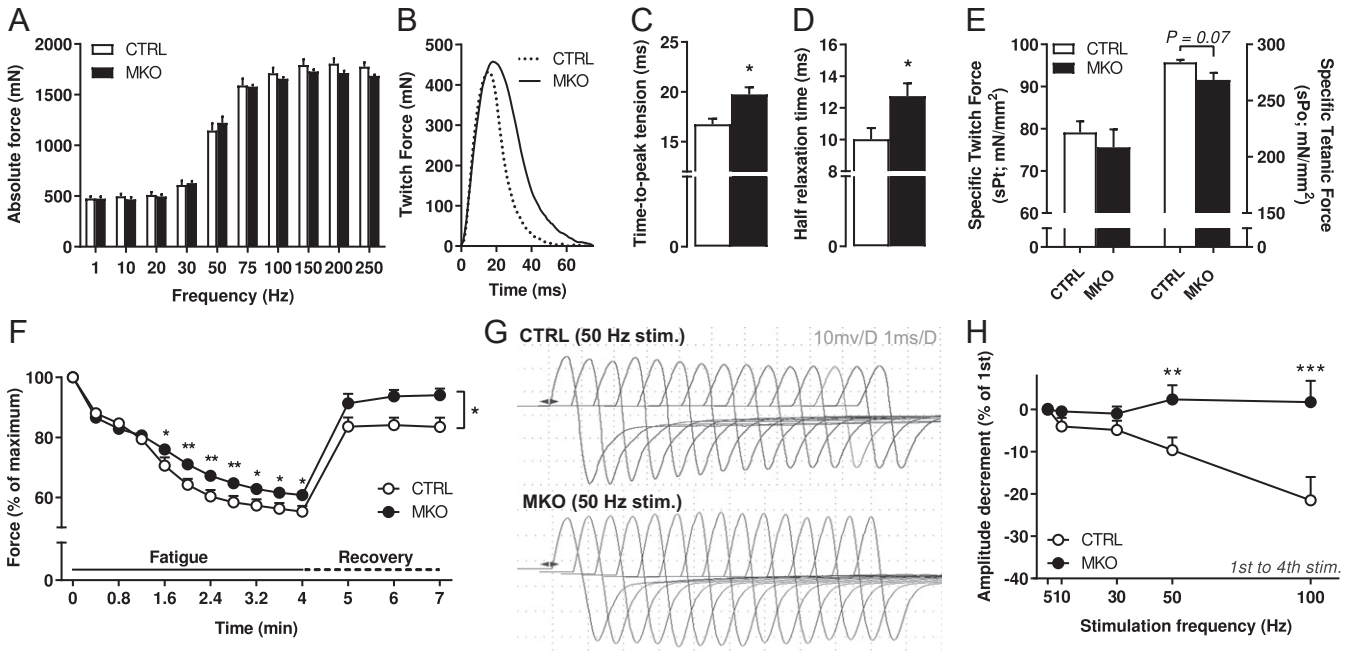

Fig. 3. Lack of BDNF promotes slow muscle contraction and enhances fatigue resistance. (*A*) In situ TA absolute muscle force frequency relationship as evoked by electrical sciatic nerve stimulation from CTRL ($n = 4$) and MKO ($n = 5$) mice. (*B*) Representative traces of twitch force from both genotypes. (*C*) Time-to-peak tension and (*D*) half-relaxation time. (*E*) CSA-normalized maximal twitch and tetanic forces. (*F*) Average curves showing the force decline during a 4-min muscle fatigue protocol and of muscle force recovery up to 3 min after fatigue. (*G*) Representative EMG traces from CTRL (*Upper*) and MKO (*Lower*) GAS muscle on 50-Hz stimulation of the sciatic nerve. (*H*) Average decrement in the amplitude of GAS CMAPs from 1st to 4th stimulation (5- to 50-Hz stimulation: $n = 9$ to 10 per genotype; 100-Hz stimulation: $n = 6$ per genotype). Results are expressed as percentage. Unpaired Student's *t* test (*C*–*E*) and 2-way ANOVA followed by Sidak's multiple comparisons (*A*, *F*, and *H*). $^{*}P < 0.05$; $^{**}P < 0.01$; $^{***}P < 0.001$.

To complement the in situ nerve–muscle stimulation experiments, we also evaluated in vivo evoked compound muscle action potentials (CMAPs) in the GAS muscle in response to supramaximal repetitive nerve stimulation using electromyography (EMG) as described previously (28). CMAPs did not significantly differ between genotypes over 15 consecutive stimuli at 5, 10, or 30 Hz (Fig. 3*H*). However, we found greater reductions of CMAPs at 50- and 100-Hz stimulation in CTRL than in MKO mice (Fig. 3 *G* and *H* and *SI Appendix*, Fig. S2*I*). Remarkably, while CMAPs dropped by ∼10 and ∼20% at 50- and 100-Hz stimulation, respectively, CMAPs reduction was completely absent after 4 stimulations in MKO mice (Fig. 3*H*). Lastly, to assess whether the changes in muscle contractile properties of MKO mice are associated with altered NMJ functionality, we evaluated both spontaneous and evoked neurotransmitter release using the levator auris longus (LAL)—a fast-twitch neck muscle—as described previously (29). Ex vivo electrophysiological recordings showed that the resting muscle membrane potential and both miniature end plate potential amplitude and frequency remained unaffected by muscle BDNF deletion (*SI Appendix*, Fig. S3 *A* and *B*, representative traces, and Tables S1 and S2). Likewise, there was no significant difference in the average amplitude of evoked neurotransmitter release, quantum content, and time constants between mouse groups (*SI Appendix*, Fig. S3 *C* and *D* and Table S3). Furthermore, short-term plasticity was indistinguishable between LAL NMJ synapses of CTRL vs. MKO animals (*SI Appendix*, Fig. S3 *E* and *F*). Together, these results indicate that glycolytic muscles lacking BDNF exhibit slower contractile properties and higher fatigue resistance in the absence of altered synaptic communication.

BDNF MKO Mice Show Improved Running Capacity. The change in NMJ morphology and the altered contractility in situ and using EMG collectively suggest a higher endurance performance. To test this, we first evaluated spontaneous wheel-running activity in both groups over a 7-d period. MKO mice exhibited a similar increase and overnight distribution of wheel activity as their CTRL littermates (*SI Appendix*, Fig. S4*A*). Because running performance as elicited by forced treadmill differs in many aspects from spontaneous mouse wheel-running activity, we then characterized the running capacity of MKO animals under dynamic treadmill exercise conditions. Untrained mice from both genotypes first performed a forced maximal running capacity test (i.e., VO_{2max} test) consisting of a speed increment of 2 m every 2 min at 15° inclination until exhaustion. In this strenuous exercise challenge, both genotypes demonstrated similar energy substrate utilization (RER) during the course of the experiment (*SI Appendix*, Fig. S4*B*). Furthermore, despite slightly higher VO_2 consumption rates toward the end of the running exercise session, muscle BDNF deletion did not significantly improve maximal aerobic capacity (*SI Appendix*, Fig. S4 *C* and *D*). Moreover, plasma lactate accumulation—a marker of muscle metabolism and fatigue—was similar in both genotypes at exhaustion (*SI Appendix*, Fig. S4*E*). Nevertheless, MKO mice were able to run significantly longer than CTRL mice (713 vs. 519 m; $n = 9$ per genotype; $P = 0.044$) (*SI Appendix*, Fig. S4 *G* and *H*). Incidentally, expression of exercise- and NT-related genes in response to an acute bout of treadmill exercise as described above was similar in the GAS muscle of both mouse genotypes (*SI Appendix*, Fig. S4 *I* and *J*).

Mice that performed the VO_{2max} test were then subjected to an endurance-type protocol, during which animals ran from 20 to 100% of their maximal running speed. Evaluation of energy fuel utilization and oxygen consumption, specifically at moderate exercise intensities [i.e., 20 to 60% of maximal speed when muscle fat oxidation is at its highest (30, 31)] did not reveal any differences between genotypes (Fig. 4 *A* and *B*). Moreover, blood lactate levels were similarly increased in both genotypes at

exhaustion (Fig. 4*C*). Conversely, blood glucose values were significantly lower in MKO mice at exhaustion (Fig. 4*D*), which could result from their altered performance. Indeed, in line with their improved maximal running capacity, BDNF MKO animals demonstrated significantly greater endurance performance, running about 1.5 times the distance of CTRL mice (BDNF MKO: 2,708 m; CTRL: 1,862 m; $P = 0.015$) (Fig. 4 *F* and *G*). In summary, deletion of BDNF in mouse skeletal muscle confers greater resistance to fatigue during physical exercise without significantly affecting whole-body aerobic capacity and energy substrate utilization.

Lack of Muscle BDNF Promotes a Fast-to-Slow Transition in Glycolytic Muscles. Muscle fiber type and oxidative capacity are essential determinants of muscle contractile properties, endurance, and fatigue (32). Therefore, we assessed whether BDNF deletion was associated with a muscle fiber transformation. Fiber composition and CSA were unchanged in the oxidative soleus (SOL) muscle of MKO mice (*SI Appendix*, Fig. S5 *A–C*). In contrast, the proportion of type IIX fibers in both glycolytic TA and EDL muscles was significantly increased in MKO animals at the expense of type IIB fibers (Fig. 5 *A* and *B*). Importantly, type IIX fibers show characteristics intermediate to types IIA and IIB fibers (e.g., in terms of contraction velocities and resistance to fatigue as evaluated above) and succinate dehydrogenase activity—a mitochondrial enzyme involved in oxidative phosphorylation (33). Accordingly, we observed that muscles depleted of BDNF showed higher succinate dehydrogenase (SDH) activity-dependent staining (Fig. 5*C*). Of note, the higher proportion of type IIX fibers in both TA and EDL muscles of MKO mice was not associated with significant change in myofiber CSA (Fig. 5*D*).

To investigate whether other fiber type-specific genes were also affected by this transition from type IIB to IIX, we measured the expression of several key oxidative and glycolytic markers by qPCR. In line, the α-cardiac form of the actin gene (*Actc1*)—a major constituent of the contractile apparatus predominantly expressed in oxidative muscles (34)—was elevated in the absence of BDNF (Fig. 5*E*). Conversely, the glycolytic marker *troponin-C fast* (*Tnnc2*) and transcriptional regulators controlling glycolytic fiber identity, such as *Baf60c*/*Smarcd3* (35) and *Tbx15* (36), were down-regulated in MKOs (Fig. 5*E*). The higher proportion of type IIX fibers was, however, not associated with elevated expression of *Ppargc1b* (37) or increased mitochondrial transcript and mitochondrial DNA levels (*SI Appendix*, Fig. S5*D*). We also examined the level of transcripts encoding key sarcoplasmic calcium-regulatory proteins in muscles of MKO mice. In particular, the fast-type calcium-transporting ATPase *Atp2a1* (also called sarco/endoplasmic reticulum Ca^{2+}-ATPase 1 [*Serca1*]) was reduced, while the slow-type form *Atp2a2* (*Serca2*) was significantly increased (Fig. 5*F*). In contrast, both the fast-type calsequestrin 1 (*Casq1*) and the slow-type *Casq2* were elevated in the MKO animals (Fig. 5*F*). Additional transcripts encoding for regulators of fast fiber Ca^{2+} homeostasis (e.g., myoregulin [*Mrln*]—a repressor of SERCA activity expressed in fast fibers [38]—and ryanodine receptor [*RyR1*] and parvalbumin [*Pvalb*]—highly expressed in fast-contracting fibers that have a more developed sarcoplasmic reticulum [33]) equally showed significantly reduced expression levels in muscle cells depleted of BDNF (Fig. 5*F*). These results collectively demonstrate that muscle-derived BDNF depletion promotes a fast-to-slow transition in glycolytic muscles.

BDNF Overexpression Increases Fast-Type Gene Expression and Glycolytic Fibers. The effect of muscle BDNF deletion on fiber-type composition prompted us to investigate the consequence of enhanced BDNF expression in skeletal muscle of adult CTRL mice. To this aim, a plasmid-based gene delivery method was used to introduce either BDNF or an empty vector (EV) into the TA muscle by electroporation. *SI Appendix*, Fig. S6*A* depicts in vivo transfection efficiency of a pCAG-EGFP (enhanced green fluorescent protein) expression vector using our established parameters, demonstrating even muscle distribution of EGFP at 7 and 21 d postelectroporation. Importantly, when TA muscles

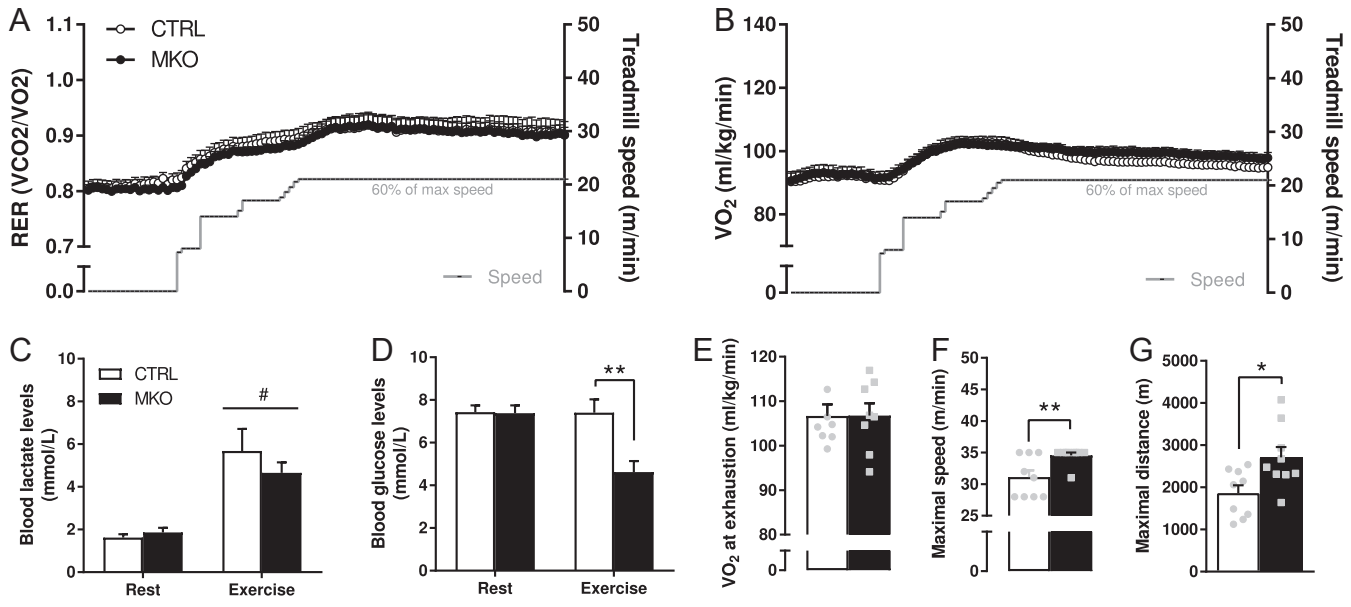

Fig. 4. BDNF MKO mice show improved running endurance capacity. (*A*) RER and (*B*) O_2 consumption as a function of speed in CTRL and MKO animals during endurance exercise challenge. Note that data in *A* and *B* are only depicted until a speed of 22 m/min (i.e., 60% of maximum speed). (*C*) Blood lactate and (*D*) glucose levels at rest and within 1 min after exhaustion. (*E*) Maximal O_2 consumption at exhaustion. (*F*) Maximal speed and (*G*) total distance reached at exhaustion. Results are expressed as mean ± SEM ($n = 9$ per genotype except in *A*, *B*, and *E*, where data from 1 CTRL and 1 MKO mouse could not be included due to O_2 artifacts during run acquisition). Unpaired Student's *t* test (*E–G*) and 2-way ANOVA followed by Sidak's multiple comparisons (*C* and *D*). $^*P < 0.05$; $^{**}P < 0.01$; $^{\#}$Significant difference ($P < 0.05$) between experimental conditions.

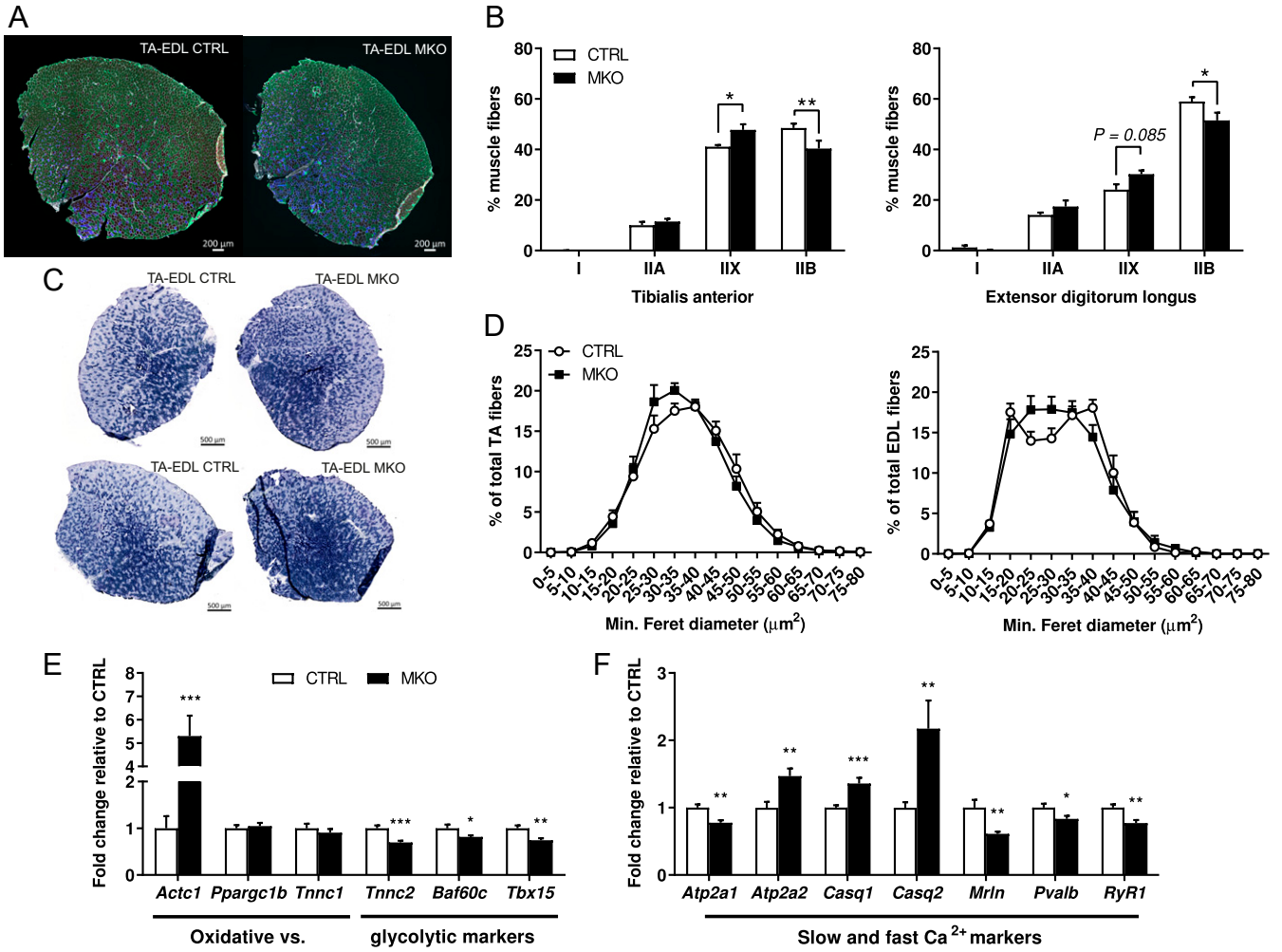

Fig. 5. Lack of BDNF leads to a type IIB to IIX transition in glycolytic muscles. (*A*) Representative fluorescence microscopy images illustrating the fiber-type composition in the TA-EDL muscle of CTRL and MKO animals. Corresponding color legend for fiber types: type I = red, type IIA = blue, type IIX = unstained (black), type IIB = green, and laminin = white. (Scale bar: 200 µm.) (*B*) Quantification of fiber-type content in (*Left*) TA and (*Right*) EDL muscles ($n = 5$ per genotype). Note that EDL and TA muscles were analyzed separately. (*C*) Representative SDH staining of TA-EDL muscles from different CTRL and MKO animals. (Scale bar: 500 µm.) (*D*) CSA based on minimal Feret's diameter of (*Left*) TA and (*Right*) EDL myofibers ($n = 5$ per genotype). Results are expressed as percentage (mean ± SEM). (*E* and *F*) Gene expression in CTRL and BDNF MKO GAS muscles. Expression values were determined by qPCR and normalized to *Hprt*. Data are shown as the average fold change ± SEM ($n = 12$ per genotype) relative to the expression in CTRL set to 1. Unpaired Student's *t* test (*E* and *F*) and 2-way ANOVA followed by Sidak's multiple comparisons (*B* and *D*). $^*P < 0.05$; $^{**}P < 0.01$; $^{***}P < 0.001$.

from CTRL mice were transfected with a BDNF-encoding vector, both pro- and mature forms of BDNF were detected 21 d after electrotransfer with 2 different antibodies (Fig. 6*A*). This clearly indicates that—alongside the drastic elevation of its transcript (Fig. 6*B*)—BDNF is further processed and cleaved in adult skeletal muscle.

Next, we found that BDNF elevation mirrored the consequences of BDNF deletion at the gene expression level. Specifically, there was a greater expression of glycolytic markers (e.g., *Serca1* and its coregulator *Mlrn*) and of transcriptional mediators of fast fiber-type gene programs, such as *Baf60c* and *Tbx15* (Fig. 6 *B* and *C*). Because electroporation is known to produce significant damage in skeletal muscle leading to satellite cell activation and the formation of new fibers (39–41), we concomitantly determined myosin heavy-chain composition in both small new fibers (i.e., based on a CSA value < 20 µm^2), nearly absent in nonelectroporated TA muscle (Fig. 5*D*), and in larger fibers (CSA > 20 µm^2) of EV- and BDNF-electroporated muscles (Fig. 6*D*). Intriguingly, on BDNF overexpression, small myofibers had a significantly lower content of the type IIX myosin heavy-chain isoform alongside an elevation of the type IIB isoform (Fig. 6*E*). Thus, overexpression of BDNF is sufficient to induce fast-twitch markers and influence fiber-type composition in skeletal muscle.

Higher Muscle Mass, Strength, and Oxidative Fibers in Old BDNF MKO Mice. NMJ structure, muscle fiber type and contractile properties, fatigue resistance, and exercise capacity are all changed in young adult BDNF MKO animals. Incidentally, altered NT signaling at the neuromuscular interface is associated with the age-related decline of muscle mass and function (15, 16, 42). Moreover, there is an age-dependent decrease of both circulating BDNF and brain *TrkB* levels in humans (43, 44) and a likewise age-dependent reduction of both *Bdnf* and *TrkB* levels in the rodent brain (45–47). However, we could not find data on muscle *Bdnf* and *TrkB* expression in the aging context and have, therefore, compared their transcript levels in 6- vs. 24-mo-old CTRL animals. We did not find any change in regard to *Bdnf* and *TrkB* expression in the old muscle (Fig. 7*A*).

In a last set of experiments, we evaluated whether the lifelong deletion of muscle BDNF would further alter muscle physiology

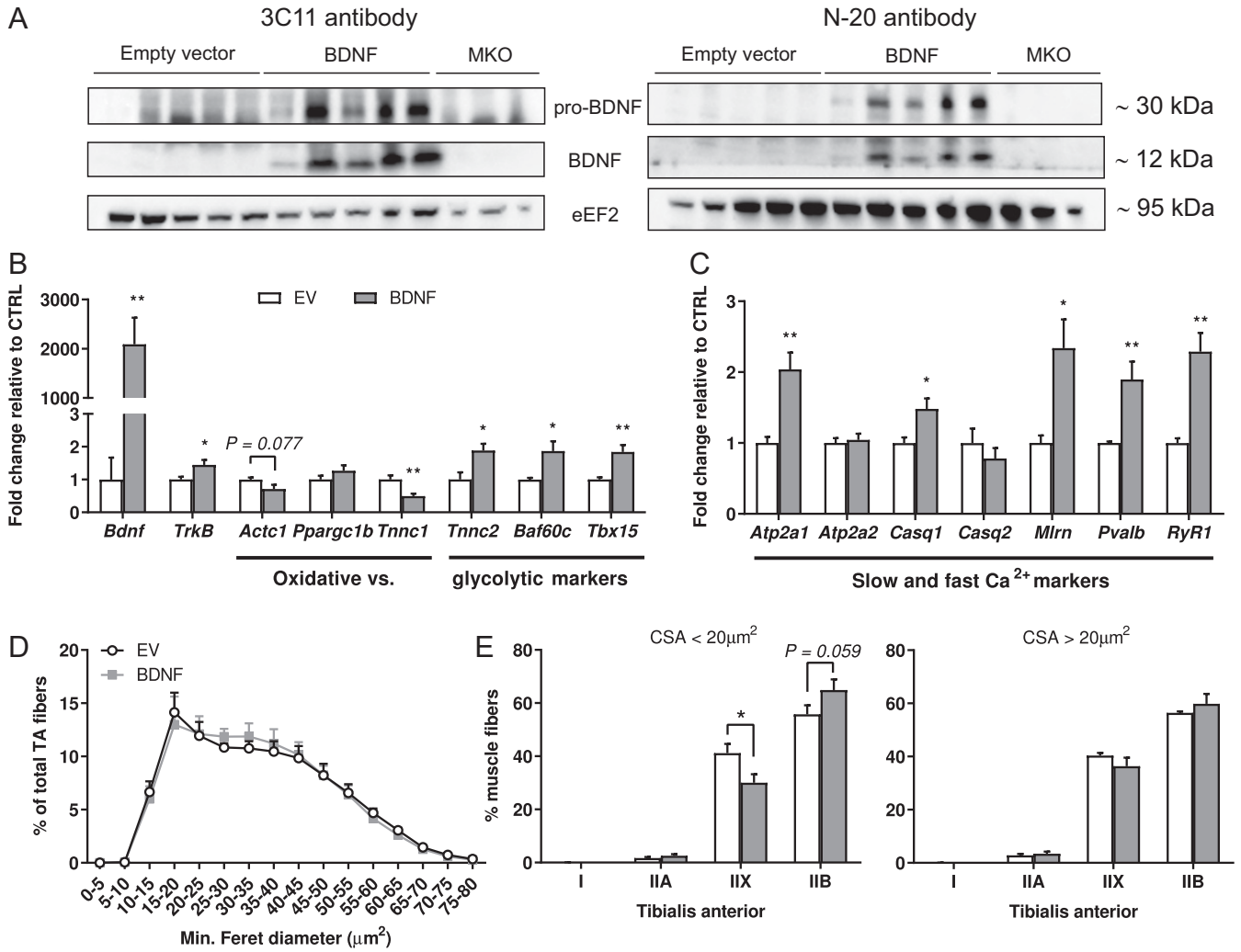

Fig. 6. BDNF influences skeletal muscle fiber-type specification. (*A*) Expression of BDNF protein in EV- and BDNF-electroporated TA muscles ($n = 5$ per condition) as determined by western blot. Note that muscle protein extracts from MKO animals were used as negative controls. (*B* and *C*) Gene expression in EV- and BDNF-electroporated TA muscles. Expression values were determined by qPCR and normalized to *Hprt*. Data are shown as the average fold change ± SEM ($n = 5$ per condition) relative to the expression in EV set to 1. (*D*) CSA based on minimal Feret's diameter of TA myofibers ($n = 5$ per genotype). (*E*) Fiber-type composition in small (*Left*) vs. large (*Right*) TA fibers ($n = 5$ per genotype). Results are expressed as percentage (mean ± SEM). Unpaired Student's *t* test (*B* and *C*) and 2-way ANOVA followed by Sidak's multiple comparisons (*E*). $*P < 0.05$; $**P < 0.01$.

in the aging context. Motor balance and coordination were unchanged in 24-mo-old MKO mice (Fig. 7 *B* and *C*). Likewise, old MKO animals demonstrated a running capacity comparable with their CTRL littermates (Fig. 7*D*). Old MKO mice, however, showed significantly higher grip strength in comparison with old CTRL mice (Fig. 7*E*). This was, furthermore, associated with significantly increased whole-body lean mass alongside elevated GAS and quadriceps hind limb muscle mass (Fig. 7 *F* and *G*). Finally, we found a higher SDH activity-dependent staining and a significantly increased proportion of type IIA fibers in TA muscles of 24-mo-old MKO mice (Fig. 7 *H* and *I*). Overall, these results suggest that lifelong expression of muscle BDNF is not required for the maintenance of neuromuscular function and that, conversely, the more oxidative phenotype of muscles lacking BDNF contributes to attenuation of some aspects of muscle aging.

Discussion

The trophic activity of BDNF and related NT family members is well recognized in the interaction between cells of the central nervous system (24, 48). In contrast, the regulation and function of BNDF in other cell types remains less understood. Here, we describe a hitherto unknown and surprising effect of skeletal muscle BNDF on the promotion of a fast-twitch glycolytic muscle fiber program using both loss- and gain-of-function approaches in vivo.

Our findings uncover BDNF as a myokine that promotes a glycolytic fiber phenotype; other factors, such as the insulin-like growth factor 2 (IGF2), have been associated with embryonic development of fast fibers (49), while IGF1 primarily promotes hypertrophy of fibers, with minimal effects on fiber-type distribution (50). In contrast, our data demonstrate that BDNF affects the gene program and fiber composition of glycolytic muscles without significantly altering muscle fiber CSA. It is, therefore, conceivable that BNDF cooperates with other factors (e.g., IGF1) in the adaptation of skeletal muscle to resistance training. Of note, the seemingly beneficial effect of muscle-specific deletion of BDNF on different parameters (e.g., fatigue resistance and endurance capacity) might be offset in other contexts. It thus will be interesting to test the performance of the BDNF MKO animals in other paradigms where adequate function of type IIB fibers is required (e.g., maximal strength or resistance

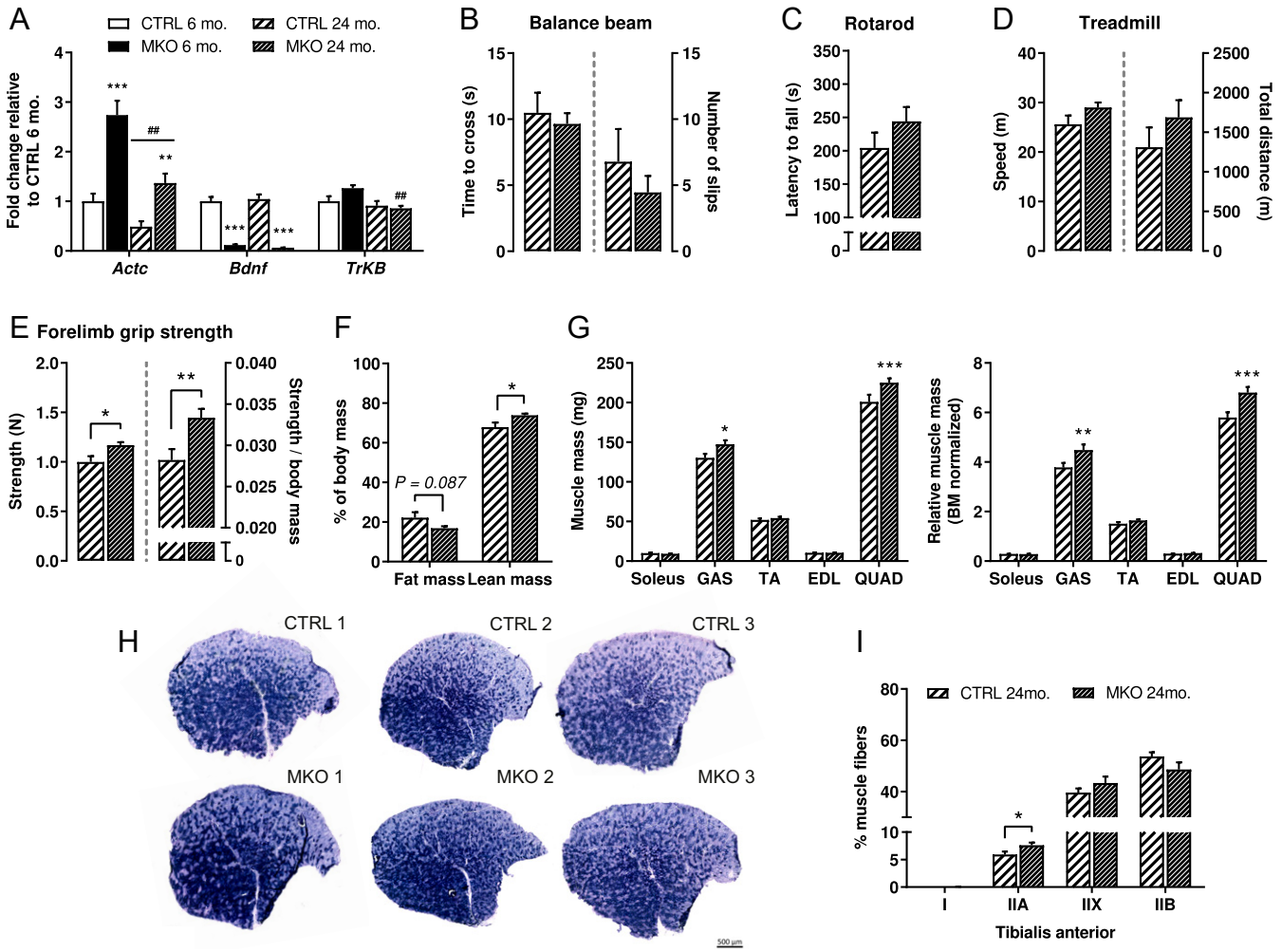

Fig. 7. The 24-mo-old BDNF MKO mice show higher muscle mass, grip strength, and oxidative fiber number. (*A*) Gene expression in young ($n = 6$ per genotype) and old ($n = 7$ to 9 per genotype) CTRL and BDNF MKO GAS muscles. Expression values were determined by qPCR and normalized to *Hprt*. Data are shown as the average foldchange ± SEM relative to the expression in young CTRL set to 1. (*B*) Balance beam (CTRL $n = 9$, MKO $n = 11$), (*C*) rotarod (CTRL $n = 9$, MKO $n = 12$), and (*D*) treadmill running data (CTRL $n = 8$, MKO $n = 9$). (*E*) Absolute and body mass-normalized forelimb muscle strength as determined by grip test (CTRL $n = 9$, MKO $n = 12$). Note that experiments were performed from the age of 23 mo and that some mice from this specific cohort spontaneously died between the start of our behavioral investigation and their euthanasia. (*F*) Normalized lean and fat mass and (*G*) absolute vs. normalized muscle mass from 24-mo-old CTRL ($n = 7$) and MKO ($n = 9$) animals just before euthanasia. QUAD, quadricep. (*H*) Representative SDH staining of TA muscles from different old CTRL and MKO animals. Note that sections with the same number originate from the same slide. (Scale bar: 500 μm.). (*I*) Evaluation of TA muscle fiber composition of old CTRL and MKO animals ($n = 6$ per genotype from randomly chosen muscles). Results are expressed as mean ± SEM. Unpaired Student's *t* test (*B*–*E*) and 2-way ANOVA followed by Sidak's multiple comparisons (*A*, *F*, *G*, and *I*). $^{*}P < 0.05$; $^{**}P < 0.01$; $^{***}P < 0.001$; $^{\#\#}$Significant difference ($P < 0.01$) between conditions.

exercise performance). Nevertheless, other pathological settings could profit from a reduction or ablation of muscle BNDF as evidenced by the improvement of lean mass, muscle weight, and grip strength in old mice.

Contrary to postnatal and whole-body disruption of TrkB (6, 15, 25), muscle-specific BDNF deletion did not adversely affect neuromuscular structure and function. Furthermore, even though we did not directly assess NMJ morphology and functionality in old MKO animals, the fact that these mice displayed similar, if not greater, muscle force, motor balance, and coordination likely rules out an essential role for postsynaptic BDNF expression in the lifelong maintenance of the motor unit. Finally, our observations of unchanged substrate utilization on BDNF deletion are contrasting with the proposed role of BDNF as an exercise-induced myokine to regulate fatty acid oxidation (17). Whether this difference stems from diverging effects of long-term deletion (these results) vs. the transient overexpression and the relatively modest induction of BDNF after acute exercise bouts (17) remains unclear. In any case, in contrast to its key function in other central and peripheral cells controlling energy homeostasis (23, 24), BDNF depletion did not alter systemic energy homeostasis. One limitation of this study, however, is the use of the HSA-Cre transgene to excise BDNF, leading to Cre expression from E9.5 in somitic cells committed to the myogenic lineage (19, 20). It thus would be interesting to initiate muscle BDNF deletion at a later stage to rule out the possibility of any developmental compensation (51).

Some of the characteristics of muscle lacking BDNF (e.g., higher SDH activity, slower contraction and relaxation times, and decreased fatigability rate) are found in endurance-trained muscle (52). However, MKO mice did not show increased spontaneous locomotor activity but rather, showed decreased spontaneous locomotor activity—as some other mouse models

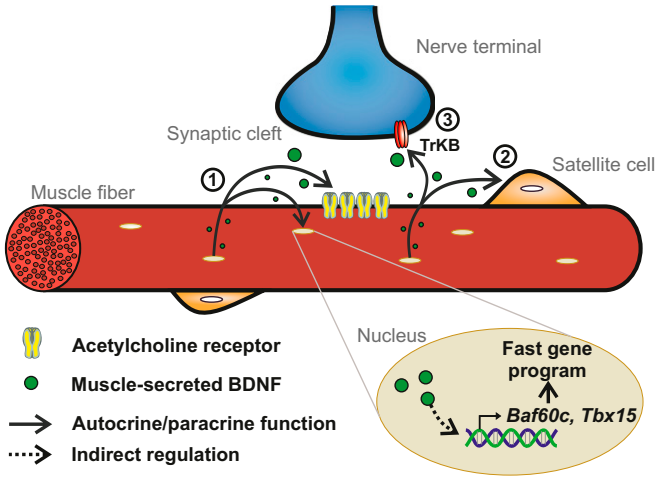

Fig. 8. Proposed model by which BDNF signaling regulates neuromuscular physiology. (*1*) BDNF could act as an autocrine factor to influence the expression of transcriptional regulators involved in fast-twitch muscle-specific gene expression or the expression of synaptic proteins involved in AChR clustering. (*2*) As a paracrine factor, BDNF could regulate the differentiation of satellite cells into slow vs. fast myofibers. (*3*) BDNF might also affect myofiber identity and motor end plate structure indirectly (e.g., by modulating the activity of the TrkB receptors present in nerve terminals of motor neurons).

exhibiting a slow-type muscle transition (36, 53)—ruling out physical activity as a primary cause of the fiber-type change. Intriguingly, there is a clear relationship between the expression of the fast IIB myosin isoform and BDNF during early postnatal development, when muscles are subjected to distinct programs of myosin isoform transitions influenced, for example, by functional demand or motor innervation (33, 54). For instance, the fast IIB myosin isoform rises in both mouse EDL and GAS muscles from day 5 until day 90 after birth (54). BDNF protein also gradually increases in glycolytic muscles of rodent neonates but not in the SOL (27, 55). Besides, combined administration of a ciliary neurotrophic factor (CNTF)–BDNF mixture after neonatal sciatic nerve crush injury can rescue a small fraction (i.e., 5%) of type IIB fibers in the EDL muscle (27). Mechanistically, it is not clear how BNDF controls the type IIB fiber program. Future studies will aim at elucidating the BDNF-activated signaling pathways that ultimately result in a transcriptional induction of *Baf60c* and *Tbx15*, 2 transcriptional regulators involved in fast-twitch muscle-specific gene expression (35, 36). BDNF might also affect these regulators indirectly [e.g., by modulating the activity of the TrkB receptors present in nerve terminals of motor neurons (5, 6)] to mediate morphological remodeling of the NMJ. In that regard, other approaches to overexpress BDNF [e.g., the tetracycline-inducible system (56)] could not only circumvent the significant changes induced by muscle electroporation but also, allow the careful functional and structural evaluation of the effect of muscle BDNF elevation at different developmental stages on the neuromuscular system. Finally, the role of extrinsic signals, such as muscle-derived BDNF, in influencing the commitment of myoblast nuclei to particular gene expression programs and thus, the differentiation of these cells into slow vs. fast myofibers needs additional investigation (Fig. 8).

In summary, we report here that BDNF is a myokine that regulates glycolytic muscle fiber-type identity. Muscle-specific loss of BDNF confers beneficial effects on endurance and mitigates loss of muscle mass and function in sarcopenia. Thus, strategies aimed at neutralizing muscle BDNF might be of interest in certain pathologies. Inversely, our findings of BNDF to promote type IIB fiber programs could be leveraged in diseases where the function of glycolytic muscle fibers is compromised or increased fast-twitch muscle fiber activity is desirable. For example, circulating BDNF levels are associated with type 2 diabetes (16, 57, 58), and chronic BDNF administration enhances glucose uptake in muscle cells (59), which could be, at least in part, mediated by a higher proportion of glycolytic type IIB muscle fibers. Moreover, BDNF may also modulate the glycolytic capabilities of muscle fibers by mechanisms similar to the fibroblast growth factor 21 myokine (60, 61). Lastly, in light of the susceptibility of certain muscle fibers to muscle diseases [e.g., Duchenne muscular dystrophy (62)] and the positive effect of essential determinants of fiber identity on muscle disease progression (63, 64), our findings warrant additional studies to determine whether modulating the activity of BDNF represents an effective therapeutic strategy to delay or even prevent muscle wasting disorders.

Materials and Methods

Animals. *HSA-Cre* transgenic mice were purchased from the Jackson Laboratory (stock no. 006149). *Bdnf*$^{flox/flox}$ mice were a gift from Yves-Alain Barde, Cardiff University, Wales, United Kingdom and have been previously characterized (ref. 65 has mutation and genotyping details). Mice were maintained on a C57BL/6J genetic background in the animal facility of the Biozentrum (University of Basel) in a temperature-controlled room (21 °C to 22 °C) under a 12:12-h light/dark cycle (lights on at 6:00 AM). Unless specifically mentioned, all experiments were performed in young adult male mice (3 to 4 mo old) housed in groups of 3 to 5 in standard cages with enrichment and free access to regular chow diet (3432; KLIBA NAFAG) and water. All experiments were performed in accordance with the principles of the Basel Declaration and with Federal and Cantonal Laws regulating the care and use of experimental animals in Switzerland as well as institutional guidelines of the Biozentrum and the University of Basel. The protocol with all methods described here was approved by the Kantonales Veterinäramt of the Kanton Basel-Stadt under consideration of the wellbeing of the animals and the 3R (replacement, reduction, and refinement) principle.

Statistical Analysis. No statistical methods were used to predetermine sample size. The *n* number used per genotype for each experiment is indicated in the figure legends. Data are expressed as mean ± SEM and were represented and analyzed with the GraphPad Prism 7.0 software. Comparisons between 2 groups were performed with unpaired Student's *t* test. For assessment between 2 independent variables, 2-way ANOVA was used followed by Sidak's multiple comparisons test if the interaction term was significant. A value of $P < 0.05$ was considered statistically significant. Symbols used to indicate the different degrees of statistical significance are as follow: $^{*}P < 0.05$, $^{**}P < 0.01$, and $^{***}P < 0.001$ between mouse genotypes and $^{\#}P < 0.05$ and $^{\#\#}P < 0.01$ between experimental conditions.

Details about body composition analysis; comprehensive laboratory animal monitoring system, glucose homeostasis, body temperature and locomotor activity recordings, gait analysis, indirect calorimetry coupled to treadmill exercise, repetitive nerve stimulation EMG, muscle force and fatigue measurements, muscle electroporation, tissue collection, enzyme-linked immunosorbent assay, histology and immunohistochemistry, slide imaging and image analysis, muscle RNA extraction and real-time qPCR, protein extraction and western blot, mitochondrial DNA number, laser capture microdissection, electrophysiology, behavioral phenotyping of old mice, and antibodies and reagents are provided in *SI Appendix, Supplementary Materials and Methods*. Primer pairs and TaqMan probes used in this study are listed in *SI Appendix*, Table S4.

ACKNOWLEDGMENTS. We thank the Imaging Core Facility of the Biozentrum for their technical help with imaging procedures and data analysis. We also thank Prof. Yves-Alain Barde (Cardiff University, Wales, United Kingdom) for providing the founder *Bdnf*$^{flox/flox}$ mice. L.T. is supported by Spanish Ministry of Economy and Competitiveness/European Regional Development Fund BFU2016-78934-P. The work in the laboratory of C.H. is funded by the Swiss National Science Foundation, European Research Council Consolidator Grant 616830-MUSCLE_NET, Swiss Cancer Research Grant KFS-3733-08-2015, the Swiss Society for Research on Muscle Diseases, SystemsX.ch, the Novartis Stiftung für Medizinisch-Biologische Forschung, and the University of Basel.

1. M. V. Chao, Neurotrophins and their receptors: A convergence point for many signalling pathways. *Nat. Rev. Neurosci.* **4**, 299–309 (2003).
2. E. J. Huang, L. F. Reichardt, Trk receptors: Roles in neuronal signal transduction. *Annu. Rev. Biochem.* **72**, 609–642 (2003).
3. G. Chevrel, R. Hohlfeld, M. Sendtner, The role of neurotrophins in muscle under physiological and pathological conditions. *Muscle Nerve* **33**, 462–476 (2006).
4. B. Kablar, M. A. Rudnicki, Development in the absence of skeletal muscle results in the sequential ablation of motor neurons from the spinal cord to the brain. *Dev. Biol.* **208**, 93–109 (1999).
5. N. Garcia *et al*., The interaction between tropomyosin-related kinase B receptors and presynaptic muscarinic receptors modulates transmitter release in adult rodent motor nerve terminals. *J. Neurosci.* **30**, 16514–16522 (2010).
6. M. Gonzalez *et al*., Disruption of Trkb-mediated signaling induces disassembly of postsynaptic receptor clusters at neuromuscular junctions. *Neuron* **24**, 567–583 (1999).
7. L. B. Tovar-Y-Romo, U. N. Ramírez-Jarquín, R. Lazo-Gómez, R. Tapia, Trophic factors as modulators of motor neuron physiology and survival: Implications for ALS therapy. *Front. Cell. Neurosci.* **8**, 61 (2014).
8. V. E. Koliatsos, R. E. Clatterbuck, J. W. Winslow, M. H. Cayouette, D. L. Price, Evidence that brain-derived neurotrophic factor is a trophic factor for motor neurons in vivo. *Neuron* **10**, 359–367 (1993).
9. S. Capsoni, F. Ruberti, E. Di Daniel, A. Cattaneo, Muscular dystrophy in adult and aged anti-NGF transgenic mice resembles an inclusion body myopathy. *J. Neurosci. Res.* **59**, 553–560 (2000).
10. P. Ernfors, K. F. Lee, J. Kucera, R. Jaenisch, Lack of neurotrophin-3 leads to deficiencies in the peripheral nervous system and loss of limb proprioceptive afferents. *Cell* **77**, 503–512 (1994).
11. R. Klein *et al*., Disruption of the neurotrophin-3 receptor gene trkC eliminates la muscle afferents and results in abnormal movements. *Nature* **368**, 249–251 (1994).
12. N. Belluardo *et al*., Neuromuscular junction disassembly and muscle fatigue in mice lacking neurotrophin-4. *Mol. Cell. Neurosci.* **18**, 56–67 (2001).
13. D. G. Wells, B. A. McKechnie, S. Kelkar, J. R. Fallon, Neurotrophins regulate agrin-induced postsynaptic differentiation. *Proc. Natl. Acad. Sci. U.S.A.* **96**, 1112–1117 (1999).
14. H. S. Je *et al*., ProBDNF and mature BDNF as punishment and reward signals for synapse elimination at mouse neuromuscular junctions. *J. Neurosci.* **33**, 9957–9962 (2013).
15. S. A. Kulakowski, S. D. Parker, K. E. Personius, Reduced TrkB expression results in precocious age-like changes in neuromuscular structure, neurotransmission, and muscle function. *J. Appl. Physiol.* **111**, 844–852 (2011).
16. K. Sakuma, A. Yamaguchi, The recent understanding of the neurotrophin's role in skeletal muscle adaptation. *J. Biomed. Biotechnol.* **2011**, 201696 (2011).
17. V. B. Matthews *et al*., Brain-derived neurotrophic factor is produced by skeletal muscle cells in response to contraction and enhances fat oxidation via activation of AMP-activated protein kinase. *Diabetologia* **52**, 1409–1418 (2009).
18. C. Clow, B. J. Jasmin, Brain-derived neurotrophic factor regulates satellite cell differentiation and skeltal muscle regeneration. *Mol. Biol. Cell* **21**, 2182–2190 (2010).
19. M. Leu *et al*., Erbb2 regulates neuromuscular synapse formation and is essential for muscle spindle development. *Development* **130**, 2291–2301 (2003).
20. M. Schwander *et al*., β1 integrins regulate myoblast fusion and sarcomere assembly. *Dev. Cell* **4**, 673–685 (2003).
21. P. Chacón-Fernández *et al*., Brain-derived neurotrophic factor in megakaryocytes. *J. Biol. Chem.* **291**, 9872–9881 (2016).
22. A. B. Klein *et al*., Blood BDNF concentrations reflect brain-tissue BDNF levels across species. *Int. J. Neuropsychopharmacol.* **14**, 347–353 (2011).
23. S. Bathina, U. N. Das, Brain-derived neurotrophic factor and its clinical implications. *Arch. Med. Sci.* **11**, 1164–1178 (2015).
24. E. E. Noble, C. J. Billington, C. M. Kotz, C. Wang, The lighter side of BDNF. *Am. J. Physiol. Regul. Integr. Comp. Physiol.* **300**, R1053–R1069 (2011).
25. C. B. Mantilla *et al*., TrkB kinase activity maintains synaptic function and structural integrity at adult neuromuscular junctions. *J. Appl. Physiol.* **117**, 910–920 (2014).
26. T. M. DeChiara *et al*., The receptor tyrosine kinase MuSK is required for neuromuscular junction formation in vivo. *Cell* **85**, 501–512 (1996).
27. K. Mousavi, B. J. Jasmin, BDNF is expressed in skeletal muscle satellite cells and inhibits myogenic differentiation. *J. Neurosci.* **26**, 5739–5749 (2006).
28. A.-S. Arnold *et al*., Morphological and functional remodelling of the neuromuscular junction by skeletal muscle PGC-1α. *Nat. Commun.* **5**, 3569 (2014).
29. R. Tejero, M. Lopez-Manzaneda, S. Arumugam, L. Tabares, Synaptotagmin-2, and -1, linked to neurotransmission impairment and vulnerability in Spinal Muscular Atrophy. *Hum. Mol. Genet.* **25**, 4703–4716 (2016).
30. J. Jeppesen, B. Kiens, Regulation and limitations to fatty acid oxidation during exercise. *J. Physiol.* **590**, 1059–1068 (2012).
31. J. A. Romijn *et al*., Regulation of endogenous fat and carbohydrate metabolism in relation to exercise intensity and duration. *Am. J. Physiol.* **265**, E380–E391 (1993).
32. J. R. Zierath, J. A. Hawley, Skeletal muscle fiber type: Influence on contractile and metabolic properties. *PLoS Biol.* **2**, e348 (2004).
33. S. Schiaffino, C. Reggiani, Fiber types in mammalian skeletal muscles. *Physiol. Rev.* **91**, 1447–1531 (2011).
34. S. Schiaffino, C. Reggiani, Molecular diversity of myofibrillar proteins: Gene regulation and functional significance. *Physiol. Rev.* **76**, 371–423 (1996).
35. Z.-X. Meng *et al*., Baf60c drives glycolytic metabolism in the muscle and improves systemic glucose homeostasis through Deptor-mediated Akt activation. *Nat. Med.* **19**, 640–645 (2013).
36. K. Y. Lee *et al*., Tbx15 controls skeletal muscle fibre-type determination and muscle metabolism. *Nat. Commun.* **6**, 8054 (2015).
37. Z. Arany *et al*., The transcriptional coactivator PGC-1β drives the formation of oxidative type IIX fibers in skeletal muscle. *Cell Metab.* **5**, 35–46 (2007).
38. D. M. Anderson *et al*., A micropeptide encoded by a putative long noncoding RNA regulates muscle performance. *Cell* **160**, 595–606 (2015).
39. C. Trollet, D. Scherman, P. Bigey, "Delivery of DNA into muscle for treating systemic diseases: Advantages and challenges" in *Electroporation Protocols: Preclinical and Clinical Gene Medicine*, S. Li, Ed. (Humana Press, Totowa, NJ, 2008), pp. 199–214.
40. J. D. Schertzer, D. R. Plant, G. S. Lynch, Optimizing plasmid-based gene transfer for investigating skeletal muscle structure and function. *Mol. Ther.* **13**, 795–803 (2006).
41. M. J. Molnar *et al*., Factors influencing the efficacy, longevity, and safety of electroporation-assisted plasmid-based gene transfer into mouse muscles. *Mol. Ther.* **10**, 447–455 (2004).
42. M. Gonzalez-Freire, R. de Cabo, S. A. Studenski, L. Ferrucci, The neuromuscular junction: Aging at the crossroad between nerves and muscle. *Front. Aging Neurosci.* **6**, 208 (2014).
43. K. I. Erickson *et al*., Brain-derived neurotrophic factor is associated with age-related decline in hippocampal volume. *J. Neurosci.* **30**, 5368–5375 (2010).
44. M. J. Webster, M. M. Herman, J. E. Kleinman, C. Shannon Weickert, BDNF and trkB mRNA expression in the hippocampus and temporal cortex during the human lifespan. *Gene Expr. Patterns* **6**, 941–951 (2006).
45. M. Silhol, V. Bonnichon, F. Rage, L. Tapia-Arancibia, Age-related changes in brain-derived neurotrophic factor and tyrosine kinase receptor isoforms in the hippocampus and hypothalamus in male rats. *Neuroscience* **132**, 613–624 (2005).
46. E. Palomer *et al*., Aging triggers a repressive Chromatin state at Bdnf promoters in hippocampal neurons. *Cell Rep.* **16**, 2889–2900 (2016).
47. F. Rage, M. Silhol, F. Binamé, S. Arancibia, L. Tapia-Arancibia, Effect of aging on the expression of BDNF and TrkB isoforms in rat pituitary. *Neurobiol. Aging* **28**, 1088–1098 (2007).
48. E. J. Huang, L. F. Reichardt, Neurotrophins: Roles in neuronal development and function. *Annu. Rev. Neurosci.* **24**, 677–736 (2001).
49. D. Merrick, T. Ting, L. K. Stadler, J. Smith, A role for Insulin-like growth factor 2 in specification of the fast skeletal muscle fibre. *BMC Dev. Biol.* **7**, 65 (2007).
50. A. C. Paul, N. Rosenthal, Different modes of hypertrophy in skeletal muscle fibers. *J. Cell Biol.* **156**, 751–760 (2002).
51. J. J. McCarthy, R. Srikuea, T. J. Kirby, C. A. Peterson, K. A. Esser, Inducible Cre transgenic mouse strain for skeletal muscle-specific gene targeting. *Skelet. Muscle* **2**, 8 (2012).
52. J. O. Holloszy, F. W. Booth, Biochemical adaptations to endurance exercise in muscle. *Annu. Rev. Physiol.* **38**, 273–291 (1976).
53. P. Klover, W. Chen, B.-M. Zhu, L. Hennighausen, Skeletal muscle growth and fiber composition in mice are regulated through the transcription factors STAT5a/b: Linking growth hormone to the androgen receptor. *FASEB J.* **23**, 3140–3148 (2009).
54. O. Agbulut, P. Noirez, F. Beaumont, G. Butler-Browne, Myosin heavy chain isoforms in postnatal muscle development of mice. *Biol. Cell* **95**, 399–406 (2003).
55. M. Nagano, H. Suzuki, Quantitative analyses of expression of GDNF and neurotrophins during postnatal development in rat skeletal muscles. *Neurosci. Res.* **45**, 391–399 (2003).
56. M. A. Grill *et al*., Tetracycline-inducible system for regulation of skeletal muscle-specific gene expression in transgenic mice. *Transgenic Res.* **12**, 33–43 (2003).
57. K. S. Krabbe *et al*., Brain-derived neurotrophic factor (BDNF) and type 2 diabetes. *Diabetologia* **50**, 431–438 (2007).
58. K. Marosi, M. P. Mattson, BDNF mediates adaptive brain and body responses to energetic challenges. *Trends Endocrinol. Metab.* **25**, 89–98 (2014).
59. M. Yamanaka *et al*., Brain-derived neurotrophic factor enhances glucose utilization in peripheral tissues of diabetic mice. *Diabetes Obes. Metab.* **9**, 59–64 (2007).
60. F. L. Mashili *et al*., Direct effects of FGF21 on glucose uptake in human skeletal muscle: Implications for type 2 diabetes and obesity. *Diabetes Metab. Res. Rev.* **27**, 286–297 (2011).
61. Y. Izumiya *et al*., FGF21 is an Akt-regulated myokine. *FEBS Lett.* **582**, 3805–3810 (2008).
62. J. Talbot, L. Maves, Skeletal muscle fiber type: Using insights from muscle developmental biology to dissect targets for susceptibility and resistance to muscle disease. *Wiley Interdiscip. Rev. Dev. Biol.* **5**, 518–534 (2016).
63. C. Handschin *et al*., PGC-1alpha regulates the neuromuscular junction program and ameliorates Duchenne muscular dystrophy. *Genes Dev.* **21**, 770–783 (2007).
64. V. Ljubicic *et al*., Chronic AMPK activation evokes the slow, oxidative myogenic program and triggers beneficial adaptations in mdx mouse skeletal muscle. *Hum. Mol. Genet.* **20**, 3478–3493 (2011).
65. S. Rauskolb *et al*., Global deprivation of brain-derived neurotrophic factor in the CNS reveals an area-specific requirement for dendritic growth. *J. Neurosci.* **30**, 1739–1749 (2010).

Acknowledgments

First, I want to thank my supervisor and “Doktorvater” Christoph Handschin for giving me the opportunity to work in his laboratory and for allowing me to work on such an interesting topic that truly became my passion. I also want to thank him for all the support given during my PhD, for the open ear to all problems, the productive feedback, and fruitful discussions.

I would like to take this opportunity to thank current and former lab members that helped me during my thesis with intellectual, mental, and experimental support. Especially, Gesa Brochmann Santana Santos, who performed many of the experiments, with constant persistence, enthusiasm, and accuracy. Due to her kindness and her great personality, I appreciated working with her very much. Further thanks go to Joaquin Perez-Schindler for productive discussions and critical input. I also want to thank all the other people on the floor with whom I had great discussions and fun times, for their support and encouragement. Many thanks go to all the collaborators, especially Pål Westermark, and the core facilities, the IMCF, the FACS, and the Proteomics facility, where special thanks go to Danilo Ritz for his support, analysis, and discussions.

I would like to thank Markus Rüegg and Urs Albrecht for intellectual guidance and constructive discussions during my Ph.D. advisory committee meetings.

Special thanks go to my family and friends, who supported me through the busy times, the ups and downs, and always believed in me. All of you were with me for many years or (almost) all my life. You formed me, and without you, I would not be where and who I am today. Thank you!

Finally, I want to thank Julien Delezie, without whom I would not have been able to succeed the way I did. He guided and supported me during day and night, stood by me during the good and the bad, dealt with my yearly, monthly, daily, and hourly fluctuations in mood, motivation, and confidence. Thank you for being a great teacher, mentor, and partner in life.